

**EFFICIENT APPROACHES FOR EVALUATING THE PLANER
MICROSTRIP GREEN'S FUNCTION AND ITS APPLICATIONS
TO THE ANALYSIS OF MICROSTRIP ANTENNAS**

DISSERTATION

Presented in Partial Fulfillment of the Requirements for
the Degree Doctor of Philosophy in the Graduate
School of The Ohio State University

By

Sina Barkeshli, B.S., M.S.

The Ohio State University

1988

Reading Committee:

Professor P.H. Pathak
Professor L. Peters, Jr.
Professor B.A. Munk
Professor R. Boyd

Approved by



Adviser

Department of Electrical Engineering

Dedication

To my parents, Sorour Aazan and Mehdi

August 1987

ACKNOWLEDGMENTS

I would like to express my gratitude to my advisor, Professor Prabhakar H. Pathak for his advice and encouragement during the production of this work. The assistance and critique of the reading committee, Professor Leon Peters, Jr. and Professor Benedikt A. Munk are greatly appreciated. Working with these Professors was a great pleasure. I also want to express my deepest thanks to my Father, Professor Mehdi Barkeshli, for his everlasting support and inspiration. I must also express my appreciation to my wife, Fariba, for her encouragement, understanding and patience during the completion of this endeavor.

Finally, I wish to express my sincere thanks and appreciation to Karen Mihalco for the careful typing of this manuscript.

August 1987

VITA

August 1, 1956 Born - Tehran, Iran

1979 B.S., The University of Kansas
Lawrence, Kansas

1982 M.S., The University of Kansas
Lawrence, Kansas

1982 to present Graduate Research Associate,
ElectroScience Laboratory,
Department of Electrical
Engineering, The Ohio State
University, Columbus, Ohio

PUBLICATIONS

Publications

"Asymptotic Closed Form Representation of the Microstrip Surface Green's Function for an Efficient Moment Method Analysis of Mutual Coupling in Microstrip Antenna Arrays," S. Barkeshli, P.H. Pathak and M. Marin, paper submitted to IEEE Trans. on Antennas and Propagation.

"Radially Propagating and Steepest Descent Path Integral Representations of the Planar Microstrip Dyadic Green's Function," S. Barkeshli and P.H. Pathak, paper submitted to Journal of Radio Science.

"On the Location of Surface and Leaky Wave Poles for the Grounded Dielectric Slab," M. Marin, S. Barkeshli and P.H. Pathak, paper submitted to IEEE Trans. on Antennas and Propagation.

Conference Papers

"An Efficient Moment Method Analysis of Finite Phased Arrays of Microstrip Dipoles Using an Asymptotic Closed Form Approximation for the Planar Microstrip Green's Function," S. Barkeshli and P.H. Pathak, presented at International IEEE/AP-S Symposium and National Radio Science Meeting at Syracuse, New York, June 6-10, 1988.

"On the Dyadic Green's Function for an Infinite Array of Dipole Source in Multilayered Dielectric/Ferrite Media," S. Barkeshli and P. Pathak, presented at the International IEEE/APS Symposium and National Radio Science Meeting at Blacksburg, Virginia, June 15-19, 1987.

"On the Dyadic Green's Function for Multilayered Dielectric/Ferrite Media," S. Barkeshli and P. Pathak, presented at the International IEEE/APS Symposium and National Radio Science Meeting at Blacksburg, Virginia, June 15-19, 1987.

"An Efficient Approach for Evaluating the Planar Microstrip Green's Function," S. Barkeshli and P.H. Pathak, presented at International IEEE/APS Symposium and National Radio Science Meeting at Philadelphia, Pennsylvania, June 9-13, 1986.

"A Prediction-Correlation Algorithm for Recognition of Noncooperative Aircraft Targets," S. Barkeshli and D.L. Moffatt, Accepted in NATO/AGARD "Target Signature" Symposium, October 8-12, 1984.

"Extraction of Modulation of Capillary Waves," T. Kirimoto, R.K. Moore, S. Barkeshli, R. Vaughn and T. Lam, Presented at National Radio Science Meeting (URSI), Boulder, Colorado, January 1983.

"Extraction of Modulation of Capillary Waves," R.K. Moore and S. Barkeshli, Presented at the IEEE 1982 International Geoscience and Remote Sensing Symposium (IGARSS'82) Meeting at Munich, West Germany, June 1-4, 1982.

"Distribution of Capillary Waves on Larger Waves as Measured by Radar," R.K. Moore, S. Barkeshli, I. Birrer and G.J. Dome, Presented at National Radio Science Meeting (URSI), Boulder, Colorado, January 13-15 1982.

"Preliminary Investigation of the Modulation Function for Radar Backscatter from the Sea," G.J. Dome, R.K. Moore, K.A. Soofi, I. Birrer, S. Barkeshli and G.P. Deloor, Presented at National Radio Science Meeting (URSI), Boulder, Colorado, January 12-15, 1981.

Technical Reports

"Near Field Scattering by Rectangular and Circular Inlet Configurations With an Impedance Surface Termination," Final Report No. 715267-1, The Ohio State University ElectroScience Laboratory, July 1984, (co-author with P.H. Pathak, A. Altintas, and C.W. Chuang).

"Interaction of the Radio Waves with the Capillary Waves of the Sea," Technical Report NO. 419-1, Remote Sensing Laboratory Center for Research, Inc. The University of Kansas, May 1982, (co-author, R.K. Moore).

FIELDS OF STUDY

Major Field: Electrical Engineering

Studies in: Electromagnetic Theory: Professor R. Kouyoumjian
Antenna Theory: Professor B. Munk
Communication Theory: Professor R. Compton
Mathematics: Professor O. Hejrab
Statistics: Professor R. Bartoszynski

TABLE OF CONTENTS

	Page
DEDICATION	ii
ACKNOWLEDGEMENTS	iii
VITA	iv
LIST OF TABLES	ix
LIST OF FIGURES	x
CHAPTER	
I INTRODUCTION	1
II DEVELOPMENT OF THE CONVENTIONAL PLANE WAVE SPECTRAL INTEGRAL SOLUTION OF THE CONONICAL PROBLEM OF THE RADIATION BY A POINT SOURCE IN THE PRESENCE OF A GROUNDED DIELECTRIC SLAB	13
A. The PWS Representation for the Free Space Electric Dyadic Green's Function	17
B. Dyadic Green's Function Formulation for the Grounded Dielectric Slab	26
III SOMMERFELD INTEGRAL REPRESENTATION FOR THE SINGLE LAYER MICROSTRIP DYADIC SURFACE GREEN'S FUNCTION	41
IV EFFICIENT ALTERNATIVE RADIALLY PROPAGATING AND STEEPEST DESCENT PATH INTEGRAL REPRESENTATION FOR THE SINGLE LAYER MICROSTRIP DYADIC SURFACE GREEN'S FUNCTION	63
A. Radially ($\hat{\rho}$) Propagating Representation for the Microstrip Green's Function	64
B. Steepest Descent Path (SDP) Representation of the Microstrip Green's Function	77

V	UNIFORM ASYMPTOTIC CLOSED FORM REPRESENTATION OF SINGLE LAYER MICROSTRIP DYADIC SURFACE GREEN'S FUNCTION	102
IV	MOMENT-METHOD SOLUTION	125
	Moment Method	125
	Mutual Coupling	132
VII	NUMERICAL RESULTS	155
VIII	CONCLUSION	165

APPENDICES

A	THE PWS SOLUTION FOR THE FREE SPACE DYADIC GREEN'S FUNCTION $\bar{G}^0(\vec{r}, \vec{r}')$	167
B	RADIATION AND EDGE CONDITIONS	180
C	SOMMERFELD INTEGRAL REPRESENTATION OF THE MICROSTRIP DYADIC GREEN'S FUNCTION	184
D	ANALYTIC PROPERTY OF $\kappa(\xi) = \sqrt{k^2 - \xi^2}$ IN THE COMPLEX ξ PLANE	191
E	$\xi = k \sin w$ TRANSFORMATION	198
F	MUTUAL IMPEDANCE BETWEEN A PAIR OF ANTENNAS	203
G	GENERAL TE AND TM POLES AND RESIDUES OF THE GROUNDED DIELECTRIC/FERRITE SLAB; (SURFACE WAVE AND LEAKY WAVES)	210
H	UNIFORM ASYMPTOTIC EXPANSION OF THE CANONICAL INTEGRAL	224
I	A UNIFORM ASYMPTOTIC EXPANSION OF	244

$$\int_{-\infty}^{\infty} \frac{H_0^2(k_0 \rho \sqrt{1-\eta^2}) e^{-jk_0 \eta z}}{\eta - \left(\frac{\zeta_p}{k_0}\right)} d\eta$$

REFERENCES	251
------------	-----

LIST OF TABLES

Table	Page
D.1 SIGNS OF $\operatorname{Re}(\kappa(\xi))$ AND $\operatorname{Im}(\kappa(\xi))$	195

LIST OF FIGURES

Figure	Page
1.1. Geometrical configuration of microstrip dyadic Green's function; electric current point source on a grounded planar dielectric slab.	2
2.1. The point source located at $r=\vec{r}'$. Imaginary plane S passing through the source at $z=z'$ and is parallel to xy plane.	18
2.2. Arbitrarily oriented electric current point source over the grounded dielectric slab.	32
2.3. Analogy of g_m'' to a voltage response of a semi-infinite transmission line excited by a current source at $z=z'$.	38
2.4. Analogy of g_m' to a current response of a semi-infinite transmission line excited by a voltage source at $z=z'$.	39
3.1. Imaginary part of the integrand of Sommerfeld type integral of Equation (3.38), versus its normalized argument, $(k_0\rho=1)$.	51
3.2. Normalized behavior of $F(\xi)$ as a function $\alpha=\frac{\xi}{k_0}$	55
3.3. Behavior of $[(F(\xi)-C e^{-\xi s}) J_0(\rho\xi)]$ versus $\frac{\xi}{k_0}$ with a $k_0\rho$ as a parameter.	56
3.4. The behavior of the integrand of the Equation (3.46) for $(k_0\rho=30)$.	60
4.1. The analytic properties of $g_m(\kappa,z,z')$ in complex ξ plane, surface wave poles, branch cuts, C1 is the path of integration of (4.2).	65
4.2. The contour deformation for ρ -propagation representation.	69
4.3. Complex ξ plane and the contour of integration.	69
4.4. Integrand of W in the Equation (4.13) versus $\xi=\alpha$.	74
4.5. Integrand of W in the Equation (4.13) versus $\xi=\alpha$.	78

Figure	Page
4.6. Integrand of W in the Equation (4.13) versus $\xi=\alpha$.	79
4.7. Mapping from complex z to γ plane (angular spectrum mapping), the original path Γ and SDP path Γ_{SDP} have been depicted in complex γ plane.	84
4.8. Complex S plane, original path Γ maps on solid curve, the SDP maps on to the real axis ($-\infty < s < \infty$) and the saddle point $\gamma_s=0$, maps on to $s=0$; the branch points exist at $S_{b1,2} = \mp\sqrt{2}e^{-j\pi/4} (\sqrt{s^2+2j} = 0)$.	86
4.9. Integrand of W in the Equation (4.37) versus s .	90
4.10. Integrand of W in the Equation (4.37) versus s .	93
4.11. Integrand of W in the Equation (4.37) versus s , with closeby leaky wave singularity extracted.	96
4.12. Integrand of W in the Equation (4.37) versus s .	97
4.12. Integrand of W in the Equation (4.37) versus s , with close by leaky wave singularity extracted.	98
4.13. Typical values of U versus ρ/λ_0 from three different representations, Sommerfeld representation, Equation (3.46), ρ -propagation representation, Equation (4.11), and steepest descent path representation, Equation (4.35).	100
4.14. Typical values of W versus ρ/λ_0 from three different representations, Sommerfeld representation, Equation (3.48), ρ -propagation representation, Equation (4.13), and steepest descent path representation, Equation (4.37).	101
5.1. The comparison between the exact numerical integration and the uniform asymptotic value of (W) versus ρ/λ_0 given in (4.13) and (5.19) for $\epsilon_r=3.25$ and different slab thicknesses.	114
5.2. The comparison between the exact numerical integration and the uniform asymptotic value of (W) versus ρ/λ_0 given in (4.13) and (5.19) for $\epsilon_r=9.6$ and different slab thicknesses.	118
5.3. The comparison between the exact numerical integration and the uniform asymptotic value of (W) versus ρ/λ_0 given in (4.13) and (5.19) for $\epsilon_r=12.8$ and different slab thicknesses.	121

Figure	Page
6.1. Pictorial configuration of the Schelkunoff field equivalence principle.	127
6.2. Different basis function used in longitudinal direction.	142
6.3. Mapping from (x, x') to (u, v) plane: $u = \frac{1}{\sqrt{2}} (x' + x)$, $v = \frac{1}{\sqrt{2}} (x' - x)$.	144
7.1. Strip dipole over a grounded dielectric slab.	156
7.2. Input impedance of thin strip dipole over a grounded dielectric slab versus its normalized length with respect to free space wave length λ_0 .	157
7.3. Two coupled very narrow strip dipole antennas.	159
7.4. Mutual impedance of two thin strip dipoles over a grounded dielectric slab, E-plane coupling (end fire) versus the normalized separation length with respect to free space wave length.	160
7.5. Mutual impedance of two thin strip dipoles over a grounded dielectric slab, H-plane coupling (broad side) versus the normalized separation with respect to free space wave length.	162
B.1. Three dimensional wedge (surface singularity); the electromagnetic energy must be finite in any small finite volume (shown by small cylinder) at the neighborhood of the wedge.	182
B.2. Current singularity close to the edges. Current is flowing in the x direction ($\vec{J}(x, y) \sim \hat{x} y^{-1+\alpha} f(x)$).	183
D.1. Regions in the complex ξ separated by curves $\text{Re}(\kappa^2(\xi))=0$ and $\text{Im}(\kappa^2(\xi))=0$.	193
D.2. Two sheeted ξ plane connected with the branch cut defined by $\text{Im}(\kappa^2(\xi))=0$.	196
D.3. Entire two-sheeted ξ -plane. (a) Top sheet $\text{Im}(\kappa(\xi))<0$, (b) Bottom sheet: $\text{Im}(\kappa(\xi))>0$	196
D.5. Two sheeted ξ plane connected with branch cut defined by $\text{Im}(\kappa^2(\xi))=0$; ($k \rightarrow 0$).	197

Figure	Page
D.6. Entire two-sheeted ξ -plane, lossless medium $\kappa'' \rightarrow 0$. (a) Top sheet $\text{Im}(\kappa(\xi)) < 0$, (b) Bottom sheet $\text{Im}(\kappa(\xi)) > 0$	197
E.1. Mapping from two sheet complex ξ plane to complex w plane, k is real; lossless case.	200
E.2. Mapping from the sheeted ξ complex plane to the complex w plane; k is the complex (lossy case).	202
F.1. Two element antenna system $I(2)$, an impressed current on antenna terminal (2); $v(1)$ is the induced open circuited voltage in antenna terminal (1).	203
F.2. Two element antenna system, $V(2)$ is an impressed voltage on antenna terminal (2); $I(1)$ is the induced short circuited current in antenna terminal (1).	204
F.3. Short circuited antenna exposed to the incident electric field \bar{E} , and its equivalent circuit.	207
F.4. Loaded antenna exposed to the incident field \bar{E} .	208
F.5. Two general coupled antennas (q) and (r).	209
H.1. Deformation contour of Γ into steepest descent path Γ' .	226
H.2. Definition of the angle ϕ_s . The direction of integration along the path SDP is indicated by the arrowhead [66].	232
H.3. Contour of integrations of $I_0^\pm(\Omega, b_r \pm j\delta)$.	239
H.4. Mapping of the two sheeted (ξb^2) plane onto $u = \sqrt{j\xi b^2}$ plane.	243
H.5. Integration path of the complex Fresnel's integral in the $u = \sqrt{j\xi b^2}$ plane.	243
I.1. Angular spectrum mapping where $n = \cos \gamma$; the leaky and surface wave poles and the contour integration of Γ and Γ_{SDP} in (I.1) and (I.12) respectively are shown.	247

CHAPTER I

INTRODUCTION

A relatively simple and efficient closed form asymptotic representation of the microstrip dyadic surface Green's function is developed. The geometrical configuration of this microstrip Green's function problem is shown in Figure 1 which illustrates an electric current point source on a grounded isotropic homogeneous planar dielectric slab in free space. The large parameter in this asymptotic development is directly proportional to the lateral separation between the source and field points along the planar microstrip configuration. However, as will be shown later, this asymptotic solution remains accurate even for very small (almost two tenths of the free space wavelength) lateral separation of the source and field points. This efficient representation [1] is expected to be useful in many applications such as in the analysis and design of microstrip antenna arrays and monolithic millimeter and microwave integrated circuit (MIMIC) elements which are gaining importance as the need for easy to fabricate conformal arrays and the push to higher frequencies continues. As pointed out later, the present asymptotic Green's function will allow an efficient calculation of the currents excited on microstrip antenna patches/feed lines based on a moment method (MM) solution of an integral

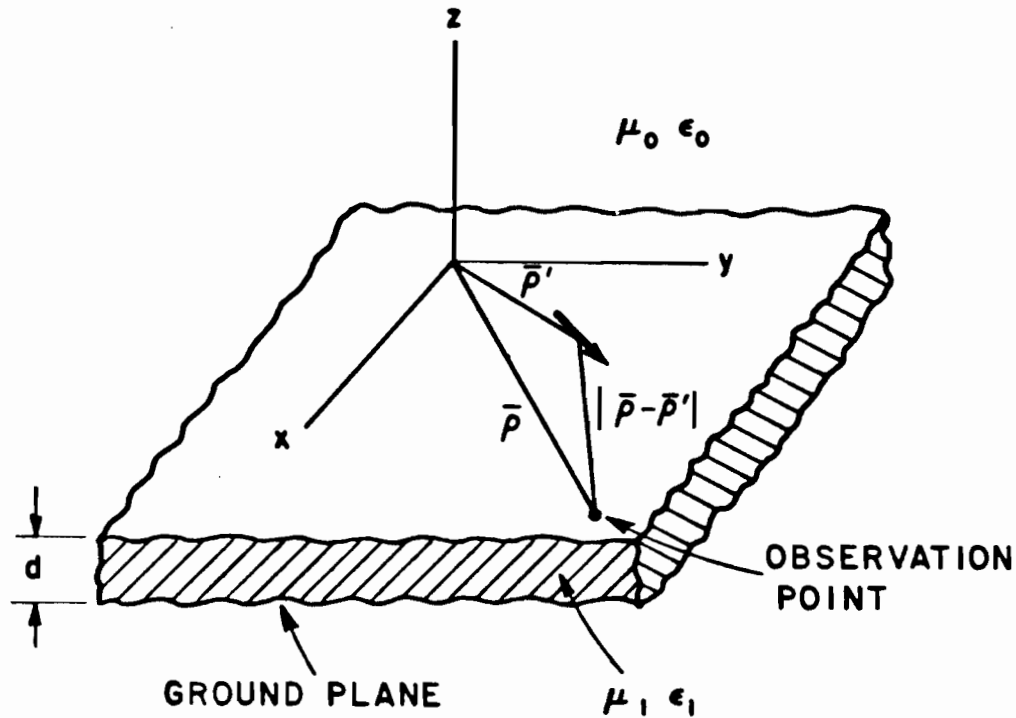


Figure 1.1. Geometrical configuration of microstrip dyadic Green's function; electric current point source on a grounded planar dielectric slab.

equation for these currents in which the Kernel is the microstrip Green's function. Such a MM solution automatically includes all the mutual coupling effects and radiation losses, etc., which most approximate analyses end up neglecting. An exact conventional Sommerfeld representation of the microstrip Green's function is very poorly convergent when used in this MM formulation which generally requires laterally separated source and field points rather than vertically separated (with respect to the planar microstrip structure). In contrast, the present asymptotic Green's function would serve to drastically improve the computational speed of the MM solution for

source and field points laterally separated by more than a couple of tenths of a wavelength; for smaller separations between those points one can switch back to either the conventional Sommerfeld integral form of the Green's function or its modification which is discussed briefly below.

In addition to the asymptotic form, an efficient exact steepest descent contour integral form of the radially propagating representation of the microstrip dyadic Green's function is also derived. The original form of the radially propagating integral representation of the microstrip Green's function (before the contour of integration is deformed into the steepest descent path) exhibits a relatively fast convergence in comparison to the conventional Sommerfeld integral representation as long as there is at least a moderate amount (between a few tenths to a couple of wavelengths) of lateral separation between the source and field points; furthermore, when deformed into the steepest descent path, the radially propagating integral representation exhibits a much faster convergence for lateral separation in excess of half a wavelength or so [1]. For observation points in the immediate vicinity of the source, a modified form of the conventional Sommerfeld representation (which is a vertically (or \hat{z}) propagating representation) of the microstrip Green's function has been utilized. This modification is achieved through an explicit removal of the source singularity [1] which is the main reason for the slow convergence of the Sommerfeld type integrals in the neighborhood of the source point. It has come to our attention that the latter modification has also been independently

developed recently by Jackson and Alexopoulos [2,3]. For laterally separated source and field points, the conventional Sommerfeld integrand exhibits rapid oscillations again making the corresponding integral very slowly convergent.

The microstrip antenna concept was first introduced by Deschamps [4] as early as 1953, and later by Gutton and Baissinot [5] in 1955. However, this class of structures was not seriously considered until the early 70's [6] when Byron [7] proposed a new phased array antenna consisting of conducting strip elements separated from a ground plane by a thin dielectric substrate. The early work by Munson [8], leading to the development of low-profile flush-mounted microstrip antennas showed that in spite of their narrow bandwidth and low gain, this was a practical concept for use in many antenna applications. Since then, this new technology has been under continuous growth over the last decade. The attractive features of microstrip structures are their low profile, low cost, high reliability, reproductivity and their conformability. Although the most practical microstrip structures have been developed for use from 300 MHz to 38 GHz [6], there is a rapid growth of interest to extend this technology to the millimeter wave region [9].

The simplest analytical description of a rectangular microstrip patch utilizes transmission line theory and approximates the patch as two parallel narrow radiating slots [8], separated by some distance. Although the transmission line model gives a simple formula for the input impedance and resonant frequency, it suffers from some serious

drawbacks. It can only be applied to the rectangular shape patches, so other patch configurations cannot be analyzed by this model. The fringing factor must be empirically determined in this model. It ignores the field variation along the radiating edge, and it also ignores the surface wave effects.

A more successful description of the microstrip antenna characteristics can be achieved by the modal expansion analysis technique wherein the patch is viewed as a thin TMz-mode cavity with magnetic side walls [10]-[15]. This theoretical model is based on the following observations:

- a) The close proximity between the microstrip patch and the ground plane implies that the electric field has only a vertical (\hat{z}) component and the magnetic field has only transverse (to \hat{z}) components.
- b) The field confined within the patch and ground plane is almost constant in the vertical (or \hat{z}) direction because the thickness of the substrate (which is the same here as the distance between the microstrip patch and the ground plane) is quite small in terms of the wavelength.
- c) As dictated by the edge condition (see Appendix B), the current on the patch must not have a component normal to the edge at any given point on the edge. This implies that tangential components of the magnetic field along the patch edges must be negligible.

The region between the microstrip and the ground plane can therefore be treated as a cavity bounded by a perfect magnetic conductor side wall. The effect of radiation is represented in terms of either an artificially increased substrate loss tangent [10] or by more elegantly lumping radiated energy effects through the complex admittance at the side (magnetic) walls which amounts to effectively using an impedance boundary condition at the side walls [12], [13]. This method can successfully predict the input impedance and resonance frequency for a variety of patches for which the cavity modes can be found. However this method cannot be applied to the general type of the microstrip elements for which the modal expansion of the field inside the cavity region cannot be derived. It also fails when the cavity model cannot accurately represent the field confined to the substrate region under the patch, such as a narrow strip dipole which is becoming increasingly important for applications in the millimeter wave regime. Also, the mutual coupling effects cannot be analyzed by the above method.

To overcome most of the difficulties of the approximate approaches described above, the moment method (MM) solution of this class of microstrip structures has been proposed by several authors. Newman and Tulyathan [16], used a method based on image theory. The unknown current on the patch was determined in [16] via an integral equation solution based on the MM technique, and the excitation was modeled by a vertically oriented electric line current source. Also, the dielectric slab was modeled by an equivalent volume polarization current

distribution similar to that done earlier by Richmond and Newman [17],[18]. Although the method gives good numerical results for the input impedance and resonance frequency of the patch, it requires an extremely accurate evaluation of the impedance matrix [16]. Later, the MM solution of an integral equation for the patch currents which employed the exact plane wave spectral representation of the microstrip Green's function was proposed by some investigators such as Azumogla, et al. [19], and Mosig and Gardiol [20]. Because of the rigorous form of the spectral Green's function, all the wave interactions are accounted for in a self-consistent manner. However, the main disadvantage with the rigorous formulation which employs the plane wave spectral form of the microstrip Green's function is the extremely large computational time. Even the transformation of the plane wave spectral integral representation to the conventional Sommerfeld type Green's function gives a highly oscillatory integrand especially for large and even moderately large lateral separation of source and field points. If the source (or current) distribution on the patches is Fourier transformable in this plane wave spectral representation, then it has been shown that the resulting six-fold integral of the mutual impedance matrix in the MM calculation can be transformed to a two-fold spectral integral [21]; this method thus becomes very useful for the calculation of the self-impedance or mutual impedance for closeby elements in a microstrip array configuration; nevertheless, even for moderate and of course large amount of lateral separation between source and field points, that plane wave spectral representation becomes inefficient. Alexapoulous and Rana

[22], [23], utilized the MM to analyze the current distribution, input impedance and the mutual impedance of a pair of printed dipoles. They used the conventional Sommerfeld integral form of the microstrip Green's function in their integral equation solution by the MM technique. In this connection, it is noted that there have been some efforts in the past that dealt with the direct evaluation of the Sommerfeld type integral which is encountered in the related classical half-space problem; namely, this has been done by Siegel and King [24], Burke and Miller [25], Johnson and Dudley [26], and others. On the other hand, the Fast Fourier Transform (FFT) technique has been employed by Tsang, et al. [27] and by Mohsen [28]. The integration along the branch cut has been suggested by Kong, et al. [29] and the deformation of the original Sommerfeld integral contour into the steepest descent path has also been used to improve the convergence of the Sommerfeld solution for the half-space problem by Parhami, et al. [30]; and that approach has been further improved by Michalski [31]. In the MM analysis of microstrip geometries where the source and observation point are both on the substrate, the evaluation of the conventional Sommerfeld type integral representation for the microstrip Green's function becomes very inefficient because of the absence of the exponential decay of the integrand which occurs only for vertically separated source and field points in this representation. A combination of numerical and analytical treatment of the Sommerfeld type microstrip Green's function has been proposed by Katehi and Alexopoulos [32] to somewhat alleviate this convergence problem; whereas, Mosig and Gardiol [33], and Choi

[34], utilize deformation of the original Sommerfeld contour to evaluate the otherwise highly oscillatory Sommerfeld integrals. An asymptotic extraction technique has also been used by some investigators [1-3],[35,36] to accelerate the convergence of the Sommerfeld representation of the microstrip surface Green's function. Recently, Choi has successfully derived an approximate but accurate closed form asymptotic solution for the microstrip surface Green's function [34]. The asymptotic development in [34] is based on some "physical considerations" rather than mathematical rigor. The asymptotic treatment presented in this work does not require the use of physical arguments employed in [34] and the asymptotic solution obtained here is quite different from that in [34].

The organization of this dissertation is as follows. Chapter II deals with the formulation and formal solution of the canonical problem of determining the fields produced by an electric point source in the presence of a grounded dielectric slab via the plane wave spectral integral representation for two appropriate vertically (z) directed Hertzian potentials. The concept of wave impedance in the plane wave spectral domain is introduced and the plane wave spectral representation of the dyadic Green's function for such a microstrip geometry is thus formulated. A transmission line interpretation of this dyadic Green's function is also presented.

The plane wave spectral form of the microstrip Green's function obtained in Chapter II is transformed into the usual Sommerfeld form of the microstrip Green's function in Chapter III. The slow convergence of

this Sommerfeld form is illustrated, and a modification of this Sommerfeld representation is developed for improved convergence when the observation point lies in the neighborhood of the source point [1]. As stated earlier, the latter modification has also been independently obtained by Jackson and Alexopoulos [2,3].

Alternative and exact efficient representations of the microstrip dyadic Green's function are next developed in Chapter IV ([1],[37]). Special attention is devoted to the convergence behavior of these alternative representations for the dyadic microstrip surface Green's function; this is studied through numerical calculations. In particular, there are two related types of alternative representations for microstrip dyadic surface Green's function that are given explicitly in Chapter IV; first, an exact radially propagating integral representation which is very efficient for relatively small to moderately large lateral separation of source and field points is obtained. Next, a transformation of the above radially propagating contour integral representation into its exact steepest descent path representation is given; this steepest descent representation is highly efficient for moderately large as well as large lateral separations. It is noted that the radially propagating integral representation before it is deformed into the more efficient form along the steepest descent path somewhat resembles but is not identical to the representation of Mosig and Gardiol [33].

The main thrust of the present work has been to obtain a useful, efficient and accurate closed form asymptotic approximation for the microstrip dyadic surface Green's function [1],[38]; this is derived in

Chapter V. Surprisingly, this new asymptotic representation remains accurate even for separations as small as two tenths of the free space wavelength (in the air region) for moderate size of substrate thickness and dielectric constants.

Chapter VI reviews some basic ideas of the moment method (MM) and its adaptation for analyzing microstrip geometries via the new representations of the microstrip surface Green's function derived in Chapters IV and V. The current expansion modes (or basis functions) suitable for representing the currents on the microstrip patches are described, and the difficulties and remedies in dealing with the calculation of the self impedance or the diagonal matrix terms in the MM solution are also addressed.

Chapter VII mostly contains numerical results. The input impedance of a microstrip dipole has been evaluated as a function of its electrical length. The mutual impedance between a pair of strip dipoles over a grounded dielectric substrate has also been evaluated. In all of these calculations, the numerical results based on the exact microstrip Green's function are used as a check on the results obtained here via the highly efficient closed form asymptotic approximation.

Finally, Chapter VIII deals with conclusions of this research. The main contribution of this dissertation has been to provide a closed asymptotic representation for the microstrip dyadic surface Green's function; these results do not appear to have been given previously in the literature and are therefore new. In Addition, alternative exact radially propagating representations of this Green's function along the

original as well as along the steepest descent contours of integration, respectively, are presented as they exhibit better convergence properties than the usual Sommerfeld integral representation for observation points outside the neighborhood of the source point. For the sake of completeness, some appendices are included. These appendices contain some derivations which have not been pursued in detail in the chapters, or they describe some concepts which have been used in the analysis but need a bit of added clarification. An $e^{+j\omega t}$ time dependence is assumed and suppressed throughout the analysis.

CHAPTER II

DEVELOPMENT OF THE CONVENTIONAL PLANE WAVE SPECTRAL INTEGRAL SOLUTION OF THE CANONICAL PROBLEM OF THE RADIATION BY A POINT SOURCE IN THE PRESENCE OF A GROUNDED DIELECTRIC SLAB

This chapter deals with the construction of the solution to the canonical problem of the electromagnetic (EM) radiation by an electric current point source which radiates in the presence of a grounded isotropic, homogeneous dielectric slab in which the external medium is free space. This solution is developed in terms of the well known vertical (or \hat{z} -propagation) plane wave spectrum (PWS) integral representation for the EM fields. The fields can be expressed compactly in terms of the dyadic Green's function for this problem.

The plane wave spectrum integral representation of the dyadic Green's function for this canonical problem may be constructed in several ways. One of the most common approaches is to express the Green's function in terms of a magnetic vector potential [39-41], whereas another less commonly used approach is to construct the Green's function from a set of appropriate electric and magnetic vector potentials [42,43]. In the former case, the magnetic vector potential in general has components which are parallel and normal to the interface even if the current moment does not possess a component which is normal to the interface. In the other approach, the magnetic and electric

vector potentials are both normal to the interface. If the electric current moment is chosen entirely normal to the interface, then the two approaches become identical since only a single normally directed magnetic vector potential suffices in this case. This is related to the fact that the normally oriented current moment excites only the TM waves (with respect to the normal \hat{z} to the interface), whereas the current moment parallel to the interface excites both TM and TE waves. Therefore the total electromagnetic field must be constructed either with the magnetic vector potential which can produce both TM and TE waves (in this case magnetic vector potential must have components normal and parallel to the interface in order to satisfy the appropriate boundary conditions), or with the magnetic and electric vector potentials which are both normal to the interface (since a normally directed magnetic vector potential produces TM waves and a normally directed electric vector potential produces TE waves). One of the main advantages of the latter formulation is that the boundary conditions associated with the differential operators for the two different types of vector potentials can be uncoupled. In the case of a choice of a single type of magnetic vector potential containing both a vertical (normal \hat{z} to interface) and a horizontal (transverse to \hat{z} or parallel to interface) components, the transverse component (parallel to interface) of the magnetic vector potential will contribute to both TE and TM waves; therefore, the boundary conditions for normal and transverse components will be coupled. This disadvantage will be more pronounced if one deals with a stratified or multi-layer dielectric

media, for which the number of coupled boundary conditions increase, and no simple approach exists.

In this study, the microstrip dyadic Green's function is constructed in terms of electric and magnetic vector potentials, ($\hat{z}\Pi''$ and $\hat{z}\Pi'$) which are directed normal (along \hat{z}) to the interface. We start with the free space case in which the point source radiates with no interface present, and construct the corresponding dyadic Green's function in terms of an integral over the spectra of plane waves guided in the preferred \hat{z} direction. This is essentially the \hat{z} -propagation plane wave spectrum representation of the free space dyadic Green's function which is usually represented by a discrete spherical vector wave expansion. The dyadic Green's function for the grounded dielectric slab is then constructed from the principle of superposition which involves the sum of the fields of the source in free space (or the free space Green's function) with the contribution of the fields reflected by the the grounded dielectric slab. In Chapter IV alternative representations of the microstrip dyadic surface Green's function which exhibit superior convergence properties for laterally separated source and field points, as is required in the moment method (MM) analysis of microstrip problems are presented. It is to be noted that all the different representations of the dyadic Green's functions can be transformed from one type to the other through function theoretic manipulations, or through the use of the characteristic Green's function procedure [42,44].

The electric field for the microstrip geometry (see Figure 1.1) \bar{E}_m ($m=0$ or 1) can be related to the microstrip dyadic Green's function $\bar{\bar{G}}^m(\bar{r}, \bar{r}')$ by [45]

$$\bar{E}_m = -j\omega\mu_0 \iiint_v \bar{\bar{G}}^m(\bar{r}, \bar{r}') \cdot \bar{J}(\bar{r}') d\nu' \quad (2.1)$$

where $\bar{J}(\bar{r}')$ is an arbitrary oriented electric current density contained in volume v in region (o), and m can take on a value of 0 or 1 for observation points in the air or dielectric regions, respectively.

If the electric current density $\bar{J}(\bar{r}')$ is taken to be a point source of strength \bar{p}_e at $\bar{r}=\bar{r}'$, then

$$\bar{J}(\bar{r}') = \bar{p}_e \delta(\bar{r}-\bar{r}') , \quad (2.2)$$

where as usual $\delta(\bar{r}-\bar{r}')$, is the Dirac Delta function which indicates that the electric point source of strength \bar{p}_e is located at $\bar{r}=\bar{r}'$ in (2.2) with

$$\bar{r} = \hat{x}x + \hat{y}y + \hat{z}z \quad ; \quad \bar{r}' = \hat{x}x' + \hat{y}y' + \hat{z}z' . \quad (2.3)$$

The electric field \bar{E}_m may now be viewed as a distribution [46], namely,

$$\bar{E}_m = -j\omega\mu_0 \bar{\bar{G}}^m(\bar{r}, \bar{r}') \cdot \bar{p}_e \quad (2.4)$$

Thus, it is important to observe that the components of the dyadic Green's function can be inferred from (2.4) by inspection if the electric field \bar{E}_m excited by an arbitrarily oriented current point source \bar{p}_e is known; this procedure will be followed here. It is noted that the units of \bar{p}_e are amp-m (and it therefore constitutes a point

current moment), whereas $\delta(\vec{r}-\vec{r}')$ has the units $1/m^3$; thus $\vec{J}=\vec{p}_e \delta(\vec{r}-\vec{r}')$ correctly has the units of amps/m².

As noted previously, the electromagnetic field for the microstrip geometry (in the air region) can be written as

$$\vec{E}_m = \vec{E}^0 + \vec{E}_s \quad ; \quad \vec{H}_m = \vec{H}^0 + \vec{H}_s \quad (2.5)$$

where (\vec{E}^0, \vec{H}^0) are the fields due to \vec{p}_e radiating in free space; i.e., in the absence of the grounded dielectric slab. Thus, (\vec{E}_s, \vec{H}_s) denote the fields scattered by the grounded dielectric slab. First, PWS representation for the fields (\vec{E}^0, \vec{H}^0) and the associated free space dyadic Green's function $\vec{\vec{G}}^0$ will be developed below in part A; the total fields (\vec{E}_m, \vec{H}_m) and the microstrip dyadic Green's function $\vec{\vec{G}}^m$ will then be found in terms of the PWS form in Part B.

A. The PWS Representation for the Free Space Electric Dyadic Green's Function

In free space, the electric field \vec{E}^0 can be expressed in terms of the free space dyadic Green's function $\vec{\vec{G}}^0$ as [45]

$$\vec{E}^0 = -j\omega\mu_0 \iiint_v \vec{\vec{G}}^0(\vec{r}, \vec{r}') \cdot \vec{J}(\vec{r}') dV' \quad (2.6)$$

where $\vec{J}(\vec{r}')$ is the volumetric current density contained in the volume v . If $\vec{J}(\vec{r}')$ is taken as a current point source $\vec{p}_e \delta(\vec{r}-\vec{r}')$, then

$$\vec{E}^0 = -j\omega\mu_0 \vec{\vec{G}}^0(\vec{r}, \vec{r}') \cdot \vec{p}_e \quad (2.7)$$

The field \vec{E}^0 due to \vec{p}_e will be found first, and $\vec{\vec{G}}^0$ will be inferred simultaneously from \vec{E}^0 via the above relation (2.7).

Let us define,

$$\nabla \times \vec{E}^< = -j\omega\mu_0 \vec{H}^< \quad (2.8a)$$

$$\nabla \times \vec{H}^< = j\omega\epsilon_0 \vec{E}^< \quad (2.8b)$$

with

$$\vec{E}^0 = \vec{E}^< \quad \text{for } z \geq 0, \quad (2.9a)$$

$$\vec{H}^0 = \vec{H}^< \quad \text{for } z \geq 0. \quad (2.9b)$$

Therefore, with \geq means the field for $z \geq z'$. The entire free space consists of two regions; namely $z > z'$ and $z < z'$. The plane $z = z'$ (normal to z -axis) which contains the source $\vec{J} = \vec{p}_e \delta(\vec{\rho} - \vec{\rho}') \delta(z - z')$ is shown in Figure 2.1.

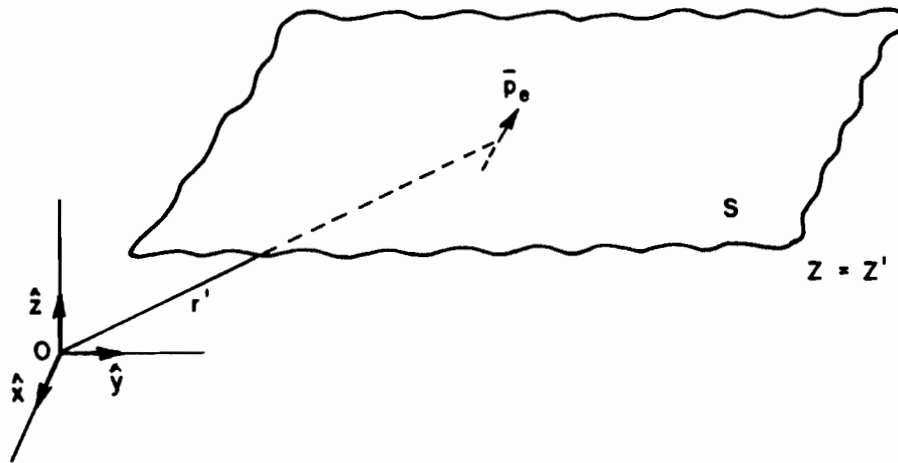


Figure 2.1. The point source located at $\vec{r} = \vec{r}'$. Imaginary plane S passing through the source at $z = z'$ and is parallel to xy plane.

Let us express \bar{E}' which is the value of \bar{E}^0 for $z \neq z'$ as

$$\bar{E}' = u(z-z')\bar{E}^> + u(z'-z)\bar{E}^< \quad (2.10)$$

where the Heaviside Unit Step Function $u(\xi)$ is defined by,

$$u(\xi) = \begin{cases} 1 & \xi > 0 \\ 0 & \xi < 0 \end{cases} \quad (2.11)$$

The \bar{E}' can be obtained in terms of only the solenoidal eigenfunctions because the electric field has a zero divergence of $z \neq z'$. Outside the source region, the Free Space dyadic Green's Function or its associated electric and magnetic fields $\bar{E}^>$ and $\bar{H}^>$ respectively produced by \bar{p}_e can be found via the two different types of vector potentials; namely, the magnetic vector potential $\hat{z}\pi_0'$ and electric vector potential $\hat{z}\pi_0''$. It is noted from (2.9a,b) and (2.10) that

$$(\bar{E}^0 = \bar{E}')_{z \neq z} \quad ; \quad (\bar{H}^0 = \bar{H}')_{z \neq z'} \quad (2.12)$$

It can be shown that

$$\bar{E}^<(\bar{r}, \bar{r}') = \nabla \times \nabla \times \hat{z}\pi_0'^<(\bar{r}, \bar{r}') - j\omega\mu_0 \nabla \times \hat{z}\pi_0''^<(\bar{r}, \bar{r}') \quad , \quad (2.13)$$

$$\bar{H}^<(\bar{r}, \bar{r}') = j\omega\epsilon_0 \nabla \times \hat{z}\pi_0'^<(\bar{r}, \bar{r}') + \nabla \times \nabla \hat{z}\pi_0''^<(\bar{r}, \bar{r}') \quad . \quad (2.14)$$

The $\hat{z}\pi_0'^<(\bar{r}, \bar{r}')$ and $\hat{z}\pi_0''^<(\bar{r}, \bar{r}')$ are solenoidal vector functions, and $\pi_0'^<(\bar{r}, \bar{r}')$ and $\pi_0''^<(\bar{r}, \bar{r}')$ satisfy the well known Helmholtz's equation:

$$\nabla^2 \begin{bmatrix} \Pi_0'' \\ \Pi_0' \\ 0 \end{bmatrix} + k_0^2 \begin{bmatrix} \Pi_0' \\ \Pi_0'' \\ 0 \end{bmatrix} = 0 \quad ; \quad k_0 = \omega \sqrt{\mu_0 \epsilon_0} \quad . \quad (2.15)$$

We impose two sets of boundary conditions. The first set are associated with the behavior of the field at infinity and the second set are associated with the source excitation. As $|r| \rightarrow \infty$ the field quantities must satisfy the Sommerfeld radiation condition (see Appendix B; Equation (B.6)). In the case when one expands the fields in terms of the spectrum of the plane waves using the \hat{z} -propagation (or guided) representation then the Sommerfeld radiation condition simply becomes:

$$\lim_{z \rightarrow \pm\infty} \left(\frac{\partial}{\partial z} \pm jk_z \right) \Pi_0(\vec{r}, \vec{r}') \rightarrow 0 \quad , \quad (2.16)$$

where

$$k_z = \sqrt{k_0^2 - (k_x^2 + k_y^2)} \quad , \quad (2.17)$$

and k_x and k_y will be defined later.

There exist at least two methods to construct the electromagnetic fields of \vec{p}_e in free space. One method is to impose the proper source conditions (see Figure 2.1).

$$[\hat{z} \times (\vec{H}^> - \vec{H}^<)] = \vec{J}_s \quad z=z' \quad (2.18)$$

and

$$[\hat{z} \times (\vec{E}^> - \vec{E}^<)] = \vec{K}_s \quad z=z' \quad (2.19)$$

where \bar{J}_S and \bar{K}_S are equivalent electric and magnetic surface current densities at $z=z'$. The magnetic surface current is equivalent to normally distributed electric current through some operator [47]. These sets of boundary conditions will specify the correct field at $z \neq z'$. However the solution is incomplete in the source region at $z=z'$. The correction term can be found via the use of the original vector wave Equations,

$$\nabla \times \nabla \times \bar{E}^0 - k_0^2 \bar{E}^0 = -j\omega\mu_0 \bar{J} \quad , \quad (2.20)$$

$$\nabla \times \nabla \times \bar{H}^0 - k_0^2 \bar{H}^0 = \nabla \times \bar{J} \quad . \quad (2.20)$$

The second method which is more straight forward and relatively simple has been recently developed by Pathak [46]. In this formulation only (2.18) will be used, and it directly leads to complete electric field representation. It also does not require the imposition of the boundary condition associated with electric field in terms of \bar{K}_S ; the latter is required in the first approach for example if the source \bar{p}_e is perpendicular to the plane S (at $z=z'$).

We follow the same procedure as that of [46] in the following. In order to impose the boundary conditions across the S, the volume current density \bar{p}_e must be expressed in terms of a distribution \bar{p}_{es} corresponding to a "surface" current density at $z=z'$; thus,

$$\bar{J} = \bar{p}_e \delta(\bar{\rho}-\bar{\rho}')\delta(z-z') = \bar{p}_{es} \delta(z-z') \quad . \quad (2.22)$$

Now the discontinuity of the tangential magnetic field across S (at $z=z'$) must be equal to the surface current density on the surface S ; namely,

$$\hat{z} \times (\bar{H}^> - \bar{H}^<) \Big|_{z=z'} = \bar{I}_t \cdot \bar{p}_{es} \quad , \quad (2.23)$$

where \bar{I}_t denotes the transverse part of the unit dyad with respect to \hat{z} :

$$\bar{I} = \bar{I}_t + \hat{z}\hat{z} \quad , \quad (2.24)$$

and

$$\bar{I}_t = \hat{x}\hat{x} + \hat{y}\hat{y} \quad . \quad (2.25)$$

But it is clear that the above equation is valid only at $z=z'$, so it can be expressed as:

$$\hat{z} \times (\bar{H}^> - \bar{H}^<) \delta(z-z') = \bar{I}_t \cdot \bar{p}_{es} \delta(z-z') \quad . \quad (2.26)$$

From Equations (2.22) and (2.23), it follows directly that the above equation becomes

$$\hat{z} \times (\bar{H}^> - \bar{H}^<) \delta(z-z') = \bar{I}_t \cdot \bar{p}_e \delta(\bar{r}-\bar{r}') \quad . \quad (2.27)$$

This simple result expresses the condition on \bar{H}^0 at the source point; this important result will directly indicate the appropriate addition to \bar{E}^1 at the source point to yield the required complete expansion of \bar{E}^0 . It is important to note that since the discontinuity condition in (2.27) relates $\bar{H}^>$ to $\bar{H}^<$ across the source point, and $\nabla \cdot \bar{H} = 0$ here, one only needs to know $\bar{H}^>$ and $\bar{H}^<$ to completely specify \bar{H}^0 due to the source $\bar{J} = \bar{p}_e \delta(\bar{r}-\bar{r}')$; thus

$$\bar{H}^0 = u(z-z') \bar{H}^> + u(z'-z) \bar{H}^< \quad , \quad (2.28)$$

and from (2.8b) and (2.10),

$$\bar{E}' = \frac{-j\omega\mu_0}{k_0^2} [u(z-z') \nabla \times \bar{H}^> + u(z'-z) \nabla \times \bar{H}^<] \quad (2.29)$$

But, from distribution theory [48], it can be shown that

$$\nabla \times (\bar{H} \hat{z} u(\pm z \mp z')) = u(\pm z \mp z') \nabla \times \bar{H} \hat{z} \pm \hat{z} \times \bar{H} \hat{z} \delta(z-z') \quad , \quad (2.30)$$

so (2.29) may be expressed via (2.30) as:

$$\bar{E}' = \frac{-j\omega\mu_0}{k_0^2} \{ \nabla \times [u(z-z') \bar{H}^> + u(z'-z) \bar{H}^<] - \hat{z} \times (\bar{H}^> - \bar{H}^<) \delta(z-z') \} \quad , \quad (2.31)$$

which from (2.27) and (2.28) will become

$$\bar{E}' = \frac{-j\omega\mu_0}{k_0^2} [\nabla \times \bar{H}^0 - \bar{I}_t \delta(\bar{r}-\bar{r}') \cdot \bar{p}_e] \quad . \quad (2.32)$$

On the other hand, the complete expression for the electric field is given via the Maxwell's equation; namely,

$$\bar{E}^0 = \frac{-j\omega\mu}{k_0^2} [\nabla \times \bar{H}^0 - \bar{I} \delta(\bar{r}-\bar{r}') \cdot \bar{p}_e] \quad , \quad (2.33)$$

where the current source \bar{J} is replaced by the point source $\bar{I} \cdot \bar{p}_e \delta(\bar{r}-\bar{r}')$.

It is evident from (2.32) and (2.33) that the complete electric field \bar{E}^0 in terms of \bar{E}' (where \bar{E}' is valid only for $z \neq z'$) is given by:

$$\bar{E}^0(\bar{r}, \bar{r}') = \bar{E}'(\bar{r}, \bar{r}') - j\omega\mu_0 \left[-\frac{\hat{z}\hat{z}}{k_0^2} \delta(\bar{r}-\bar{r}') \right] \cdot \bar{p}_e \quad , \quad (2.34)$$

since $\bar{I} - \bar{I}_t = \hat{z}\hat{z}$.

Recall from (2.12) that

$$\bar{E}^0(\bar{r}, \bar{r}') \Big|_{z \neq z'} = \bar{E}'(\bar{r}, \bar{r}') \Big|_{z \neq z'} \quad (2.35)$$

Next, let us denote $\bar{\bar{G}}'(r, r')$ the dyadic analog of \bar{E}' just as $\bar{\bar{G}}^0(r, r')$ constitutes the dyadic analog of \bar{E}^0 . Let,

$$\bar{\bar{G}}'(\bar{r}, \bar{r}') = u(z-z')\bar{\bar{G}}^> + u(z-z')\bar{\bar{G}}^< \quad , \quad (2.36)$$

Corresponding to (2.10), where $\bar{\bar{G}}'$ satisfies the same differential equation and boundary conditions as $\bar{\bar{G}}(r, r')$ for $\bar{r} \neq \bar{r}'$; thus

$$\bar{\bar{G}}(r, r') \Big|_{z \neq z'} = \bar{\bar{G}}'(r, r') \Big|_{z \neq z'} \quad (2.37)$$

The precise relation between \bar{E}' and $\bar{\bar{G}}'$ can be obtained via the same procedure as that used in obtaining (2.17). In particular

$$\bar{E}'(r') = j\omega\mu_0 \bar{\bar{G}}'(\bar{r}, \bar{r}') \cdot \bar{p}_e \quad . \quad (2.38)$$

Finally, from (2.7), (2.34) and (2.38), it is obvious the required complete expansion of $\bar{\bar{G}}(\bar{r}, \bar{r}')$ in terms of its solenoidal eigenfunction expansion $\bar{\bar{G}}'$ (which is complete only if $z \neq z'$) is given by,

$$\bar{\bar{G}}^0(\bar{r}, \bar{r}') = \bar{\bar{G}}'(\bar{r}, \bar{r}') - \frac{\hat{z}\hat{z}}{k_0^2} \delta(\bar{r} - \bar{r}') \quad (2.39)$$

The detailed derivation of the PWS representation for the electromagnetic fields (\bar{E}^0, \bar{H}^0) due to \bar{p}_e in free space and also the corresponding free space dyadic Green's function $\bar{\bar{G}}^0$ are given in Appendix A. The PWS form of \bar{E}^0 can be written as

$$\vec{E}^0 = \hat{x} E_x^0 + \hat{y} E_y^0 + \hat{z} E_z^0 ,$$

and

$$E_x^0 = \frac{1}{4\pi^2} \iint_{-\infty}^{\infty} \left[jk_y \left[\frac{-jk_x p_{ey} + jk_y p_{ex}}{k_t^2} \right] g''^> + \right. \\ \left. \frac{-jk_x}{j\omega\epsilon_0} \left[\frac{1}{j\omega\epsilon_0} \frac{jk_x p_{ex} + jk_y p_{ey}}{k_t^2} \right] \frac{\partial^2}{\partial z \partial z'} g'^> + \right. \\ \left. \left[\frac{1}{j\omega\epsilon_0} p_{ez} \right] \frac{\partial}{\partial z} g_o'^> \right] e^{-j\vec{k}_t \cdot (\vec{\rho} - \vec{\rho}')} dk_x dk_y , \quad (2.40a)$$

$$E_y^0 = \frac{1}{4\pi^2} \iint_{-\infty}^{\infty} \left[-jk_x \left[\frac{-jk_x p_{ey} + jk_y p_{ex}}{k_t^2} \right] g''^> + \right. \\ \left. \frac{-jk_y}{j\omega\epsilon_0} \left[\frac{1}{j\omega\epsilon_0} \frac{jk_x p_{ex} + jk_y p_{ey}}{k_t^2} \right] \frac{\partial^2}{\partial z \partial z'} g'^> + \right. \\ \left. \left[\frac{1}{j\omega\epsilon_0} p_{ez} \right] \frac{\partial}{\partial z} g_o'^> \right] e^{-j\vec{k}_t \cdot (\vec{\rho} - \vec{\rho}')} dk_x dk_y , \quad (2.40b)$$

$$\begin{aligned} \vec{E}_z^0 = \frac{1}{4\pi^2} \iint_{-\infty}^{\infty} & \left[\frac{1}{j\omega\epsilon_0} \left[\frac{1}{j\omega\epsilon_0} \left[\frac{-jk_x p_{ex} + jk_y p_{ey}}{k_t^2} \right] \frac{\partial}{\partial z'} g_{<}^{\prime} + \right. \right. \\ & \left. \left[\frac{1}{j\omega\epsilon_0} p_{ez} \right] g_{<}^{\prime} k_t^2 \right] \left[e^{-jk_t \cdot (\vec{\rho} - \vec{\rho}')} dk_x dk_y - \frac{1}{j\omega\epsilon_0} p_{ez} \delta(\vec{r} - \vec{r}') \right] \end{aligned} \quad (2.40c)$$

where

$$g_{<}^{\prime\prime} = j\omega\mu_0 \frac{e^{-jk_z |z-z'|}}{2jk_z}, \quad (2.41)$$

$$g_{<}^{\prime} = j\omega\epsilon_0 \frac{e^{-jk_z |z-z'|}}{2jk_z}, \quad (2.42)$$

$$k_z = \sqrt{k_0^2 - k_t^2}, \quad (2.43)$$

$$k_t^2 = k_x^2 + k_y^2; \quad \vec{k}_t = \hat{x} k_x + \hat{y} k_y, \quad (2.44)$$

and

$$\vec{\rho} - \vec{\rho}' = \hat{x}(x-x') + \hat{y}(y-y'). \quad (2.41)$$

B. Dyadic Green's Function Formulation for the Grounded Dielectric Slab

The PWS representation for the free space dyadic Green's function \vec{G}^0 , and hence for the corresponding fields (\vec{E}^0 and \vec{H}^0) of \vec{p}_e in free

space given in part A provides information on the general form of the PWS solution for the fields \vec{E}_m and \vec{H}_m due to \vec{p}_e radiating in the presence of the grounded dielectric slab. The latter would then provide the complete dyadic Green's function $\vec{\vec{G}}^m$ for the grounded dielectric slab.

The electric dyadic Green's function for the grounded dielectric slab can be expressed as a sum of $\vec{\vec{G}}^0$ and another PWS contribution to account for the field scattered by the grounded dielectric layer. The scattered contribution can be expressed in terms of a PWS resembling that for $\vec{\vec{G}}^0$ except that now the amplitude of the spectrum in the integrands must be weighted by spectral reflection and transmission coefficients to be found by enforcing the boundary conditions. We will show how one can make use of the transmission line analogy to the PWS integral representation for waves guided in the \hat{z} -direction for this situation. This analogy enables one to formulate the Green's function for the general multilayered media in a more systematic way.

Let us consider an arbitrarily oriented electric point source radiating in the presence of a grounded dielectric slab as shown in Figure 2.2. Medium (0) is free space with the constitutive parameters μ_0, ϵ_0 , and medium (1) corresponds to the grounded dielectric slab with constitutive parameters μ_1, ϵ_1 and thickness d . The dipole is located at $z=z'$ plane in region (0).

One may write the general form of the solutions for the fields in this problem following the results given earlier in (2.40a) - (2.40c) for the free space case. The only difference is that the general form

of the PWS integrals for the fields in regions (0) and (1) will now be weighted by unknown spectral coefficients g_0'' , g_1'' , g_0' and g_1' instead of the known g'' and g' as in the free space case. By applying the boundary conditions at the interfaces and radiation condition at $z \rightarrow \infty$, the explicit expressions of g_m'' and g_m' will be determined; here $m=0$ or 1 as before. Note that

$$\vec{E}_m = \hat{x} E_{mx} + \hat{y} E_{my} + \hat{z} E_{mz}$$

and

$$E_{mx} = \frac{1}{4\pi^2} \iint_{-\infty}^{\infty} \left[jk_y \left[\frac{-jk_x p_{ey} + jk_y p_{ex}}{k_t^2} \right] g_m'' + \right. \\ \left. \frac{-jk_x}{j\omega\epsilon_m} \left[\frac{1}{j\omega\epsilon_0} \frac{jk_x p_{ex} + jk_y p_{ey}}{k_t^2} \right] \frac{\partial^2}{\partial z' \partial z} g_m' + \right. \\ \left. \left[\frac{1}{j\omega\epsilon_0} p_{ez} \right] \frac{\partial}{\partial z} g_m' \right] e^{-j\vec{k}_t \cdot (\vec{\rho} - \vec{\rho}')} dk_x dk_y, \quad (2.46a)$$

$$\begin{aligned}
E_{my} = \frac{1}{4\pi^2} \iint_{-\infty}^{\infty} & \left[-jk_x \left[\frac{-jk_x p_{ey} + jk_y p_{ex}}{k_t^2} \right] g_m^{>} + \right. \\
& \frac{-jk_y}{j\omega\epsilon_m} \left[\left[\frac{1}{j\omega\epsilon_0} \frac{jk_x p_{ex} + jk_y p_{ey}}{k_t^2} \right] \frac{\partial^2}{\partial z' \partial z} g_m^{>} + \right. \\
& \left. \left. \left[\frac{1}{j\omega\epsilon_0} p_{ez} \right] \frac{\partial}{\partial z} g_m^{>} \right] \right] e^{-j\bar{k}_t \cdot (\bar{\rho} - \bar{\rho}')} dk_x dk_y \quad (2.46b)
\end{aligned}$$

$$\begin{aligned}
E_{mz} = \frac{1}{4\pi^2} \iint_{-\infty}^{\infty} & \left[\frac{1}{j\omega\epsilon_m} \left[\left[\frac{1}{j\omega\epsilon_0} \frac{jk_x p_{ex} + jk_y p_{ey}}{k_t^2} \right] \frac{\partial}{\partial z'} g_m^{>} + \right. \right. \\
& \left. \left. \left[\frac{1}{j\omega\epsilon_0} p_{ez} \right] g_m^{>} k_t^2 \right] \right] e^{-j\bar{k}_t \cdot (\bar{\rho} - \bar{\rho}')} dk_x dk_y \\
& - \frac{1}{j\omega\epsilon_0} p_{ez} \delta(\bar{r} - \bar{r}') , \quad (2.46c)
\end{aligned}$$

$$\bar{H}_m = \hat{x} H_{mx} + \hat{y} H_{my} + \hat{z} H_{mz} ,$$

$$H_{mx} = \frac{1}{4\pi^2} \iint_{-\infty}^{\infty} \left[\frac{-jk_x}{j\omega\mu_m} \left[\frac{-jk_x p_{ey} + jk_y p_{ex}}{k_t^2} \right] \frac{\partial}{\partial z} g_m^{>\zeta} + \right. \\ \left. -jk_y \left[\frac{1}{j\omega\epsilon_0} \frac{jk_x p_{ex} + jk_y p_{ey}}{k_t^2} \right] \frac{\partial}{\partial z'} g_m^{>\zeta} + \right. \\ \left. \left[\frac{1}{j\omega\epsilon_0} p_{ez} \right] g_m^{>\zeta} \right] e^{-j\bar{k}_t \cdot (\bar{\rho} - \bar{\rho}')} dk_x dk_y , \quad (2.47a)$$

$$H_{my} = \frac{1}{4\pi^2} \iint_{-\infty}^{\infty} \left[\frac{-jk_y}{j\omega\mu_m} \left[\frac{-jk_x p_{ey} + jk_y p_{ex}}{k_t^2} \right] \frac{\partial}{\partial z} g_m^{>\zeta} + \right. \\ \left. +jk_x \left[\frac{1}{j\omega\epsilon_0} \frac{jk_x p_{ex} + jk_y p_{ey}}{k_t^2} \right] \frac{\partial}{\partial z'} g_m^{>\zeta} + \right. \\ \left. \left[\frac{1}{j\omega\epsilon} p_{ez} \right] g_m^{>\zeta} \right] e^{-j\bar{k}_t \cdot (\bar{\rho} - \bar{\rho}')} dk_x dk_y , \quad (2.47b)$$

and

$$H_{mz} = \frac{1}{4\pi^2} \iint_{-\infty}^{\infty} \left[\frac{1}{j\omega\mu_m} \left[\frac{-jk_x p_{ey} + jk_y p_{ex}}{1} \right] \cdot \hat{g}_m^{\rightarrow} + e^{-j\vec{k}_t \cdot (\vec{\rho} - \vec{\rho}')} \right] dk_x dk_y,$$

where

$$m = \begin{cases} 0 & \text{if } z > 0 \\ 1 & \text{if } z < 0 \end{cases} \quad (2.47c)$$

Due to the radiation condition at infinity and the presence of the interface at $z=0$, let us write \hat{g}_0'' and \hat{g}_0' as a superposition of the two waves traveling along the $(+\hat{z})$ and $(-\hat{z})$ directions:

$$\hat{g}_0'' = j\omega\mu_0 \frac{e^{-jk_{oz}|z-z'|} + B_0'' e^{-jk_{oz}(z+z')}}{2jk_{oz}}, \quad z > 0, \quad (2.48)$$

$$\hat{g}_0' = j\omega\epsilon_0 \frac{e^{-jk_{oz}|z-z'|} + B_0' e^{-jk_{oz}(z+z')}}{2jk_{oz}}, \quad z > 0. \quad (2.49)$$

Due to the ground plane, the tangential components of the electric field must vanish at $z=-d$. Equations (2.46a) and (2.46b) simply imply that

$$g_1''(z, z') = 0 \Big|_{z=-d}, \quad (2.50)$$

and

$$\frac{\partial}{\partial z} g_1'(z, z') = 0 \Big|_{z=-d}. \quad (2.51)$$

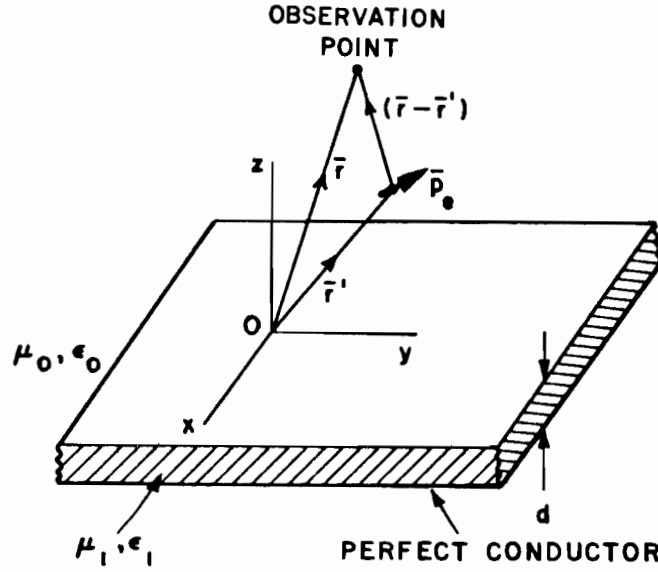


Figure 2.2. Arbitrarily oriented electric current point source over the grounded dielectric slab.

Hence, one can write g_1'' and g_1' as the superposition of the standing waves, knowing the fact that g_1'' and $\frac{\partial g_1'}{\partial z}$ must vanish at $z=-d$, so

$$g_1''(z, z') = j\omega\mu_0 e^{-jk_{0z}z'} C_1'' \sin k_{1z}(z+d) \quad (2.52)$$

$$g_1'(z, z') = j\omega\epsilon_0 e^{-jk_{0z}z'} C_1' \cos k_{1z}(z+d) \quad (2.53)$$

Now with these expressions for g_m'' and g_m' , we impose the boundary conditions at the interface $z=0$. the tangential electric and magnetic fields must be continuous at the air/dielectric interface:

$$\hat{z} \times \vec{E}_m \Big|_{z \rightarrow 0^+} = \hat{z} \times \vec{E}_m \Big|_{z \rightarrow 0^-} \quad (2.54)$$

$$\hat{z} \times \bar{H}_m \Big|_{z \rightarrow 0^+} = \hat{z} \times \bar{H}_m \Big|_{z \rightarrow 0^-} \quad (2.55)$$

in which (\bar{E}_m, \bar{H}_m) are the electromagnetic fields of \bar{p}_e in the presence of the grounded dielectric slab. Also, as mentioned earlier,

$$\bar{E}_m = \begin{cases} \bar{E}_0 & \text{in region (0)} \\ \bar{E}_1 & \text{in region (1)} \end{cases} ; \quad (2.56)$$

likewise,

$$\bar{H}_m = \begin{cases} \bar{H}_0 & \text{in region (0)} \\ \bar{H}_1 & \text{in region (1)} \end{cases} . \quad (2.57)$$

The preceeding equations can be written in component form:

$$E_{ox} = E_{1x} \Big|_{z=0} ; E_{oy} = E_{1y} \Big|_{z=0} , \quad (2.58)$$

$$H_{ox} = H_{1x} \Big|_{z=0} ; H_{oy} = H_{1y} \Big|_{z=0} . \quad (2.59)$$

From (2.46a), (2.46b), (2.47a) and (2.47b), one may deduce that at $z=0$ it suffices to have:

$$g_0'' = g_1'' ; \frac{1}{\mu_0} \frac{\partial}{\partial z} g_0'' = \frac{1}{\mu_1} \frac{\partial}{\partial z} g_1'' \quad (2.60)$$

and

$$g_0' = g_1' ; \frac{1}{\epsilon_0} \frac{\partial}{\partial z} g_0' = \frac{1}{\epsilon_1} \frac{\partial}{\partial z} g_1' . \quad (2.61)$$

The decoupling of the boundary conditions into the TE_z , involving only g'' , and TM_z , involving only g' , should to be noted. From (2.48), (2.52) and (2.60), one will get:

$$\frac{1+B_0''}{2jk_{oz}} = C_1'' \sin(k_{1z}d) \quad , \quad (2.62)$$

and

$$\frac{1-B_0''}{2} = \frac{\mu_0}{\mu_1} C_1'' (k_{1z}) \cos(k_{1z}d) \quad . \quad (2.63)$$

The two equations above can be solved for the two unknowns B_0'' and C_1'' as

$$B_0'' = \frac{+j \frac{k_{1z}}{\mu_1} \cotan(k_{1z}d) + \frac{k_{oz}}{\mu_0}}{\frac{k_{oz}}{\mu_0} - j \frac{k_{1z}}{\mu_1} \cotan(k_{1z}d)} \quad , \quad (2.64)$$

and

$$C_1'' = \frac{\frac{1}{2jk_{oz}} \frac{2k_{oz}}{\mu_0 \sin(k_{1z}d)}}{\frac{k_{oz}}{\mu_0} - j \frac{k_{oz}}{\mu_1} \cotan(k_{1z}d)} \quad . \quad (2.65)$$

Also from (2.49), (2.53) and (2.61), one obtains

$$\frac{1-B_0'}{2jk_{oz}} = C_1' \cos k_{1z}(z+d) \quad (2.66)$$

$$\frac{1-B_0'}{2} = \frac{\epsilon_0}{\epsilon_1} C_1'' (-k_{1z}) \sin(k_{1z}d) \quad (2.67)$$

$$B_0' = \frac{\frac{k_{0z}}{\epsilon_0} - j \frac{k_{1z}}{\epsilon_1} \tan k_{1z}d}{\frac{k_{0z}}{\epsilon_0} + j \frac{k_{1z}}{\epsilon_1} \tan k_{1z}d}, \quad (2.68)$$

and

$$C_1' = \frac{\frac{1}{2jk_{0z}} \frac{2k_{0z}}{\epsilon_0} \cos(k_{1z}d)}{\frac{k_{0z}}{\epsilon_0} + j \frac{k_{1z}}{\epsilon_1} \tan k_{1z}d}. \quad (2.69)$$

Before proceeding further, it is beneficial to introduce the concept of wave impedance in the plane wave spectral domain. From (2.46) through (2.47), it is noted that the transverse part (to \hat{z}) of the field components $\bar{E}_{mt}, \bar{H}_{mt}$ outside the source point can be expressed symbolically as

$$\bar{E}_{mt} = \frac{1}{4\pi^2} \iint_{-\infty}^{\infty} \left[\bar{\tilde{E}}_{mt}''(k_x, k_y) + \bar{\tilde{E}}_{mt}'(k_x, k_y) \right] e^{-jk_t \cdot (\bar{\rho} - \bar{\rho}')} dk_x dk_y, \quad (2.70)$$

$$\bar{H}_{mt} = \frac{1}{4\pi^2} \iint_{-\infty}^{\infty} \left[\bar{\tilde{H}}_{mt}''(k_x, k_y) + \bar{\tilde{H}}_{mt}'(k_x, k_y) \right] e^{-jk_t \cdot (\bar{\rho} - \bar{\rho}')} dk_x dk_y. \quad (2.71)$$

with

$$\bar{E}_{mt} = \hat{x} E_{mx}^t + \hat{y} E_{my}^t, \quad (2.72)$$

$$\bar{H}_{mt} = \hat{x} H_{mx}^t + \hat{y} H_{my}^t, \quad (2.73)$$

There exists, a relationship between $\tilde{\tilde{E}}_t$ and $\tilde{\tilde{H}}_t$; namely

$$\hat{z} \times \tilde{\tilde{E}}_{mt} = \pm Z_m \tilde{\tilde{H}}_{mt} \quad , \quad (2.74)$$

where the prime (') and double prime (") have been omitted for convenience. Explicit form of $\tilde{\tilde{E}}_{mt}$, $\tilde{\tilde{H}}_{mt}$ can be identified via (2.40) and (2.41) where the wave impedance Z_m will be:

$$Z_m'' = \frac{1}{Y''} = \frac{\omega \mu_m}{k_{mz}} \quad , \quad (2.75)$$

and

$$Z_m' = \frac{k_{mz}}{\omega \epsilon} \quad . \quad (2.76)$$

Here, Z_m'' is the impedance (Y'' is the admittance) of the TE_z waves and Z_m' is the impedance of the TM_z waves. In the Equation (2.74), the plus sign (+) is for the waves going in $+\hat{z}$ direction and the minus sign (-) is for the waves going in the $-\hat{z}$ direction. Also note that the total fields in (2.72) and (2.73) are the superposition of plane waves traveling in $\pm\hat{z}$ directions with a continuous spectrum of wave numbers.

Now the coefficients in (2.64), (2.65), (2.68) and (2.69) can be written in terms of the wave admittance. The expression for g_m'' will be:

$$g_0'' = \frac{1}{2Y_0''} \left[e^{-jk_{0z}|z-z'|} + \Gamma'' e^{jk_{0z}(z+z')} \right] \quad , \quad (2.77)$$

$$g_1'' = \frac{1}{2Y_0''} T'' \frac{\sin k_{1z}(z+d)}{\sin(k_{1z}d)} e^{-jk_{0z}z'} \quad . \quad (2.78)$$

where

$$\Gamma'' = \frac{Y_0'' + jY_1'' \cotan(k_{1z}d)}{Y_0'' - jY_1'' \cotan(k_{1z}d)}, \quad (2.79)$$

$$T'' = \frac{2Y_0''}{Y_0'' - jY_1'' \cotan(k_{1z}d)}, \quad (2.80)$$

$$Y_0'' = \frac{k_{0z}}{\omega\mu_0}, \quad Y_1'' = \frac{k_{1z}}{\omega\mu_1}, \quad (2.81)$$

and the admittance Y_0'' and Y_1'' denote the values of $(Z_m'')^{-1}$ in regions (0) and (1), respectively. Also,

$$k_{0z} = \sqrt{k_0^2 - k_t^2}, \quad k_{1z} = \sqrt{k_1^2 - k_t^2} \quad (2.82)$$

The expression of g'' , Equations (2.77) and (2.78), are exactly the same as the voltage response of a transmission line, excited by a unit current source at $z=z'$, with an intrinsic impedance change at $z=0$ and a short circuit termination at $z=-d$ (see Figure 2.3). The expression for g_m' can be written as

$$g_0' = \frac{1}{2Z_0'} \left[e^{-jk_{0z}|z-z'|} - \Gamma' e^{jk_{0z}(z+z')} \right], \quad (2.83)$$

and

$$g_1' = \frac{1}{2Z_1'} T' \frac{\cos k_{1z}(z+d)}{\cos(k_{1z}d)} e^{-jk_{0z}z'}, \quad (2.84)$$

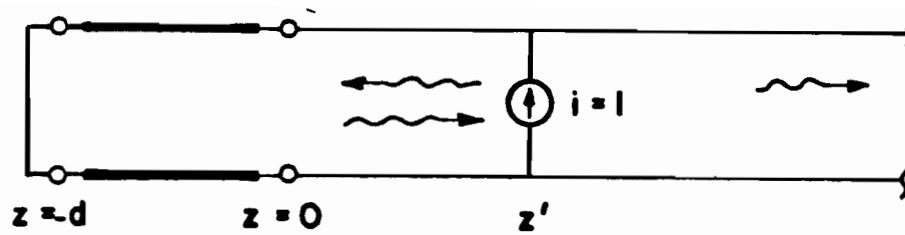


Figure 2.3. Analogy of g_m'' to a voltage response of a semi-infinite transmission line excited by a current source at $z=z'$.

where

$$\Gamma' = \frac{j Z_1' \tan(k_{1z}d) - Z_0'}{j Z_1' \tan(k_{1z}d) + Z_0'} \quad , \quad (2.85)$$

and

$$T' = \frac{2Z_0'}{j Z_1' \tan(k_{1z}d) + Z_0'} \quad , \quad (2.86)$$

$$Z_0' = \frac{k_{0z}}{\omega \epsilon_0} \quad , \quad Z_1' = \frac{k_{1z}}{\omega \epsilon_1} \quad . \quad (2.87)$$

Again, Z_0' and Z_1' denote the values of Z' in regions (0) and (1), respectively. The expression of g_m' , Equations (2.83) and (2.84), are exactly the same as the current response of a transmission line, excited by a unit voltage source at $z=z'$, with the intrinsic impedance change at $z=0$ and a short circuit termination at $z=-d$ (see Figure 2.4).

The explicit expressions of g_m'' and g_m' in air and dielectric have been found. The electric and magnetic field components and corresponding dyadic Green's function for a grounded dielectric slab can be calculated via (2.46) and (2.47).

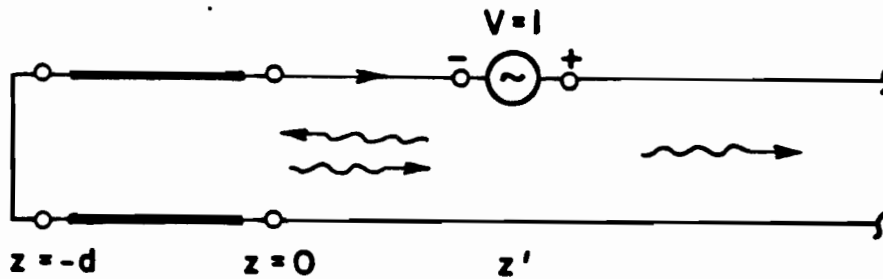


Figure 2.4. Analogy of g_m' to a current response of a semi-infinite transmission line excited by a voltage source at $z=z'$.

The utilization of the transmission line analogy to the z and z' dependance of the field components enables one to investigate more complicated problems such as an arbitrarily oriented dipole in a multi-layered media environment in which the stratification is along planes defined by z -constant. The latter problems are of importance in the design of substrate and superstrate antenna configuration, or an array within multi-layered dielectric slabs [49,50].

The PWS representation for the microstrip Green's function obtained above is in general very cumbersome in applications. It involves a double infinite integral and it is extremely slowly convergent for laterally separated source and field points. Nevertheless, this representation is being used within a Moment Method (MM) formulation of the integral equation for the currents on a microstrip patch in which the current is expanded in terms of basis functions which are Fourier transformable in both x and y domains [21].

CHAPTER III

SOMMERFELD INTEGRAL REPRESENTATION FOR THE SINGLE LAYER MICROSTRIP DYADIC SURFACE GREEN'S FUNCTION

This chapter deals with the Sommerfeld integral representation of the dyadic Green's function for single layer microstrip geometries. This integral representation consists of semi-infinite integrals with oscillatory integrand. Through numerical calculations a convergence problem associated with this conventional integral representation will be addressed. A technique for improving the convergence of this representation will be proposed, and its limitation will be studied. In the next two chapters more efficient alternative representations of the microstrip surface dyadic Green's function will be sought.

One recalls that (2.40a)-(2.40c) of the previous chapter constitute the plane wave spectrum (PWS) representation of the dyadic Green's function for single layer microstrip geometries. The conventional Sommerfeld representation of this dyadic Green's function can be obtained for this double spectrum (or PWS) representations given in detail in the previous chapter.

This PWS representation of the electric field \bar{E}_m ($m=0$ or 1) given in (2.46) can also be written as

$$\begin{aligned}\bar{E}_m = & \left[-j\omega\mu_m \frac{\partial \pi''_m}{\partial y} + \frac{\partial^2 \pi'_m}{\partial x \partial z} \right] \hat{x} + \left[j\omega\mu_m \frac{\partial \pi''_m}{\partial x} + \frac{\partial^2 \pi'_m}{\partial y \partial z} \right] \hat{y} \\ & + \left[\frac{\partial^2}{\partial z^2} + k_m^2 \right] \pi'_m \hat{z} - \frac{1}{j\omega\epsilon_0} p_{ez} \delta(\bar{r}-\bar{r}') \hat{z} \quad ,\end{aligned}\quad (3.1)$$

where

$$\begin{aligned}\pi''_m = & \frac{1}{4\pi^2} \frac{1}{j\omega\mu_m} \iint_{-\infty}^{\infty} \frac{-(\hat{z}_x \hat{p}_e)}{k_t^2} \\ & \cdot \nabla_t g''_m(\kappa, z, z') e^{-j(k_x(x-x') + k_y(y-y'))} dk_x dk_y \quad ,\end{aligned}\quad (3.2)$$

and

$$\begin{aligned}\pi'_m = & \frac{1}{4\pi^2} \frac{1}{(j\omega\epsilon_m)} \frac{1}{(j\omega\epsilon_0)} \iint_{-\infty}^{\infty} \left(\frac{-\bar{p}_{et}}{k_t^2} \cdot \frac{\partial}{\partial z'} \nabla_t + p_{ez} \right) \\ & g'_m(\kappa, z, z') e^{-j(k_x(x-x') + k_y(y-y'))} dk_x dk_y \quad ,\end{aligned}\quad (3.3)$$

with

$$\bar{p}_e = \bar{p}_{et} + \hat{z} p_{ez} \quad . \quad (3.2)$$

As usual, ∇_t denotes the transverse (to z) Laplacian operator,

$$\nabla_t = \hat{x} \frac{\partial}{\partial x} + \hat{y} \frac{\partial}{\partial y} \quad , \quad (3.5)$$

and g''_m and g'_m have been given in (2.71) (2.72), (2.77), (2.78), with $\kappa_0 = k_{0z}$ and $\kappa_1 = k_{1z}$; also the symbols $(\begin{smallmatrix} < \\ > \end{smallmatrix})$ have been omitted for convenience.

If the derivative and integral operations in (3.2) and (3.3) are interchanged, then one obtains

$$\pi_m'' = \frac{1}{j\omega\mu_m} [-\hat{z} \times \bar{p}_e \cdot \nabla_t] G_m'' \quad , \quad (3.6)$$

and

$$\pi_m' = \frac{1}{j\omega\epsilon_m} \frac{1}{j\omega\epsilon_0} \left[[-\bar{p}_e \cdot \frac{\partial}{\partial z'} \nabla_t] G_m' - p_{ez} \nabla^2 G_m' \right] \quad , \quad (3.7)$$

where

$$G_m'' = \frac{1}{4\pi^2} \iint_{-\infty}^{\infty} \frac{g_m''(\kappa, z, z')}{k_t^2} e^{-j(k_x(x-x') + k_y(y-y'))} dk_x dk_y \quad , \quad (3.8)$$

and

$$G_m' = \frac{1}{4\pi^2} \iint_{-\infty}^{\infty} \frac{g_m'(\kappa, z, z')}{k_t^2} e^{-j(k_x(x-x') + k_y(y-y'))} dk_x dk_y \quad . \quad (3.9)$$

After some manipulation the dyadic Green's function in component form, i.e., in terms of its associated electromagnetic fields can be written as

$$\begin{aligned} E_{mx} = & \left\{ p_{ex} \left[\nabla_t^2 G_m'' - \frac{\partial^2}{\partial x^2} \left(G_m'' + \frac{1}{j\omega\epsilon_m} \frac{1}{j\omega\epsilon_0} \frac{\partial^2}{\partial z \partial z'} G_m' \right) \right] \right. \\ & + p_{ey} \left[-\frac{\partial}{\partial x} \frac{\partial}{\partial y} \left(G_m'' + \frac{1}{j\omega\epsilon_m} \frac{1}{j\omega\epsilon_0} \frac{\partial^2}{\partial z \partial z'} G_m' \right) \right] \\ & \left. + p_{ez} \left[\frac{1}{j\omega\epsilon_m} \frac{1}{j\omega\epsilon_0} \frac{\partial^2}{\partial x \partial z} \left(-\nabla_t^2 G_m' \right) \right] \right\} \quad , \quad (3.10) \end{aligned}$$

$$\begin{aligned}
E_{my} = \{ & p_{ex} \left[-\frac{\partial^2}{\partial x \partial y} \left(G_m'' + \frac{1}{j\omega\epsilon_m} \frac{1}{j\omega\epsilon_0} \frac{\partial^2}{\partial z \partial z'} G_m' \right) \right] \\
& + p_{ey} \left[\nabla_t^2 G_m'' - \frac{\partial^2}{\partial y^2} \left(G_m'' + \frac{1}{j\omega\epsilon_m} \frac{1}{j\omega\epsilon_0} \frac{\partial^2}{\partial z \partial z'} G_m' \right) \right] \\
& + p_{ez} \left[\frac{1}{j\omega\epsilon_m} \frac{1}{j\omega\epsilon_0} \frac{\partial^2}{\partial y \partial z} (-\nabla_t^2 G_m') \right] \} , \quad (3.11)
\end{aligned}$$

and

$$\begin{aligned}
E_{mz} = \{ & \frac{1}{j\omega\epsilon_m} \frac{1}{j\omega\epsilon_0} \left[p_{ex} \frac{-\partial^2}{\partial x \partial z'} (-\nabla_t^2 G_m') + p_{ey} \frac{-\partial^2}{\partial y \partial z'} (-\nabla_t^2 G_m') + p_{ez} \nabla_t^2 (\nabla_t^2 G_m') \right] \\
& - \frac{p_{ez}}{j\omega\epsilon_0} \delta(\vec{r}-\vec{r}') \} , \quad (3.12)
\end{aligned}$$

where use has been made of $(\nabla_t^2 = \frac{\partial^2}{\partial x^2} + \frac{\partial^2}{\partial y^2})$. The above PWS representation of the fields will be next transformed into the Sommerfeld representation as follows [42].

Consider the function I (a double Fourier integral) which essentially constitutes a typical PWS integral:

$$I = \iint_{-\infty}^{\infty} F(k_t) e^{-j(k_x(x-x') + k_y(y-y'))} dk_x dk_y , \quad (3.13)$$

The above integral has a Fourier-Bessel representation given by

$$I = 2\pi \sum_{n=-\infty}^{\infty} e^{-jn(\phi-\phi')} \int_0^{\infty} F(\xi) J_n(\xi\rho) J_n(\xi\rho') \xi d\xi , \quad (3.14)$$

which can be obtained from (3.13) by employing the following transformations:

$$k_t = \xi \quad ; \quad k_x = \xi \cos \alpha \quad ; \quad k_y = \xi \sin \alpha \quad , \quad (3.15)$$

and

$$(x-x') = \rho \cos \phi - \rho' \cos \phi' \quad ; \quad y-y' = \rho \sin \phi - \rho' \sin \phi' \quad (3.16)$$

If the coordinate system is chosen so that $\rho'=0$, then the expression (3.14) reduces (in view of $J_0(0)=1$, $J_m(0)=0$; $m \neq 0$) to

$$I = 2\pi \int_0^\infty F(\xi) J_0(\xi \rho) \xi d\xi \quad . \quad (3.17)$$

The expression in (3.17) is the Sommerfeld type integral representation of the Function I which was given in terms of its PWS representation in (3.13) (see Appendix C; Equation (C.1) -(C.12)). Now with this introduction, the Sommerfeld representation of G_m'' and G_m' given in (3.8) and (3.9) are likewise given by:

$$G_m'' = \frac{1}{2\pi} \int_0^\infty \frac{g_m''(\kappa, z, z')}{\xi} J_0(\xi \rho) d\xi \quad , \quad (3.18)$$

and

$$G_m' = \frac{1}{2\pi} \int_0^\infty \frac{g_m'(\kappa, z, z')}{\xi} J_0(\xi \rho) d\xi \quad , \quad (3.19)$$

where

$$\rho = \sqrt{(x-x')^2 + (y-y')^2} \quad . \quad (3.20)$$

It is noted that

$$\frac{\partial}{\partial x} \leftrightarrow \cos \phi \frac{\partial}{\partial \rho} - \frac{1}{\rho} \sin \phi \frac{\partial}{\partial \phi} \quad ; \quad \frac{\partial}{\partial y} \leftrightarrow \sin \phi \frac{\partial}{\partial \rho} + \frac{1}{\rho} \cos \phi \frac{\partial}{\partial \phi} \quad , \quad (3.21a)$$

and

$$\phi = \tan^{-1} \left(\frac{y-y'}{x-x'} \right) . \quad (3.21b)$$

Recall that the g_m'' and g_m' in (3.18) and (3.19) have $m=0$ and 1 are given in (2.77), (2.78), (2.83) and (2.84) with k_t replaced by ξ in (2.82) via (3.15) so that

$$k_{0z} = \kappa_0 = \sqrt{k_0^2 - \xi^2} \quad ; \quad k_{1z} = \kappa_0 = \sqrt{k_1^2 - \xi^2} . \quad (3.22)$$

The integrands of the (3.18) and (3.19) exhibit a spurious pole at $\xi=0$. This leads to an integral with a logarithmic singularity and it is a consequence of interchanging the derivative and integration operations. Strictly speaking, this interchange is not allowed (because of the convergence difficulty as $\xi \rightarrow 0$). However the expressions in (3.10) and (3.11) as a whole converge, which means that the integrand of

$$\left(G_m'' + \frac{1}{j\omega\epsilon_m} \frac{1}{j\omega\epsilon_0} \frac{\partial^2}{\partial z \partial z'} G_m' \right) \quad (3.23)$$

is regular at $\xi=0$. This can be shown by explicit substitution of g_m'' and g_m' and taking the limit of the integrand of the above expression as $\xi \rightarrow 0$. So in a distributional sense an interchange of the operators is justified. The expression of $\nabla_t^2 G_m''$, $\nabla_t^2 G_m'$ and $\nabla_t^2 (\nabla_t^2 G_m')$ are,

$$\nabla_t^2 G_m'' = \frac{-1}{2\pi} \int_0^\infty g_m''(\kappa, z, z') J_0(\xi \rho) \xi d\xi , \quad (3.24)$$

$$\nabla_t^2 G_m' = \frac{-1}{2\pi} \int_0^\infty g_m'(\kappa, z, z') J_0(\xi \rho) \xi d\xi , \quad (3.25)$$

and

$$\nabla_t^2 (\nabla_t^2 G_m') = \frac{1}{2\pi} \int_0^\infty g_m'(\kappa_m, z, z') J_0(\xi \rho) \xi^3 d\xi \quad (3.26)$$

Equations (3.10) through (3.12) essentially provide the dyadic Green's function in component form for the single layer geometries in terms of the conventional Sommerfeld representation for G_m'' , G_m' , $\nabla_t^2 G_m''$, $\nabla_t^2 G_m'$ and $\nabla_t^2 (\nabla_t^2 G_m')$ which are given explicitly in (3.18) through (3.26). From (2.77) and (2.83), together with (3.22) it is clear that if

$$\xi^2 < k_0^2 \quad ; \quad \xi^2 < k_1^2 \quad (3.27)$$

then g_m'' and g_m' exhibit waves traveling in the $\pm \hat{z}$ directions with

$$\kappa_0 = \sqrt{k_0^2 - \xi^2} \quad ; \quad \kappa_1 = \sqrt{k_1^2 - \xi^2} \quad (3.28)$$

On the other hand, if in those equations the following is true:

$$\xi^2 > k_0^2 \quad ; \quad \xi^2 > k_1^2 \quad (3.29)$$

then g_m'' , g_m' exhibit evanescent waves in $\pm \hat{z}$ directions, with

$$\kappa_0 = -j \sqrt{k_0^2 - \xi^2} \quad ; \quad \kappa_1 = -j \sqrt{k_1^2 - \xi^2} \quad (3.30)$$

in which the negative branch of the square root has been properly chosen in (3.30) to be consistent with the radiation condition as $z \rightarrow \pm \infty$. As κ_0 and κ_1 in (3.30) are imaginary, the expressions for g_m'' and g_m' decay very fast as $\xi \rightarrow \infty$ for the cases when the source and field points are displaced vertically; i.e., when $|z - z'|$ is non zero. However, in the situation when the source and field points are both on the interface, or they are laterally separated, then as $\xi \rightarrow \infty$, g_m'' and g_m' decay very slowly if $|z - z'|$ is small.

It is recalled that the microstrip dyadic Green's functions $\bar{\bar{G}}^m$ can be obtained from the electric field \bar{E}^m via (2.4); in matrix form, (2.4) becomes

$$\begin{bmatrix} E_{mx} \\ E_{my} \\ E_{mz} \end{bmatrix} = -j\omega\mu_0 \begin{bmatrix} G_{xx}^m & G_{xy}^m & G_{xz}^m \\ G_{yx}^m & G_{yy}^m & G_{yz}^m \\ G_{zx}^m & G_{zy}^m & G_{zz}^m \end{bmatrix} \begin{bmatrix} P_{ex} \\ P_{ey} \\ 0 \end{bmatrix} \quad (3.31)$$

with \bar{P}_e given by

$$\bar{P}_e = P_{ex} \hat{x} + P_{ey} \hat{y} \quad .$$

The elements of the matrix for \bar{E}_m in (3.31) above can be found explicitly from (3.10)-(3.12) and consequently the elements of the matrix for $\bar{\bar{G}}^m$ can then be found from those equations by inspection via (3.31). For example, in the region $m=0$, one identifies

$$-j\omega\mu_0 G_{xx}^0(\bar{r},0) = \frac{-1}{2\pi\omega\epsilon_0} \left\{ k_0^2 U + \frac{\partial^2}{\partial x^2} \left(U - \frac{\epsilon_r^{-1}}{\epsilon_r} W \right) \right\} \quad , \quad (3.32)$$

$$-j\omega\mu_0 G_{yx}^0(\bar{r},0) = \frac{-1}{2\pi\omega\epsilon_0} \left\{ \frac{\partial^2}{\partial x \partial y} \left(U - \frac{\epsilon_r^{-1}}{\epsilon_r} W \right) \right\} \quad , \quad (3.33)$$

$$-j\omega\mu_0 G_{zx}^0(\bar{r},0) = \frac{1}{2\pi\omega\epsilon_0} \left\{ \frac{\partial}{\partial x} (V) \right\} \quad , \quad (3.34)$$

$$-j\omega\mu_0 G_{xy}^0(\bar{r},0) = -j\omega\mu_0 G_{yx}^0(\bar{r},0) \quad (3.35)$$

$$-j\omega\mu_0 G_{yy}^0(\vec{r},0) = \frac{-1}{2\pi\omega\epsilon_0} \left\{ k_0^2 U + \frac{\partial^2}{\partial y^2} \left(U - \frac{\epsilon_r^{-1}}{\epsilon_r} W \right) \right\} , \quad (3.36)$$

and

$$-j\omega\mu_0 G_{zy}^0(\vec{r},0) = \frac{1}{2\pi\omega\epsilon_0} \left\{ \frac{\partial}{\partial y} (V) \right\} , \quad (3.37)$$

where

$$U = \int_0^\infty \frac{J_0(\xi\rho)\xi e^{-j\sqrt{k_0^2-\xi^2}\delta}}{\sqrt{k_0^2-\xi^2} - j\sqrt{\epsilon_r k_0^2-\xi^2} \cot \text{and} \sqrt{\epsilon_r k_0^2-\xi^2}} d\xi , \quad (3.38)$$

$$V = \int_0^\infty \frac{\frac{j\sqrt{\epsilon_r k_0^2-\xi^2}}{\epsilon_r} \text{tand} \sqrt{\epsilon_r k_0^2-\xi^2} J_0(\xi\rho)\xi e^{-j\sqrt{k_0^2-\xi^2}\delta}}{\sqrt{k_0^2-\xi^2} + \frac{j\sqrt{\epsilon_r k_0^2-\xi^2}}{\epsilon_r} \text{tand} \sqrt{\epsilon_r k_0^2-\xi^2}} d\xi , \quad (3.39)$$

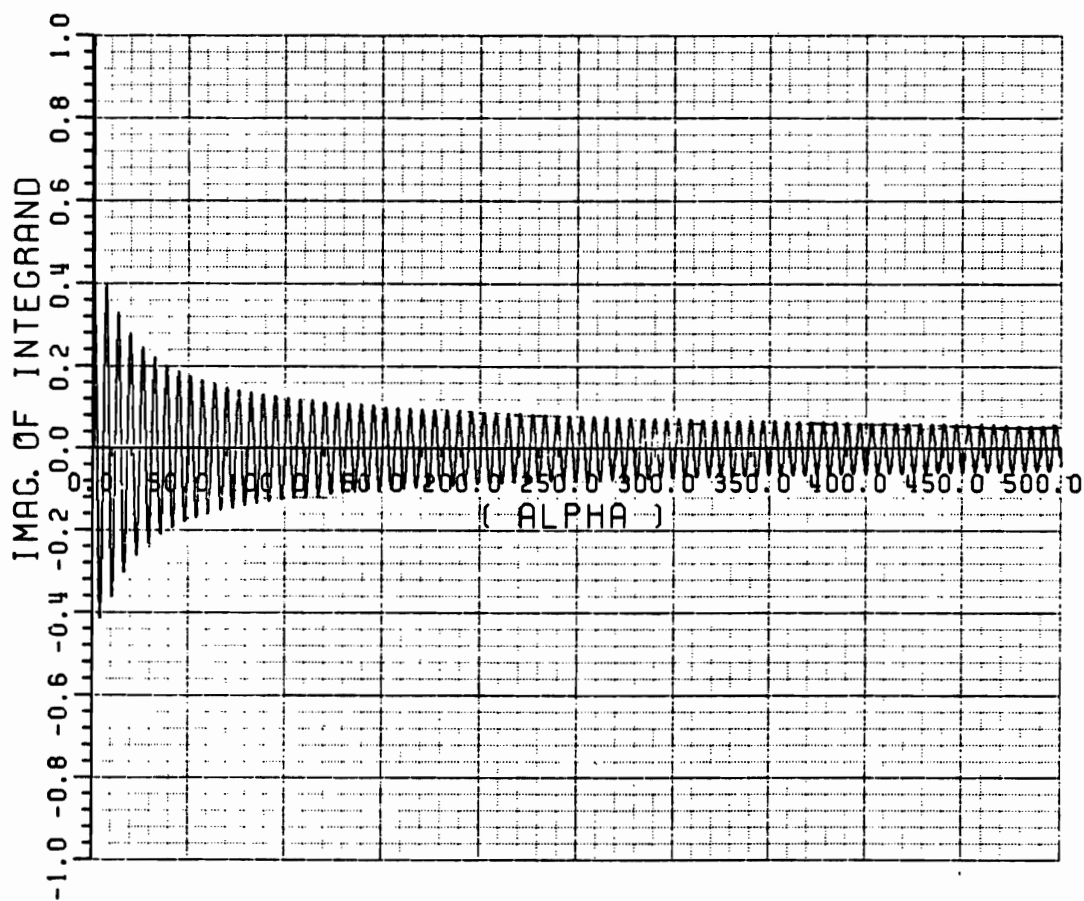
and

$$W = \int_0^\infty \frac{\sqrt{k_0^2-\xi^2} J_0(\xi\rho)\xi e^{-j\sqrt{k_0^2-\xi^2}\delta}}{(\sqrt{k_0^2-\xi^2} - j\sqrt{\epsilon_r k_0^2-\xi^2} \cot \text{and} \sqrt{\epsilon_r k_0^2-\xi^2}) (\sqrt{k_0^2-\xi^2} + \frac{j\sqrt{\epsilon_r k_0^2-\xi^2}}{\epsilon_r} \text{tan}(\text{d} \sqrt{\epsilon_r k_0^2-\xi^2}))} , \quad (3.40)$$

Also, $\delta=z$ (vertical separation between the source and observation points). The regularity of U , V and W at $\xi=0$ is to be noted, (see also Equation (3.23)).

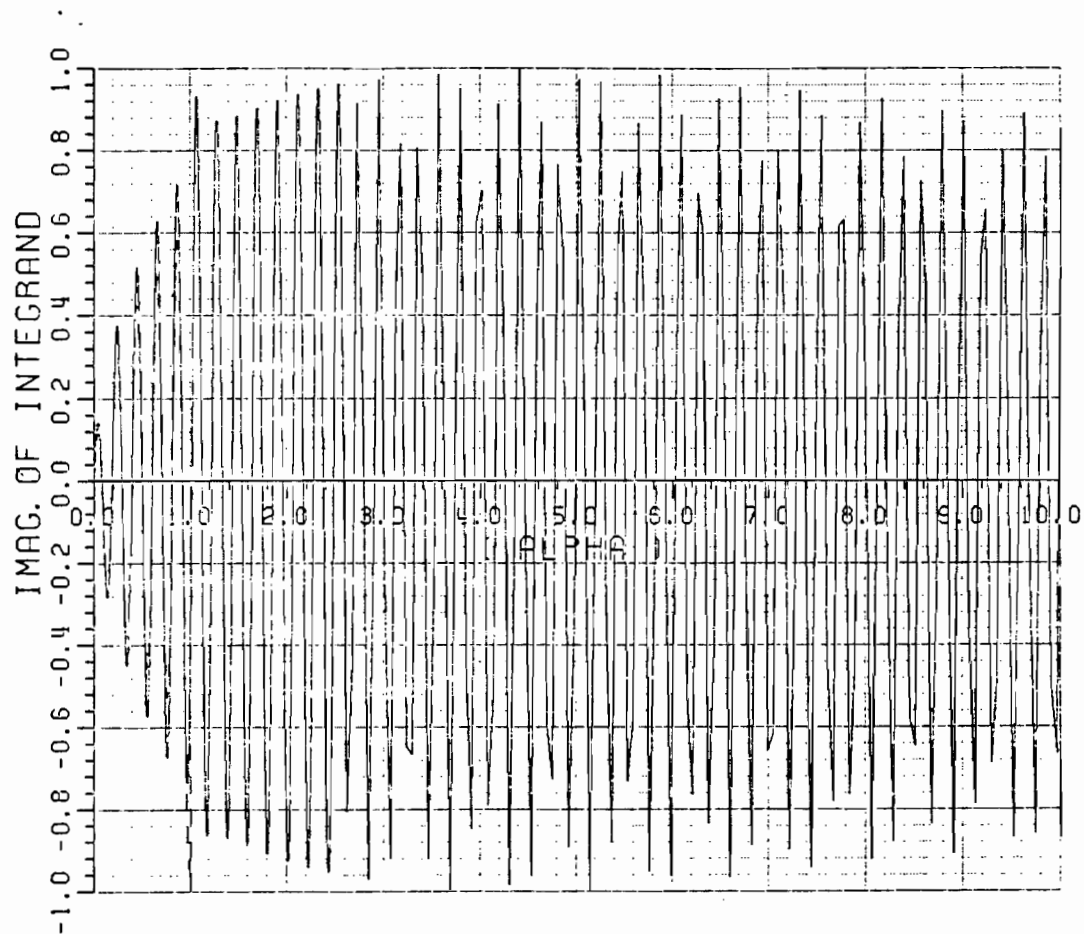
The convergence behavior of these functions depends strongly upon the value of δ (vertical separation between the source and observation points). For almost all of the planar structures, such as microstrip arrays, $\delta \rightarrow 0$ in the MM solution for the currents as the microstrip patches, and the factor which exhibits an exponential decay goes to unity. Thus, as $\xi \rightarrow \infty$, the Sommerfeld type integrands decay algebraically as $\sim \frac{1}{\sqrt{\xi\rho}}$ rather than exponentially; the algebraic decay results from the asymptotic behavior of $J_0(\xi\rho)$ for large $\xi\rho$. Figure 3.1(a) shows the typical behavior of the integrand of the function U , for $k_0\rho=1$ versus $\alpha=\frac{\xi}{k_0}$ as $\delta \rightarrow 0$. The integrand is an oscillatory function (typical behavior of the Bessel function), and decays very slowly. As $k_0\rho$ becomes larger (the lateral separation between the source and field point increases), the integrand oscillates more rapidly (see Figure 3.1(b)).

It is a well known fact that the numerical integration of oscillatory functions are very time consuming, particularly when they have an end point at infinity. To overcome this difficulty, which is inherent in any open structure involving multilayered media, four distinct methods have been proposed. The first method which is referred to as the envelope extraction or singularity removal technique is very efficient when the lateral separation ($k_0\rho$) is small (i.e., if $k_0\rho < 1$). It deals with asymptotic behavior of the integrands, which in turn is dictated by the behavior of $J_0(\xi\rho)$. These asymptotic values can be integrated in closed form; therefore, if one subtracts these asymptotic values from the integrands, then the resulting integrands are relatively smooth and fast decaying so that they can be integrated efficiently. Only this latter method is discussed below;



(a) $k_0\rho = 1.0$

Figure 3.1. Imaginary part of the integrand of Sommerfeld type integral of Equation (3.38), versus its normalized argument, ($k_0\rho=1$).



(b) $k_0\rho=30$

Figure 3.1. (continued)

the other three methods are discussed in detail in the next two chapters which present more efficient alternative representations for the microstrip Green's function.

The Envelope Extraction Technique [1] which improves the convergence of the conventional Sommerfeld integral representation is described as follows.

Consider again (3.32) through (3.37). Let I be a typical value of U , W , or V , which in general has the form

$$I = \int_0^{\infty} F(\xi) J_0(\rho\xi) d\xi \quad (3.41)$$

where $F(\xi)$ is recognizable from (3.38) through (3.40). As $\xi \rightarrow \infty$, the value of $F(\xi)$ asymptotically approaches some complex value, say " $C e^{-\xi\delta}$ ".

But

$$\int_0^{\infty} J_0(\rho\xi) e^{-\xi\delta} d\xi = \frac{1}{\sqrt{(\rho^2 + \delta^2)}} \quad (3.42)$$

Therefore, one can write (3.41) via (3.42) as

$$I = \int_0^{\infty} (F(\xi) - C e^{-\xi\delta}) J_0(\rho\xi) d\xi + \frac{C}{\sqrt{(\rho^2 + \delta^2)}} \quad (3.43)$$

Mathematically, Equations (3.41) and (3.43) are equivalent; numerically however, the integral of (3.43) possesses a much smoother function. Therefore an eight or sixteen point Gaussian integration routine is sufficient to achieve a reasonable accuracy in evaluating such an integral. Figure 3.2 shows a typical behavior of an appropriately

normalized $F(\xi)$ corresponding to $U(k_0\rho)$ as a function $\alpha = \frac{\xi}{k_0}$.

Referring to Equation (3.38), one identifies $F(\xi)$ corresponding to the $U(k_0\rho)$ in that equation as:

$$F(\xi) = \frac{\xi e^{-j\sqrt{k_0^2 - \xi^2} \delta}}{\sqrt{k_0^2 - \xi^2} - j\sqrt{\epsilon_r k_0^2 - \xi^2} \cot \alpha \sqrt{\epsilon_r k_0^2 - \xi^2}} \quad (3.44)$$

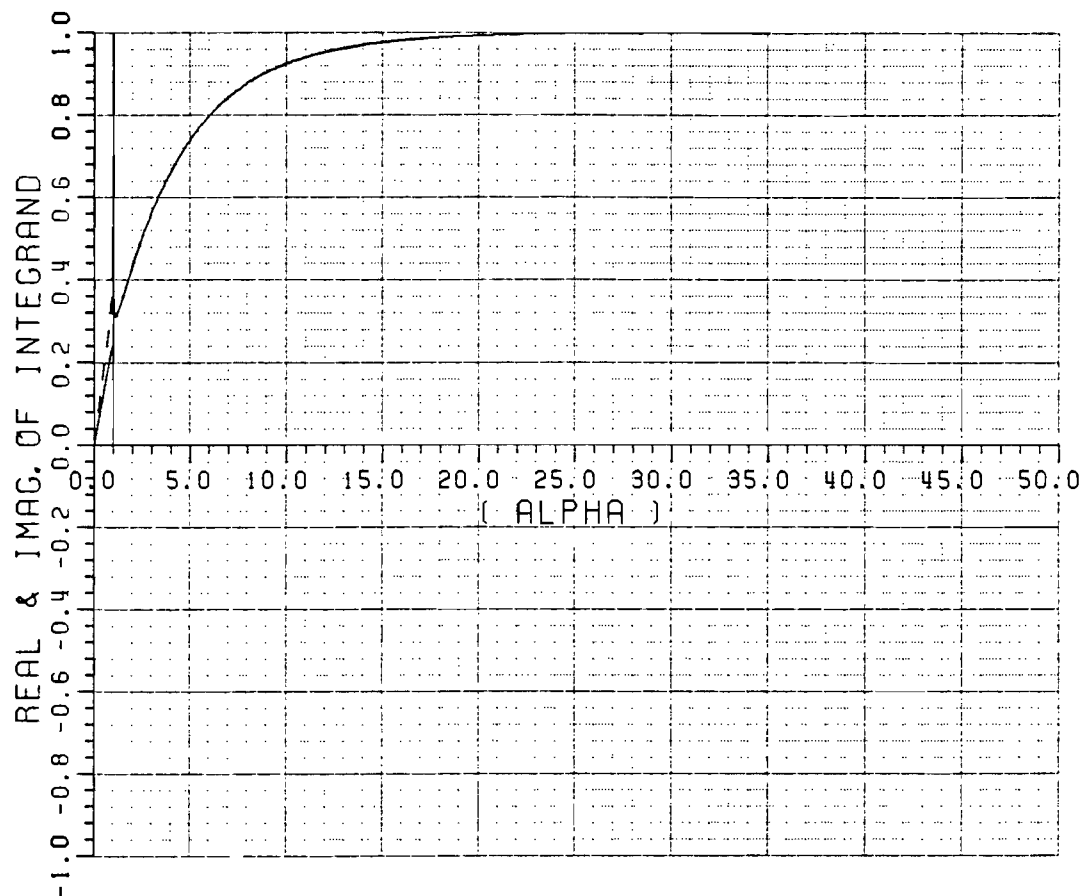
Next, one notes from (3.39) that

$$\lim_{\xi \rightarrow \infty} F(\xi) = C e^{-\xi \delta} = j(0.5) e^{-\xi \delta} \quad (3.45)$$

So, one can write U of (3.38) via (3.43) and (3.45) as

$$U = \int_0^\infty (F(\xi) - j(0.5)e^{-\xi \delta}) J_0(\rho \xi) d\xi + \frac{jk_0 0.5}{\sqrt{k_0^2(\rho^2 + \delta^2)}} \quad (3.46)$$

Figures 3.3(a) through 3.3(c), show the numerical behavior of the integrand of the above equation for $k_0\rho=0.2, 0.5$ and 1.0 , respectively as a function of $\alpha=\frac{\xi}{k_0}$. The significance of this "envelope removal" is more vivid if one compares the smoothness of the plots in Figures 3.3(c) and 3.1(a), for the case of $k_0\rho = 1.0$.



$$\lim_{\xi \rightarrow \infty} F(\xi) = C e^{-\xi \delta}$$

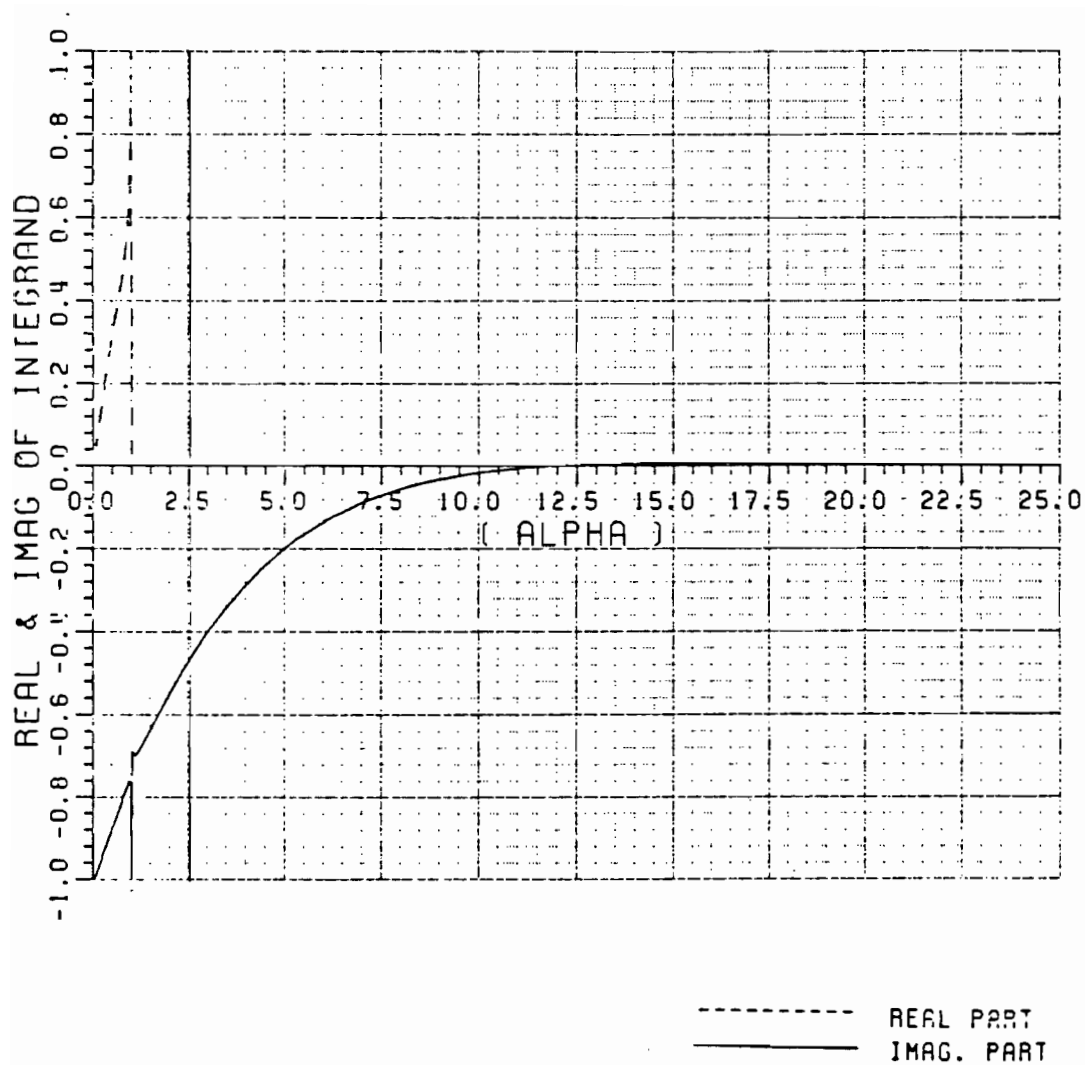
$$\xi \rightarrow \infty$$

---- Real Part

—— Imag. Part

$$C \int_0^{\infty} J_0(\rho \xi) e^{-\xi \delta} d\xi = C \frac{k_0}{k_0 \sqrt{\rho^2 + \delta^2}}$$

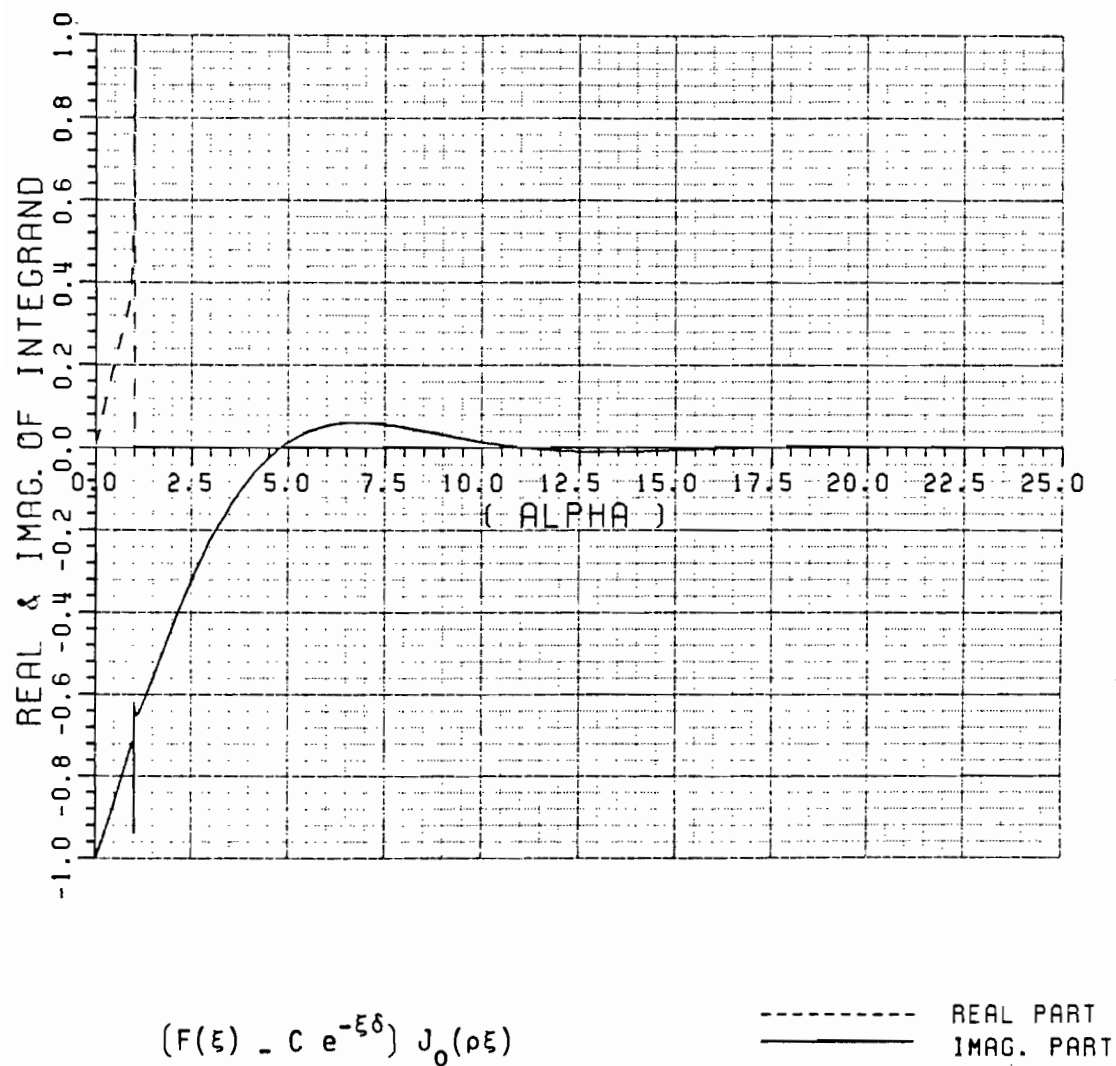
Figure 3.2. Normalized behavior of $F(\xi)$ as a function $\alpha = \frac{\xi}{k_0}$



$$(F(\xi) - C e^{-\xi\delta}) J_0(\rho\xi)$$

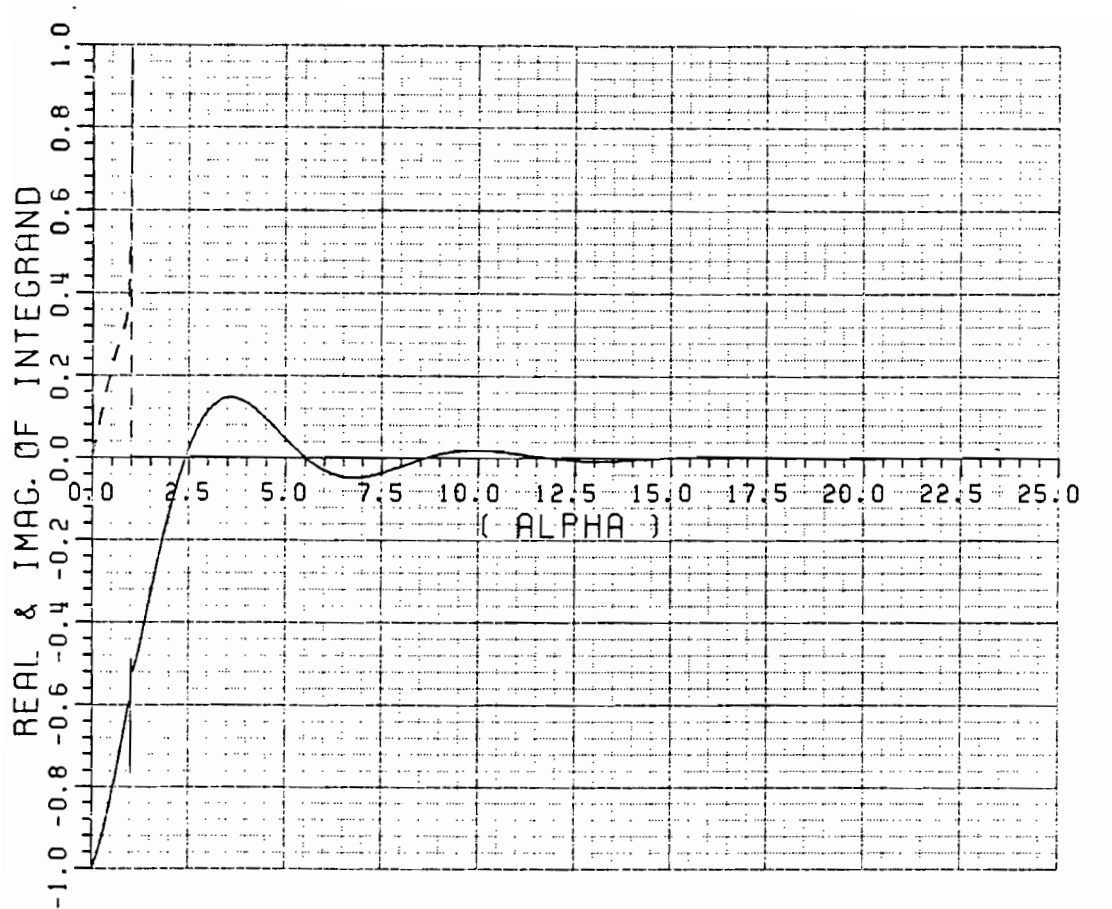
(a) Typical behavior of the integrand of the Equation (3.46) for $k_0\rho=0.2$.

Figure 3.3. Behavior of $[(F(\xi)-C e^{-\xi\delta}) J_0(\rho\xi)]$ versus $\frac{\xi}{k_0}$ with a $k_0\rho$ as a parameter.



(b) Typical behavior of the integrand
 of the Equation (3.46) for $k_0\rho=0.5$.

Figure 3.3. (continued)



$$(F(\xi) - C e^{-\xi\delta}) J_0(\rho\xi)$$

----- REAL PART
 ————— IMAG. PART

(c) Typical behavior of the integrand
 of the Equation (3.46) for $k_0\rho=1.0$.

Figure 3.3. (continued)

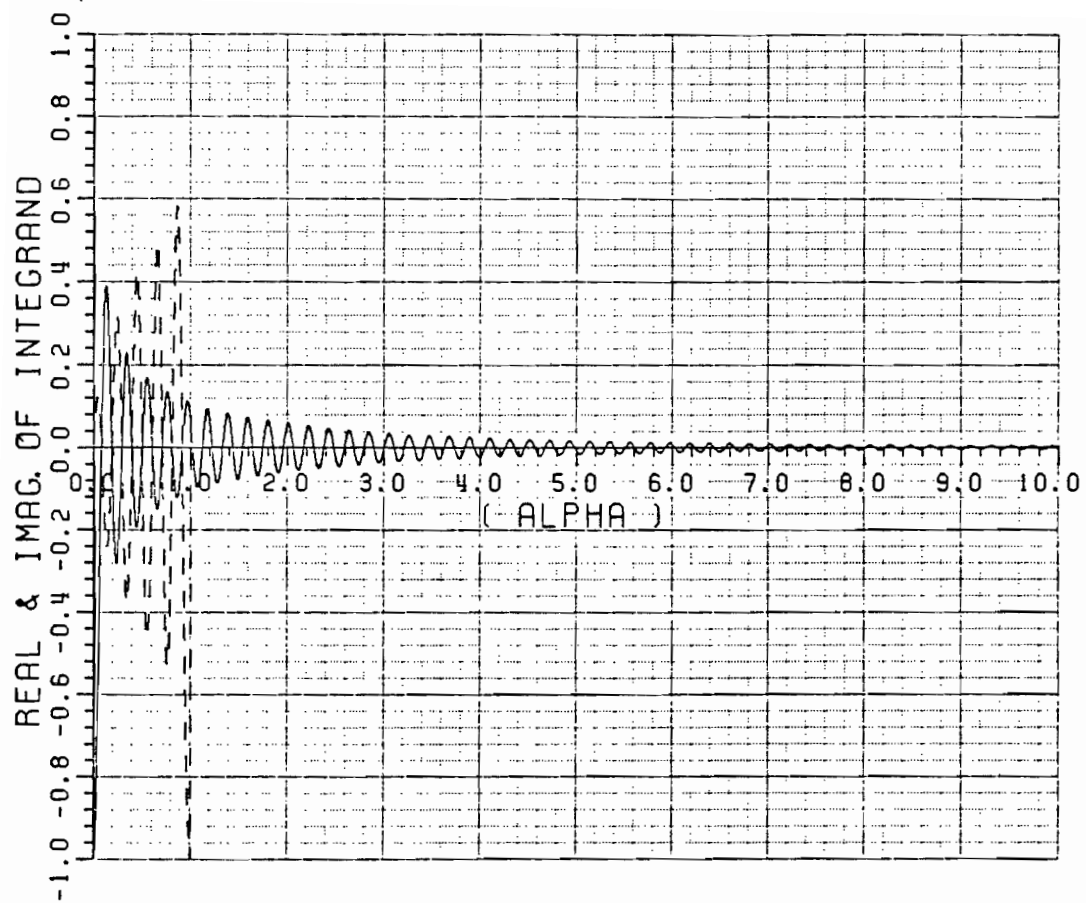
The integrands occurring in V and W can be treated similarly; thus,

$$V = \int_0^\infty \left[\frac{\frac{j\sqrt{\epsilon_r k_0^2 - \xi^2}}{\epsilon_r} \tanh \sqrt{\epsilon_r k_0^2 - \xi^2} e^{-j\sqrt{k_0^2 - \xi^2} \delta}}{\sqrt{k_0^2 - \xi^2} + \frac{j\sqrt{\epsilon_r k_0^2 - \xi^2}}{\epsilon_r} \tanh \sqrt{\epsilon_r k_0^2 - \xi^2}} + \left(\frac{e^{-\xi \delta}}{\epsilon_r + 1} \right) \right] J_0(\xi \rho) \xi d\xi - \left(\frac{1}{\epsilon_r + 1} \right) \frac{-d}{d\delta} \left[\frac{k_0}{\sqrt{k_0^2 (\rho^2 + \delta^2)}} \right] \quad (3.47)$$

and

$$W = \int_0^\infty \left[\frac{\sqrt{k_0^2 - \xi^2} \xi e^{-j\sqrt{k_0^2 - \xi^2} \delta}}{(\sqrt{k_0^2 - \xi^2} - j\sqrt{\epsilon_r k_0^2 - \xi^2} \coth \sqrt{\epsilon_r k_0^2 - \xi^2}) \left(\sqrt{k_0^2 - \xi^2} + \frac{j\sqrt{\epsilon_r k_0^2 - \xi^2}}{\epsilon_r} \tanh \sqrt{\epsilon_r k_0^2 - \xi^2} \right)} - \frac{j}{2} \left(\frac{\epsilon_r e^{-\xi \delta}}{\epsilon_r + 1} \right) \right] J_0(\xi \rho) d\xi + \frac{j}{2} \left(\frac{\epsilon_r}{\epsilon_r + 1} \right) \frac{k_0}{\sqrt{k_0^2 (\rho^2 + \delta^2)}} \quad (3.48)$$

It is now evident that (for the small lateral separation) this method "envelope removal technique", can efficiently be utilized to evaluate the dyadic Green's function. Nevertheless as the lateral separation of the source and observation points increases ($k_0 \rho$ becomes large) the integrand starts to oscillate. Figure 3.4 shows the typical behavior of the integrand of (3.46) for $k_0 \rho = 30$. This oscillation is due to the rapid growth of the argument of the Bessel function which causes the



$$(F(\xi) - C e^{-\xi\delta}) J_0(\rho\xi)$$

----- REAL PART
 _____ IMAG. PART

Figure 3.4. The behavior of the integrand of the Equation (3.46) for $(k_0\rho=30)$.

method to lose its efficiency. This is the main difficulty of envelope extraction which motivates us to construct the alternative ρ -propagation representation of the microstrip dyadic surface Green's function in the next chapter. Before we discuss this alternative, it is important to note that the denominator of the Sommerfeld integrands in (3.46) through (3.48) contain some pole singularities in the interval $k_0 \leq \xi \leq k_1$. The significance of these singularities will be discussed in the next chapter. In the lossless case these singularities are on the real axis along the path of integration; therefore, in order to efficiently perform the numerical integration one should remove these singularities by the following means. Let

$$I = \int_0^{\infty} F(\xi) d\xi \quad , \quad (3.49)$$

where $F(\xi)$ has a first order pole at ξ_0 with $\xi_1 < \xi_0 < \xi_2$. Then one can write

$$I = \int_0^{\xi_1} F(\xi) d\xi + \int_{\xi_1}^{\xi_2} \left[F(\xi) - \frac{\text{Res}(\xi_0)}{\xi - \xi_0} \right] d\xi + \text{Res}(\xi_0) \int_{\xi_1}^{\xi_2} \frac{d\xi}{\xi - \xi_0} + \int_{\xi_2}^{\infty} F(\xi) d\xi \quad (3.50)$$

where $\text{Res}(\xi_0)$ is the residue of the pole ξ_0 ; i.e.,

$$\text{Res}(\xi_0) = \lim_{\xi \rightarrow \xi_0} F(\xi)(\xi - \xi_0) \quad (3.51)$$

Finally,

$$I = \int_0^{\xi_1} F(\xi) d\xi + \int_{\xi_2}^{\infty} F(\xi) d\xi + \int_{\xi_1}^{\xi_2} \left(F(\xi) - \frac{\text{Res}(\xi_0)}{\xi - \xi_0} \right) d\xi + \text{Res}(\xi_0) \ln \left(\frac{\xi_2 - \xi_0}{\xi_0 - \xi_1} \right) \quad (3.52)$$

where all integrands are smooth and suitable for numerical integration.

Finally it is noted that the complete expressions for all the components of the Sommerfeld integral representation of the microstrip dyadic Green's function in which the spatial derivatives within the integrands have been explicitly evaluated are developed in detail in Appendix C (see (C.26) -(C.28)), for the sake of completeness.

CHAPTER IV

EFFICIENT ALTERNATIVE RADially PROPAGATING AND STEEPEST DESCENT PATH INTEGRAL REPRESENTATION FOR THE SINGLE LAYER MICROSTRIP DYADIC SURFACE GREEN'S FUNCTION

This chapter deals with the function theoretic manipulations for transforming the conventional Sommerfeld (z-propagation) representation into an alternative ρ -propagation and steepest descent path forms of the microstrip dyadic surface Green's function given in (3.10) -(3.12) and (3.32) -(3.37). The ρ -propagation representation for the microstrip surface Green's function overcomes the difficulty associated with the first method (envelope removal technique) which was discussed in the previous chapter. The alternative ρ -propagation representation of the microstrip dyadic surface Green's function converges very fast if the source and observation points are separated laterally (rather than vertically), i.e., when $k_0\rho$ is non-zero even if ($|z-z'|=\delta\rightarrow 0$). This technique also leads to the extremely efficient uniform asymptotic closed form representation for the microstrip dyadic surface Green's function developed in Chapter V.

Also discussed in this chapter is the deformation of the original path of integration for the ρ -propagation representation into the steepest descent path (SDP) on which the integrands decay most rapidly; this latter SDP representation is most efficient for large as well as

moderately large to even relatively small lateral separation between source and field points. On the other hand, the original ρ -propagation representation works best for relatively small to moderately large separation between the source and field point; for larger lateral separation; this representation eventually exhibits an oscillatory integrand which limits its usefulness and it then becomes necessary to use the SDP representation instead. The radially propagating representation and its SDP form are developed below in parts A and B, respectively.

A. Radially ($\hat{\rho}$) Propagating Representation for the Microstrip Green's Function

The starting point in the derivation of the radially propagating microstrip Green's function are Equations (3.18), (3.19), which constitute the Sommerfeld representation of G_m'' and G_m' . In particular, one may write G_m'' and G_m' in general as

$$G_m = \frac{1}{2\pi} \int_0^\infty \frac{g_m(\kappa, z, z')}{\xi} J_0(\xi \rho) d\xi, \quad (4.1)$$

where the prime (') and double prime (") symbols have been omitted for convenience. The above integral can be written in terms of the Hankel function where the integral has the lower limit as $\infty e^{-j\pi}$, and the upper limit as ∞ , provided that g_m is an even function of ξ [42]. Thus, (4.1) becomes

$$G_m = \frac{1}{4\pi} \int_{\infty e^{-j\pi}}^{\infty} \frac{g_m(\kappa, z, z')}{\xi} H_0^{(2)}(\xi \rho) d\xi, \quad (4.2)$$

in which the contour of integration is such that the branch point at $\xi=0$ introduced by the transformation and also a spurious pole at $\xi=0$ is avoided as in Figure 4.1.

An alternative ρ propagating representation of the microstrip Green's function can be derived by deforming the integration contour of the type in (4.2) so that it encloses all the singularities of the z -dependent characteristic Green's function g_m in the integrand. It is easy to show that $\nabla_t^2 G_m$ and $\nabla_t^2 G_m$ satisfy the three dimensional Green's function differential Equation; therefore, alternative representations

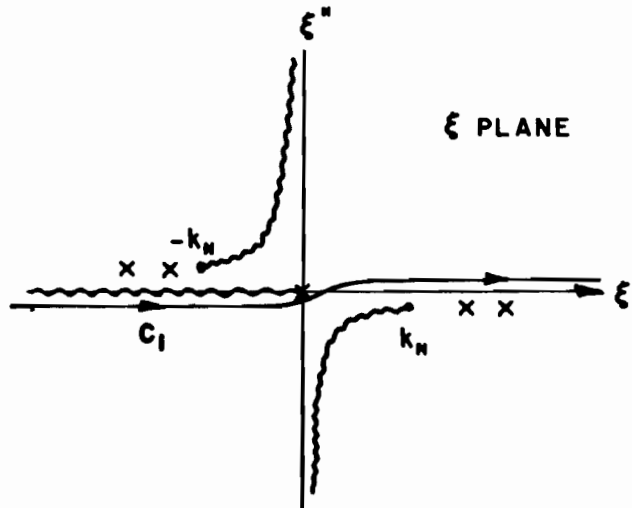


Figure 4.1. The analytic properties of $g_m(\kappa, z, z')$ in complex ξ plane, surface wave poles, branch cuts, C_1 is the path of integration of (4.2).

of G_m'' and G_m' follow directly from the characteristic Green's functions pertaining to $\nabla_t^2 G_m''$ and $\nabla_t^2 G_m'$ [42]. This is due to the fact that the functional dependence of G_m and $\nabla_t^2 G_m$ are the same except for the factor $(\xi)^{-2}$, (see the Equations (3.18), (3.19), (3.24) and (3.25)). The prime (') and double prime (") have been omitted here for convenience.

In order to enclose all the singularities of $g_m(\kappa, z, z')$ in the ξ plane, the analytic property of $g_m(\kappa, z, z')$ ought to be studied. The explicit expressions for g_m'' and g_m' in the single layer microstrip geometry (grounded dielectric slab) have been given in (2.71), (2.72), (2.77) and (2.78). The g_m'' and g_m' are functions of the propagation constants $\kappa_n = \sqrt{k_n^2 - \xi^2}$; $n=0,1$. In the complex ξ plane they have a pair of branch points at $\xi = \pm k_0$ and a pair of branch cuts from $\xi = \pm k_0$ to infinity. These branch cuts must be defined in such a way that $\text{Im}(\sqrt{k_0^2 - \xi^2}) < 0$ on the entire top sheet. This is the only pair of branch cuts that allow the analytic continuation of g_m'' and g_m' into the entire top sheet of ξ such that they satisfy the radiation condition (see (D.13) and (D.14) in Appendix D). Therefore, the deformation of the real axis path of integration into the complex plane is possible as long as it stays on the top Riemann sheet as $|\xi| \rightarrow \infty$; of course, one must account for residues associated with any poles in the integrals (g_m'' and g_m') which are enclosed in this contour deformation. As mentioned previously, Figure 4.1 shows a typical complex ξ plane in which the branch cuts due to the Hankel function and g_m in the integrand of (4.2) and the path of integration from $\infty e^{-j\pi}$ to ∞ have been depicted. In general there also exists a finite number of pole singularities in the

top Riemann sheet called surface wave poles (whose residues are modal waves because they satisfy the radiation condition at infinity), and an infinite number of singularities in the bottom Riemann sheet called leaky wave poles (giving rise to non modal waves since they do not satisfy the radiation condition at infinity). A finite number of surface wave poles have also been depicted in Figure 4.1.

One may refer to Equation (4.2) for the Sommerfeld integral representation over infinite rather than semi-infinite limits of integration; thus, the ρ -propagation representation for G_m can be derived by enclosing all the singularities of g_m in the ξ plane via contour deformation. The original contour is thus deformed as shown in Figure 4.2 to arrive at

$$G_m = \frac{1}{4\pi} \left(\int_C \frac{g_m(\kappa, z, z')}{\xi} H_0^{(2)}(\xi \rho) d\xi - 2\pi j \sum_{p=1}^N \text{Res} \left(g_m(\kappa_p, z, z') \frac{H_0^{(2)}(\xi_p \rho)}{\xi_p} \right) \right) \quad (4.3)$$

where the finite sum refers to the discrete spectral or pole wave contribution to G_m and the integral on C is the continuous spectral contribution to G_m ; also, at the poles $\xi = \xi_p$ one has

$$\kappa_p = \kappa(\xi) \Big|_{\xi = \xi_p} \quad . \quad (4.4)$$

The integral contour C can be transformed to a real axis integration in the following manner. Introducing the change of variable

$$z = \sqrt{k_0^2 - \xi^2} \quad , \quad d\xi = \frac{-z \, dz}{\sqrt{k_0^2 - z^2}} \quad . \quad (4.5)$$

It is noted that as ξ varies along the contour C , the new variable of integration z will vary from $+\infty$ to $-\infty$ along the real z axis. Note that the circular contour C' which encircles the branch point does not contribute. This can be seen by expanding the integrand around the branch point k_0 and then performing the integration along a small circle of radius δ enclosing the branch point; it is easy to see that the integral around this branch point grows as $O(\sqrt{\delta})$, and if $\delta \rightarrow 0$, that integral will vanish. Finally, one will have (see Figure 4.3).

$$G_m = \frac{1}{4\pi} \left(\int_{-\infty}^{\infty} \frac{g_m(z, z, z')}{(k_0^2 - z^2)} H_0^2(\rho \sqrt{k_0^2 - z^2}) z dz - 2\pi j \left(\sum_p \text{Res} (g_m(\kappa_p, z, z')) \frac{H_0^2(\xi_p \rho)}{\xi_p} \right) \right). \quad (4.6)$$

The above result in (4.6) represents the alternative ρ -propagation representation of G_m which is obtained from its Sommerfeld representation in (4.1). The spurious poles at $z = \pm k_0$ ought to be noted in (4.6). These are the images of the pole at $\xi = 0$ occurring in the z plane. The ρ -propagation representation of the microstrip dyadic surface Green's function can be constructed via (3.32) through (3.37), where U , V and W are re-written in the ρ -propagating representation as:

$$U = \frac{1}{2} \left[\int_{-\infty}^{\infty} \frac{H_0^2(\rho \sqrt{k_0^2 - z^2}) z e^{-jz\delta} dz}{z - j \sqrt{(\epsilon_r - 1)k_0^2 + z^2} \cotan(d \sqrt{(\epsilon_r - 1)k_0^2 + z^2})} \right] + 2\pi j \sum_{n''} \text{Res}_U(z_{n''}), \quad (4.7)$$

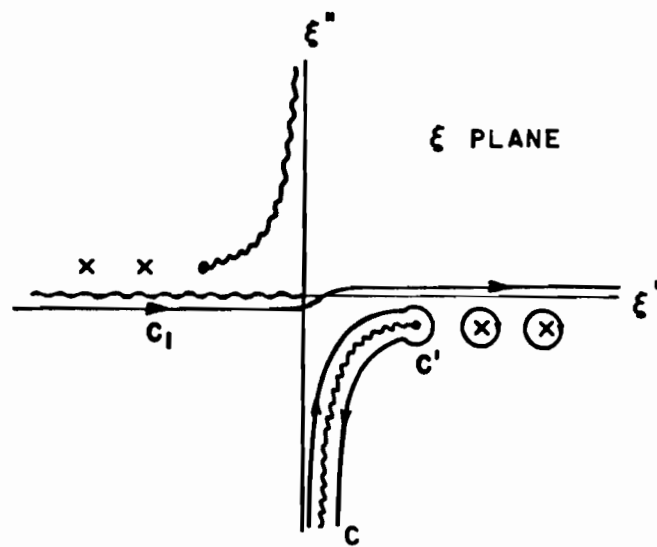


Figure 4.2. The contour deformation for ρ -propagation representation.

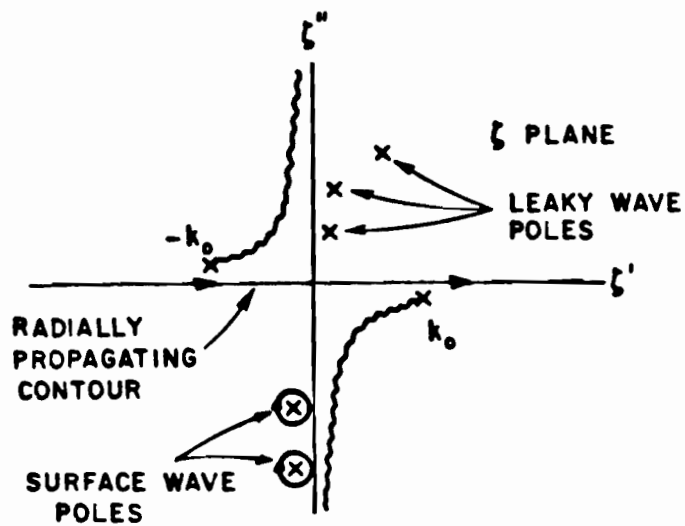


Figure 4.3. Complex ζ plane and the contour of integration.

$$V = \frac{1}{2} \left[\int_{-\infty}^{\infty} \frac{\frac{\sqrt{(\epsilon_r-1)k_0^2+\zeta^2}}{\epsilon_r} \tan(d\sqrt{(\epsilon_r-1)k_0^2+\zeta^2}) H_0^2(\rho\sqrt{k_0^2-\zeta^2}) \zeta e^{-j\zeta\delta} d\zeta}{\zeta + j \frac{\sqrt{(\epsilon_r-1)k_0^2+\zeta^2}}{\epsilon_r} \tan(d\sqrt{(\epsilon_r-1)k_0^2+\zeta^2})} \right] + 2\pi j \sum_n \text{Res}_V(\zeta_n') ,$$

(4.8)

and

$$W = \frac{1}{2} \left[\int_{-\infty}^{\infty} \frac{H_0^2(\rho\sqrt{k_0^2-\zeta^2})}{(\zeta - j\sqrt{(\epsilon_r-1)k_0^2+\zeta^2} \cotan(d\sqrt{(\epsilon_r-1)k_0^2+\zeta^2}))} \cdot \frac{\zeta^2 e^{-j\zeta\delta} d\zeta}{\frac{(\zeta + j\sqrt{(\epsilon_r-1)k_0^2+\zeta^2} \tan(d\sqrt{(\epsilon_r-1)k_0^2+\zeta^2}))}{\epsilon_r}} \right] + 2\pi j \sum_{n''} \text{Res}_W(\zeta_{n''}) + 2\pi j \sum_n \text{Res}_W(\zeta_n') .$$

(4.9)

The $\text{Res}_U(\zeta_{n''})$ and $\text{Res}_V(\zeta_n')$ and $\text{Res}_W(\zeta)$ are the residues of the poles in the integrands U, V and W . In Appendix G, a perturbation technique for finding these poles of Γ_0'' and Γ_0' is discussed. The residues at these poles are also given in the same appendix (see (G.14), (G.16), (G.18) and (G.20)).

The logarithmic singularity of the Hankel function at $\zeta = \pm k_0$ can be removed via the following transformation

$$\begin{aligned} \zeta &= k_0 \sqrt{1-\xi^2} & |\zeta| < k_0 \\ \zeta &= k_0 \sqrt{1+\xi^2} & |\zeta| > k_0 \end{aligned} \quad (4.10)$$

therefore the actual form of the U, V and W, which is ultimately being used, is as follows:

$$\begin{aligned}
 U = \frac{k_0}{2} & \left[\int_0^1 H_0^2(k_0 \rho \xi) \xi \left[\frac{e^{-jk_0 \sqrt{1-\xi^2} \delta}}{\sqrt{1-\xi^2} + \gamma} + \frac{e^{jk_0 \sqrt{1-\xi^2} \delta}}{\sqrt{1-\xi^2} - \gamma} \right] d\xi \right]_{\zeta^2 = k_0^2(1-\xi^2)} \\
 & + \int_0^\infty H_0^2(-jk_0 \rho \xi) \xi \left[\frac{e^{-jk_0 \sqrt{1+\xi^2} \delta}}{\sqrt{1+\xi^2} + \gamma} + \frac{e^{jk_0 \sqrt{1+\xi^2} \delta}}{\sqrt{1+\xi^2} - \gamma} \right] d\xi \Big|_{\zeta^2 = k_0^2(1+\xi^2)} \\
 & + 2\pi j \sum_n \text{Res}_U(\zeta_n), \quad (4.11)
 \end{aligned}$$

$$\begin{aligned}
 V = \frac{k_0^2}{2} & \left[\int_0^1 H_0^2(k_0 \rho \xi) \xi \left[-jZ \left[\frac{e^{-jk_0 \sqrt{1-\xi^2} \delta}}{\sqrt{1-\xi^2} + Z} + \frac{e^{jk_0 \sqrt{1-\xi^2} \delta}}{\sqrt{1-\xi^2} - Z} \right] d\xi \right]_{\zeta^2 = k_0^2(1-\xi^2)} \right. \\
 & + \int_0^\infty H_0^2(-jk_0 \rho \xi) \xi \left[-jZ \left[\frac{e^{-jk_0 \sqrt{1+\xi^2} \delta}}{\sqrt{1+\xi^2} + Z} + \frac{e^{jk_0 \sqrt{1+\xi^2} \delta}}{\sqrt{1+\xi^2} - Z} \right] d\xi \right]_{\zeta^2 = k_0^2(1+\xi^2)} \\
 & + 2\pi j \sum_n \text{Res}_V(\zeta_n), \quad (4.12)
 \end{aligned}$$

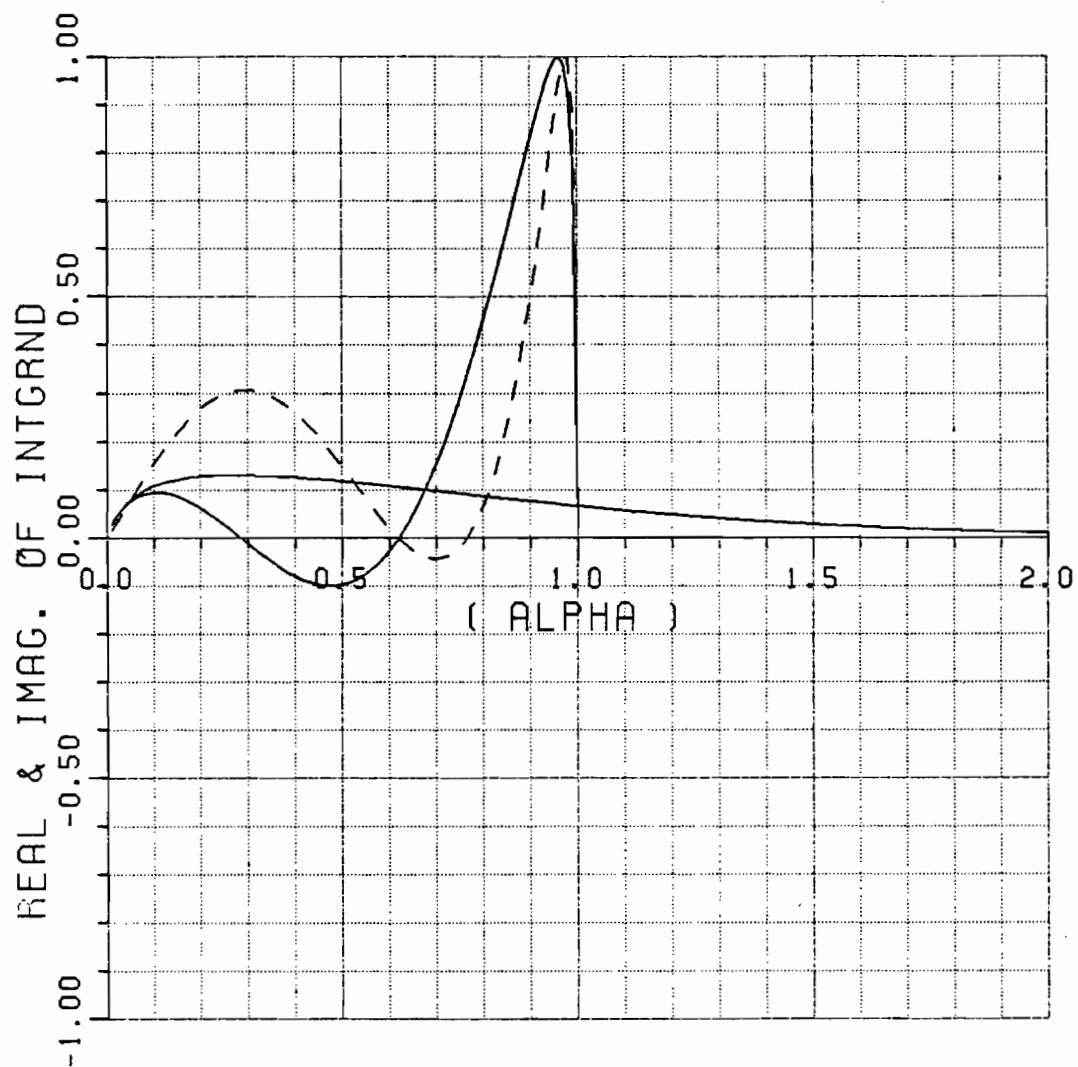
$$\begin{aligned}
W = \frac{k_0}{2} & \left[\int_0^1 H_0^2(k_0 \rho \xi) \xi \left[\frac{e^{-jk_0 \sqrt{1-\xi^2} \delta}}{(\sqrt{1-\xi^2}+Y)(\sqrt{1-\xi^2}+Z)} \right. \right. \\
& \left. \left. + \frac{e^{-jk_0 \sqrt{1-\xi^2} \delta}}{(\sqrt{1-\xi^2}-Y)(\sqrt{1-\xi^2}-Z)} \right] \right] \bigg|_{\zeta^2=k_0^2(1-\xi^2)} d\xi \\
& + \int_0^\infty H_0^2(-jk_0 \rho \xi) \xi \left[\frac{e^{-jk_0 \sqrt{1+\xi^2} \delta}}{(\sqrt{1+\xi^2}+Y)(\sqrt{1+\xi^2}+Z)} \right. \\
& \left. \left. + \frac{e^{-jk_0 \sqrt{1+\xi^2} \delta}}{(\sqrt{1+\xi^2}-Y)(\sqrt{1+\xi^2}-Z)} \right] \right] \bigg|_{\zeta^2=k_0^2(1+\xi^2)} d\xi \\
& + 2\pi j \sum_{n''} \text{Res}_W(\zeta_{n''}) + 2\pi j \sum_{n'} \text{Res}_W(\zeta_{n'}) \quad , \quad (4.13)
\end{aligned}$$

where

$$Y = -j \frac{\sqrt{(\epsilon_r - 1)k_0^2 + \zeta^2}}{k_0} \cotan(d \sqrt{(\epsilon_r - 1)k_0^2 + \zeta^2}) \quad (4.14)$$

$$Z = +j \frac{\sqrt{(\epsilon_r - 1)k_0^2 + \zeta^2}}{k_0 \epsilon_r} \tan(d \sqrt{(\epsilon_r - 1)k_0^2 + \zeta^2}) \quad (4.15)$$

Figures 4.4(a) through 4.4(c) show a typical behavior of the integrand W (Equation (4.15)) as the function of its argument ξ for a single layer microstrip configuration with a dielectric constant $\epsilon_r=2.54$ and of thickness equal to $0.0795\lambda_0$ for different lateral distances, $\rho=0.5\lambda_0$, $1.\lambda_0$ and $2.\lambda_0$. It is important to note that the real part of this integral always exists over finite limits that have their end points at 0. and 1.0; and the imaginary part which exists over semi-infinite limits is always exponentially decaying as the function of the argument. As the lateral separation between the source and observation points increases, the infinite integral decays faster, but the number of oscillations in the finite integrals increases. This can be seen from the Figure 4.5 when $\rho=4.775 \lambda_0$. These oscillations are due to the behavior of the Hankel function as its argument becomes larger. It is interesting to note that in the Sommerfeld representation, the total number of oscillations of the integrand between 0 and 1.0 of its semi-infinite interval of integration are the same as the number of oscillations of the integrand of the radially propagating representation which exists only over finite limits from 0. to 1. as noted earlier. Over the rest of the interval of integration from 1.0 to infinity however, the Sommerfeld integrand exhibits an infinite number of oscillations; no such oscillations exist for the radially propagating representation. The advantage of the radially propagating representation against the conventional Sommerfeld representation is now apparent. Figures 4.6(a), (b) and (c) show the same integrand but for



$$\epsilon_r = 2.54$$

Radially Propagating Representation

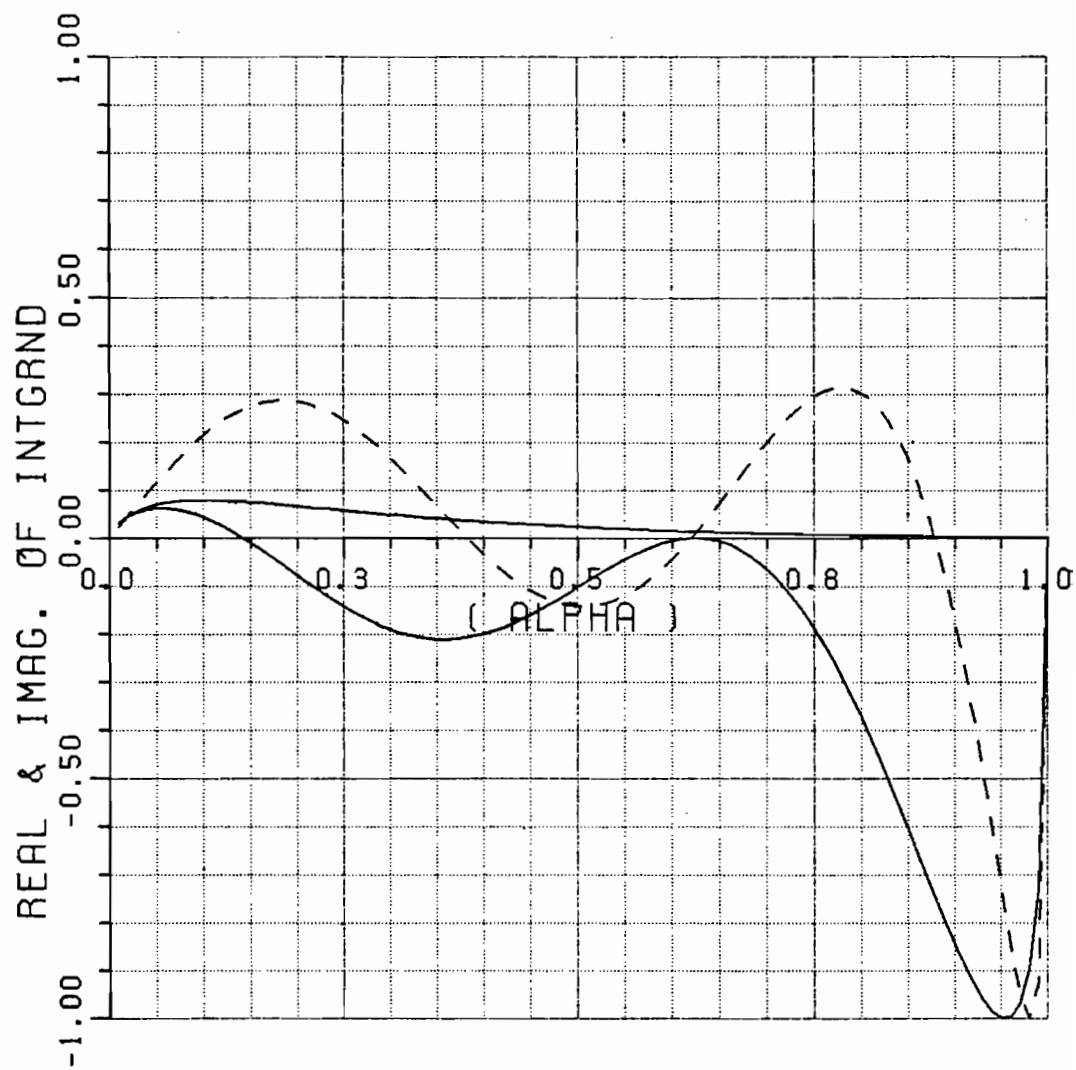
$$K_0 d = 0.5 \quad (d/\lambda_0 = 0.0795)$$

---- Real Part

—— Imag. Part

$$(a) \quad \rho = 0.5 \lambda_0$$

Figure 4.4. Integrand of W in the Equation (4.13) versus $\xi = \alpha$.



$$\epsilon_r = 2.54$$

$$K_0 d = 0.5 \quad (d/\lambda_0 = 0.0795)$$

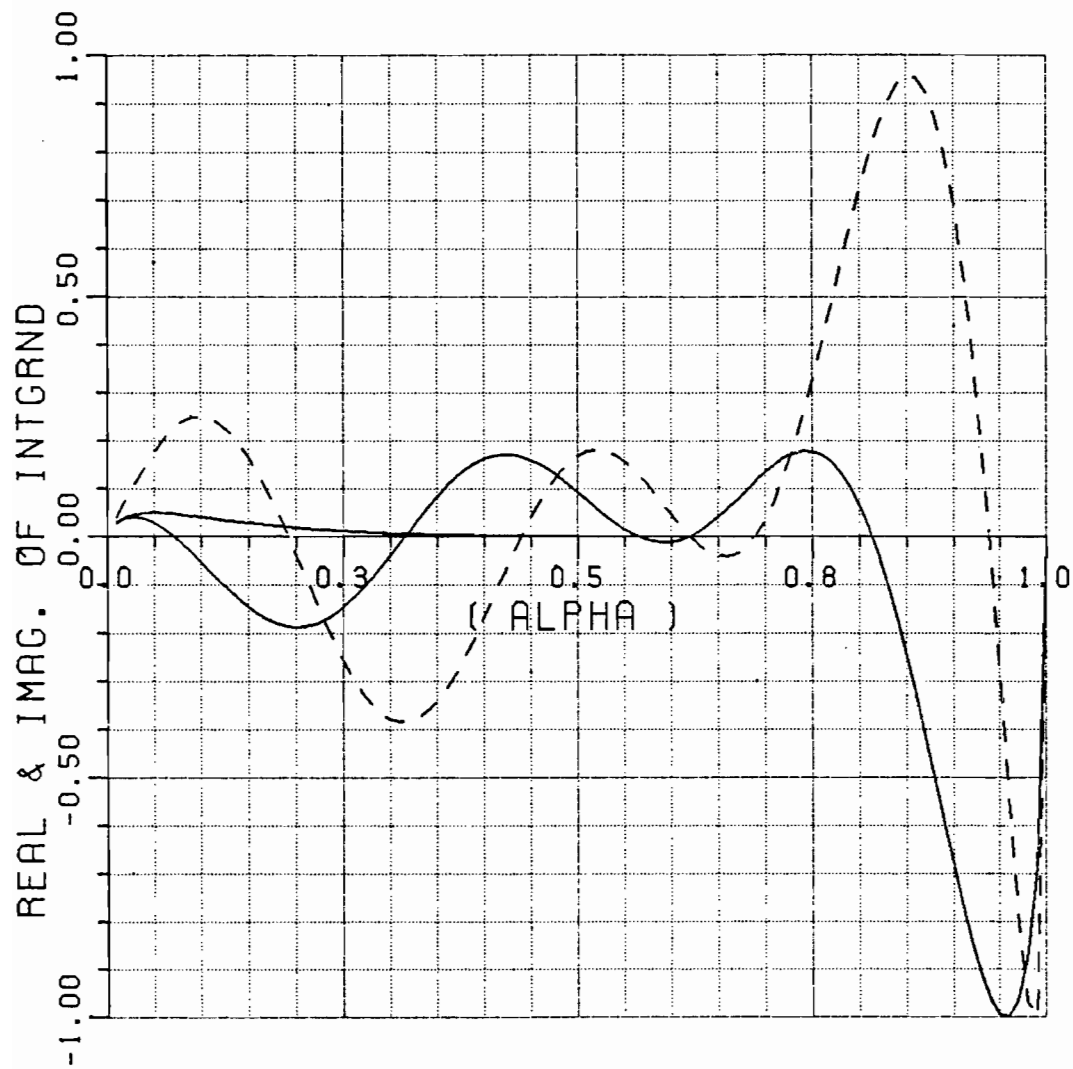
Radially Propagating Representation

---- Real Part

—— Imag. Part

$$(b) \quad \rho = \lambda_0$$

Figure 4.4. (continued)



$$\epsilon_r = 2.54$$

$$K_0 d = 0.5 \quad (d/\lambda_0 = 0.0795)$$

Radially Propagating Representation

---- Real Part

—— Imag. Part

$$(c) \quad \rho = 2.0 \lambda_0$$

Figure 4.4. (Continued)

the denser dielectric material ($\epsilon_r=10.2$). The trend of the integrands versus the argument are the same as the lateral distance increases. In the following we will derive the (SDP) form of the radially propagating microstrip Green's function to eliminate these oscillations in the integrands for larger later separations of the source and field points.

B. Steepest Descent Path (SDP) Representation of the Microstrip Green's Function

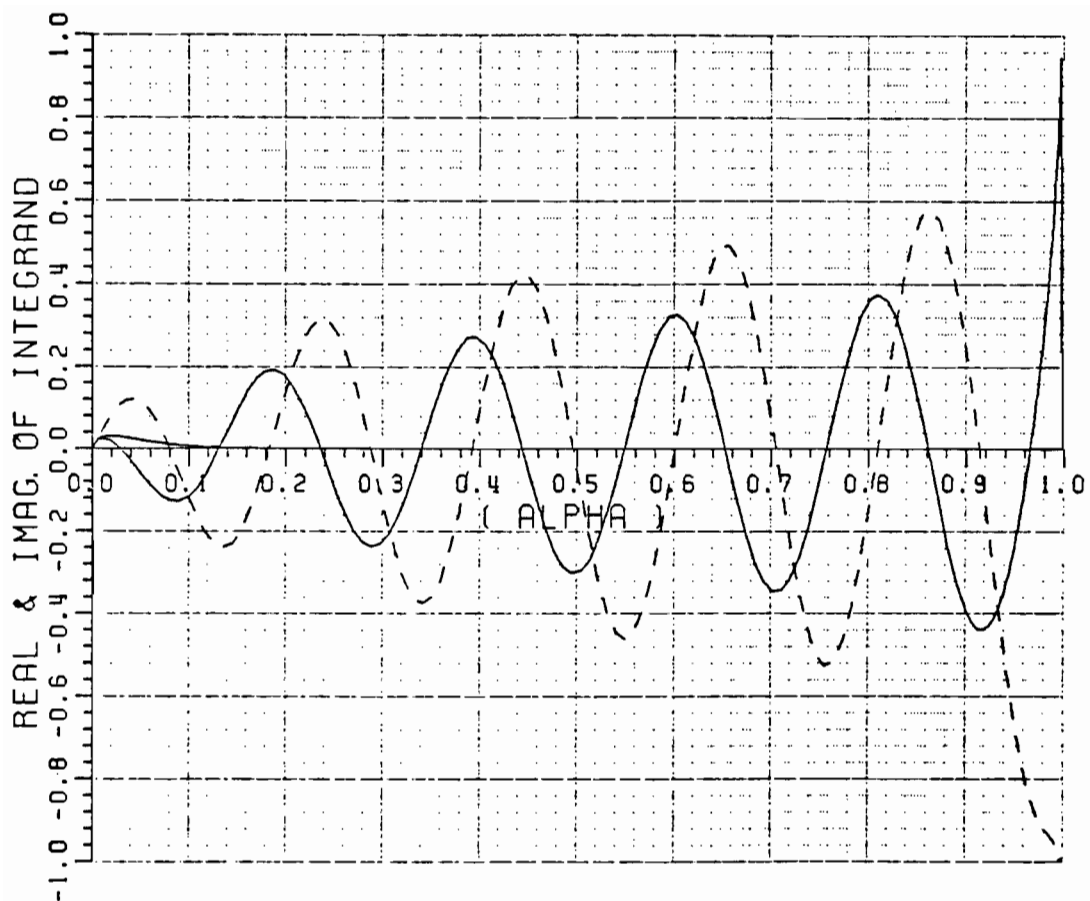
This method deals with the deformation of the original contour for the radially propagation representation of the microstrip Green's function (obtained earlier in part A) into its steepest descent path (SDP) of integration. It is a technique which allows numerical integration to be employed over the SDP on which the integrand decays most rapidly. In this case, as the separation between the source and observation point increases, the numerical integration becomes even faster and easier to perform.

Consider the integral in the form

$$I = \int_{-\infty}^{\infty} F(\zeta) H_0^2(\rho \sqrt{k_0^2 - \zeta^2}) e^{-j\zeta z} d\zeta \quad , \quad (4.16)$$

$$= k_0 \int_{-\infty}^{\infty} F(k_0 \zeta) H_0^2(k_0 \rho \sqrt{1 - \zeta^2}) e^{-jk_0 \zeta z} d\zeta \quad , \quad (4.17)$$

where I can be a typical expression for the integrals occurring in G_m'' or G_m' . Let's assume for the time being that $k_0 \rho \gg 1$, and the use of the large argument asymptotic form of the Hankel function is permissible.



$$\epsilon_r = 2.54$$

Radially Propagating Representation

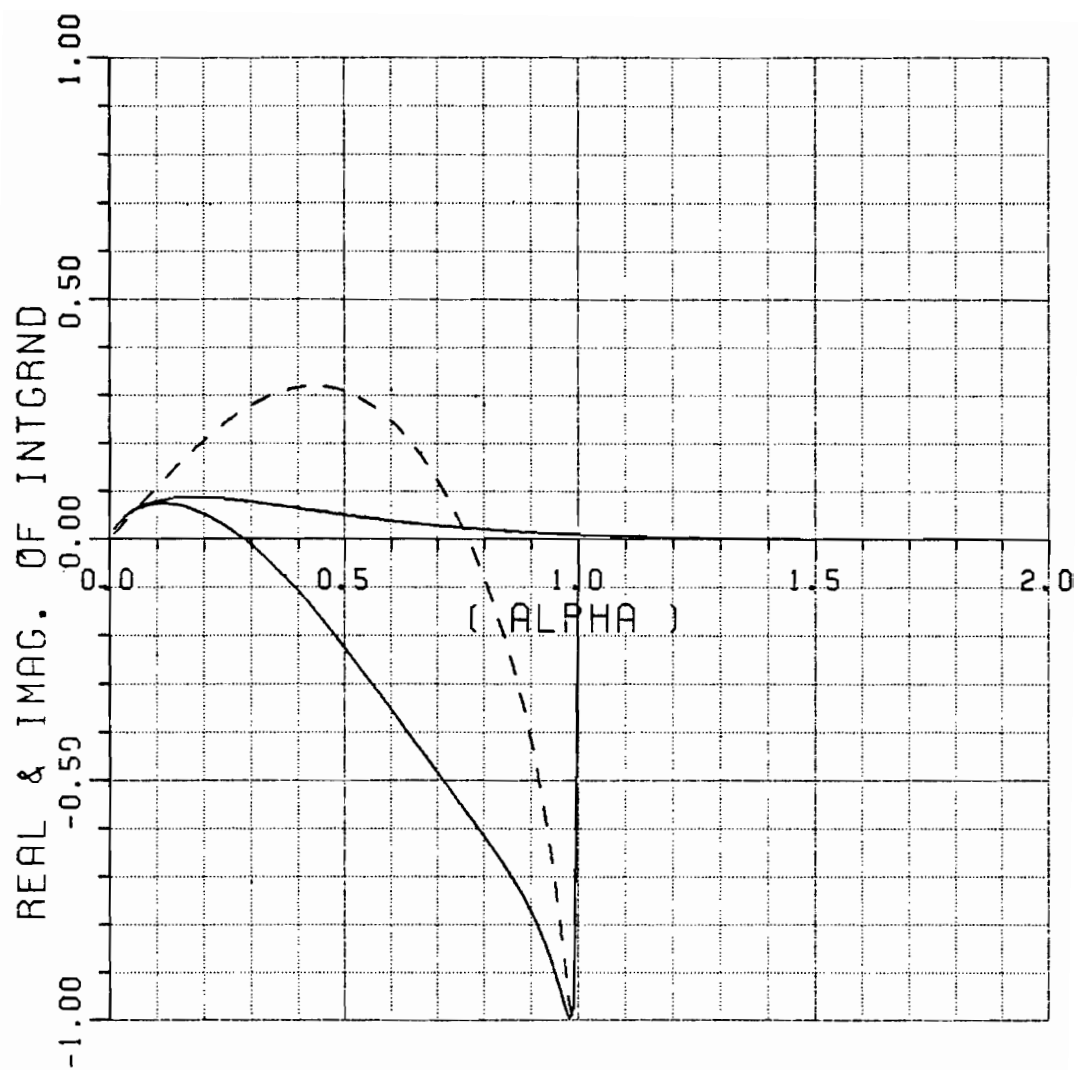
$$K_0 d = 0.5 \quad (d/\lambda_0 = 0.0795)$$

---- Real Part

—— Imag. Part

$$\rho = 4.775 \lambda_0$$

Figure 4.5. Integrand of W in the Equation (4.13) versus $\xi = \alpha$.



$$\epsilon_r = 10.2$$

Radially Propagating Representation

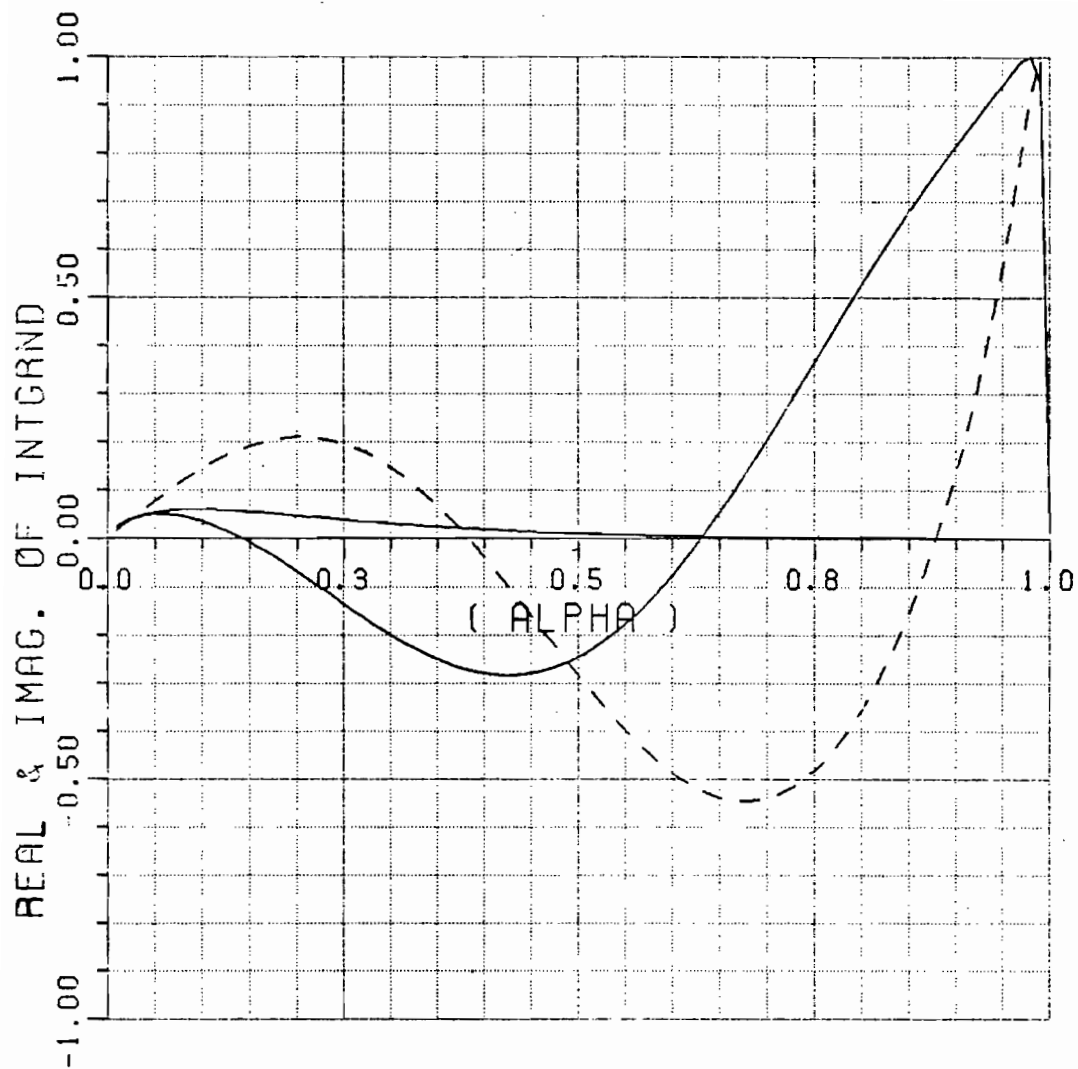
$$K_0 d = 0.5 \quad (d/\lambda_0 = 0.0795)$$

---- Real Part

—— Imag. Part

$$(a) \quad \rho = 0.5 \lambda_0$$

Figure 4.6. Integrand of W in the Equation (4.13) versus $\xi = \alpha$.



$$\epsilon_r = 10.2$$

$$K_0 d = 0.5 \quad (d/\lambda_0 = 0.0795)$$

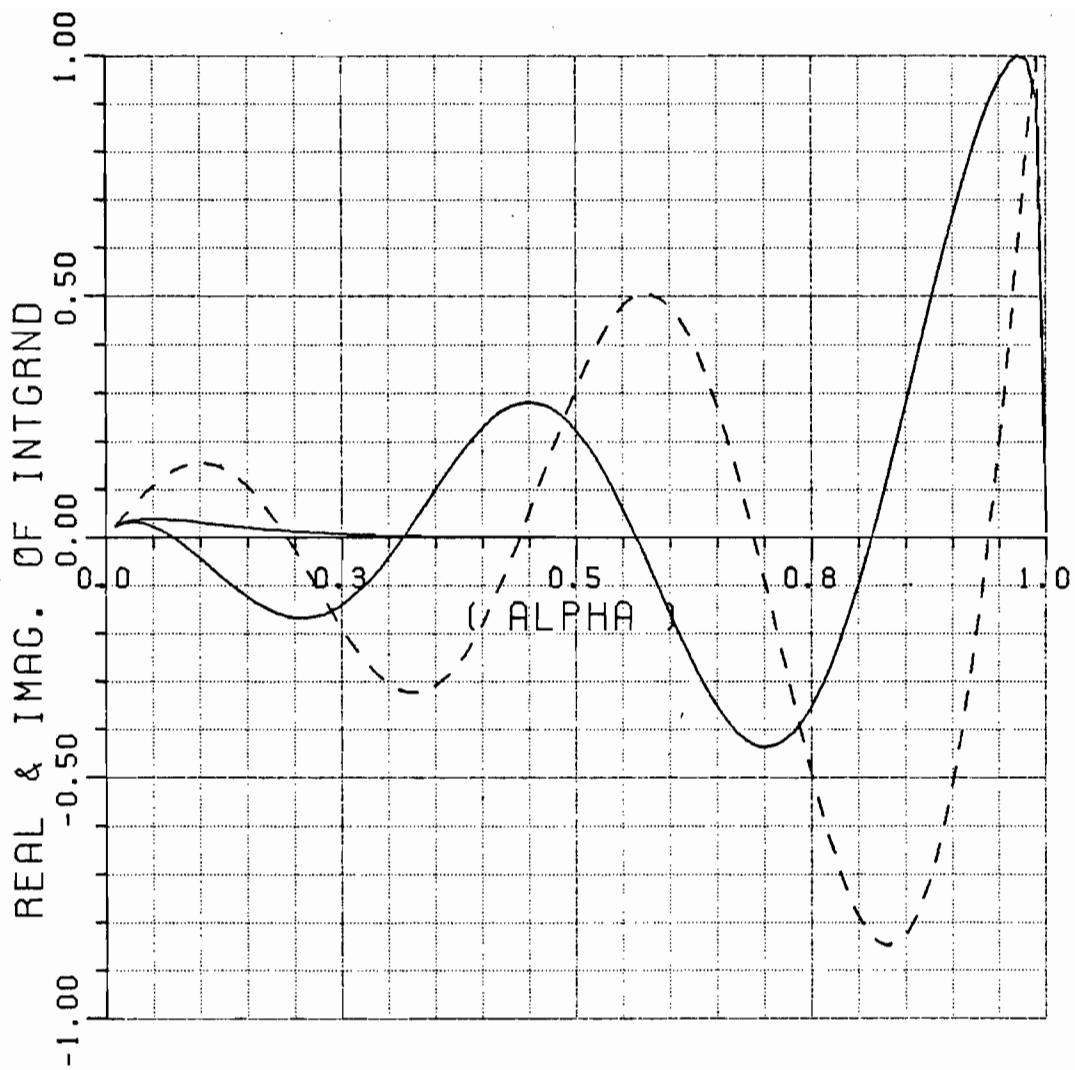
Radially Propagating Representation

---- Real Part

—— Imag. Part

$$(b) \quad \rho = \lambda_0$$

Figure 4.6. (Continued)



$$\epsilon_r = 10.2$$

Radially Propagating Representation

$$K_0 d = 0.5 \quad (d/\lambda_0 = 0.0795)$$

---- Real Part

—— Imag. Part

$$(c) \quad \rho = 2.0 \lambda_0$$

Figure 4.6. (Continued)

Then

$$I \sim k_0 \int_{-\infty}^{\infty} F(k_0 \zeta) \sqrt{\frac{2}{\pi k_0 \rho \sqrt{1-\zeta^2}}} e^{+j\frac{\pi}{4}} e^{-jk_0(\rho \sqrt{1-\zeta^2} + z\zeta)} d\zeta. \quad (4.18)$$

Although the saddle point and the steepest descent path can be directly found in the complex ζ plane, we will perform the angular spectrum mapping for convenience, (see Appendix E).

Let

$$\zeta = \cos \gamma \quad ; \quad d\zeta = -\sin \gamma d\gamma \quad (4.19)$$

so

$$\sqrt{1-\zeta^2} = \sin \gamma \quad , \quad (4.20)$$

then

$$I \sim k_0 \int_{\Gamma} F(k_0 \cos \gamma) \sqrt{\frac{2}{\pi k_0 \rho \sin \gamma}} e^{+j\frac{\pi}{4}} e^{-jk_0 r \cos(\theta-\gamma)} (\sin \gamma) d\gamma \quad (4.21)$$

where

$$\rho = r \sin \theta \quad ; \quad z = r \cos \theta \quad \text{and} \quad \tan \theta = \frac{\rho}{z} \quad (4.22)$$

The integrand exhibits a saddle point at $\gamma_s = \theta$, (see Appendix H).

Let

$$q(\gamma) = -j \cos(\theta-\gamma) \quad (4.23)$$

$$q'(\gamma) = j \sin(\theta-\gamma) \quad ; \quad \gamma_s = \theta \text{ (saddle point)} \quad ; \quad q(\gamma_s) = -j \quad (4.24)$$

Figure 4.7 shows the original path Γ and steepest descent path Γ_{SDP} in the complex γ plane. Note that the steepest descent path is the path on which the following condition holds,

$$\text{Im}(q(\gamma)) = \text{Im}(q(\gamma_s)) \quad (4.25)$$

or

$$\text{Re}(\cos(\theta - \gamma)) = 1 \quad (4.26)$$

so

$$I \sim k_0 \left\{ \int_{\Gamma_{\text{SDP}}} F(k_0 \cos \gamma) \sqrt{\frac{2}{\pi k_0 \rho \sin \gamma}} e^{+j \frac{\pi}{4}} e^{-jk_0 r \cos(\theta - \gamma)} (\sin \gamma) d\gamma \right. \\ \left. \pm 2\pi j \sum_n \text{Res}(\gamma_n) \right\} \quad (4.27)$$

where Γ_{SDP} is the SDP contour, and the summation term stands for the total of the residue contributions arising from the presence of the surface wave and leaky wave poles which may be intercepted during the path deformation (it is seen that no branch points and branch cuts intercepted). It is noted that unless $\theta \approx \frac{\pi}{2}$ ($k_0 \rho \gg 1; k_0 z \ll 1$), there exists the possibility of crossing one or more of those surface wave poles which are closest to the Real γ axis (see Figure 4.2) that have been captured during the derivation of ρ -propagation representation (see the Equation (4.6). This results in the cancellation of some of the surface wave residue contributions in the sum on the right hand side of (4.6). Therefore, not all of the possible surface waves will contribute to the SDP representation of the field. It is also to be noted that the same SDP representation will result if one starts from the Sommerfeld

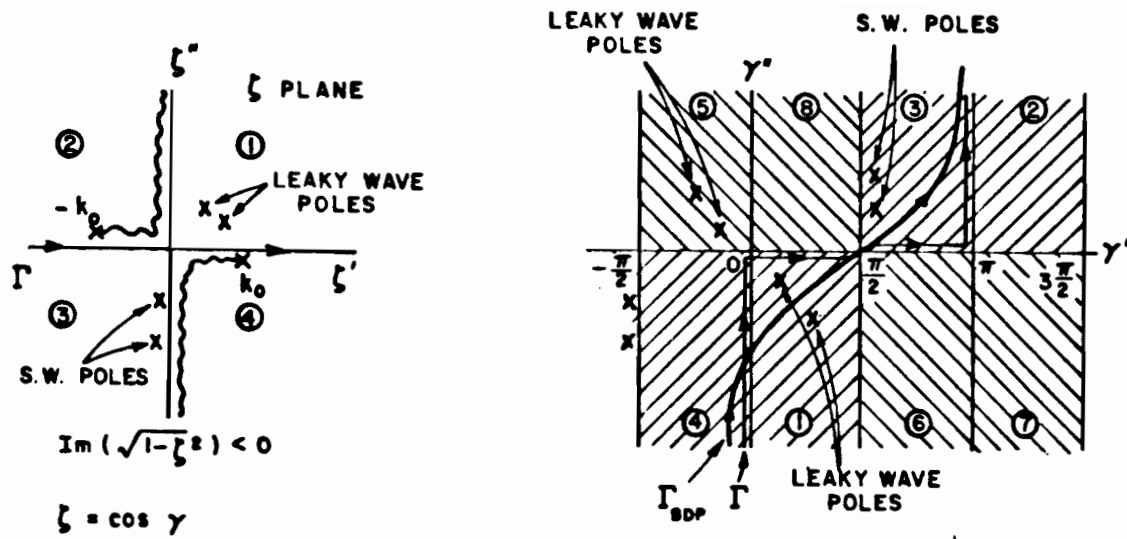


Figure 4.7. Mapping from complex ζ to γ plane (angular spectrum mapping), the original path Γ and SDP path Γ_{SDP} have been depicted in complex γ plane.

representation (rather than the ρ -propagation representation) since only one SDP exists in each strip of 2π radians in the γ plane. A typical uniform asymptotic evaluation of such an integral has been carried out in the Appendix H and will not be repeated here. In the following we will map the SDP onto a contour along the real axis in the new complex plane s defined by

$$q(\gamma) - q(\gamma_s) = s^2 \quad (4.28)$$

or

$$\cos(\theta - \gamma) = 1 - js^2 \quad (4.29)$$

This transformation maps the steepest descent path, Γ_{SDP} on the real axis of the complex s plane as indicated above. The saddle point at $\gamma_s = \theta$ is now mapped to $s=0$, (see Figure 4.8). The explicit expression of γ on the SDP can be inferred via Equation (4.29), that is

$$\gamma = \theta \pm \left(\frac{\pi}{2} + j \ln (s^2 + j + |s| \sqrt{s^2 + 2j}) \right) ; \quad \left\{ \begin{array}{ll} + & \gamma > \theta, s > 0 \\ - & \gamma < \theta, s < 0 \end{array} \right. , \quad (4.30)$$

and the Jacobian, $\frac{d\gamma}{ds}$ is given by

$$\frac{d\gamma}{ds} = \frac{2j}{\sqrt{s^2 + 2j}} ; \quad (\text{Branch points at } \sqrt{s^2 + 2j} = 0) \quad (4.31)$$

The exact SDP representation of I in the S -plane will be

$$I = k_0 \left\{ \int_{-\infty}^{\infty} F(k_0 \cos \gamma) H_0^2(k_0 \rho \sin \gamma) e^{-jk_0 z \cos \gamma} (\sin \gamma) \right\} \bigg|_s^{\frac{2j}{\sqrt{s^2 + 2j}}} ds + \pm 2\pi j \sum_n \text{Res}(\gamma_n) \} \quad (4.32)$$

For $\theta \approx \frac{\pi}{2}$ the source and observation points lie on the interface and hence $k_0 z \approx 0$; hence, one will have

$$\sin \gamma = 1 - js^2 , \quad \cos \gamma = |s| \sqrt{s^2 + 2j} . \quad (4.33)$$

Therefore

$$H_0^2(k_0 \rho \sin \gamma) = H_0^2(k_0 \rho (1 - js^2)) . \quad (4.34)$$

The final SDP representation for microstrip dyadic surface Green's function which is suitable for numerical integration can be found from (3.26) - (3.31) and the following results:

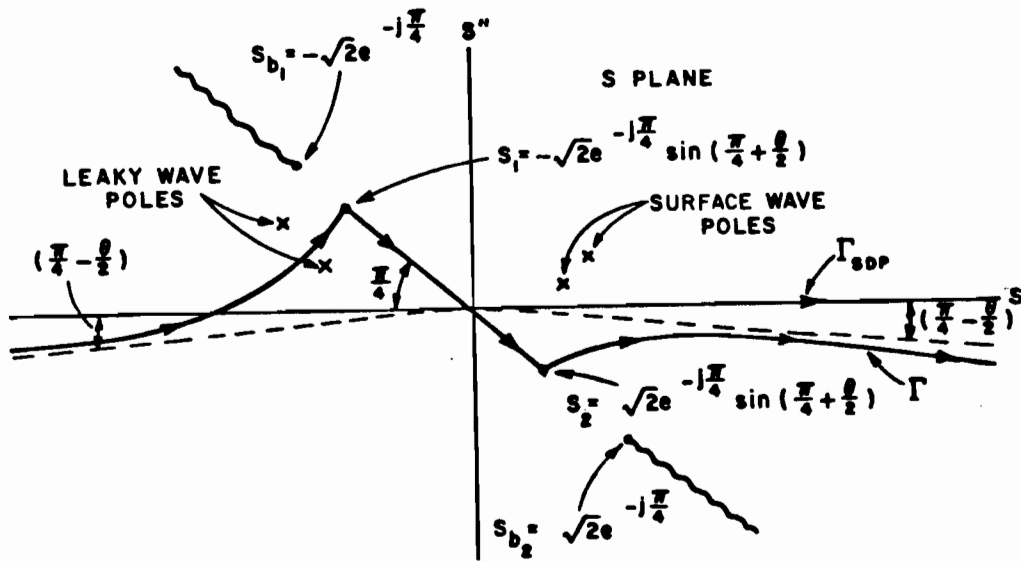


Figure 4.8. Complex S plane, original path Γ maps on solid curve, the SDP maps on to the real axis ($-\infty < s < \infty$) and the saddle point $\gamma_s = \theta$, maps on to $s = 0$; the branch points exist at $s_{b1,2} = \pm \sqrt{2}e^{-j\pi/4} (\sqrt{s^2 + 2j} = 0)$.

$$U = \frac{1}{2} \left[k_0 \int_0^\infty H_0^2(k_0 \rho (1 - js^2)) 2(s^2 + j)s \left(\frac{1}{\cos \gamma + \gamma} + \frac{1}{\cos \gamma - \gamma} \right) ds \right]_{\cos \gamma = s\sqrt{s^2 + 2j}}$$

$$\pm 2\pi j \sum_{m''} \text{Res}_U(\gamma_{m''}) + 2\pi j \sum_{n''} \text{Res}_U(\gamma_{n''}) \quad , \quad (4.35)$$

$$V = \frac{1}{2} \left[k_0^2 \int_0^\infty H_0^2 (k_0 \rho (1 - js^2)) 2(s^2 + j)s \left[-jZ \left(\frac{1}{\cos \gamma + Z} + \frac{1}{\cos \gamma - Z} \right) \right] \right]_{\cos \gamma = s\sqrt{s^2 + 2j}} ds \pm 2\pi j \sum_{m'} \text{Res}_V(\gamma_{m'}) + 2\pi j \sum_{n'} \text{Res}_V(z_{n'}) \quad , \quad (4.36)$$

and

$$W = \frac{1}{2} \left[k_0 \int_0^\infty H_0^2 (k_0 \rho (1 - js^2)) 2(s^2 + j)s \left[\cos \gamma \left(\frac{1}{\cos \gamma + Z} + \frac{1}{\cos \gamma - Z} \right) \right] \right]_{\cos \gamma = \sqrt{s^2 + 2j}} ds \pm 2\pi j \sum_{m'} \text{Res}_W(\gamma_{m'}) \pm 2\pi j \sum_m \text{Res}_W(\gamma_m) + 2\pi j \sum_{n''} \text{Res}_W(z_{n''}) + 2\pi j \sum_{n'} \text{Res}_W(z_{n'}) \quad (4.37)$$

where

$$\gamma = -j \sqrt{(\epsilon_r - 1) + \cos^2 \gamma} \cotan (k_0 d \sqrt{(\epsilon_r - 1) + \cos \gamma}) \quad , \quad (4.38)$$

and

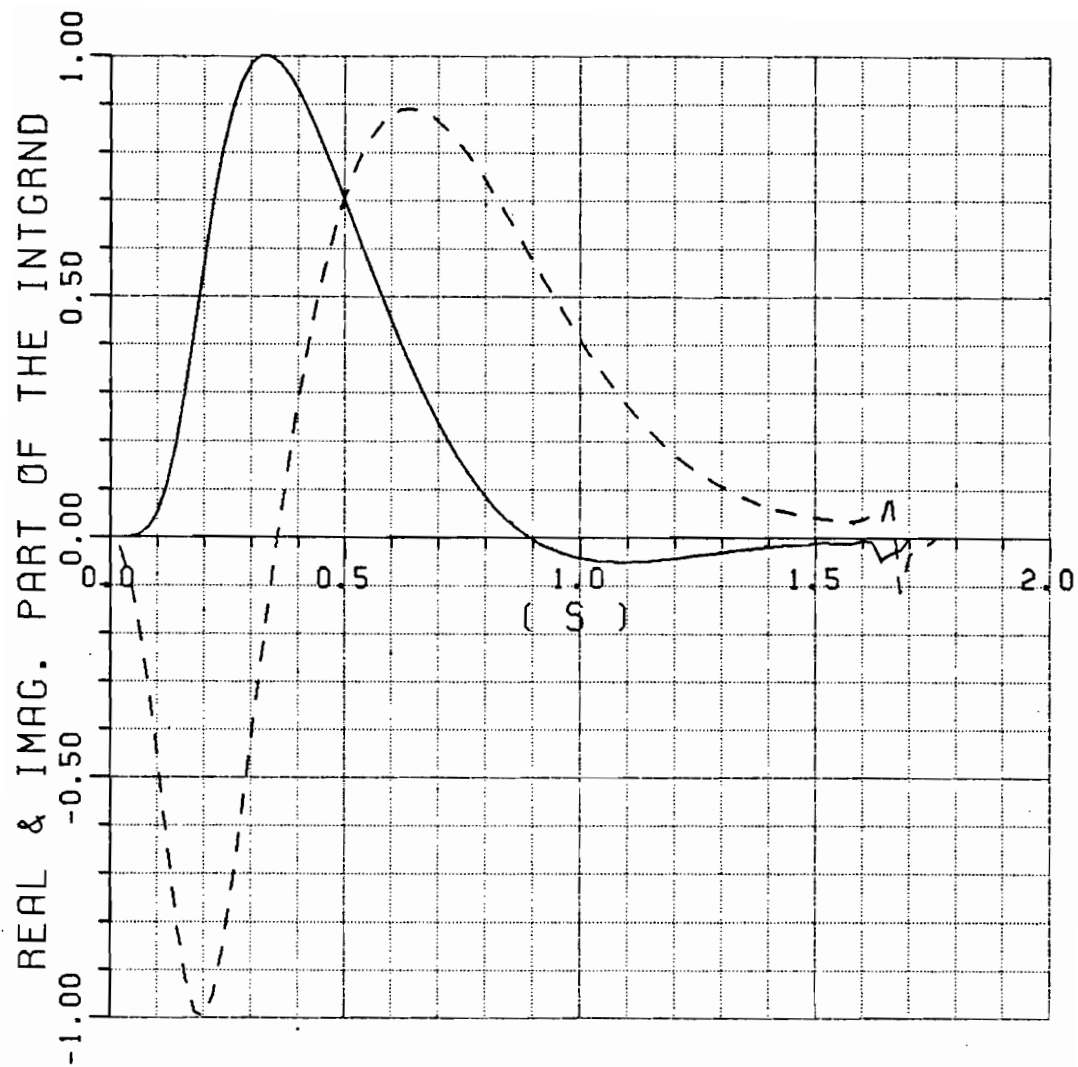
$$Z = j \sqrt{(\epsilon_r - 1) + \cos^2 \gamma} \tan (k_0 d \sqrt{(\epsilon_r - 1) + \cos^2 \gamma}) \quad . \quad (4.39)$$

The next six figures deal with the numerical results based on this steepest descent path (SDP) representation. Figures 4.9(a) through (c) and 4.10(a) through (c) depict the integrand of the SDP representation of W given in Equation (4.37) versus its argument(s) for a slab thickness of $0.0795\lambda_0$ with low and high dielectric constants $\epsilon_r=2.54$ and $\epsilon_r=10.2$, respectively. Unlike the previous cases, the integrands now become smoother as the lateral separation between the source and observation points increases; therefore, they will be easier to evaluate. Nevertheless, for small separations, a numerical irregularity appears in the integrand of the SDP representation, (see Figures 4.9(a) and 4.10(a)). These irregularities, and rapid changes in the integrands are mostly due to the unexcited leaky wave poles (not being captured by SDP in these instances) which are very close to the SDP path. One can use the following procedure to avoid these irregularities and thereby improve the numerical behavior of the integrand. Let a typical integral of the type being considered be expressed as

$$\int_{s_1}^{s_2} F(s) ds = \int_{s_1}^{s_2} \left[F(s) - \frac{\text{Res}(s_p)}{s-s_p} \right] ds + \text{Res}(s_p) \ln \left| \frac{s_2-s_p}{s_1-s_p} \right| + j \text{Arg} \left(\frac{s_2-s_p}{s_1-s_p} \right) \quad (4.40)$$

where the integrand, given in the bracket is a regular and slow varying function. Figure 4.11 depicts the same integrand as 4.10(a) with the leaky wave pole singularity being subtracted. Although the integrand with the singularity subtracted is easier to evaluate as can be seen from the comparison between the Figures 4.10(a) and 4.11, it is now

necessary to find the leaky wave poles via a numerical search technique before these pole effects can be subtracted. However, for moderate sized substrate thickness, this leaky wave pole subtraction procedure is not necessary if one uses the SDP representation for lateral distances from the source point larger than $(0.5\lambda_0)$ for $\epsilon_r=2.54$ and $(0.8\lambda_0)$ for $\epsilon_r=10.2$, as is evident from Figures 4.9(b), 4.9(c), 4.10(b) and 4.10(c); the main reason why this is so is because the Hankel function with the large complex argument decays fast exponentially for larger lateral separation between source and field points and dominates any irregularities or any contribution that comes from the nearby singularities; hence, most of the contribution to the integral comes from the vicinity of the saddle point at $s=0$. The SDP representation can indeed be used to evaluate the field points arbitrarily close to the source, but the nearby leaky wave poles ought to be determined in order to have an efficient and accurate representation. A careful numerical study reveals that the exact SDP representation is a more efficient representation than the other exact ones for lateral source and field point separations as small as $0.1\lambda_0$ if the nearest singularity to the SDP were removed analytically. Figures 4.12(a) and (b) show the integrand of the SDP representation for the surface field when the lateral separation between the source and field points is $(0.1\lambda_0)$ before and after the singularity has been removed, respectively. It is to be noted that in all these figures, the values of the integrand are normalized to their absolute maximum, hence all values of the integrand lie between -1.0 and 1.0.



$$\epsilon_r = 2.54$$

$$K_0 d = 0.5 \quad (d/\lambda_0 = 0.0795)$$

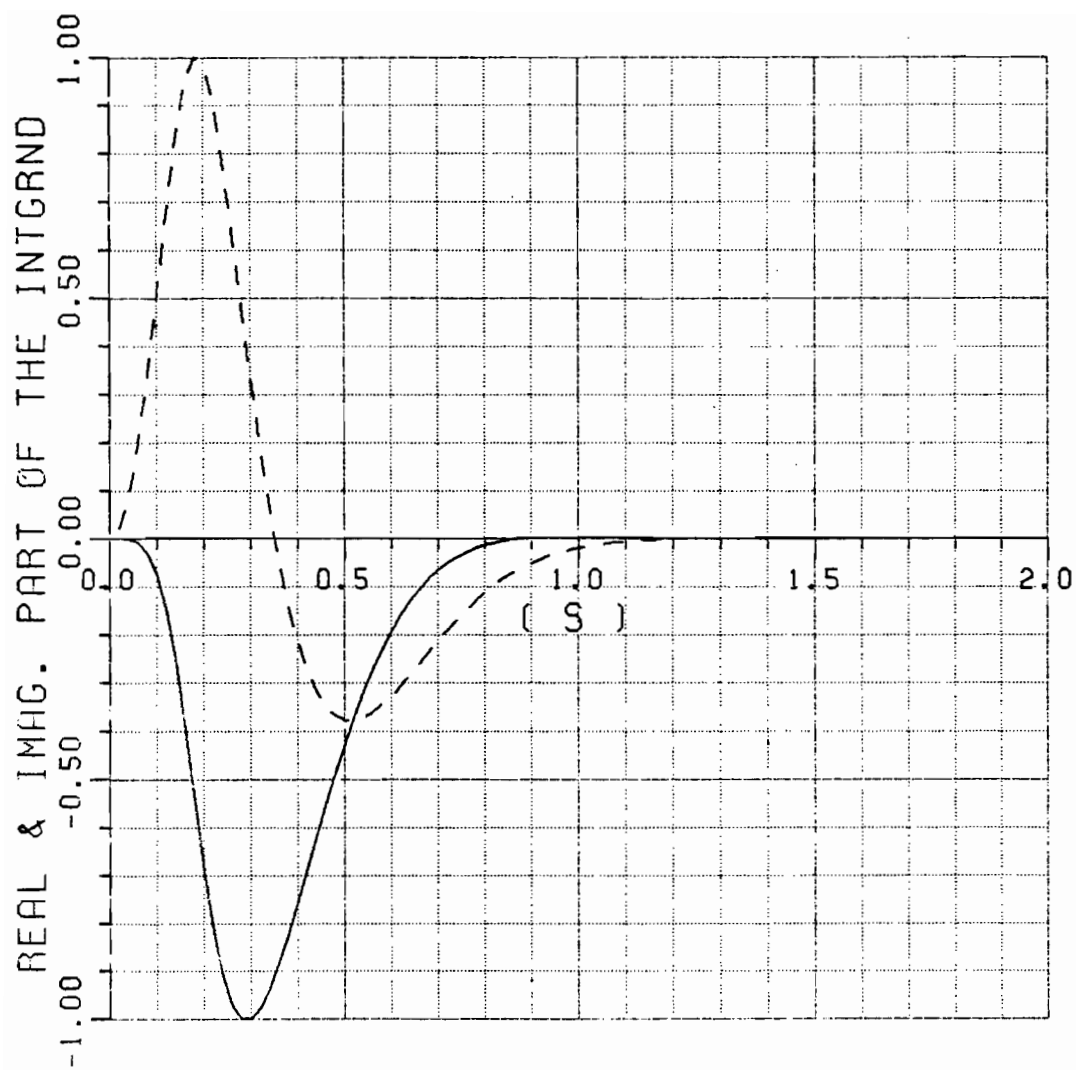
Steepest Descent Path

---- Real Part

—— Imag. Part

$$(a) \quad \rho = 0.5 \lambda_0$$

Figure 4.9. Integrand of W in the Equation (4.37) versus s .



$$\epsilon_r = 2.54$$

$$K_0 d = 0.5 \quad (d/\lambda_0 = 0.0795)$$

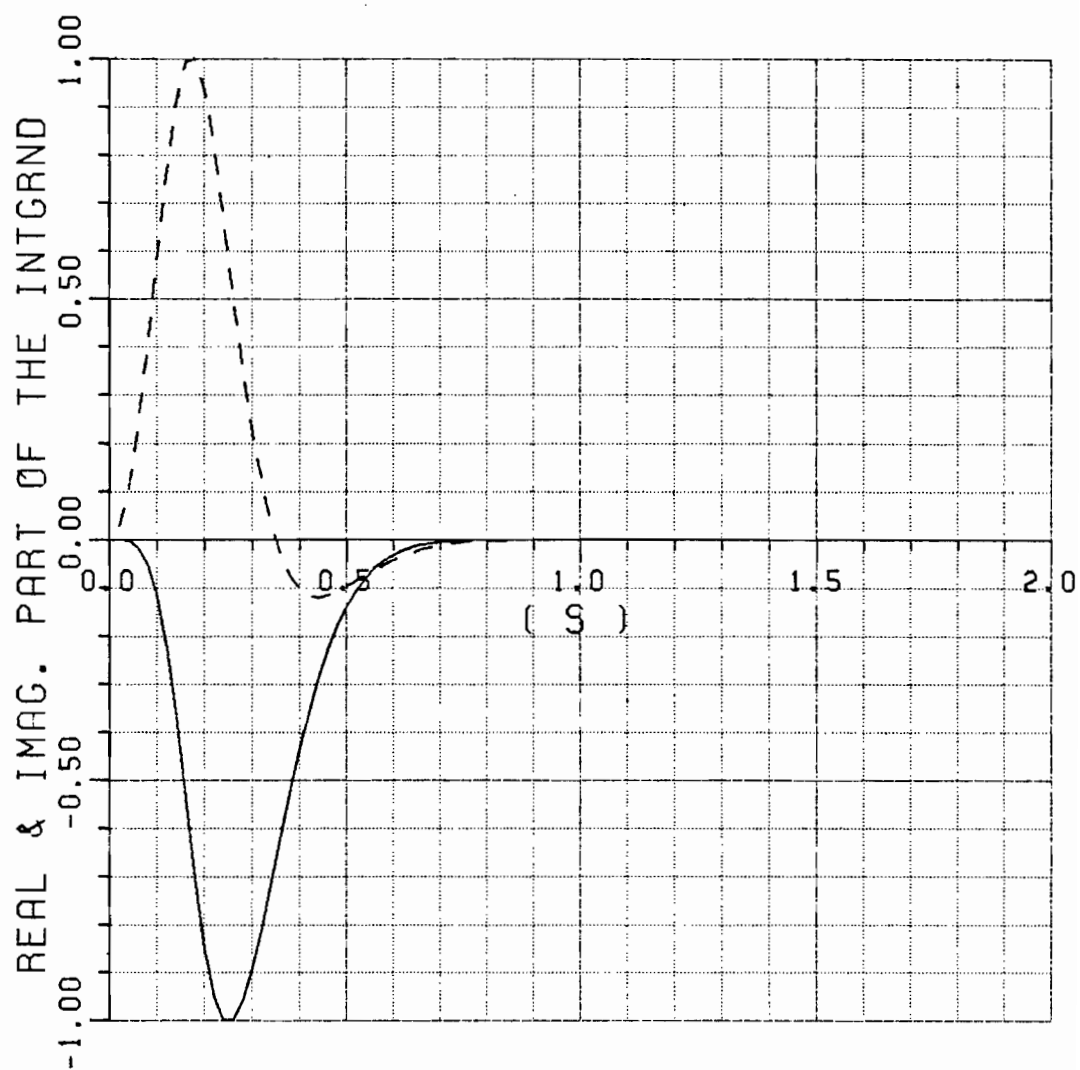
Steepest Descent Path

---- Real Part

—— Imag. Part

$$(b) \quad \rho = 1.0 \lambda_0$$

Figure 4.9. (Continued).



$$\epsilon_r = 2.54$$

$$K_0 d = 0.5 \quad (d/\lambda_0 = 0.0795)$$

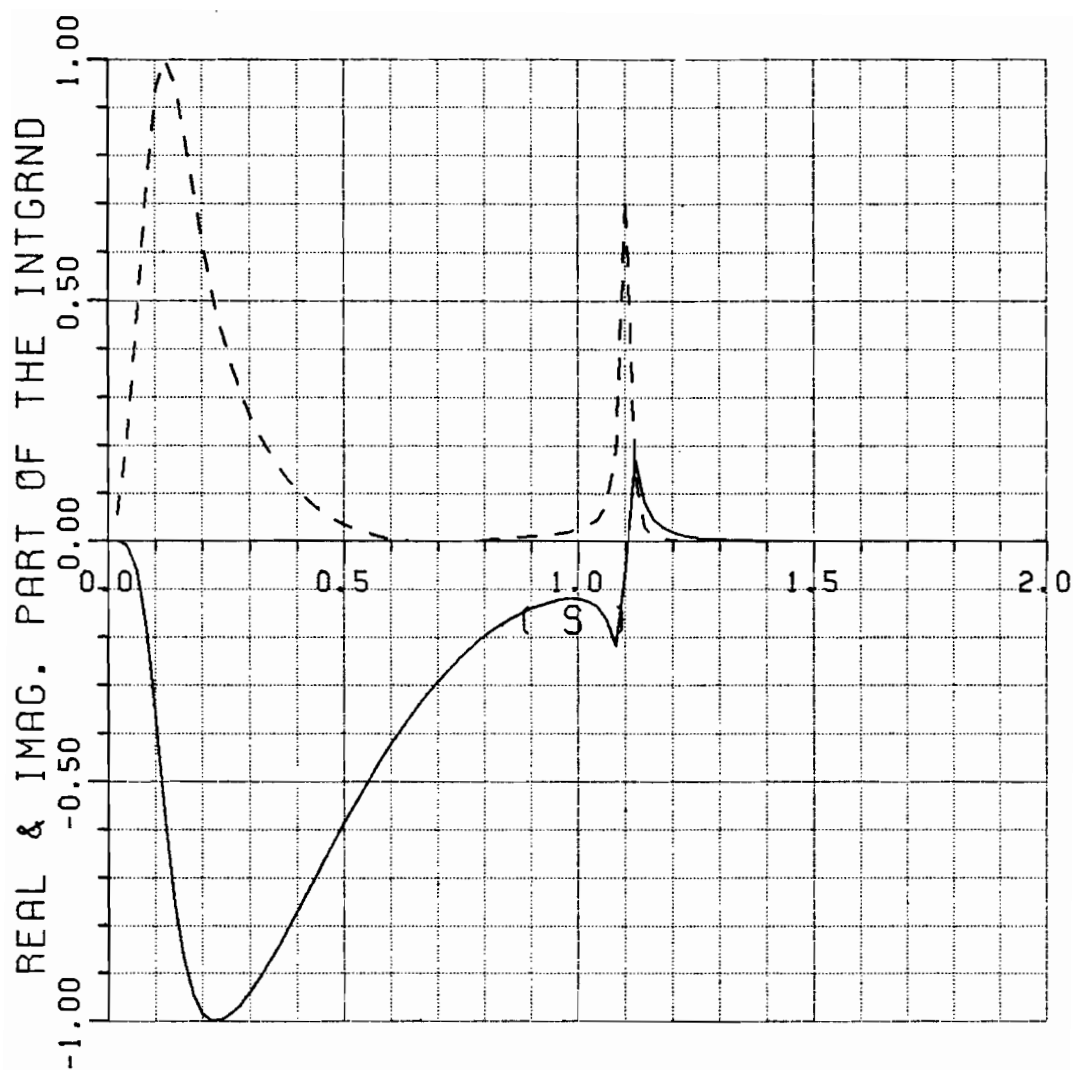
Steepest Descent Path

---- Real Part

—— Imag. Part

$$(c) \quad \rho = 2.0 \lambda_0$$

Figure 4.9. (Continued).



$$\epsilon_r = 10.2$$

$$K_0 d = 0.5 \quad (d/\lambda_0 = 0.0795)$$

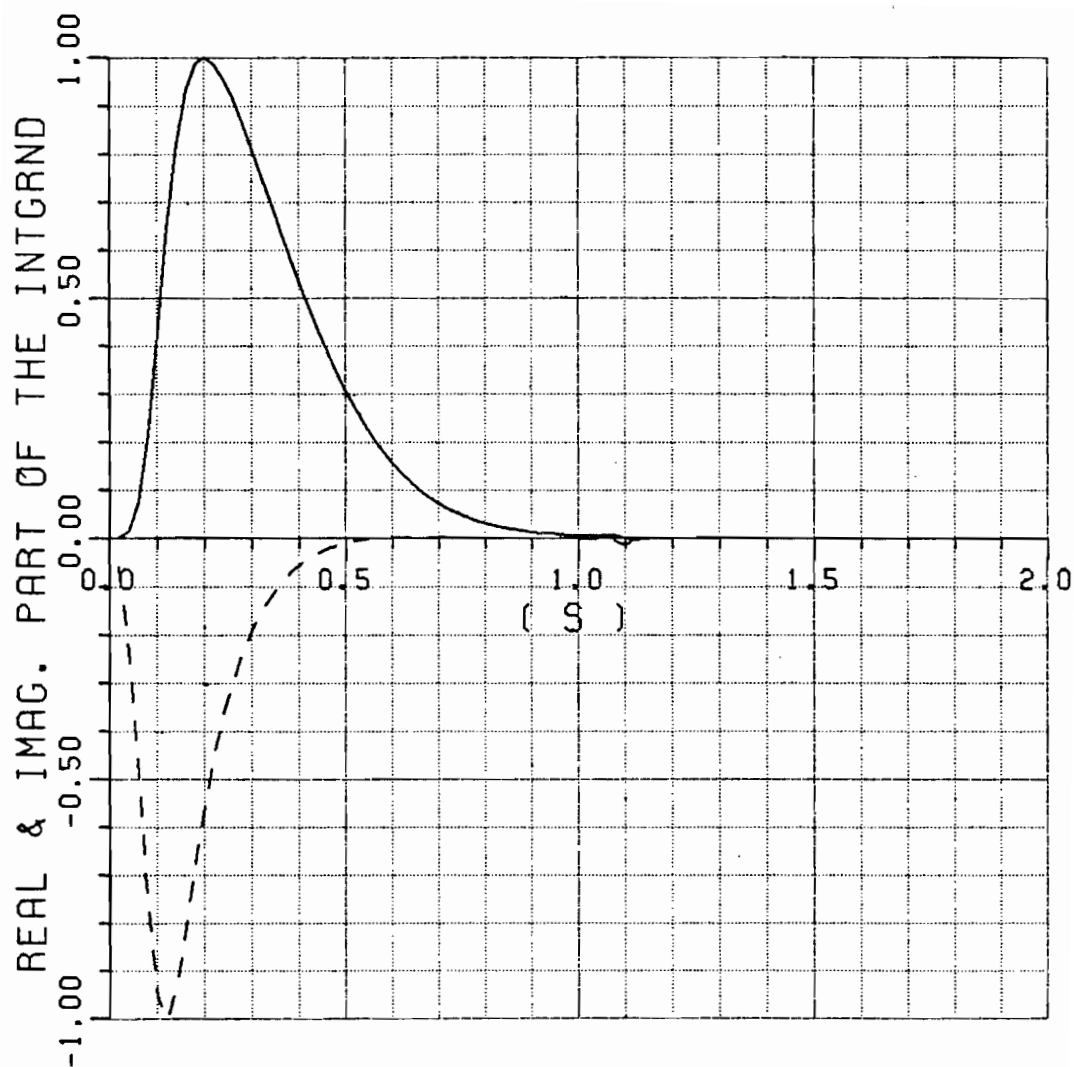
Steepest Descent Path

---- Real Part

—— Imag. Part

$$(a) \quad \rho = 0.5 \lambda_0$$

Figure 4.10. Integrand of W in the Equation (4.37) versus s.



$$\epsilon_r = 10.2$$

$$K_0 d = 0.5 \quad (d/\lambda_0 = 0.0795)$$

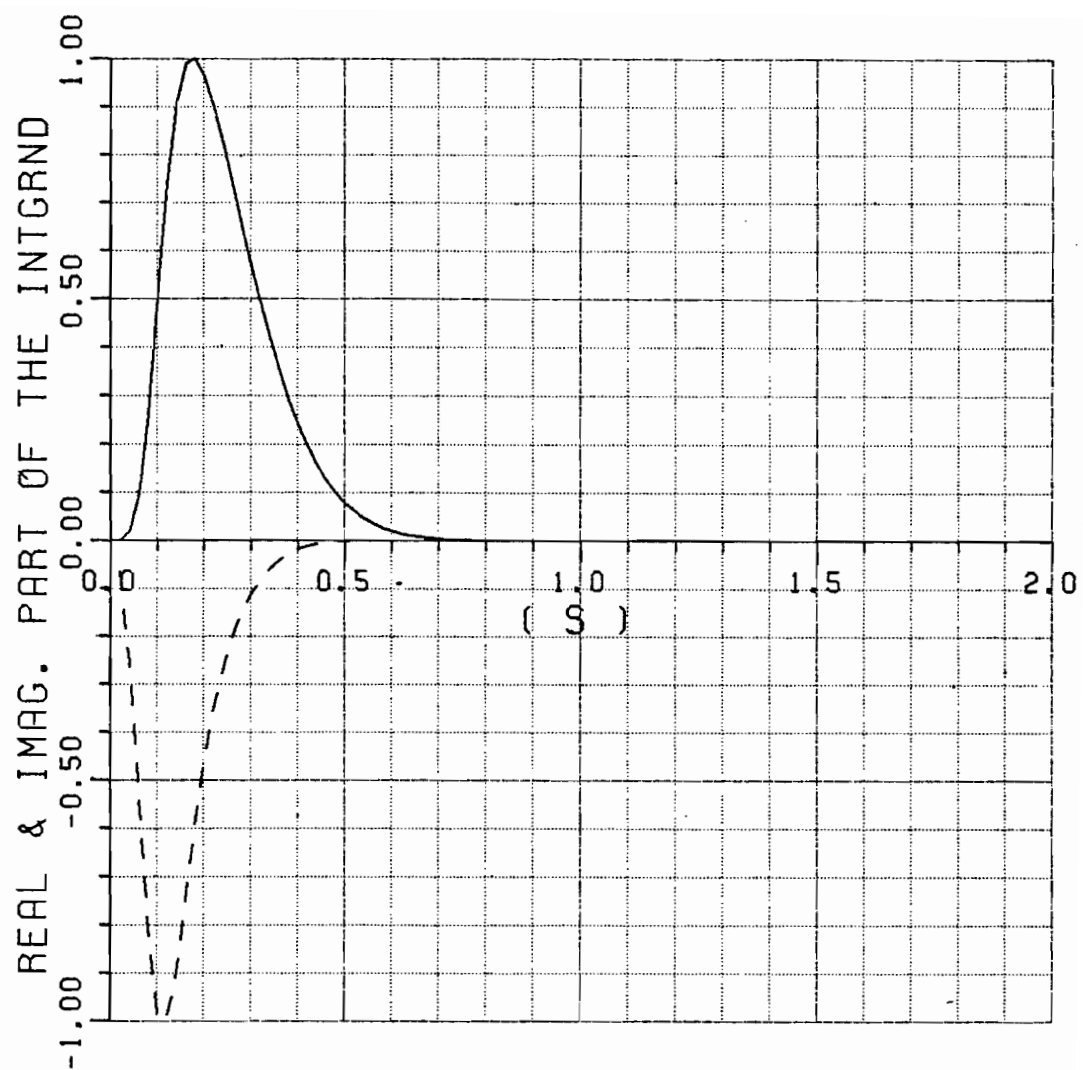
Steepest Descent Path

---- Real Part

—— Imag. Part

$$(b) \quad \rho = \lambda_0$$

Figure 4.10. (Continued).



$$\epsilon_r = 10.2$$

$$K_0 d = 0.5 \quad (d/\lambda_0 = 0.0795)$$

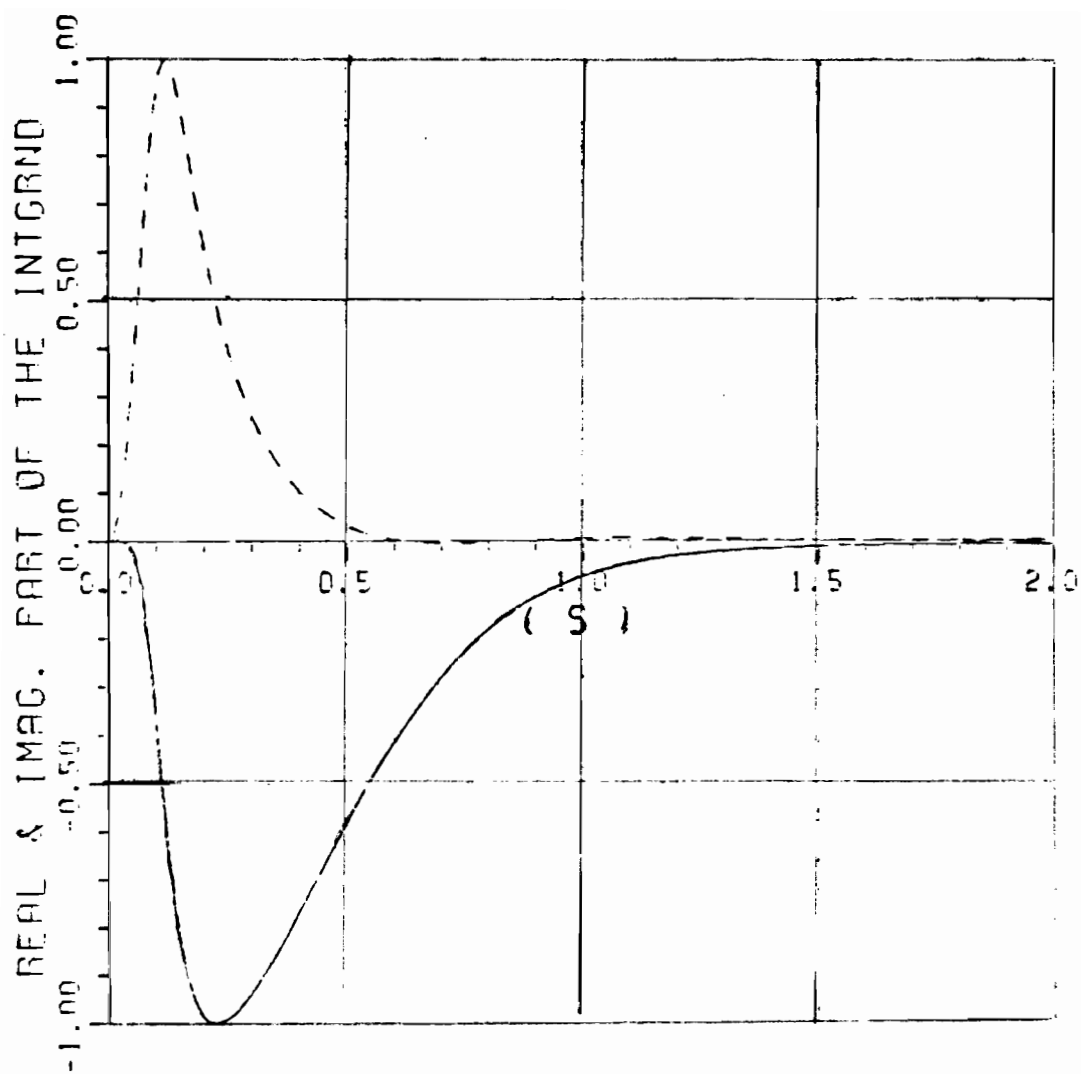
Steepest Descent Path

---- Real Part

—— Imag. Part

$$(c) \quad \rho = 2.0 \lambda_0$$

Figure 4.10. (Continued).



$$\epsilon_r = 10.2$$

$$K_0 d = 0.5 \quad (d/\lambda_0 = 0.0795)$$

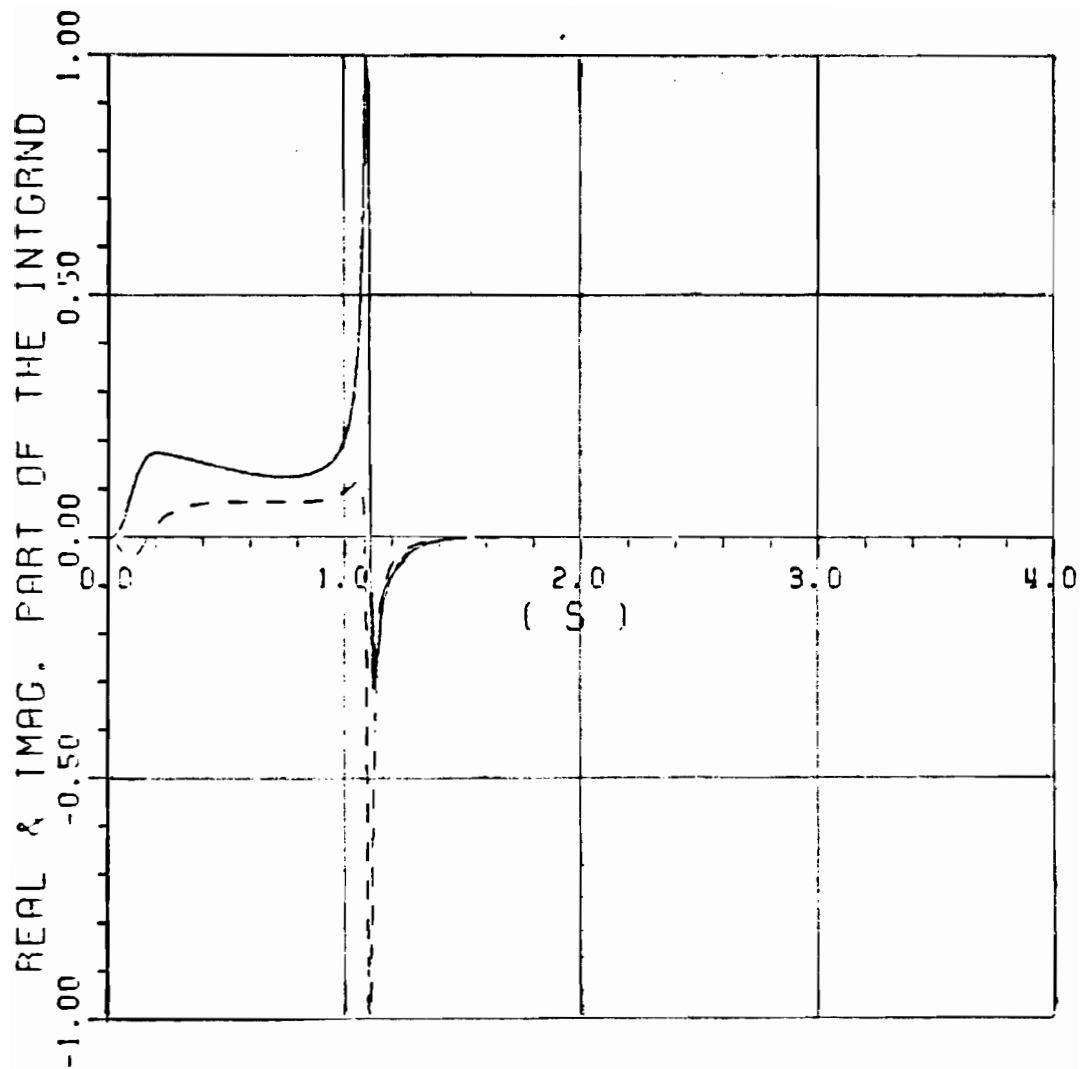
Steepest Descent Path

---- Real Part

—— Imag. Part

$$\rho = 0.5 \lambda_0$$

Figure 4.11. Integrand of W in the Equation (4.37) versus s , with closeby leaky wave singularity extracted.



$$\epsilon_r = 10.2$$

$$K_0 d = 0.5 \quad (d/\lambda_0 = 0.0795)$$

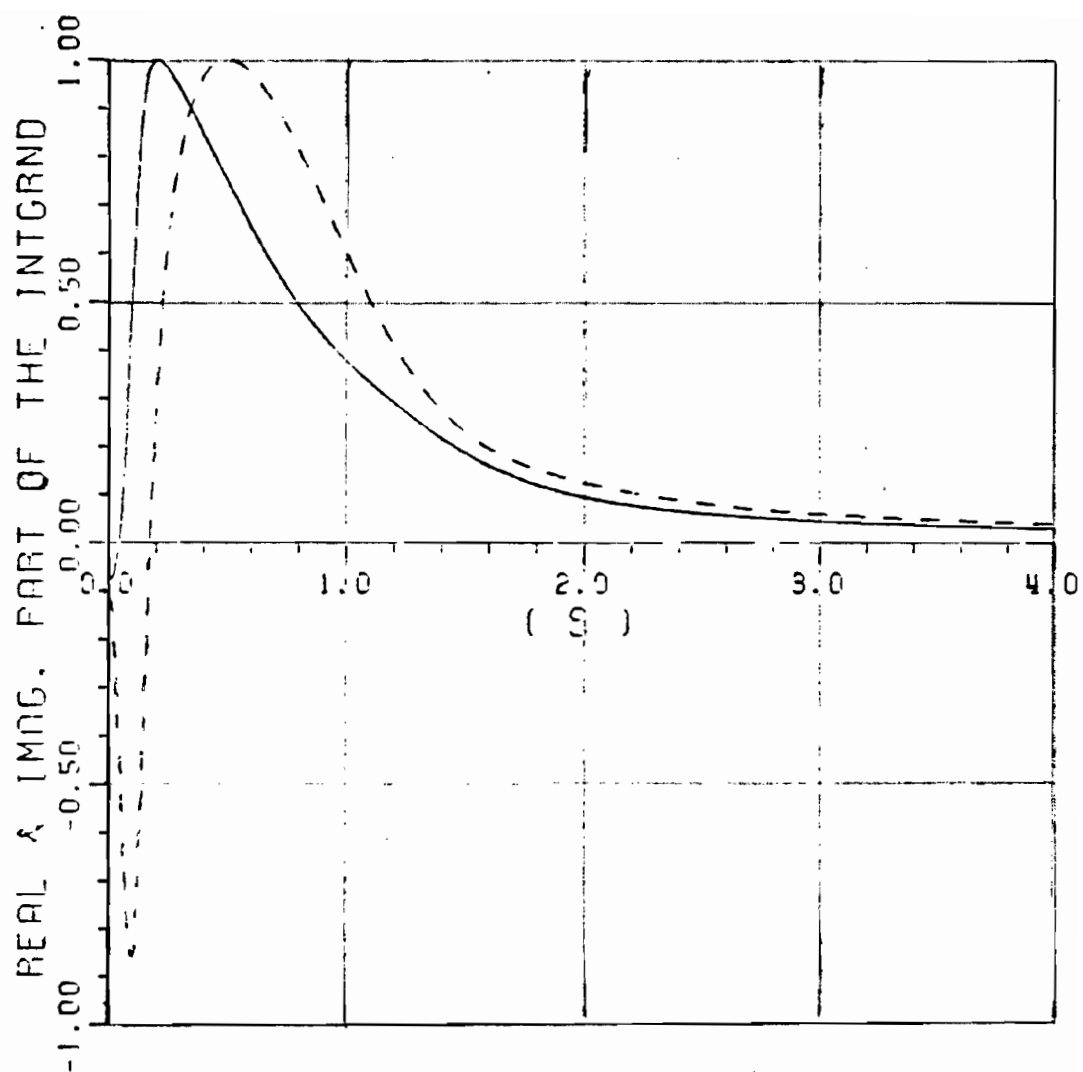
Steepest Descent Path

---- Real Part

—— Imag. Part

(a) $\rho = 0.1 \lambda_0$

Figure 4.12. Integrand of W in the Equation (4.37) versus s.



$$\epsilon_r = 10.2$$

$$K_0 d = 0.5 \quad (d/\lambda_0 = 0.0795)$$

Steepest Descent Path

----- Real Part

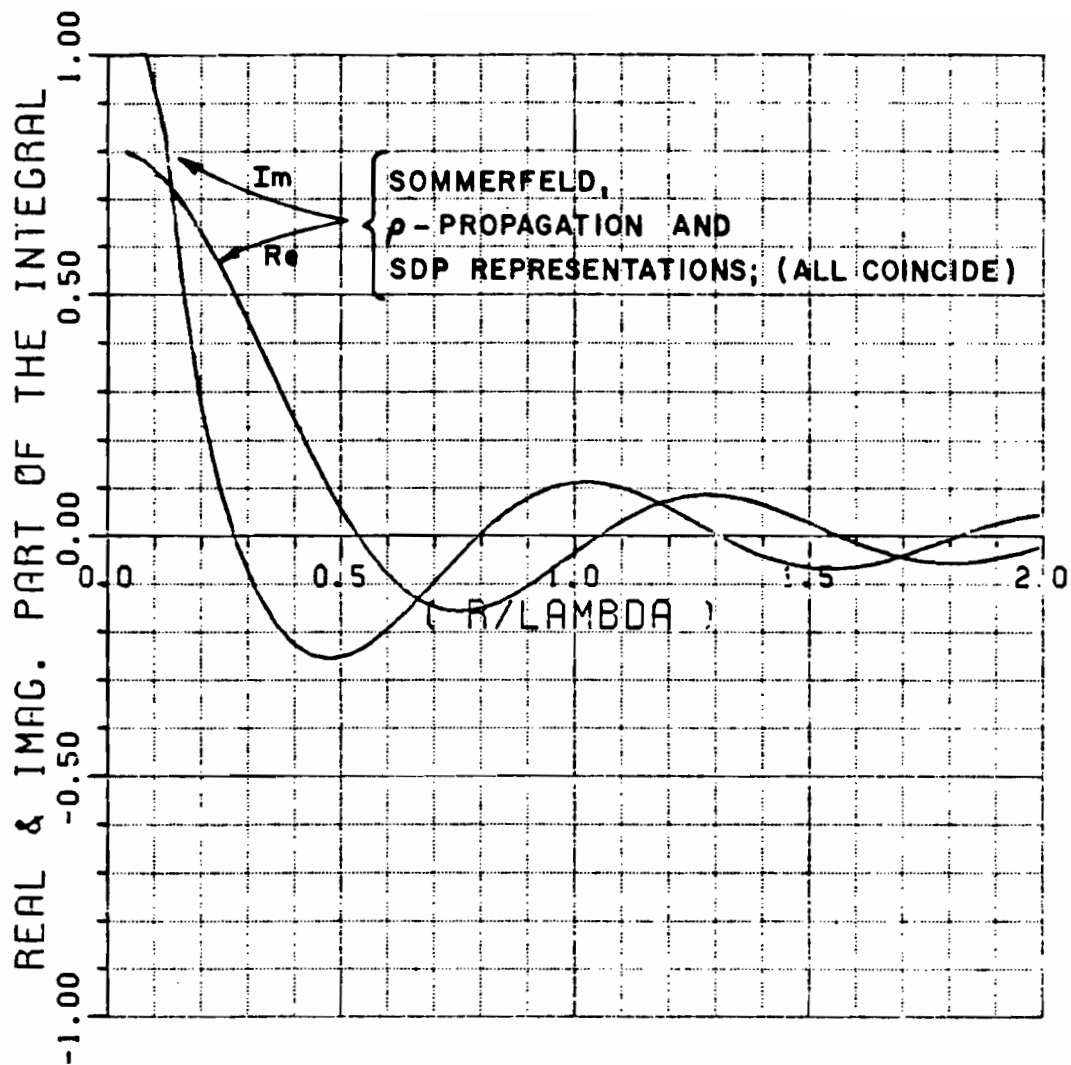
——— Imag. Part

$$(b) \quad \rho = 0.1 \lambda_0$$

Figure 4.12. Integrand of W in the Equation (4.37) versus s, with close by leaky wave singularity extracted.

Figures 4.13 and 4.14 depict the typical values of (U) and (W) versus ρ/λ_0 , which have been calculated from three different representations; namely, by the standard Sommerfeld representation, (with the envelope removal technique); by the method corresponding to the radially propagating representation; and by the steepest descent path (SDP) representation, respectively. It is apparent from the figures that all three different methods give rise to the same numerical results, (irregularities for very small lateral separations of $\rho/\lambda_0 < 0.1$ in the SDP based evaluation are due to the small number of sampling points in the integration routine). Nevertheless, as it has been shown in the previous figures, the integrands in these three different approaches are quite different; therefore, the computational costs are very much different for a given achievable accuracy and for a given ρ/λ_0 .

In the next chapter, a uniform closed form asymptotic result for the microstrip Green's function will be presented. It will be shown that the new asymptotic solution is surprisingly very accurate even for very small separation of source and field points.



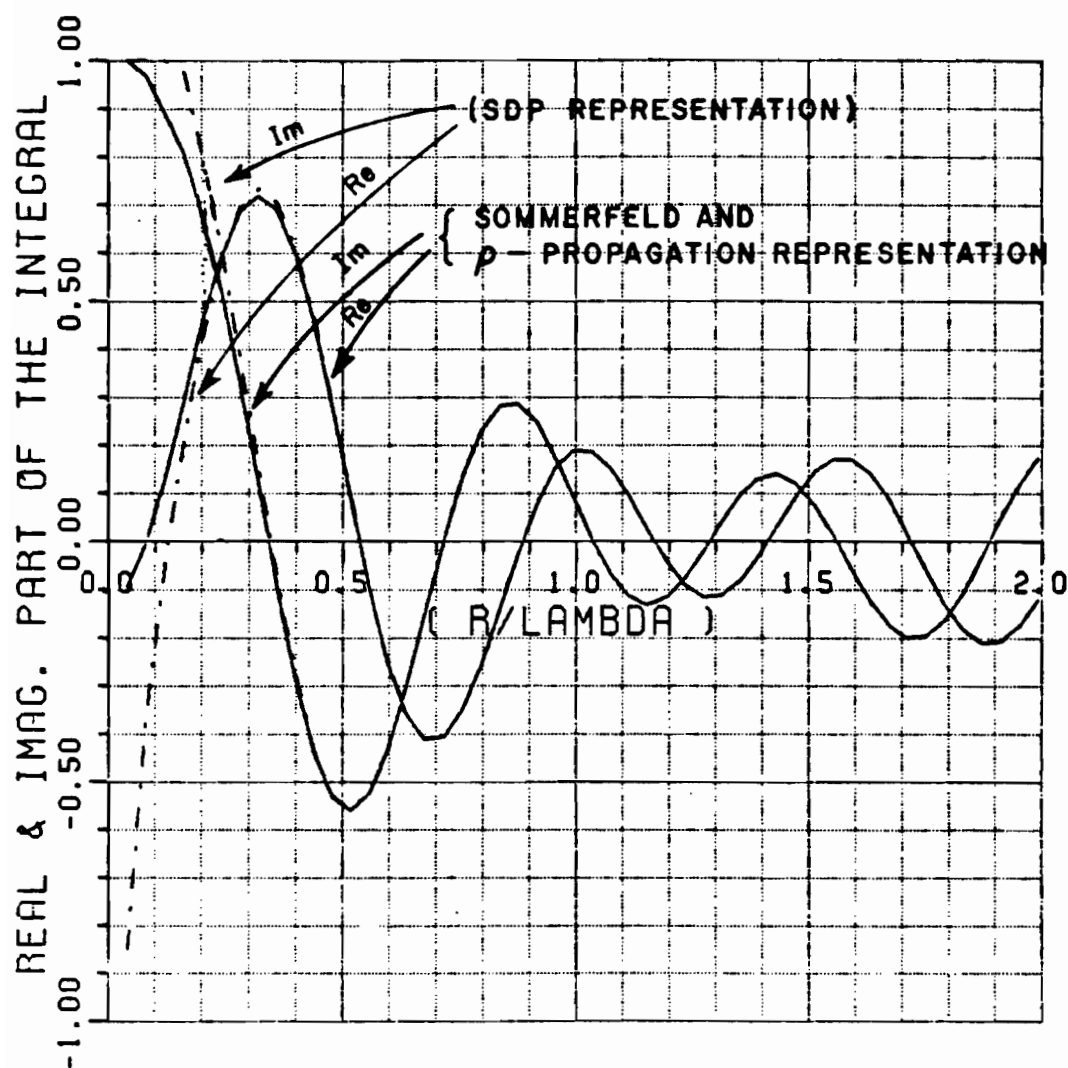
$$\epsilon_r = 10.2$$

$$K_0 d = 0.5 \quad (d/\lambda_0 = 0.0795)$$

Three Different Representations

— Sommerfeld
 ---- ρ -propagation
 -.- Steepest Descent Path

Figure 4.13. Typical values of U versus ρ/λ_0 from three different representations, Sommerfeld representation, Equation (3.46), ρ -propagation representation, Equation (4.11), and steepest descent path representation, Equation (4.35).



$$\epsilon_r = 10.2$$

$$K_0 d = 0.5 \quad (d/\lambda_0 = 0.0795)$$

Three Different Representations

— Sommerfeld
 ---- ρ -propagation
 -... Steepest Descent Path

Figure 4.14. Typical values of $(U - \frac{\epsilon_r}{\epsilon_r - 1} W)$ versus ρ/λ_0 from three different representations, Sommerfeld representation, Equations (3.36), (3.48), ρ -propagation representation, Equations (4.11), (4.13), and steepest descent path representation, Equations (4.35), (4.37).

CHAPTER V

UNIFORM ASYMPTOTIC CLOSED FORM REPRESENTATION OF THE SINGLE LAYER MICROSTRIP DYADIC SURFACE GREEN'S FUNCTION

This chapter deals with the development of an approximate asymptotic form representation for the microstrip dyadic surface Green's function which remains valid for any range of lateral separation between the source and observation points as long as it excludes the region in the neighborhood of the source point. This asymptotic solution remains uniformly valid within the surface and leaky wave poles transition regions.

As mentioned in the previous chapter, the ρ -propagation representation can be used as a starting point to find a closed form approximate (but accurate) solution of the dyadic microstrip surface Green's function which remains valid in almost the entire range of $(k_0\rho)$. The details of this asymptotic development are shown below.

Consider the integral I, which has the following functional form.

$$I = \int_{-\infty}^{\infty} F(\zeta) H_0^2(\rho \sqrt{k_0^2 - \zeta^2}) e^{-j\zeta z} d\zeta, \quad (5.1)$$

in which $(k_0\rho)$ is assumed to be a large parameter. Although in general a conventional procedure can be used to construct a uniform asymptotic

expansion of the integral in (5.1) from the formal saddle point integration technique formulated in (4.16) through (4.32) and Appendix H, one can instead use a more straight forward procedure for this special problem. One may assume in general that $F(\zeta)$ in (5.1) has a finite number of poles (surface wave and leaky wave poles) at ζ_p 's, then one can write

$$F(\zeta) = \sum_p \frac{R_F(\zeta_p)}{\zeta - \zeta_p} = \sum_n a_n \zeta^n \quad (5.2)$$

where $R_F(\zeta_p)$ is the residue of $F(\zeta)$ at $\zeta = \zeta_p$, and the radius of convergence of the series is uninfluenced by the presence of the poles so,

$$\begin{aligned} I \cong & \int_{-\infty}^{\infty} \sum_n a_n \zeta^n H_0^2(k_0 \rho \sqrt{1 - \frac{\zeta^2}{k_0^2}}) e^{-j\zeta z} d\zeta \\ & + \sum_p R_F(\zeta_p) \int_{-\infty}^{\infty} \frac{H_0^2(k_0 \rho \sqrt{1 - \frac{\zeta^2}{k_0^2}})}{\zeta - \zeta_p} e^{-j\zeta z} d\zeta \end{aligned} \quad (5.3)$$

or

$$\begin{aligned} I \sim & k_0 \sum_n a_n \frac{1}{(-j)^n} \frac{\partial}{\partial z^n} \int_{-\infty}^{\infty} H_0^2(k_0 \rho \sqrt{1 - \eta^2}) e^{-jk_0 \eta z} d\eta \\ & + \sum_p R_F(\zeta_p) \int_{-\infty}^{\infty} \frac{H_0^2(k_0 \rho \sqrt{1 - \eta^2})}{\eta - (\frac{\zeta_p}{k_0})} d\eta, \end{aligned} \quad (5.4)$$

where use has been made from the change of variable

$$\zeta = k_0 n \quad ; \quad d\zeta = k_0 dn \quad . \quad (5.5)$$

But the first integral can be evaluated in closed form,

$$\int_{-\infty}^{\infty} H_0^2(k_0 \rho \sqrt{1-n^2}) e^{-jk_0 n z} dn = 2j \frac{e^{-jk_0 \sqrt{\rho^2+z^2}}}{k_0 \sqrt{\rho^2+z^2}} \quad . \quad (5.6)$$

It is interesting to note that an asymptotic expansion of the preceding integral for large $(k_0 \sqrt{\rho^2+z^2})$ gives exactly the same result; all higher order terms in $(\frac{1}{k_0 \sqrt{\rho^2+z^2}})$ identically vanish. The second integral in (5.4) has a uniform asymptotic expansion for large parameter $(k_0 \rho)$. The detailed derivation of this asymptotic expansion has been carried out in Appendix I, (see (I.29)); and only the final result will be given below,

$$\int_{-\infty}^{\infty} \frac{H_0^2(k_0 \rho \sqrt{1-n^2})}{n - (\frac{\zeta_p}{k_0})} e^{-jk_0 n z} dn \sim M(k_0 \rho, \zeta_p) \quad , \quad (5.7)$$

where

$$\begin{aligned} M(k_0 \rho, \zeta_p) &\equiv 2\pi j [N(\zeta_p)] H_0^2(\rho \sqrt{k_0^2 - \zeta_p^2}) e^{-j\zeta_p z} \\ &\quad - 2j \frac{e^{-jk_0 \rho}}{k_0 \rho \eta_p} \cdot (1 + \frac{j}{8k_0 \rho}) \\ &\quad \left[1 - \frac{\eta_p}{\sqrt{2}} \frac{1}{\sqrt{1-\eta_p^2} \sqrt{1-\sqrt{1-\eta_p^2}}} (1 - F(\mp \sqrt{k_0 \rho (1-\sqrt{1-\eta_p^2})})) \right], \quad (5.8) \end{aligned}$$

where η_p is defined as,

$$\eta_p = \frac{z_p}{k_0} \quad , \quad (5.9)$$

and

$$F(\pm \sqrt{x}) = \pm \sqrt{x} e^{jx} \int_{\pm \sqrt{x}}^{\infty} e^{-ju^2} du \quad (5.10)$$

is called the transition function (see discussion below (H.50) in Appendix H), which makes the present asymptotic development uniformly valid across the surface wave and leaky wave poles transition regions of I as will be explained later on. It is noted that,

$$N(z_p) = \begin{cases} +1 \\ -1 \\ 0 \end{cases} \quad , \quad (5.11)$$

where the proper value of $N(z_p)$, (0, -1 or +1) depends on the location of the pole in the complex z plane (see (I.14), (I.15) and Figure I.1). If the following condition holds (the pole gets very close to the saddle point):

$$\eta_p = \frac{z_p}{k_0} \ll 1 \quad , \quad (5.12)$$

the expression of $M(k_0 \rho, p)$ given in (5.8) simplifies (see Appendix I, (I.33)), to

$$M(k_0 \rho, z_p) \cong 2\pi j [N(z_p)] H_0^2(\rho \sqrt{k_0^2 - z_p^2}) e^{-jz_p z} \\ - 2jk_0 \frac{e^{-jk_0 \rho}}{k_0 \rho z_p} \left(1 + \frac{j}{8k_0 \rho}\right) F\left(\mp \frac{z_p}{k_0} \sqrt{\frac{k_0 \rho}{2}}\right) \quad , \quad (5.13)$$

where use has been made from the Taylor expansion of $(1-x)^n$ around zero, that is

$$(1-x)^n \approx 1-nx \quad . \quad (5.14)$$

Therefore in (5.8) the first two terms inside the bracket cancels,

$$\begin{aligned} 1 - \frac{\eta_p}{\sqrt{2}} \frac{1}{\sqrt{1-\eta_p^2}} &\approx 1 - \frac{\eta_p}{\sqrt{2}} \frac{1}{(1-\frac{1}{4}\eta_p^2)} \frac{1}{\frac{\eta_p}{\sqrt{2}}} \\ &\approx \frac{-\frac{1}{4}\eta_p^2}{1 - \frac{1}{4}\eta_p^2} \bigg|_{\eta_p \ll 1} \approx 0 \quad . \end{aligned} \quad (5.15)$$

From the above discussion the uniform asymptotic approximation of I given in (5.1) can be written as

$$\begin{aligned} I \sim k_0 \sum_n a_n \frac{1}{(-j)^n} \frac{\partial}{\partial z^n} \left(2j \frac{e^{-jk_0\sqrt{\rho^2+z^2}}}{k_0\sqrt{\rho^2+z^2}} \right) \\ + \sum_p R_F(\zeta_p) M(k_0\rho, \zeta_p) \end{aligned} \quad (5.16)$$

where $M(k_0\rho, \zeta_p)$ is introduced in (5.8) and for $(\zeta_p/k_0) \ll 1$ is approximated by (5.13).

The technique discussed above for evaluating I is utilized to find the uniform asymptotic approximation of the microstrip dyadic surface Green's function given in (3.32)-(3.37) when $k_0\rho \gg 1$. First it is noted that this Green's function is given in terms of U , V and W whose

ρ -propagation representations have been given in (4.7)-(4.9). The explicit uniform asymptotic approximation for these U , V and W functions can be found first and the uniform asymptotic form of the microstrip surface Green's function can be obtained directly from the forms via (3.32)-(3.37). Thus the uniform asymptotic approximations of U , V and W are:

$$\begin{aligned}
 U = & \left[\left(\frac{R_U(z_{p''}^{SW})}{z_{p''}^{SW}} + \frac{R_U(z_{p''}^{\ell W})}{z_{p''}^{\ell W}} \right) k_0 I_0 + \right. \\
 & \left(\frac{1}{2Y(0)} + \frac{R_U(z_{p''}^{SW})}{(z_{p''}^{SW})^2} + \frac{R_U(z_{p''}^{\ell W})}{(z_{p''}^{\ell W})^2} \right) k_0^2 I_1 + \\
 & \left(\frac{-1}{2Y^2(0)} + \frac{R_U(z_{p''}^{SW})}{(z_{p''}^{SW})^3} + \frac{R_U(z_{p''}^{\ell W})}{(z_{p''}^{\ell W})^3} \right) k_0^3 I_2 + \\
 & + R_U(z_{p''}^{SW}) M(k_0^0, z_{p''}^{SW}) + R_U(z_{p''}^{\ell W}) M(k_0^0, z_{p''}^{\ell W}) \\
 & \left. + 2\pi j \sum_{n''} \text{Res}_U(z_{n''}) \right] , \tag{5.17}
 \end{aligned}$$

$$\begin{aligned}
 V = & \left[\left(\frac{R_V(\zeta_{p'}^{SW})}{\zeta_{p'}^{SW}} + \frac{R_V(\zeta_{p'}^{LW})}{\zeta_{p'}^{LW}} \right) k_0 I_0 + \right. \\
 & \left(-\frac{j}{2} + \frac{R_V(\zeta_{p'}^{SW})}{(\zeta_{p'}^{SW})^2} + \frac{R_V(\zeta_{p'}^{LW})}{(\zeta_{p'}^{LW})^2} \right) k_0^2 I_1 + \\
 & \left(\frac{j}{2Z(0)} + \frac{R_V(\zeta_{p'}^{SW})}{(\zeta_{p'}^{SW})^3} + \frac{R_V(\zeta_{p'}^{LW})}{(\zeta_{p'}^{LW})^3} \right) k_0^3 I_2 \\
 & + R_V(\zeta_{p'}^{SW}) M(k_0 \rho, \zeta_{p'}^{SW}) + R_V(\zeta_{p'}^{LW}) M(k_0 \rho, \zeta_{p'}^{LW}) \\
 & \left. + 2\pi j \sum_{n,1} \text{Res}_V(\zeta_{n,1}) \right] , \tag{5.18}
 \end{aligned}$$

and

$$\begin{aligned}
 W = & \left[\left(\frac{R_W(z_W^{SW})}{z_W^{SW}} + \frac{R_W(z_W^{LW})}{z_W^{LW}} \right) k_0 I_0 + \right. \\
 & \left(\frac{R_W(z_W^{SW})}{(z_W^{SW})^2} + \frac{R_W(z_W^{LW})}{(z_W^{LW})^2} \right) k_0^2 I_1 + \\
 & \left(\frac{\epsilon_r}{2k_0(\epsilon_r-1)} + \frac{R_W(z_W^{SW})}{(z_W^{SW})^3} + \frac{R_W(z_W^{LW})}{(z_W^{LW})^3} \right) k_0^3 I_2 \\
 & + R_W(z_W^{SW}) M(k_0 \rho, z_W^{SW}) + R_W(z_W^{LW}) M(k_0 \rho, z_W^{LW}) \\
 & \left. + 2\pi j \sum_{n''} \text{Res}_W(z_{n''}) + 2\pi j \sum_{n'} \text{Res}_W(z_{n'}) \right] , \quad (5.19)
 \end{aligned}$$

where

$$Y(o) = -jk_0 \sqrt{\epsilon_r - 1} \cotan(k_0 d \sqrt{\epsilon_r - 1}) \quad , \quad (5.20)$$

$$Z(o) = jk_0 \frac{\sqrt{\epsilon_r - 1}}{\epsilon_r} \tan(k_0 d \sqrt{\epsilon_r - 1}) \quad , \quad (5.21)$$

$$I_0 = \int_{-\infty}^{\infty} H_0^2(k_0 \rho \sqrt{1 - \zeta^2}) e^{-jk_0 \zeta z} d\zeta = 2j \frac{e^{-jk_0 r}}{k_0 r} \quad , \quad (5.22)$$

$$I_1 = \int_{-\infty}^{\infty} H_0^2(k_0 \rho \sqrt{1 - \zeta^2}) e^{-jk_0 \zeta z} \zeta d\zeta = 2j \left(\frac{z}{r}\right) \frac{e^{-jk_0 r}}{k_0 r} \left(1 + \frac{1}{jk_0 r}\right) \quad , \quad (5.23)$$

$$\begin{aligned} I_2 &= \int_{-\infty}^{\infty} H_0^2(k_0 \rho \sqrt{1 - \zeta^2}) e^{-jk_0 \zeta z} \zeta^2 d\zeta \\ &= \frac{-2e^{-jk_0 r}}{(k_0 r)^2} \left[\left(1 + \frac{1}{jk_0 r}\right) \left(1 - jk_0 z \left(\frac{z}{r}\right) - 2\left(\frac{z}{r}\right)^2\right) - \frac{1}{jk_0 r} \left(\frac{z}{r}\right)^2 \right] \quad , \quad (5.24) \end{aligned}$$

and one assumes that

$$r = \sqrt{\rho^2 + z^2} \quad ; \quad z = 0 \quad , \quad (5.25)$$

which indicates that source and observation points both lie on the dielectric substrate (see Figure 1.1). $R_T(\zeta_p^{sw})$, $R_T(\zeta_p^{lw})$ with $(T=U, V \text{ and } W)$ are the residues of the surface wave poles (ζ_p^{sw}) and leaky wave poles (ζ_p^{lw}) associated with the integrands of U , V and W , respectively obtained excluding the factor $(H_0^2(\rho \sqrt{k_0^2 - \zeta^2}) e^{-j\zeta z})$ and explicitly are given in (G.14), (G.17), (G.19) and (G.21). Once again, $M(k_0 \rho, \zeta_p)$ is

introduced in (5.8) and for $\frac{\zeta_p}{k_0} \ll 1$ (which holds for the first TM surface wave pole of thin substrates) is approximated via (5.13). It is also noted that $N(\zeta_p^{SW})$ in (5.8) and (5.13) in the expression of $M(k_0\rho, \zeta_p^{SW})$ associated with the surface wave pole ζ_p^{SW} is always zero; since the SDP will never capture the surface wave poles for the source and observation points lie on the grounded dielectric slab.

In arriving at the above expressions, use has been made of a power series expansion about $\zeta=0$ for the integrands of U, V and W (excluding the factor $(H_0^2(\rho\sqrt{k_0^2-\zeta^2}) e^{-j\zeta z})$) in Equations (4.7) through (4.9); and use is also made of Equations (5.6), (5.7) and (5.8). One notes that the power series expansions around $\zeta=0$ involve the following:

$$\frac{\zeta}{\zeta - j \frac{(\epsilon_r - 1)k_0^2 - \zeta^2}{\epsilon_r} \cotand \frac{(\epsilon_r - 1)k_0^2 - \zeta^2}{\epsilon_r}} \approx \frac{\zeta}{Y(0)} \left(1 - \frac{\zeta}{Y(0)} + O(\zeta^2) + \dots \right) \quad (5.26)$$

$$\frac{\frac{(\epsilon_r - 1)k_0^2 - \zeta^2}{\epsilon_r} \tan d \frac{(\epsilon_r - 1)k_0^2 - \zeta^2}{\epsilon_r}}{\zeta + j \frac{(\epsilon_r - 1)k_0^2 - \zeta^2}{\epsilon_r} \tan d \frac{(\epsilon_r - 1)k_0^2 - \zeta^2}{\epsilon_r}} \approx -j\zeta \left(1 - \frac{\zeta}{Z(0)} + O(\zeta^2) + \dots \right) \quad (5.27)$$

$$\begin{aligned}
& \frac{\zeta}{(\zeta - j\sqrt{(\epsilon_r - 1)k_0^2 - \zeta^2} \cot \alpha \text{ and } \sqrt{(\epsilon_r - 1)k_0^2 - \zeta^2})(\zeta + j \frac{\sqrt{(\epsilon_r - 1)k_0^2 - \zeta^2}}{\epsilon_r} \tan \alpha \text{ and } \sqrt{(\epsilon_r - 1)k_0^2 - \zeta^2})} \\
& \approx \zeta^2 \left(\frac{\epsilon_r}{k_0^2(\epsilon_r - 1)} + O(\zeta^3) + \dots \right) , \quad (5.28)
\end{aligned}$$

and

$$\frac{\text{Res}(\zeta_p)}{\zeta - \zeta_p} \approx - \frac{\text{Res}(\zeta_p)}{\zeta_p} \left(1 + \frac{\zeta}{\zeta_p} + \frac{\zeta^2}{\zeta_p^2} + \dots \right) . \quad (5.29)$$

The uniform closed asymptotic form of the complete planar microstrip surface dyadic Green's function of (3.32) through (3.37) can now be constructed via (5.17) through (5.19). In the above derivations, it has been assumed that one set of TE and TM surface wave poles, and likewise one set of TE and TM leaky wave poles are close to SDP. However, the method is versatile so that any number of pole singularities can be included in principle. Also it has been assumed that $z \ll \rho$; ($z \neq 0$). This condition can be relaxed by expanding the integrands not around zero but around $\zeta = \zeta_S$, where

$$\zeta_S = k_0 \cos(\gamma_S) , \quad (5.30)$$

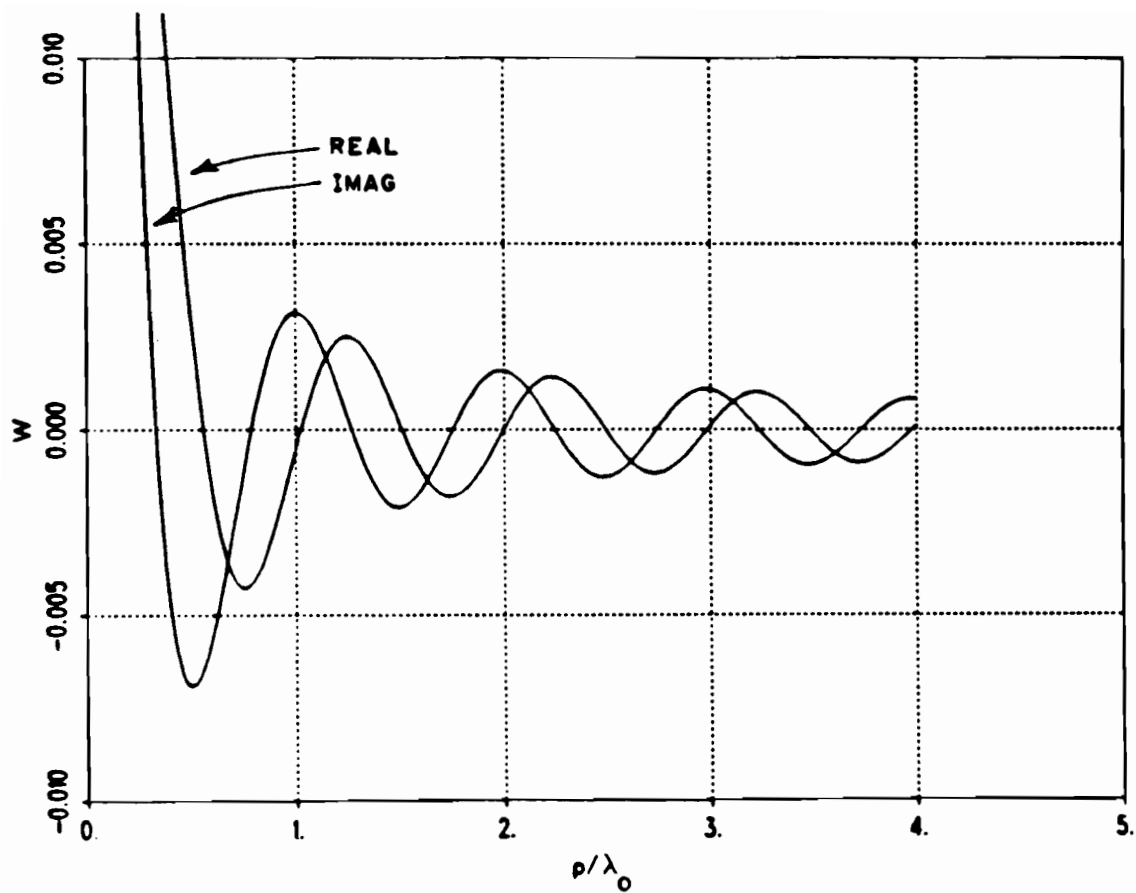
and

$$\gamma_S = \tan^{-1} \frac{z}{\rho} , \quad (5.31)$$

(see the (4.22), (4.24) and Appendix I).

It is emphasized that the method is completely general, and is simple and accurate. This method can in principle be extended to treat an arbitrary number of dielectric layers; however, care must be used for finding all of the close by singularities, including leaky wave poles.

Figures 5.1(a)-5.1(d), 5.2(a)-5.2(c) and 5.3(a)-5.3(c) show the results based on numerical integration and the uniform asymptotic representation of the function W given in (4.13) and (5.19) as a function of ρ/λ_0 for various substrate thicknesses with low and high dielectric constants ($\epsilon_r=3.25$, $\epsilon_r=9.6$ and $\epsilon_r=12.8$). The accuracy of the new representation is quite impressive. This new asymptotic solution remains valid even for field points very close to the source. The numerical behavior of U and V in (5.17) and (5.18) has also been extensively studied. It turns out that the results of the asymptotic closed form solution for U and V are at least as good as the results presented here for W . It is found that the accuracy of the new representation particularly for small lateral separations of source and field points is indeed a function of dielectric thickness and dielectric constants the dominant effect is due to space waves arising from the saddle point contribution whereas for the thick substrate with high dielectric constants, the dominant effect is due to the surface waves. It is noted that in the above examples, the uniform asymptotic approximation only requires one TM surface wave pole to be considered close to the saddle point for a very thin dielectric substrate. For denser or thicker dielectric substrate, an unexcited TE leaky wave pole also becomes close to the saddle point, and as $k_0 d \sqrt{\epsilon_r - 1}$ becomes greater



$$\epsilon_r = 3.25$$

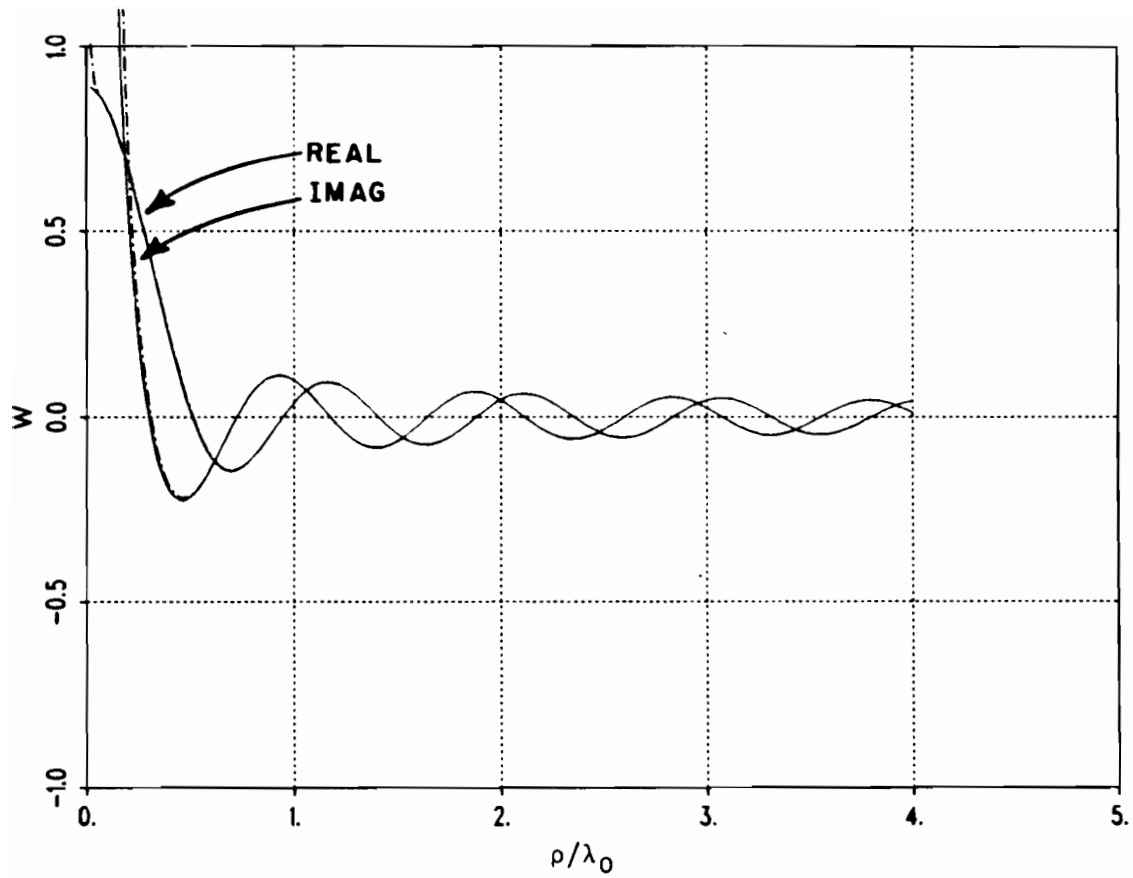
$$d/\lambda_0 = 0.01$$

— Exact Numerical Integration

--- Uniform Asymptotic Closed Form

(a)

Figure 5.1. The comparison between the exact numerical integration and the uniform asymptotic value of (W) versus ρ/λ_0 given in (4.13) and (5.19) for $\epsilon_r=3.25$ and different slab thicknesses.



$$\epsilon_r = 3.25$$

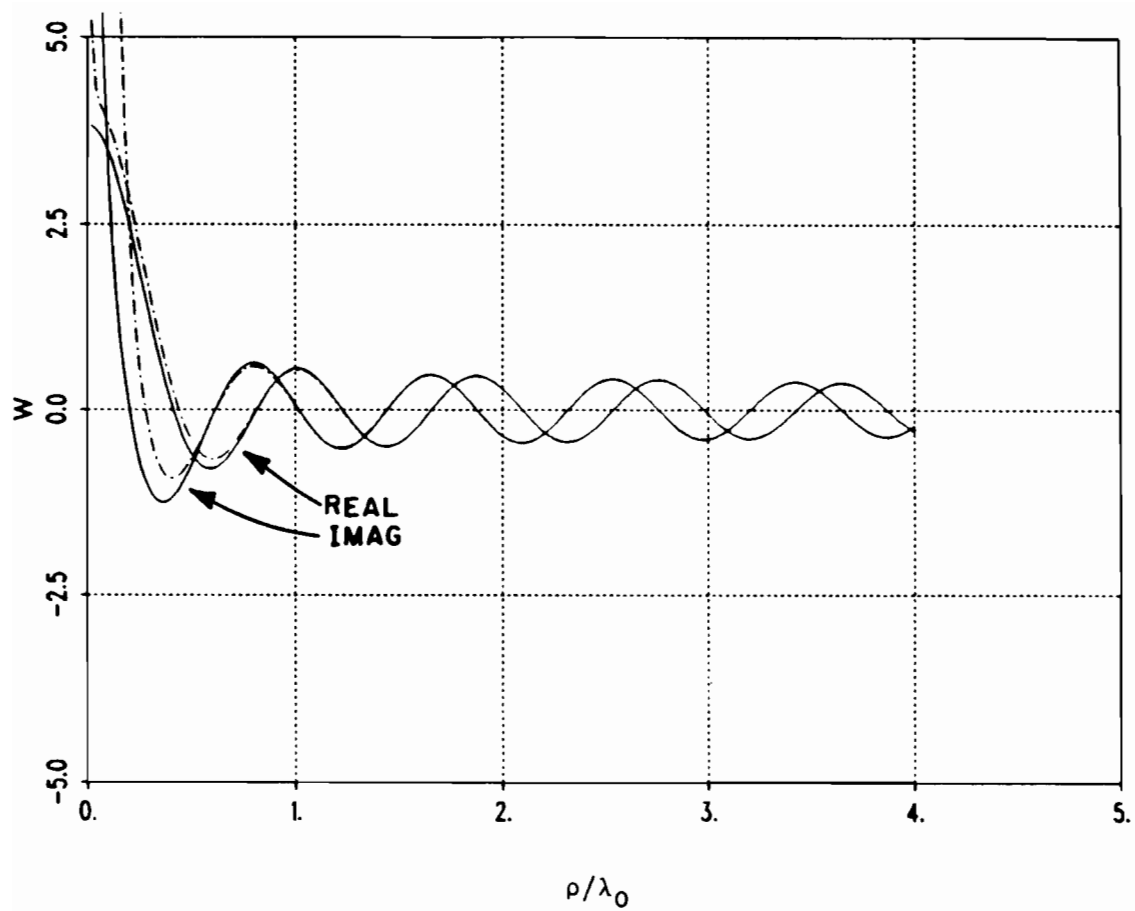
$$d/\lambda_0 = 0.05$$

— Exact Numerical Integration

- - - Uniform Asymptotic Closed Form

(b)

Figure 5.1. (continued)



$$\epsilon_r = 3.25$$

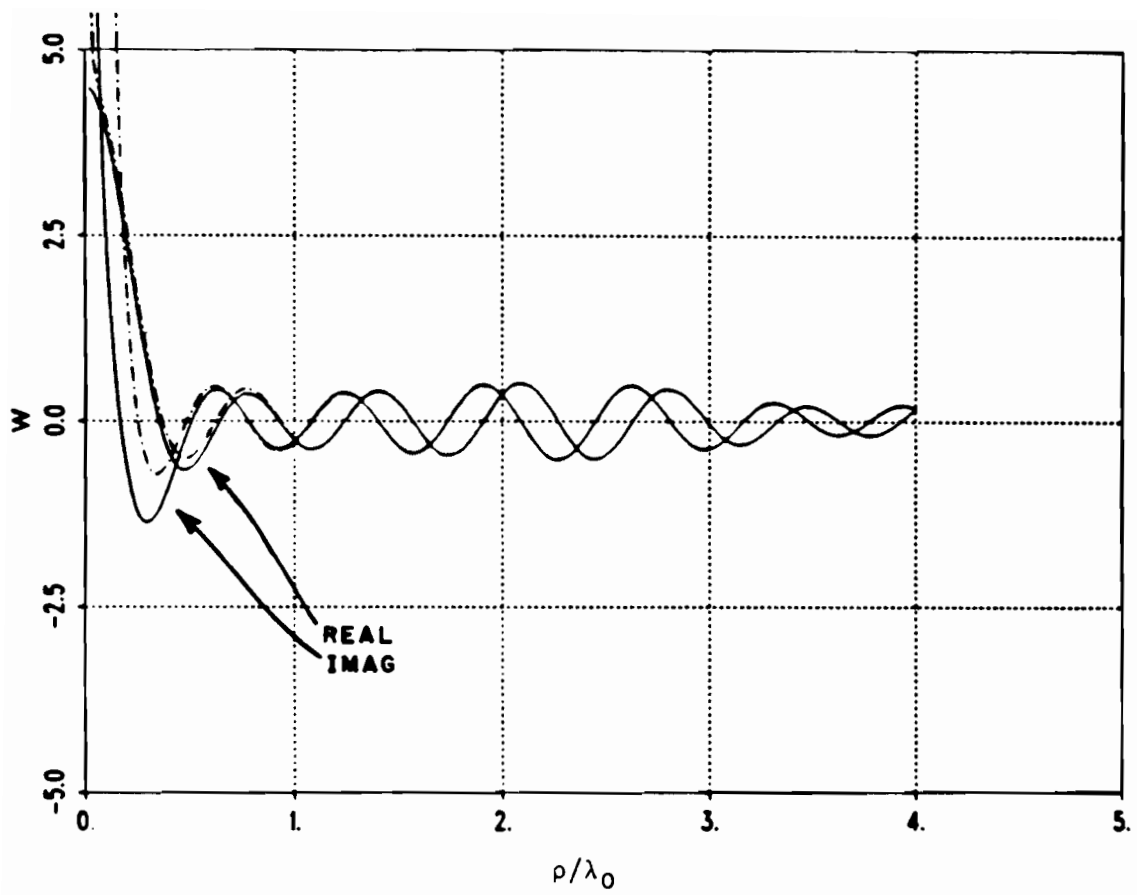
$$d/\lambda_0 = 0.1$$

— Exact Numerical Integration

- - - Uniform Asymptotic Closed Form

(c)

Figure 5.1. (continued)



$$\epsilon_r = 3.25$$

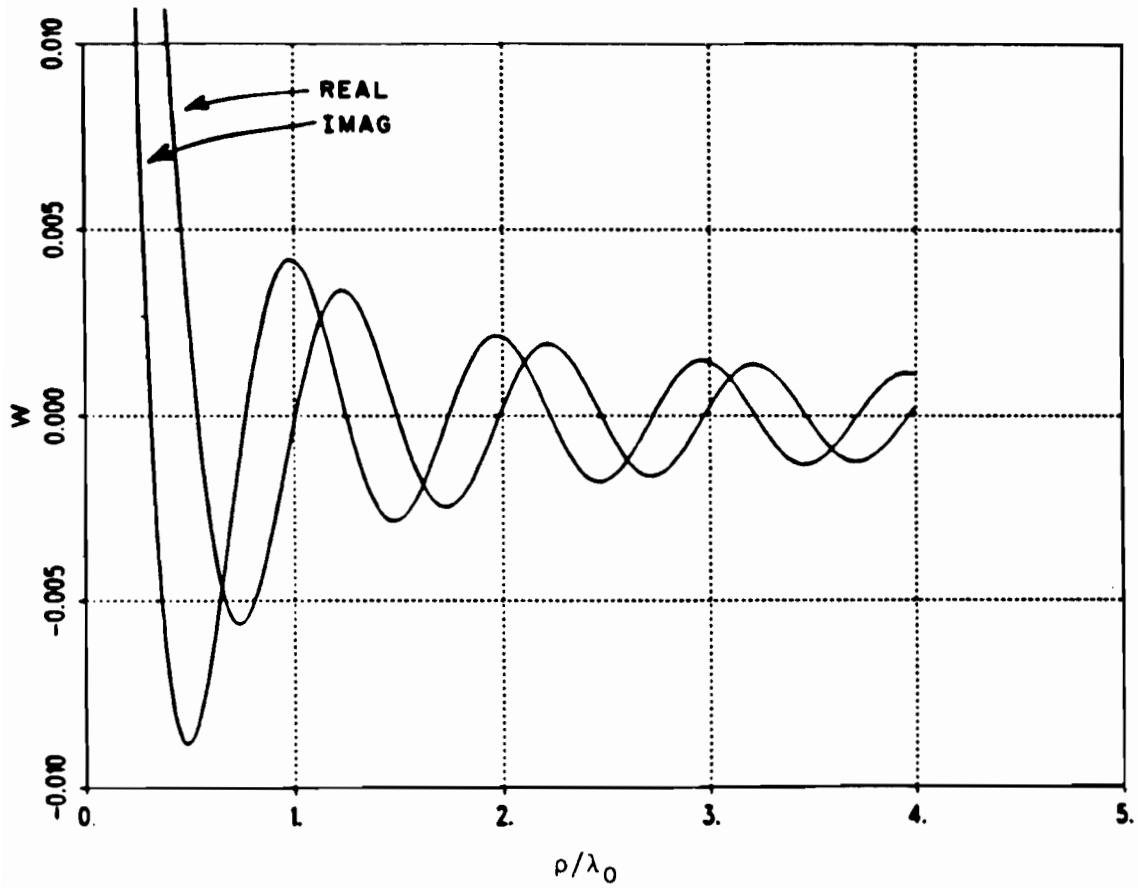
$$d/\lambda_0 = 0.2$$

— Exact Numerical Integration

- - - Uniform Asymptotic Closed Form

(d)

Figure 5.1. (continued)



$$\epsilon_r = 9.6$$

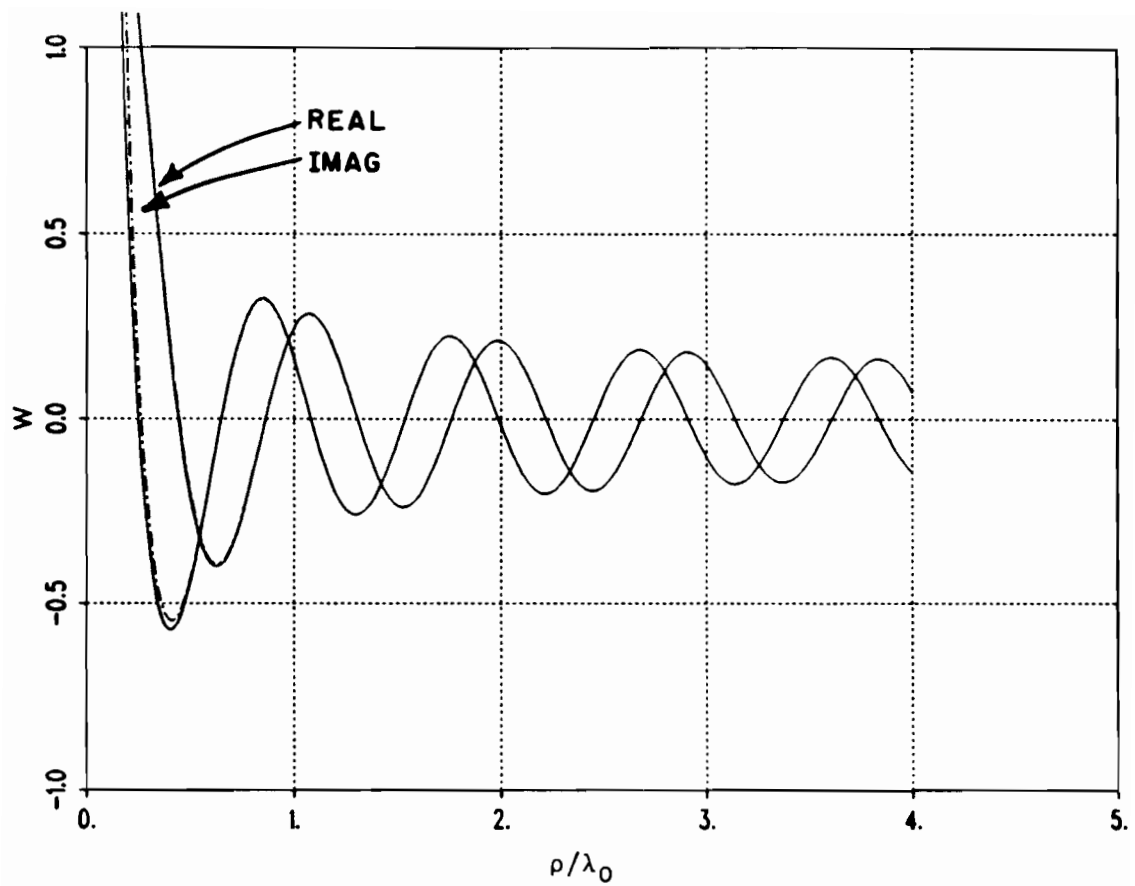
$$d/\lambda_0 = 0.01$$

— Exact Numerical Integration

- - - Uniform Asymptotic Closed Form

(a)

Figure 5.2. The comparison between the exact numerical integration and the uniform asymptotic value of (W) versus ρ/λ_0 given in (4.13) and (5.19) for $\epsilon_r=9.6$ and different slab thicknesses.



$$\epsilon_r = 9.6$$

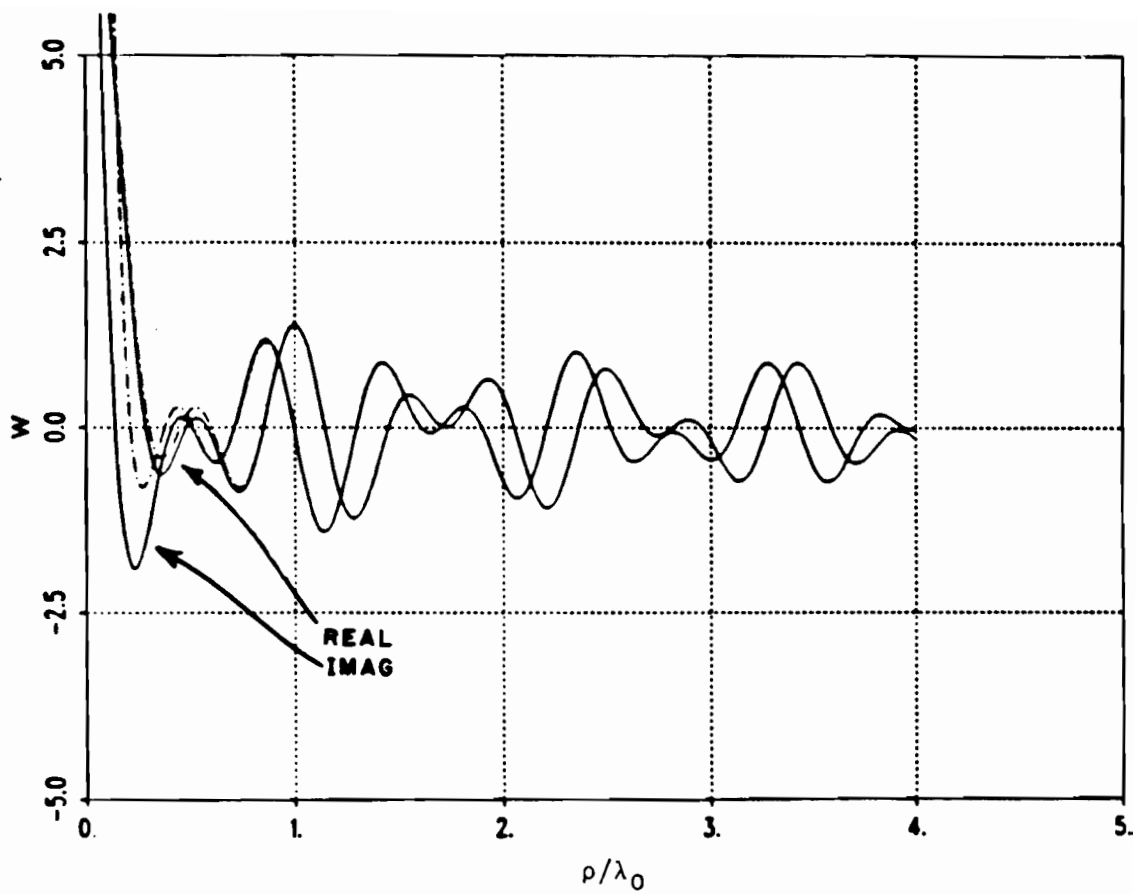
$$d/\lambda_0 = 0.05$$

— Exact Numerical Integration

- - - Uniform Asymptotic Closed Form

(b)

Figure 5.2. (Continued).

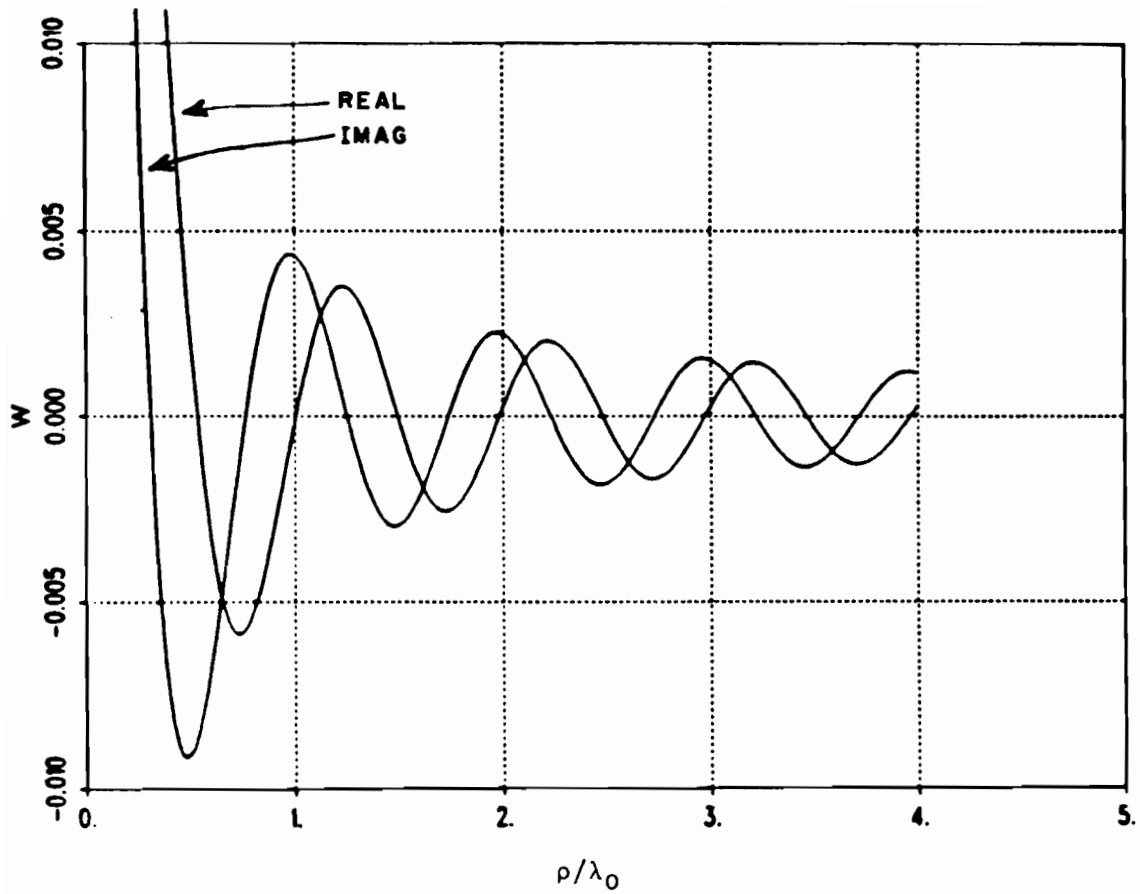


$$\epsilon_r = 9.6$$

$$d/\lambda_0 = 0.1$$

(c)

Figure 5.2. (continued)

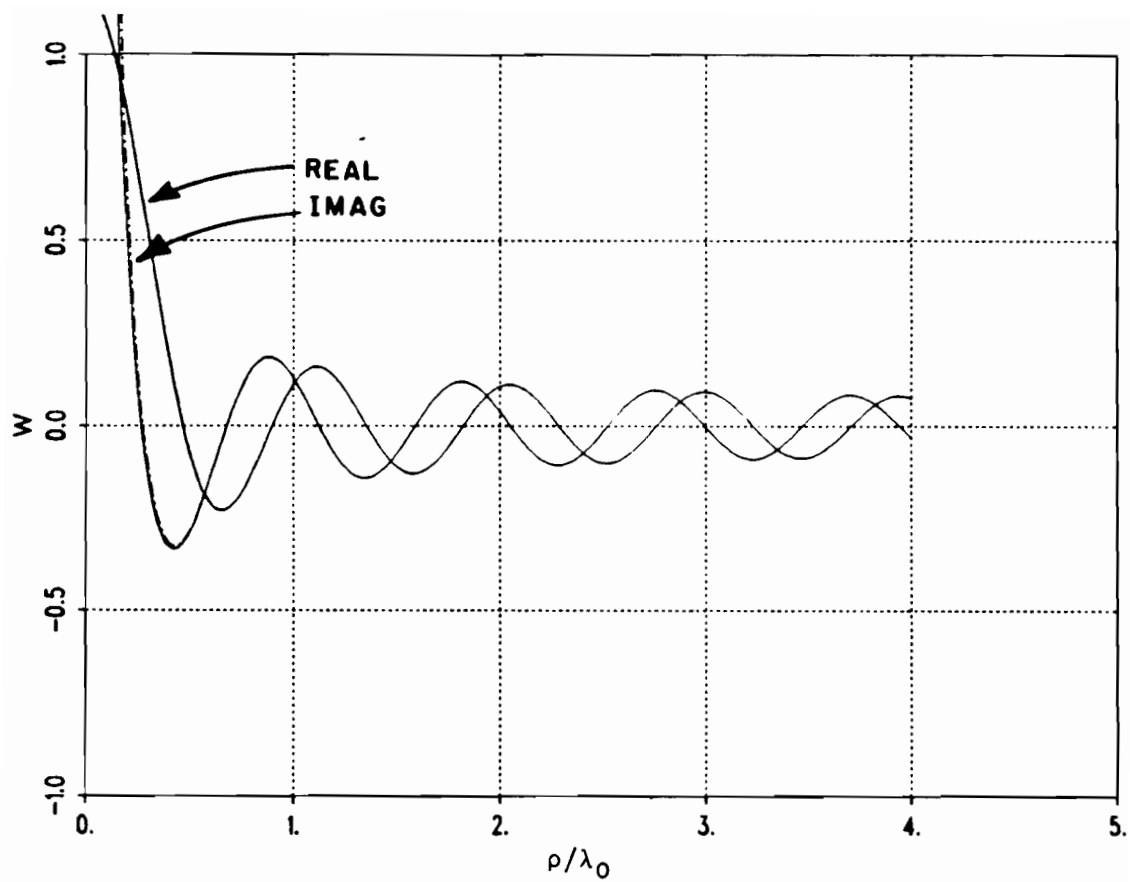


$\epsilon_r = 12.8$
 $d/\lambda_0 = 0.01$

— Exact Numerical Integration
 - - - Uniform Asymptotic Closed Form

(a)

Figure 5.3. The comparison between the exact numerical integration and the uniform asymptotic value of (W) versus ρ/λ_0 given in (4.13) and (5.19) for $\epsilon_r=12.8$ and different slab thicknesses.



$$\epsilon_r = 12.8$$

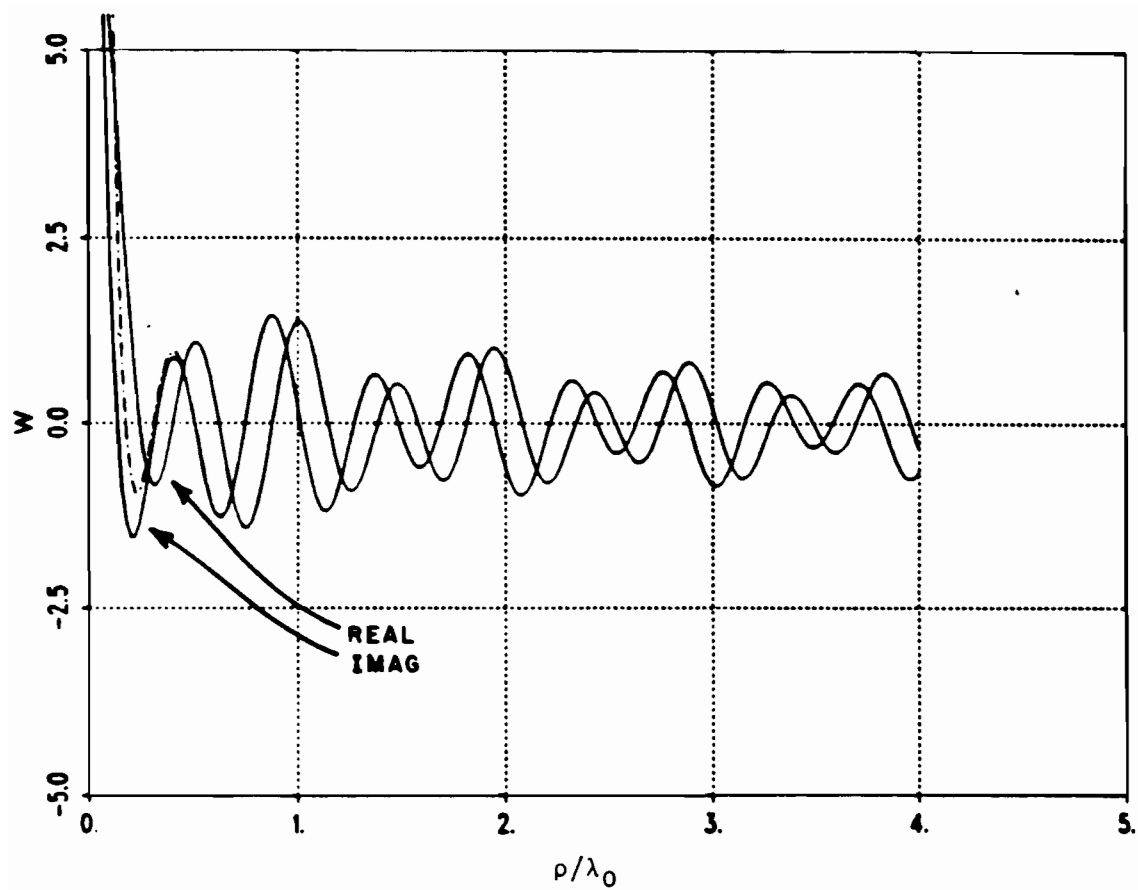
$$d/\lambda_0 = 0.04$$

— Exact Numerical Integration

- - - Uniform Asymptotic Closed Form

(b)

Figure 5.3. (Continued).



$$\epsilon_r = 12.8$$

$$d/\lambda_0 = 0.08$$

— Exact Numerical Integration

--- Uniform Asymptotic Closed Form

(c)

Figure 5.3. (continued)

than $\frac{\pi}{2}$, this TE leaky wave pole becomes the first TE surface wave pole [38,70]. In most practical cases, the uniform asymptotic approximation developed here at most needs only one TM surface wave and one TE leaky or surface wave pole singularities to be considered close to the saddle point. However, it has been found that two extra leaky wave poles occur for $(k_0 d \sqrt{\epsilon_r - 1})$ close to π [38,70]. In such case, these poles have to be considered for the solution to remain accurate for the small lateral separation of the field and source points. It is noted these leaky wave poles are located on the positive imaginary axis of the ζ plane (radially propagating plane; see Figure 4.3), which are the same leaky wave poles lying on the positive real axis of the bottom sheet of the original Sommerfeld plane, where the usual Sommerfeld integral representation for the microstrip Green's function is derived.

The results presented in this chapter will be used to formulate a highly efficient moment method solution for microstrip antenna and arrays.

CHAPTER VI

MOMENT-METHOD SOLUTION

Moment Method

In this chapter the results derived in the previous chapters are used to formulate moment-method (MM) solutions for microstrip antennas and arrays. One starts with a brief review of this technique, following which the definitions of input impedance, mutual impedance and port impedance used in MM terminology are discussed. Expressions for the MM self and mutual impedances associated with piecewise sinusoidal expansion modes for representing the unknown current on the microstrip patch are formulated along with those for the entire domain expansion modes used for the same purpose; these different choices of expansion functions are employed in different examples presented in the next chapter.

The MM formulation begins by considering an electric current source (\mathbf{J}_i) which radiates the "incident" fields $\bar{\mathbf{E}}_i$ and $\bar{\mathbf{H}}_i$ (Figure 6.1a) when it is placed within a grounded dielectric slab. Now consider the exterior scattering configuration shown in Figure 6.1b which is the same as the one in Figure 6.1a, except that now there also exists a metal patch (microstrip patch) on the dielectric-air interface. The metal patch may be viewed as being a scatterer which perturbs the

incident fields \bar{E}_i and \bar{H}_i . The objective is to find the total electric and magnetic fields everywhere in the presence of the scatterer which is excited by (\bar{E}_i, \bar{H}_i) . It is noted that \bar{E}_i, \bar{H}_i are the fields produced by the source \bar{J}_i in the presence of the grounded dielectric slab but without the microstrip patch. From the field equivalence theorem of Schelkunoff [51], one may replace the conducting scatterer by the equivalent surface-current density:

$$\bar{J}_s = \hat{n} \times \bar{H} \quad (6.1)$$

which actually exists on the surface of the scatterer (or patch) as in Figure 6.1(c). The current \bar{J}_s in the equivalent problem of Figure 6.1(c) generates the same scattered field (\bar{E}_s, \bar{H}_s) in the exterior region as in the original problem of Figure 6.1(c) but with the patch removed; the effect of the patch is contained in \bar{J}_s . Note that

$$\bar{E} = \bar{E}_i + \bar{E}_s \quad , \quad (6.2)$$

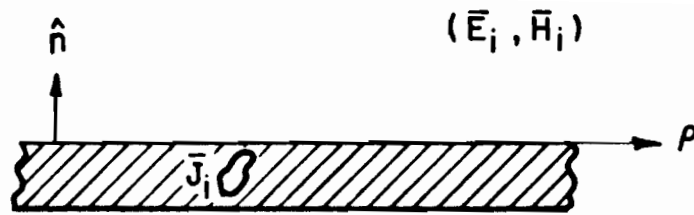
and

$$\bar{H} = \bar{H}_i + \bar{H}_s \quad . \quad (6.3)$$

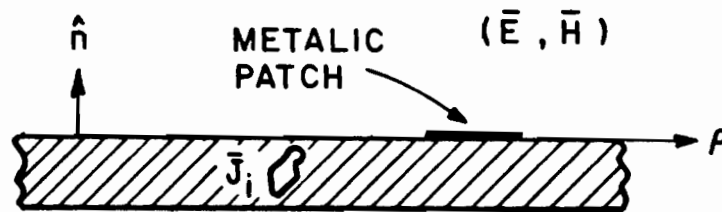
Since the scatterer is a perfect conductor, the total tangential electric field will vanish on the surface of the scatterer; i.e.,

$$0 = \hat{n} \times (\bar{E}_i + \bar{E}_s) \quad , \text{ on the scatterer (or patch)} \quad , \quad (6.4)$$

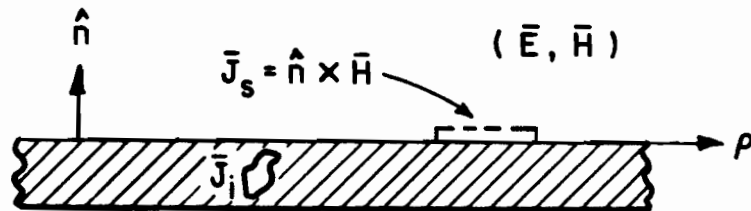
where \hat{n} is outward normal to the scatterer surface. It is clear that (6.4) above can be written as



(a) Impressed Current Source \bar{J}_i radiates an incident field $(\bar{E}_i$ and $\bar{H}_i)$.



(b) Impressed current source \bar{J}_i radiates in the presence of a metallic scatterer (microstrip patch); $\bar{E} = \bar{E}_i + \bar{E}_s$, $\bar{H} = \bar{H}_i + \bar{H}_s$.



(c) Impressed current source \bar{J}_i radiates in the presence of an equivalent surface current $\bar{J}_s = \hat{n} \times \bar{H}$ replacing the metallic scatterer (microstrip patch).

Figure 6.1. Pictorial configuration of the Schelkunoff field equivalence principle.

$$0 = \hat{n} \times \left[-j\omega\mu_0 \iiint_V \bar{\bar{G}}^1(\bar{r}, \bar{r}') \cdot \bar{J}_i(\bar{r}') dv' - j\omega\mu_0 \iint_{S_j} \bar{\bar{G}}^0(\bar{r}, \bar{r}') \cdot \bar{J}_s(\bar{r}') ds' \right] \quad (6.5)$$

Equation (6.5) is the electric field integral equation (EFIE) for the unknown surface current density \bar{J}_s where the two terms on the right hand side within the square brackets are \bar{E}_i due to \bar{J}_i and \bar{E}_s due to \bar{J}_s , respectively. Symbolically, (6.5) can be written as,

$$\bar{\bar{L}}(\bar{J}_s) = \bar{P} \quad (6.6)$$

where $\bar{\bar{L}}$ is a dyadic operator acting on \bar{J}_s and \bar{P} is related to excitation. The objective is to determine the \bar{J}_s when the operator $\bar{\bar{L}}$ and the excitation \bar{P} are specified. This is a typical functional equation which in general does not have an analytic solution. However there exist several methods to solve the functional equation in an approximate sense. The method discussed here to solve (6.6) is called the Moment-Method (MM) [52]. The basic idea of the MM is to transform the linear functional (integral) equation into a system of simultaneous linear algebraic equations which can be solved via matrix algebra.

Consider again (6.6). In order to solve this equation by the MM, one expands the \bar{J}_s in terms of a set of some known functions \bar{J}_n 's in the domain of $\bar{\bar{L}}$,

$$\bar{J}_s = \sum_{n=1}^N I_n \bar{J}_n \quad (6.7)$$

where I_n are the expansion coefficients that are to be determined. The \bar{J}_n are called expansion functions or basis functions. Generally, for an exact solution (6.7) is an infinite summation and the \bar{J}_n 's form a complete set of basis functions. This is like a Fourier type expansion; however, in practice (6.7) is usually a finite summation. The convergence of (6.7) depends on the choice of the basis functions in a given problem. Substituting (6.7) into (6.6) and making use of the linearity of \bar{L} , one obtains

$$\sum_{n=1}^N I_n \bar{L}(\bar{J}_n) = \bar{P}_N \quad (6.8)$$

and the residual \bar{R}_N is defined as

$$\bar{R}_N = \|\bar{P} - \bar{P}_N\| \quad (6.9)$$

which is:

$$\bar{R}_N = \|\bar{P} - \sum_{n=1}^N I_n \bar{L}(\bar{J}_n)\| \quad (6.10)$$

\bar{R}_N is now minimized with respect to a certain inner product with a weighting function $\bar{\omega}_j$ in the range of operator \bar{L} ; in particular, this inner product yields under the condition of minimizing the weighted residual the following result:

$$\langle \bar{R}_N, \bar{\omega}_j \rangle = \langle \bar{P} - \sum_{n=1}^N I_n \bar{L}(\bar{J}_n), \bar{\omega}_j \rangle = 0 \quad (6.11)$$

The unknown constants I_n 's can now be determined from the preceeding equation via the matrix equation obtained from (6.11) if $j=1,2,3,\dots,N$; this matrix equation becomes

$$\begin{bmatrix} \langle \bar{L}(\bar{J}_1), \bar{\omega}_1 \rangle & \dots & \langle \bar{L}(\bar{J}_1), \bar{\omega}_N \rangle \\ \vdots & & \vdots \\ \langle \bar{L}(\bar{J}_N), \bar{\omega}_1 \rangle & \dots & \langle \bar{L}(\bar{J}_N), \bar{\omega}_N \rangle \end{bmatrix} \begin{bmatrix} I_1 \\ I_2 \\ \vdots \\ I_N \end{bmatrix} = \begin{bmatrix} \langle \bar{P}, \bar{\omega}_1 \rangle \\ \langle \bar{P}, \bar{\omega}_2 \rangle \\ \vdots \\ \langle \bar{P}, \bar{\omega}_N \rangle \end{bmatrix} . \quad (6.12)$$

In compact matrix notation, the above can be expressed as

$$[Z] [I] = [V] , \quad (6.13)$$

where

$$[I] = \begin{bmatrix} I_1 \\ I_2 \\ \vdots \\ I_N \end{bmatrix} \text{ and } [V] = \begin{bmatrix} \langle \bar{P}, \bar{\omega}_1 \rangle \\ \langle \bar{P}, \bar{\omega}_2 \rangle \\ \vdots \\ \langle \bar{P}, \bar{\omega}_N \rangle \end{bmatrix} , \text{ etc.} \quad (6.14)$$

Therefore the unknown $[I]$ can be solved in terms of the known $[Z]$ and $[V]$ via

$$[I] = [Z]^{-1} [V] . \quad (6.15)$$

For a choice of $\bar{\omega}_j = \bar{J}_j$, the MM reduces to Galerkin's method [53]. If the inner product has a stationary property with respect to \bar{J}_s , then Galerkin's method is equivalent to the Rayleigh-Ritz variational method, which provides the best approximation to the stationary quantity obtainable from the given class of expansion

functions [44]. In general, a stationary inner product can be sought for the scattering problems using the concept of reaction which is based on the reciprocity theorem [54]. By definition, the reaction of a source (\bar{a}) on another source (\bar{b}) is given by

$$\langle \bar{L}(\bar{a}), \bar{b} \rangle = \iiint_V (\bar{E}^a \cdot \bar{J}^b - \bar{H}^a \cdot \bar{M}^b) dv \quad . \quad (6.16)$$

In this context, the reciprocity theorem states:

$$\langle \bar{L}(\bar{a}), \bar{b} \rangle = \langle \bar{a}, \bar{L}(\bar{b}) \rangle \quad . \quad (6.17)$$

Now, from (6.7), (6.11) can be written as:

$$\begin{aligned} \langle (\bar{L}(\bar{J}_i) + \sum_n I_n \bar{L}(\bar{J}_n)), \bar{\omega}_j \rangle \\ = \langle (\bar{J}_i + \sum_n I_n \bar{J}_n), \bar{L}(\bar{\omega}_j) \rangle \\ = 0 \end{aligned} \quad (6.18)$$

where the inner product is defined by (6.16), and $\bar{\omega}_j$ must be in the range of \bar{L} . Equation (6.18) states that the test source $\bar{\omega}_j$ has a zero reaction with the other sources ($\bar{J}_i + \bar{J}_s$). If we let $\bar{\omega}_m = \bar{J}_m$ (Galerkin's method), then (6.18) can be written as:

$$\langle \sum_{n=1}^N I_n \bar{J}_n, \bar{L}(\bar{J}_m) \rangle = - \langle \bar{J}_i, \bar{L}(\bar{J}_m) \rangle \quad . \quad (6.19)$$

The preceding equation is the operator form of the following equation:

$$-\sum_{n=1}^N I_n \iint_{S_n} \bar{J}_n \cdot \bar{E}_m ds = + \iiint_{V_i} \bar{J}_i \cdot \bar{E}_m dv \quad , \quad (6.20)$$

in which \bar{E}_m is the field generated by $\bar{\omega}_m$ ($=\bar{J}_m$ here) according to \bar{L} (\bar{J}_m), where s_n is the surface of the n^{th} expansion mode (n^{th} basis function), and v_i is the volume of the current source \bar{J}_i . Thus, (6.20) can be written as:

$$\sum_{n=1}^N I_n Z_{mn} = V_m \quad , \quad (6.21)$$

where

$$Z_{mn} = - \iint_{s_n} \bar{E}_m \cdot \bar{J}_n \, ds \quad , \quad (6.22)$$

$$V_m = \iiint_{v_i} \bar{J}_i \cdot \bar{E}_m \, dv \quad , \quad (6.23)$$

also from the reciprocity theorem,

$$V_m = \iint_{s_m} \bar{E}_i \cdot \bar{J}_m \, ds \quad . \quad (6.24)$$

It is to be noted that the reaction (inner product) is a stationary quantity for variations of \bar{J}_s . This implies that the convergence property of the MM strongly depends upon the basis (expansion) functions that one may choose for a given problem.

MUTUAL COUPLING

In the light of the above discussion one may next proceed to analyze the general microstrip configuration. Let us suppose that the general microstrip configuration consists of L metallic scatterers (which could for example be L metallic microstrip patches) within the dielectric which are excited by R sources of which P of these sources

are assumed to be constant line current filaments $\bar{J}_{ip} = \hat{z} j_{ip} \delta(\bar{\rho} - \bar{\rho}_{ip})$ [18] and the remaining Q sources ($R=P+Q$) are delta gap type $\bar{E}_{iq} = \hat{\rho} v_{iq} \delta(\bar{r} - \bar{r}_{iq})$ excitations. The subscript i emphasizes the j_{ip} and v_{iq} are impressed sources. One is interested in the current distribution, the mutual and port impedances of these elements. For the MM solution, one first expands the current on each element in terms of a known set of basis functions whose unknown amplitudes (or expansion coefficients) are to be determined using the MM. It is noted that the number of expansion modes may not necessarily be the same for all scatterers. The total electric current \bar{J}_s on the whole set of L scatterers is thus given by

$$\bar{J}_s = \sum_{\ell=1}^L \bar{J}^{\ell} \quad , \quad (6.25)$$

where

$$\bar{J}^{\ell} = \sum_{n=1}^{N_{\ell}} I_n^{\ell} \bar{J}_n^{\ell} \quad , \quad (6.26)$$

in which N_{ℓ} is the number of basis functions for the current \bar{J}^{ℓ} on the ℓ^{th} scatterer. Thus,

$$\bar{J}_s = \sum_{\ell=1}^L \sum_{n=1}^{N_{\ell}} I_n^{\ell} \bar{J}_n^{\ell} \quad , \quad (6.27)$$

in which \bar{J}_n^{ℓ} is the n^{th} expansion mode of the ℓ^{th} element, and I_n^{ℓ} is the unknown coefficient or amplitude of this expansion mode. From (6.13) to (6.24), with $\bar{\omega}_m^j = \bar{J}_m^j$ (Galerkin method) as being the source which excites the electric field \bar{E}_m^j , one gets:

$$\sum_{\ell=1}^L \sum_{n=1}^{N_{\ell}} I_n^{\ell} Z_{mn}^{j\ell} = V_m^j \quad (6.28)$$

where the impedance matrix elements $Z_{mn}^{j\ell}$ and the excitation coefficients V_m^j are given explicitly as

$$Z_{mn}^{j\ell} = - \iint_{S_{n\ell}} \vec{E}_m^j \cdot \vec{J}_n^{\ell} ds \quad (6.29)$$

$$V_m^j = \sum_{p=1}^P \iiint_{V_p} \vec{J}_{ip} \cdot \vec{E}_m^j dv + \sum_{q=1}^Q \iint_{V_q} \vec{E}_{iq} \cdot \vec{J}_m^j ds$$

(6.30)

or

$$V_m^j = \sum_{p=1}^P j_{ip} \int_{\ell_p} \hat{z} \cdot \vec{E}_m^j d\ell + \sum_{q=1}^Q v_{iq} \hat{\rho} \cdot \vec{J}_m^j(r_q)$$

where \vec{E}_m^j is the electric field due to the surface current \vec{J}_m^j and it is evaluated at the location of constant impressed current

$\vec{J}_{ip} = \hat{z} j_{ip} \delta(\vec{\rho} - \vec{\rho}_{ip})$ of the length ℓ . Also $\vec{J}_m^j(r_q)$ is the surface current \vec{J}_m^j evaluated at $\vec{r} = \vec{r}_q$ corresponding to the q^{th} delta gap location.

In compact matrix form, the above equations in (6.28) become

$$\begin{matrix} [Z] & [I] & = & [V] \\ N \times N & N \times 1 & & N \times 1 \end{matrix} \quad (6.31)$$

where the impedance matrix $[Z]$ has an $(N \times N)$ dimension; $(N = L \times N_{\ell})$

$$\begin{bmatrix} [Z^{11}] & [Z^{12}] & \dots & [Z^{1L}] \\ [Z^{21}] & [Z^{22}] & \dots & [Z^{2L}] \\ \vdots & \vdots & \ddots & \vdots \\ [Z^{L1}] & [Z^{L2}] & \dots & [Z^{LL}] \end{bmatrix} \begin{bmatrix} [I^1] \\ [I^2] \\ \vdots \\ [I^L] \end{bmatrix} = \begin{bmatrix} [V^1] \\ [V^2] \\ \vdots \\ [V^L] \end{bmatrix}, \quad (6.32)$$

in which, for example,

$$[I^2] = \begin{bmatrix} I_1^2 \\ I_2^2 \\ I_2^3 \\ \vdots \end{bmatrix}, \quad (6.33)$$

and the submatrix $[Z^{jk}]$ is given by

$$[Z^{jk}] = \begin{bmatrix} Z_{11}^{jk} & Z_{12}^{jk} & \dots & Z_{1,N_\ell}^{jk} \\ \vdots & \vdots & \ddots & \vdots \\ Z_{N_\ell 1}^{jk} & \dots & \dots & Z_{N_\ell, N_\ell}^{jk} \end{bmatrix}. \quad (6.34)$$

The unknown current amplitude $[I_n^L]$ can be determined via the matrix inversion:

$$[I] = [Y] [V]; \quad [Y] = [Z]^{-1}. \quad (6.35)$$

where, as usual,

$$[I] = \begin{bmatrix} [I^1] \\ [I^2] \\ \vdots \end{bmatrix}, \text{ etc.} \quad (6.36)$$

So the current in each element can be found. Having the current distribution on each element, one can talk about the input impedance, mutual impedance and active impedance.

According to (F.19) in Appendix F, (where the volumetric current density \bar{J}^{tq} in (F.19) has been replaced by surface current density \bar{J}_q) the input impedance at port q is given by

$$Z_{in}^q = \frac{-\iint_{s_q} \bar{E}^q \cdot \bar{J}_q \, ds}{[I_q]^2} \quad (6.37)$$

or

$$= \frac{1}{I_q^2} \sum_{n=1}^{N_q} I_n^q V_n^{qq}, \quad (6.38)$$

where s_q is the surface of the q^{th} patch and I_q is the transmitted mode terminal current at port q and \bar{E}^q is the total electric field due to \bar{J}_q which is the current density induced on the microstrip patch element q by the impressed terminal current I_q . As indicated earlier,

$$\bar{J}_q = \sum_{n=1}^{N_q} I_n^q \bar{J}_n^q. \quad (6.39)$$

V_n^{qq} is the voltage induced at port q due to each of the current

expansion modes \bar{J}_n^q .

The mutual impedance between the two ports (elements) r , and q is defined by (see (F.18) in Appendix F),

$$Z_{qr} = \frac{-\iint_{s_q} \bar{E}^r \cdot \bar{J}^q ds}{I_q I_r} , \quad (6.40)$$

where \bar{E}^r is the electric field due to \bar{J}^r which is the current density induced on the r^{th} microstrip patch element by the impressed current I_r at the terminal r ; this \bar{E}^r is calculated at the q^{th} element when all other elements are open circuited. Also,

$$\bar{J}^r = \sum_{n=1}^N I_n^r \bar{J}_n^r . \quad (6.41)$$

I_q and I_r are the terminal currents at ports q and r when they are operated in the transmitted mode, respectively. Therefore,

$$Z_{qr} = \frac{1}{I_q I_r} \sum_{n=1}^N I_n^r V_n^{qr} , \quad (6.42)$$

with

$$-\iint_{s_q} \bar{E}^r \cdot \bar{J}^q ds = \sum_{n=1}^N I_n^r V_n^{qr} \quad (6.43)$$

in which

$$V_n^{qr} = -\iint_{s_q} \bar{E}^r \cdot \bar{J}_n^q ds . \quad (6.44)$$

where V_n^{qr} is the voltage induced at port q due to the current expansion \bar{J}_n^r . If r and q were the same, i.e., if $q=r$, then Z_{qq} is called the self

impedance of the port q . The active input impedance of a port is defined as the port impedance when all elements are active. Thus, the active impedance Z_p at the p^{th} port is given by

$$Z_p = \frac{V_p}{I_p} = \frac{1}{I_p} \sum_{\ell=1}^L Z_{p\ell} I_{\ell} \quad (6.45)$$

or

$$Z_p = Z_{pp} + \frac{1}{I_p} \sum_{\substack{\ell=1 \\ \ell \neq p}}^L Z_{p\ell} I_{\ell} \quad . \quad (6.46)$$

This is the total port impedance seen by the p^{th} port; I_{ℓ} is the terminal current for the ℓ^{th} element in the total of L active elements. The active impedance depends on the terminal current in all elements and on the mutual impedance between the elements. If the elements are weakly coupled, then the self impedance of each of the elements is almost the same as the input impedance of the element [55] (see (6.37)); in this case,

$$Z_{pp} \approx Z_{in}^p \quad . \quad (6.47)$$

Also from the reciprocity,

$$Z_{qr} = Z_{rq} \quad . \quad (6.48)$$

In practice, the mutual coupling is usually measured in terms of the scattering parameters s_{qr} ; the relationship between the scattering matrix [5] whose elements are s_{qr} and impedance matrix is given by [56],

$$[S] = ([Z] + [I])^{-1} ([Z] - [I]) \quad , \quad (6.49)$$

where $[I]$ is the identity matrix.

It is noted that in the moment method the mutual impedance can be found via the admittance matrix $[Y]$ given in (6.35). Consider (6.32) and (6.35)

$$\begin{bmatrix} [Y^{11}] & [Y^{12}] & \cdots & [Y^{1L}] \\ \vdots & \vdots & \ddots & \vdots \\ [Y^{L1}] & [Y^{L2}] & \cdots & [Y^{LL}] \end{bmatrix} \begin{bmatrix} [V^1] \\ [V^2] \\ \vdots \\ [V^L] \end{bmatrix} = \begin{bmatrix} [I^1] \\ [I^2] \\ \vdots \\ [I^L] \end{bmatrix}, \quad (6.50)$$

where $[Y^{jk}]$ is the counter part of $[Z^{jk}]$ in (6.34). The $(L \times L)$ impedance matrix is given by

$$\begin{bmatrix} Z_{11} & Z_{12} & \cdots & Z_{1L} \\ Z_{21} & Z_{22} & \cdots & \vdots \\ \vdots & \vdots & \ddots & \vdots \\ Z_{L1} & Z_{L2} & \cdots & Z_{LL} \end{bmatrix} = \begin{bmatrix} Y_{11} & Y_{12} & \cdots & Y_{1L} \\ Y_{21} & Y_{22} & \cdots & \vdots \\ \vdots & \vdots & \ddots & \vdots \\ Y_{L1} & Y_{L2} & \cdots & Y_{LL} \end{bmatrix}^{-1} \quad (6.51)$$

where

$$Y_{jk} = Y_{nm}^{jk}, \quad (6.52)$$

and Y_{nm}^{jk} is the counterpart of Z_{nm}^{jk} of (6.34); furthermore, n and m correspond to the location of the physical terminals n and m in the N_j and N_k expansion modes as shown in Equation (6.32). Y_{jk} can also be written as, [57]

$$Y_{jk} = \frac{1}{v_j v_k} [V_j]^T [Y] [V_k] \quad , \quad (6.53)$$

where $[Y]$ is given by (6.35), with a normalized unit current I_q in all q terminals. $[V_j]$ and $[V_k]$ are the column voltage matrices that result from the voltage sources v_j and v_k at the terminals j and k , respectively, when all other terminals are short circuited.

In general

$$Y_{jk} \neq \frac{1}{Z_{jk}} \quad , \quad (6.54)$$

but the following relationship always holds

$$[Y] = [Z]^{-1} \quad . \quad (6.55)$$

In order to calculate all interested quantities, such as the current distribution, mutual impedance and active impedance, it is essential to calculate the self and mutual impedances associated with the current expansion modes. In the following, the mutual and self impedance of the piecewise sinusoidal (PS) and entire domain basis function (EB) will be formulated. The PS is generally better suited for thin strips and strip dipoles, whereas the (EB) is used for patches and larger size surfaces.

Consider Equation (6.24),

$$Z_{mn} = -(-j\omega\mu_0 \iint_{S_n} \iint_{S_m} \bar{J}_n(x,y) \cdot \bar{G}^0 \cdot \bar{J}_m(x',y') dx' dy' dx dy) \quad (6.56)$$

where \bar{G}^0 is the microstrip dyadic Green's Function explicitly given in (3.32) - (3.37) and \bar{J}_n and \bar{J}_m are the n^{th} and m^{th} expansion modes over

the surface s_n and s_m , respectively. For the (PS), (see Figure 6.2a) one will have

$$\bar{J}_m(x', y') = \frac{\hat{x}}{\sin k_e a} \sin k_e (a - |x' - x_m|) f_m(y') ; |x' - x_m| \leq a \quad (6.57)$$

where k_e is the effective wave number of the (PS) and $\sin k_e a$ is the normalization constant; also, $f_m(y')$ is the y' dependence of the current mode.

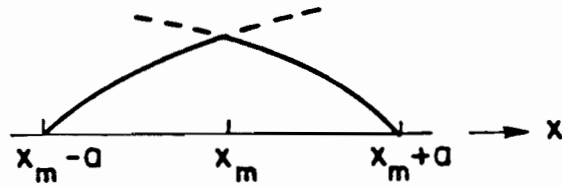
The mutual impedance for the current modes which are flowing in the same arbitrary direction \hat{x} , is given by

$$Z_{nm} = - \int_{y_n-b}^{y_n+b} \int_{y_m-b}^{y_m+b} \int_{x_n-a}^{x_n+a} \int_{x_m-a}^{x_m+a} -j\omega\mu_0 G_{xx}^0 f_n(y) f_m(y') \frac{\sin k_e (a - |x' - x_m|)}{\sin k_e a} \frac{\sin k_e (a - |x - x_n|)}{\sin k_e a} dx' dx dy' dy \quad (6.58)$$

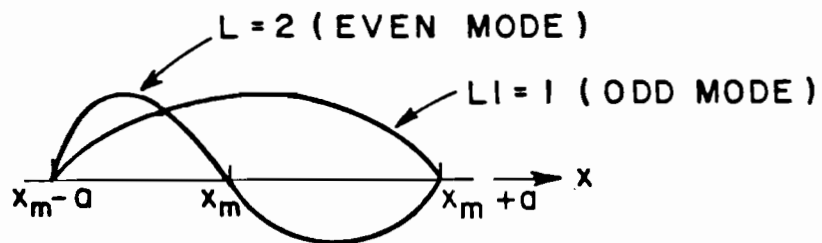
where $-j\omega\mu_0 G_{xx}^0$ is the $\hat{x}\hat{x}$ component of the microstrip surface dyadic Green's function given in (3.32); namely,

$$-j\omega\mu_0 G_{xx}^0 = \frac{-1}{2\pi\omega\epsilon_0} \left\{ \frac{\partial^2}{\partial x^2} \left(U - \frac{\epsilon_r - 1}{\epsilon_r} W \right) + k_0^2 U \right\} , \quad (6.59)$$

and U , and W were defined in (3.38) and (3.40).



(a) Piecewise sinusoidal (PS) mode.



(b) Entire basis function (EB).

Figure 6.2. Different basis function used in longitudinal direction.

If one substitutes (6.59) into (6.58), and uses integration by parts to remove the derivatives with respect to x , then

$$\begin{aligned}
 Z_{nm} = & \frac{1}{2\pi\omega\epsilon_0} \int_{-b}^b \int_{-b}^b \frac{f_n(y_n+y)f_m(y_m+y')}{(\sin k_e a)^2} \int_{x_n-a}^{x_n+a} \left[k_e \left[P(x_m+a) + P(x_m-a) \right. \right. \\
 & \left. \left. - 2\cos(k_e a)P(x_m) \right] - k_e^2 \left[\int_{x_m-a}^{x_m} [Q] \sin(k_e(x'-x_m-a)) dx' \right. \right. \\
 & \left. \left. + \int_{x_m}^{x_m+a} [Q] \sin(k_e((x_m+a)-x')) dx' \right] \right] \cdot \sin(k_e(a-|x-x_n|)) dx dy' dy
 \end{aligned} \quad (6.60)$$

where

$$P = U - \frac{\epsilon_r - 1}{\epsilon_r} W, \quad (6.61)$$

and

$$Q = \left(1 - \frac{k_0^2}{k_e^2}\right) U - \frac{\epsilon_r - 1}{\epsilon_r} W. \quad (6.62)$$

Note that if $k_e = k_0$, then Q is given by a constant times W . The double integrals can be transformed to a single integral via a rotation of coordinate systems; that is

$$\begin{aligned}
 \int_{x_{1n}}^{x_{2n}} \int_{x_{1m}}^{x_{2m}} F((x'+x), (x'-x)) dx' dx = & \int_{v_0}^{v_2} \int_{v+\sqrt{2}x_{1n}}^{-v+\sqrt{2}x_{2m}} F(u,v) du dv \\
 & + \int_{v_1}^{v_0} \int_{-v+\sqrt{2}x_{1m}}^{v+\sqrt{2}x_{2n}} F(u,v) du dv
 \end{aligned} \quad (6.63)$$

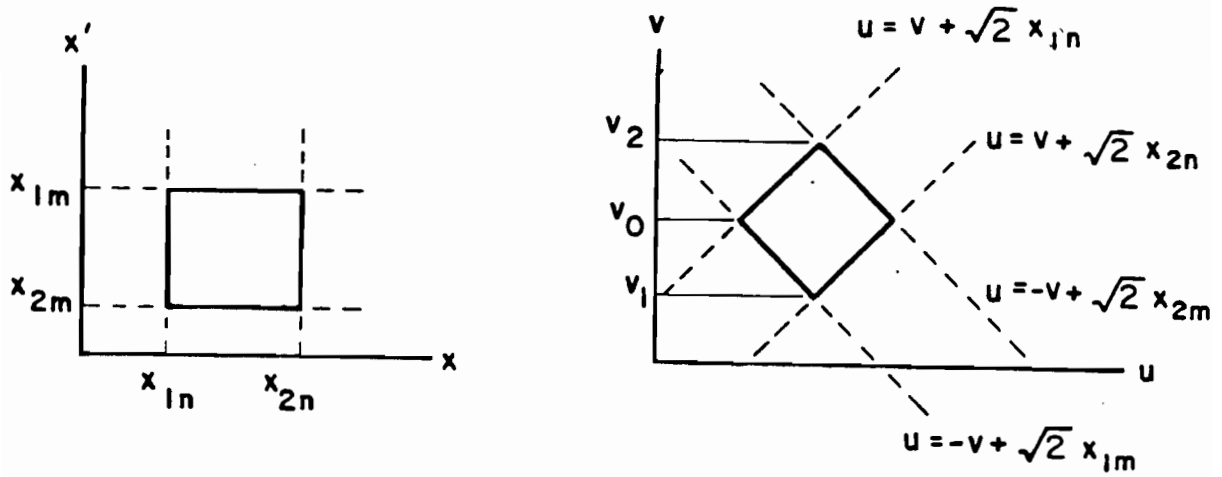


Figure 6.3. Mapping from (x, x') to (u, v) plane: $u = \frac{1}{\sqrt{2}} (x' + x)$,
 $v = \frac{1}{\sqrt{2}} (x' - x)$.

In this case the u dependence can be integrated analytically. Use has been made of the following.

$$v = \frac{1}{\sqrt{2}} (x' - x) \quad ; \quad u = \frac{1}{\sqrt{2}} (x' + x) \quad ; \quad (6.64)$$

$$dx' dx = du dv \quad , \quad (6.65)$$

and

$$v_2 = \frac{1}{\sqrt{2}} (x_{2m} - x_{1n}) \quad ; \quad x_{2m} - x_{1m} = x_{2n} - x_{1n} \quad (6.66)$$

$$v_0 = \frac{1}{\sqrt{2}} (x_{1m} - x_{1n}) \quad ; \quad v_1 = \frac{1}{\sqrt{2}} (x_{1m} - x_{2n}) \quad . \quad (6.67)$$

For very narrow strip configurations, the functional dependence of the current modes on y can be approximated by the Dirac delta function when $m \neq n$. This is due to the fact that for the very narrow strip case, the transverse dependence of the current does not have any significant effect on the mutual impedance calculation for $m \neq n$. Therefore, the mutual impedance can be given by a single integral in spatial domain; that is,

$$Z_{mn} = \frac{1}{2\pi\omega\epsilon_0} \frac{k_e a}{\sin^2 k_e a} \left\{ \int_0^1 [(P_1 + P_2 + P_3 + P_4) - 2\cos(k_e a)(P_5 + P_6)] \sin(k_e a(1-\alpha)) d\alpha \right. \\ \left. - 2k_e a \left[\int_0^{0.5} [Q^+ + Q^-] [S_1] d\alpha + \int_{0.5}^{1.0} [Q^+ + Q^-] [S_2] d\alpha \right] \right\} \quad (6.68)$$

where

$$\left. \begin{matrix} P_1 = P \\ 2 \end{matrix} \right| \rho = \sqrt{Y_{mn}^2 + (X_{mn} + a(1 \pm \alpha))^2} ; \quad \left. \begin{matrix} P_3 = P \\ 4 \end{matrix} \right| \rho = \sqrt{Y_{mn}^2 + (X_{mn} - a(1 \pm \alpha))^2} ; \quad (6.69)$$

$$\left. \begin{matrix} P_5 = P \\ 6 \end{matrix} \right| \rho = \sqrt{Y_{mn}^2 + (X_{mn} \pm a\alpha)^2} ; \quad \left. \begin{matrix} Q^\pm = Q \end{matrix} \right| \rho = \sqrt{Y_{mn}^2 + (X_{mn} \pm 2a\alpha)^2} ;$$

$$Y_{mn} = Y_m - Y_n ; \quad X_{mn} = X_m - X_n , \quad (6.70)$$

with P and Q as given in (6.57) and (6.58) respectively. Also

$$S_1 = (1 - \alpha(2 + \cos(2k_e a))) \cos(2k_e a\alpha) - \alpha \sin(2k_e a) \sin(2k_e a\alpha) \\ + \frac{1}{2k_e a} [(2 + \cos(2k_e a)) \sin(2k_e a\alpha) - \sin(2k_e a) \cos(2k_e a\alpha)] , \quad (6.71)$$

and

$$S_2 = -\cos(2k_e a) (1-\alpha) \cos(2k_e a \alpha) - (1-\alpha) \sin(2k_e a) \sin(2k_e a \alpha) \\ + \frac{1}{2k_e a} [-\cos(2k_e a) \sin(2k_e a \alpha) + \sin(2k_e a) \cos(2k_e a \alpha)] \quad (6.72)$$

For the self impedance (Z_{mm}) term, the transverse functional dependence of the current which satisfies the edge condition (see (B.8) in Appendix B) can be used. This choice is closer to the physical configuration of the current on the strip. The Dirac delta function is still being used for the testing function in the transverse domain, so

$$Z_{mm} = \frac{1}{2\pi\omega\epsilon_0} \frac{2k_e a}{\sin^2 k_e a} \int_{-b}^b \frac{1}{\pi \sqrt{b^2 - \beta^2}} \\ \left\{ \int_0^{1.0} (P_1 + P_2 - 2\cos(k_e a) P_5) \sin(k_e a(1-\alpha)) d\alpha \right. \\ \left. - 2k_e a \left[\int_0^{0.5} [Q^+] [S_1] d\alpha + \int_{0.5}^{1.0} [Q^+] [S_2] d\alpha \right] \right\} d\beta \quad (6.73)$$

where

$$\left. \begin{matrix} P_1 = P \\ 2 \end{matrix} \right|_{\rho = \sqrt{\beta^2 + (a(1 \pm \alpha))^2}} ; \quad \left. \begin{matrix} P_5 = P \\ 2 \end{matrix} \right|_{\rho = \sqrt{\beta^2 + (a\alpha)^2}} ; \quad \left. \begin{matrix} Q^+ = Q \\ 2 \end{matrix} \right|_{\rho = \sqrt{\beta^2 + (2a\alpha)^2}} \quad (6.74)$$

and (2b) is the strip width. The numerical integration in the α domain can be efficiently improved by adding and subtracting the asymptotic behavior of (P_5) and (Q^+), (see (3.46) through (3.48)) in the small interval of integration from zero to δ_α for $k_e a \delta_\alpha \ll 1$; thus,

$$\begin{aligned}
Z_{mm} = & \frac{1}{2\pi\omega\epsilon_0} \frac{2k_e a}{\sin^2 k_e a} \int_{-b}^b \frac{1}{\pi \sqrt{b^2 - \beta^2}} \left\{ \int_0^{1.0} (P_1 + P_2) \sin(k_e a(1-\alpha)) d\alpha \right. \\
& - 2\cos k_e a \left(\int_{\delta_\alpha}^{1.0} P_5 \sin(k_e a(1-\alpha)) d\alpha \right. \\
& + \int_0^{\delta_\alpha} \left(P_5 - \frac{C_p}{k_0 \sqrt{\beta^2 + (a\alpha)^2}} \right) \sin(k_e a(1-\alpha)) d\alpha + \frac{C_p}{k_0} \int_0^{\delta_\alpha} \frac{\sin(k_e a(1-\alpha)) d\alpha}{\sqrt{\beta^2 + (a\alpha)^2}} \\
& - 2k_e a \left[\int_{\delta_\alpha}^{0.5} Q^+ [S_1] d\alpha + \int_0^{\delta_\alpha} \left[Q^+ - \frac{C_Q}{k_0 \sqrt{\beta^2 + (2a\alpha)^2}} \right] [S_1] d\alpha \right. \\
& \left. \left. + \frac{C_Q}{k_0} \int_0^{\delta_\alpha} \frac{1}{\sqrt{\beta^2 + (2a\alpha)^2}} [S_1] d\alpha + \int_{0.5}^{1.0} Q^+ [S_2] d\alpha \right] \right\} d\beta, \quad (6.75)
\end{aligned}$$

where

$$C_p = j(\epsilon_r + 1) \quad , \quad C_Q = \frac{j}{2} \left(\left(1 - \frac{k_0^2}{k_e^2} \right) - \frac{\epsilon_r - 1}{\epsilon_r + 1} \right) \quad . \quad (6.76)$$

Alternatively,

$$\begin{aligned}
 Z_{mm} = & \frac{1}{2\pi\omega\epsilon_0} \frac{4k_e a}{\sin^2 k_e a} \int_0^b \frac{1}{\pi \sqrt{b^2 - \beta^2}} \left\{ \int_0^{1.0} (P_1 + P_2) \sin(k_e a(1-\alpha)) d\alpha \right. \\
 & - 2\cos k_e a \left[\int_{\delta_\alpha}^{1.0} P_5 \sin(k_e a(1-\alpha)) d\alpha \right. \\
 & + \int_0^\delta (P_5 - \frac{C_p}{k_0 \sqrt{\beta^2 + (a\alpha)^2}}) \sin(k_e a(1-\alpha)) d\alpha \\
 & + \frac{C_p}{k_0 a} \left[\sin k_e a \left[\ln(\delta_\alpha + \sqrt{\frac{\beta^2}{a^2} + \delta_\alpha^2}) - \ln\left(\frac{\beta}{a}\right) \right] \right. \\
 & \left. \left. - (k_e a) \cos(k_e a) \left(\sqrt{\frac{\beta^2}{a^2} + \delta_\alpha^2} - \frac{\beta}{a} \right) \right] \right\} \\
 & - 2k_e a \left[\int_{\delta_\alpha}^{0.5} Q^+[S_1] d\alpha + \int_0^\delta \left[Q^+ - \frac{C_Q}{k_0 \sqrt{\beta^2 + (2a\alpha)^2}} \right] [S_1] d\alpha \right. \\
 & \left. + \int_{0.5}^{1.0} Q^+[S_2] d\alpha + \frac{C_Q}{2ak_0} \left(1 - \frac{\sin 2k_e a}{2k_e a} \right) \left(\ln(\delta_\alpha + \sqrt{\frac{\beta^2}{4a^2} + \delta_\alpha^2}) - \ln\left(\frac{\beta}{2a}\right) \right) \right] d\beta.
 \end{aligned} \tag{6.77}$$

In obtaining (6.72) use has been made of the following identities

$$\begin{aligned}
 \int \frac{1}{\sqrt{\beta^2 + (a\alpha)^2}} d\alpha &= \frac{1}{a} \left(\ln(\alpha + \sqrt{\frac{\beta^2}{a^2} + \alpha^2}) \right) ; \\
 \int \frac{\alpha}{\sqrt{\beta^2 + (a\alpha)^2}} d\alpha &= \frac{1}{a} \left(\sqrt{\frac{\beta^2}{a^2} + \alpha^2} \right) ,
 \end{aligned} \tag{6.78}$$

and use has also been made of the expansions of $[S_1]$ and $\text{sink}_e a(1-\alpha)$ around $\alpha=0$; namely,

$$[S_1] \approx 1 - \frac{\sin 2k_e a}{2k_e a} ; \text{sink}_e a(1-\alpha) \approx \text{sink}_e a - (k_e a \alpha) \cos k_e a . \quad (6.79)$$

For a Dirac delta function type transverse dependence, (6.77) is still applicable provided the integrand $\frac{\pi}{\sqrt{b^2 - \beta^2}}$ is replaced by $\delta(\beta - \delta_\beta)$, where δ_β is a finite separation between the two closely spaced current filaments in the x-direction.

For the (EB) case which is shown in the Figure 6.2b, the current expansion mode is given by,

$$\bar{J}_m(x, y) = \frac{\hat{x}}{2b} \sin\left(\frac{L\pi}{2a} (a+x-x_m)\right) ; |x-x_m| < a \quad (6.80)$$

where

$$L = \begin{cases} 2N-1 & \text{odd mode} \\ 2N & \text{even mode} \end{cases} ; N=1,2,3,\dots \quad (6.81)$$

The mutual impedance between two conducting microstrip patches can be written as:

For odd mode; $L = 2N-1$; $N=1,2,3,\dots$

$$\begin{aligned} Z_{mn}^0 = & \frac{1}{2\pi\omega\epsilon_0} \frac{1}{(2b)^2} (2a)^2 \left\{ -\left(\frac{(2N-1)\pi}{2a}\right)^2 \int_0^1 \int_0^1 (1-\beta) [P_1+P_2+P_3+P_4] [S_1^0] d\alpha d\beta \right. \\ & \left. + k_0^2 \int_0^1 \int_0^1 (1-\beta) [U_1+U_2+U_3+U_4] [S_2^0] d\alpha d\beta \right\} \end{aligned} \quad (6.82)$$

where the superscript o in Z_{mn}^0 denotes the moment method mutual impedance between two odd modes; also,

$$S_1^0 = (1-\alpha)\cos((2N-1)\pi\alpha) - \frac{1}{(2N-1)\pi} \sin((2N-1)\pi\alpha) \quad , \quad (6.83)$$

and

$$S_2^0 = (1-\alpha)\cos((2N-1)\pi\alpha) + \frac{1}{(2N-1)\pi} \sin((2N-1)\pi\alpha) \quad . \quad (6.84)$$

For the even mode; $L = 2N$; $N=1,2,3\dots$

$$\begin{aligned} Z_{mn}^e = & \frac{1}{2\pi\omega\epsilon_0} \frac{1}{(2b)^2} (2a)^2 \left\{ -\left(\frac{N\pi}{a}\right)^2 \int_0^1 \int_0^1 (1-\beta) [P_1+P_2+P_3+P_4] [S_1^e] d\alpha d\beta \right. \\ & \left. + k_0^2 \int_0^1 \int_0^1 (1-\beta) [U_1+U_2+U_3+U_4] [S_2^e] d\alpha d\beta \right\} \end{aligned} \quad (6.85)$$

where the superscript e on Z_{nm}^e denotes the even mode case; also,

$$S_1^e = (1-\alpha)\cos(2N\pi\alpha) + \frac{1}{2N\pi} \sin(2N\pi\alpha) \quad , \quad (6.86)$$

and

$$S_2^e = (1-\alpha)\cos(2N\pi\alpha) - \frac{1}{2N\pi} \sin(2N\pi\alpha) \quad . \quad (6.87)$$

P_i and U_i for $i = 1,2,3,4$ are the values of $P(Y_{mn}, X_{mn}, \alpha, \beta)$ and $U(Y_{mn}, X_{mn}, \alpha, \beta)$ evaluated at

$$\rho_i = \sqrt{(Y_{mn} \pm 2b\beta)^2 + (X_{mn} \pm 2a\alpha)^2} \quad . \quad (6.88)$$

For the derivation of Equations (6.82) through (6.85), use has been made of the following formula [34]

$$\frac{\partial^2}{\partial x^2} = - \frac{\partial}{\partial x'} \frac{\partial}{\partial x} \quad (6.89)$$

to remove the second order derivative of P with respect to x via an integration by parts; in particular one integration by parts has been

performed over the domain of x and another over the domain of x' . Also the rotation of the coordinates has been used to convert the four fold integral into a two-fold integral.

For the self (impedance) term of the patch (or EB) mode, one can use the same technique which was employed for the (PS) mode pertaining to the strip dipole case; however, it turns out to be more straight forward to add and subtract the singular terms of (P) and (U) (see Equations (3.38) through (3.40)), and then carry the integration over the spatial domain whose limits go from zero to unity. It is to be noted that a constant current variation in transverse direction is still being used. Hence,

$$\begin{aligned}
 Z_{mm}^0 = & \frac{1}{2\pi\omega\epsilon_0} \frac{4}{(2b)^2(2a)^2} \left\{ -\left(\frac{(2N-1)\pi}{2a}\right)^2 \right. \\
 & \cdot \left[\int_0^1 \int_0^1 (1-\beta) \left(P_1 - \frac{C_p}{k_0 \sqrt{(2b\beta)^2 + (2a\alpha)^2}} \right) [S_1^0] d\alpha d\beta \right. \\
 & + \left. \int_0^1 \int_0^1 (1-\beta) \frac{C_p}{k_0 \sqrt{(2b\beta)^2 + (2a\alpha)^2}} [S_1^0] d\alpha d\beta \right] \\
 & + k_0^2 \left[\int_0^1 \int_0^1 (1-\beta) \left(U_1 - \frac{C_u}{k_0 \sqrt{(2b\beta)^2 + (2a\alpha)^2}} \right) [S_2^0] d\alpha d\beta \right. \\
 & + \left. \left. \int_0^1 \int_0^1 (1-\beta) \frac{C_u}{k_0 \sqrt{(2b\beta)^2 + (2a\alpha)^2}} [S_2^0] d\alpha d\beta \right] \right\} \quad (6.90)
 \end{aligned}$$

where

$$P_1 = P \left| \rho = \sqrt{(2b\beta)^2 + (2a\alpha)^2} \right. ; \quad U_1 = U \left| \rho = \sqrt{(2b\beta)^2 + (2a\alpha)^2} \right. \quad (6.91)$$

and

$$C_p = j \left(\frac{1}{\epsilon_r + 1} \right) , \quad C_u = j \, 0.5 \quad . \quad (6.92)$$

It turns out that the second and fourth integral can be expressed in closed form [34]; thus,

$$\begin{aligned} Z_{mm}^0 = & \frac{1}{2\pi\omega\epsilon_0} \frac{4}{(2b)^2} (2a)^2 \left\{ - \left(\frac{(2N-1)\pi}{2a} \right)^2 \right. \\ & \left[\int_0^1 \int_0^1 (1-\beta) \left(P_1 - \frac{C_p}{k_0 \sqrt{(2b\beta)^2 + (2a\alpha)^2}} \right) [S_1^0] \, d\alpha d\beta \right] \\ & + k_0^2 \int_0^1 \int_0^1 (1-\beta) \left(U_1 - \frac{C_u}{k_0 \sqrt{(2b\beta)^2 + (2a\alpha)^2}} \right) [S_2^0] \, d\alpha d\beta \\ & + \frac{1}{2bk_0} \left[\int_0^1 \left(\ln \left(1 + \sqrt{1 + \frac{a^2}{b^2} \alpha^2} \right) - \sqrt{1 + \frac{a^2}{b^2} \alpha^2} \right) \right. \\ & \left[(C_u k_0^2 - C_p \left(\frac{(2N-1)\pi}{2a} \right)^2) (1-\alpha) \cos((2N-1)\pi\alpha) \right. \\ & + (C_u k_0^2 + C_p \left(\frac{(2N-1)\pi}{2a} \right)^2) \frac{\sin((2N-1)\pi\alpha)}{(2N-1)\pi}] \, d\alpha \\ & + (C_u k_0^2 - C_p \left(\frac{(2N-1)\pi}{2a} \right)^2) \left(\int_0^1 \alpha \cos((2N-1)\pi\alpha) \ln \left(\frac{a}{b} \alpha \right) \, d\alpha \right. \\ & + \frac{1}{(2N-1)\pi} \int_0^{(2N-1)\pi} \frac{\sin x}{x} \, dx) + (C_u k_0^2 + C_p \left(\frac{(2N-1)\pi}{2a} \right)^2) \left(- \frac{1}{(2N-1)\pi} \right. \\ & \left. \left. \cdot \int_0^1 \sin((2N-1)\pi\alpha) \ln \left(\frac{a}{b} \alpha \right) \, d\alpha + \frac{a}{b} \frac{1}{[(2N-1)\pi]^2} \right) \right] \left. \right\} \quad (6.93) \end{aligned}$$

where use has been made of the following identity

$$\int \frac{(1-\beta)}{\sqrt{(2b\beta)^2 + (2a\alpha)^2}} d\beta = \frac{1}{2b} \left[\text{Ln} \left(\beta + \sqrt{\beta^2 + \left(\frac{a}{b}\right)^2 \alpha^2} \right) - \sqrt{\beta^2 + \left(\frac{a}{b}\right)^2 \alpha^2} \right] \quad (6.94)$$

together with an integration by parts formula. By the same token,

$$\begin{aligned} Z_{mm}^e &= \frac{1}{2\pi\omega\epsilon_0} \frac{4}{(2b)^2(2a)^2} \left\{ -\left(\frac{N\pi}{2a}\right)^2 \right. \\ &\quad \cdot \left[\int_0^1 \int_0^1 (1-\beta) \left(P_1 - \frac{C_p}{k_0 \sqrt{(2b\beta)^2 + (2a\alpha)^2}} \right) [S_1^e] d\alpha d\beta \right] \\ &\quad + k_0^2 \int_0^1 \int_0^1 (1-\beta) \left(U_1 - \frac{C_u}{k_0 \sqrt{(2b\beta)^2 + (2a\alpha)^2}} \right) [S_2^e] d\alpha d\beta \\ &\quad + \frac{1}{2bk_0} \left[\int_0^1 \left(\text{Ln} \left(1 + \sqrt{1 + \frac{a^2}{b^2} \alpha^2} \right) - \sqrt{1 + \frac{a^2}{b^2} \alpha^2} \right) \right. \\ &\quad \cdot \left[(C_u k_0^2 - C_p \left(\frac{N\pi}{a}\right)^2) (1-\alpha) \cos(2N\pi\alpha) \right. \\ &\quad \left. \left. - (C_u k_0^2 + C_p \left(\frac{N\pi}{a}\right)^2) \frac{\sin(2N\pi\alpha)}{2N\pi} \right] d\alpha \right. \\ &\quad + (C_u k_0^2 - C_p \left(\frac{N\pi}{a}\right)^2) \left(\int_0^1 \alpha \cos(2N\pi\alpha) \text{Ln} \left(\frac{a}{b} \alpha \right) d\alpha \right. \\ &\quad + \frac{1}{2N\pi} \int_0^{2N\pi} \frac{\sin x}{x} dx \left. \right) - (C_u k_0^2 + C_p \left(\frac{N\pi}{a}\right)^2) \left(-\frac{1}{2N\pi} \right. \\ &\quad \left. \left. \cdot \int_0^1 \sin(2N\pi\alpha) \text{Ln} \left(\frac{a}{b} \alpha \right) d\alpha + \frac{a}{b} \frac{1}{(2N\pi)^2} \right) \right] \left. \right\} \quad (6.95) \end{aligned}$$

It is to be noted that the self impedance of the patch does not have any singular terms, and all integrands in Equations (6.93) and (6.95) are regular over the entire domain of integration. The moment method mutual impedance Z_{mn}^{eo} between the odd and even mode for the same patch is zero; however, for these modes in different patches the Z_{mn}^{eo} will not vanish in general; the derivation for this is straight forward and it will not be presented here.

Equations (6.68), (6.77), (6.82) and (6.93) have been used in conjunction with an efficient evaluation of one microstrip Green's function discussed in Chapter V, to evaluate the interested quantities for which the numerical results will be presented in the next chapter.

CHAPTER VII

NUMERICAL RESULTS

Part of the numerical results have already been presented in Chapter III, IV, and V where numerical integration of the alternative representations and also numerical results based on the closed form asymptotic representation of the planar microstrip Green's function, respectively are discussed. In this chapter, more useful quantities, such as input impedance and mutual impedance of the microstrip geometries will be presented. Also the mutual impedance of two strip dipoles on a grounded dielectric slab are presented. The effects of the dielectric constant and dielectric thickness on the coupling are shown.

Figure 7.2 is the numerical value of the input impedance (real and imaginary part) of the microstrip dipole shown in Figure 7.1 versus normalized length with respect to free space wavelengths. Calculations are based on the Moment Method (MM) discussed in Chapter VI. The microstrip dipole antenna has a width of $(0.01\lambda_0)$ and is center fed by a delta gap generator. The unknown longitudinal current on the strip has been expanded by overlapping piecewise sinusoidal (PS) current modes and the transversal current variation is chosen such that the current satisfies the edge condition (see (6.73)). For the microstrip dipole antennas with a length of less than $0.2\lambda_0$, only a single (PS) mode is

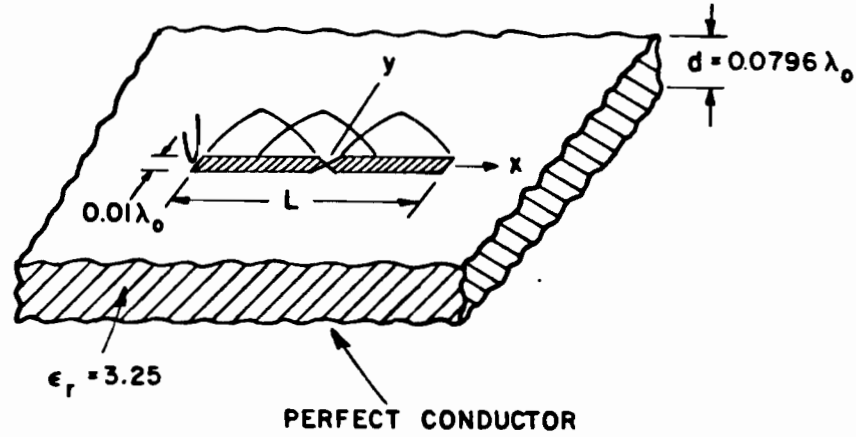


Figure 7.1. Strip dipole over a grounded dielectric slab.

used, and for longer dipoles three expansion (PS) modes with an effective wave number ($k_e = k_0 \sqrt{\frac{\epsilon_r + 1.0}{2}}$) have been utilized. For the calculation of the impedance matrix elements given in Equation (6.12), the results of Equations (6.68) and (6.77) have been utilized. The values of (P) and (Q) (see Equations (6.61) and (6.62)) in Equations (6.68) and (6.77) are explicitly given in (5.17) and (5.19). An efficient representation of these functionals have been discussed in Chapter V. It is noted that the resonant length of the microstrip dipole is a function of the substrate thickness and dielectric constant; it is less than the resonant length of the strip dipole in free space. This is due to the fact that the presence of the grounded dielectric slab increases the effective electrical length of the strip dipole. Two

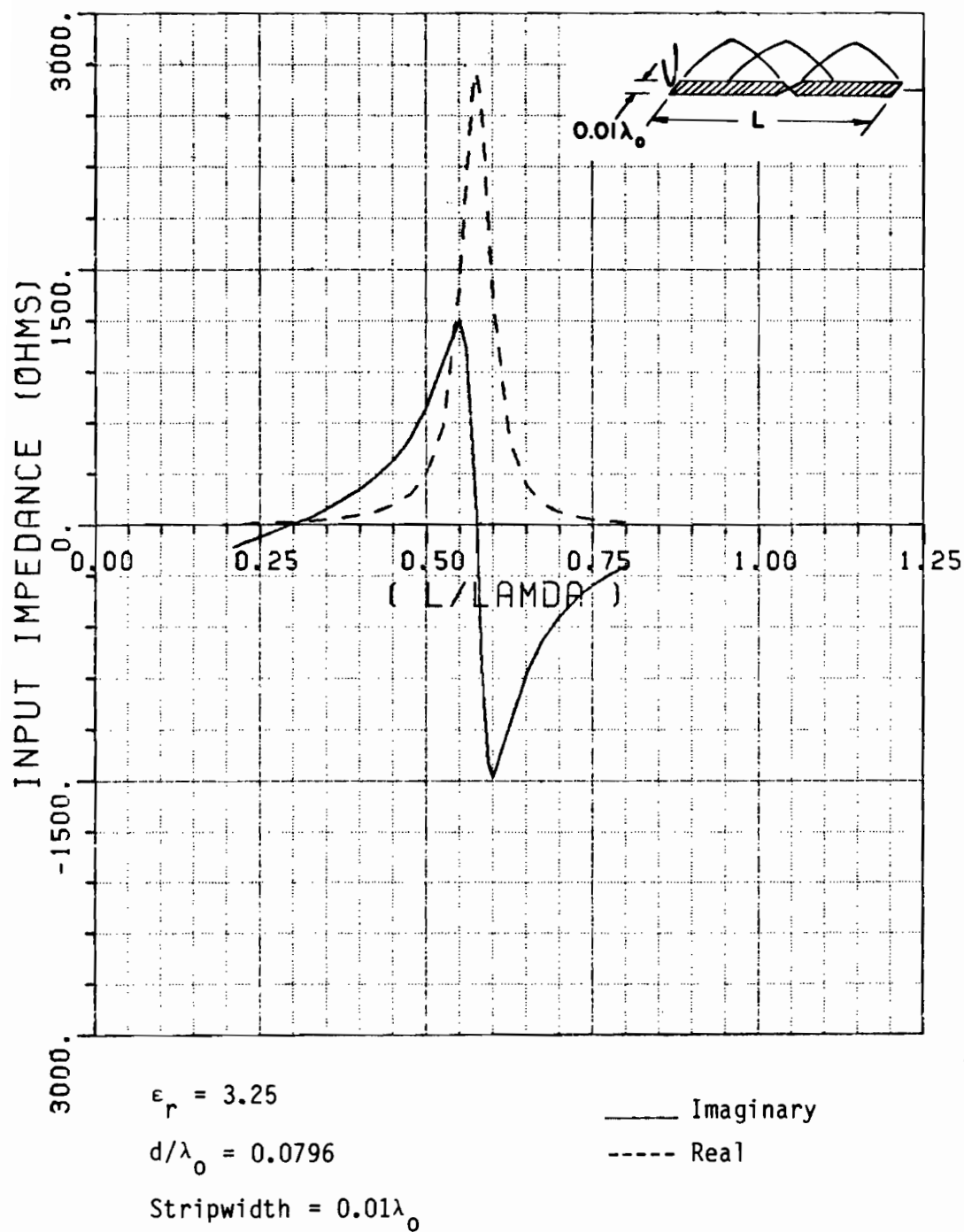
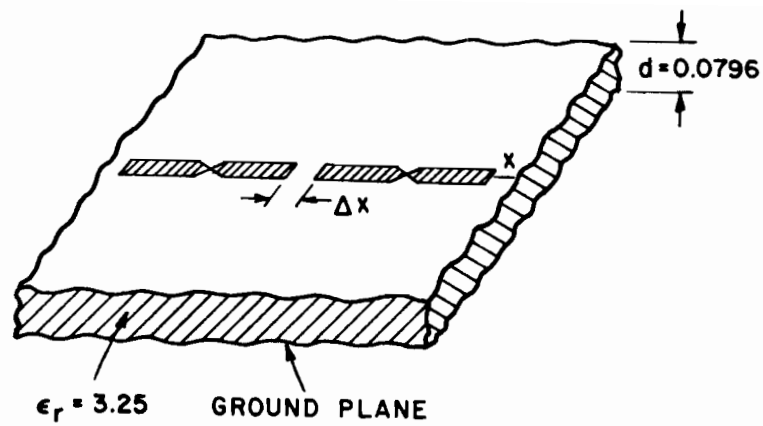


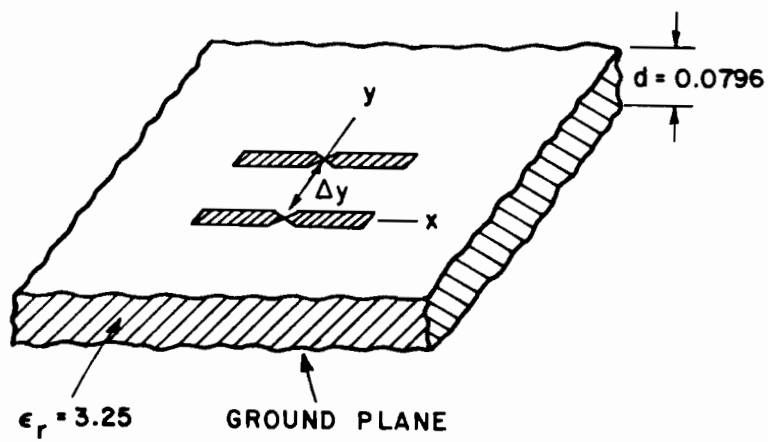
Figure 7.2. Input impedance of thin strip dipole over a grounded dielectric slab versus its normalized length with respect to free space wave length λ_0 .

resonance phenomena have been observed (which yield a purely real input impedance). The first one is at $L \approx 0.29\lambda_0$, and the second one is at $L \approx 0.58\lambda_0$ where L =length of the dipole. The quantities $(0.29\lambda_0)$ and $(0.58\lambda_0)$ are "effective" half and full wavelength of the air-dielectric substrate structure. It is also noted that the reactive part of the impedance is strongly dependent on the width of the strip dipole. This can be seen by modeling the input impedance of the strip dipole as the mutual impedance between the two closeby filaments current over the grounded dielectric slab in which their lengths are equal to the length of the original strip dipole and their lateral separation is a function of its width [58]. In this configuration, the real part of the mutual impedance is almost constant; however, the reactive part is proportional to the logarithm of inverse of the lateral separation.

Figures 7.4 and 7.5 are the plots of the mutual coupling of the two strip dipoles in the E-plane (end fire) and H-plane (broad side) as a function of the separation (see Figures 7.3(a) and 7.3(b)). Figures 7.4(a) and 7.5(a) are the numerical calculations with the exact Sommerfeld representation of the microstrip surface Green's function and 7.4(b) and 7.5(b) are the same calculations with the closed form asymptotic representation of the surface Green's function. Figures 7.4(a) and 7.4(b), 7.5(a) and 7.5(b) are almost identical, except for a very small separation of less than $0.1 \lambda_0$. The usefulness of the closed form asymptotic solution is now evident. The closed form asymptotic representation of the microstrip surface Green's function can thus be

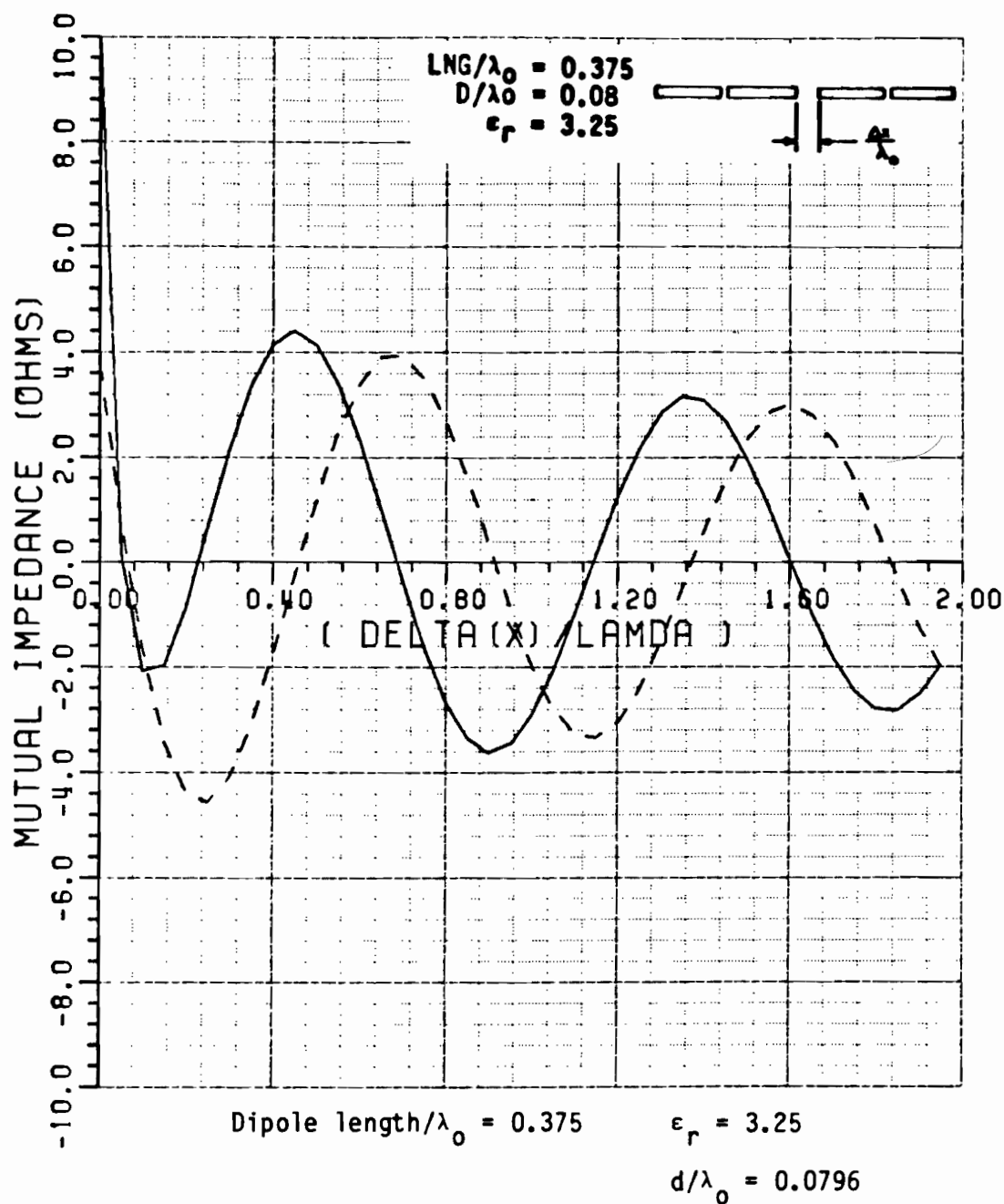


(a) E-plane coupling



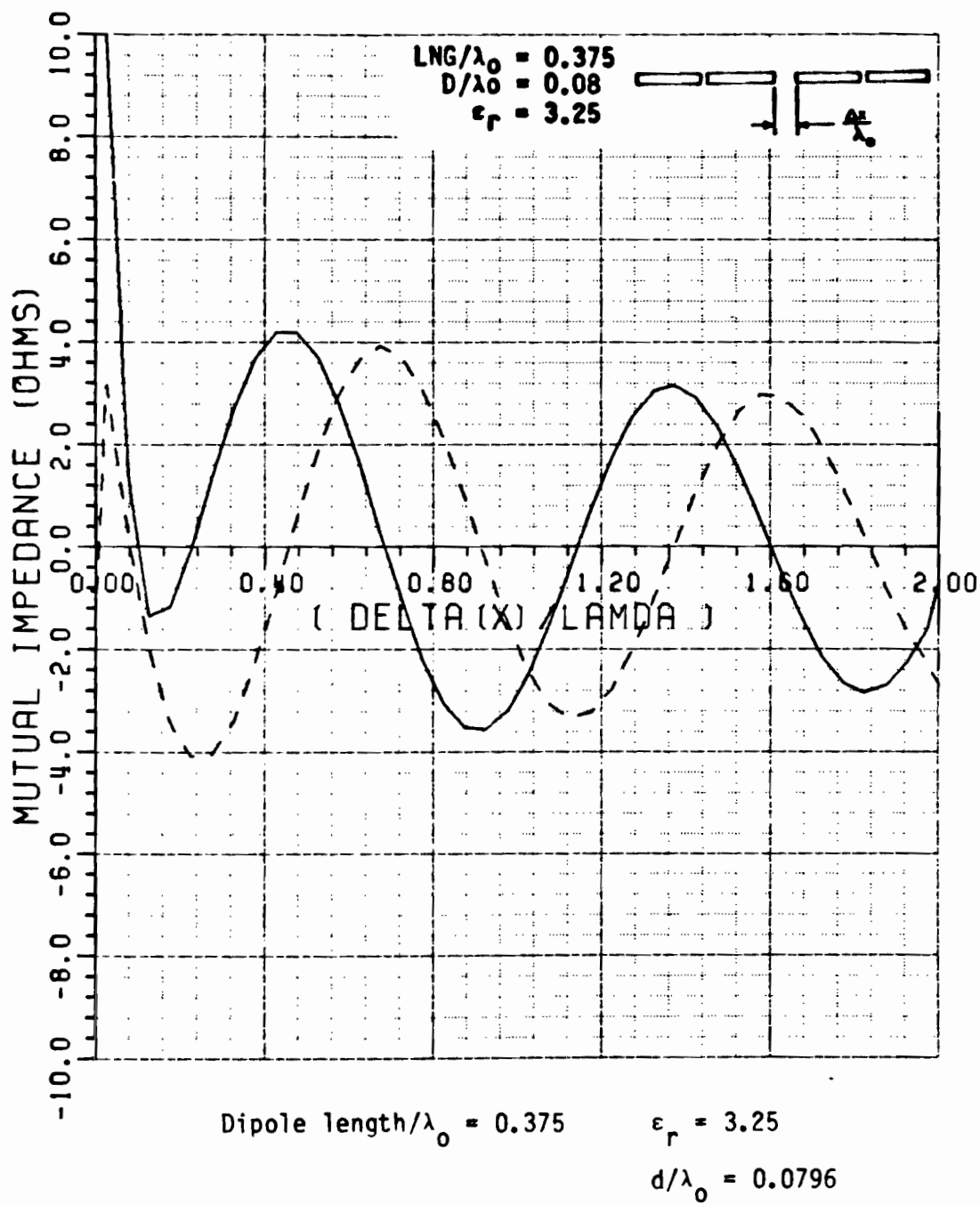
(b) H-plane coupling

Figure 7.3. Two coupled very narrow strip dipole antennas.



(a) With the exact numerical integration of the microstrip Green's function

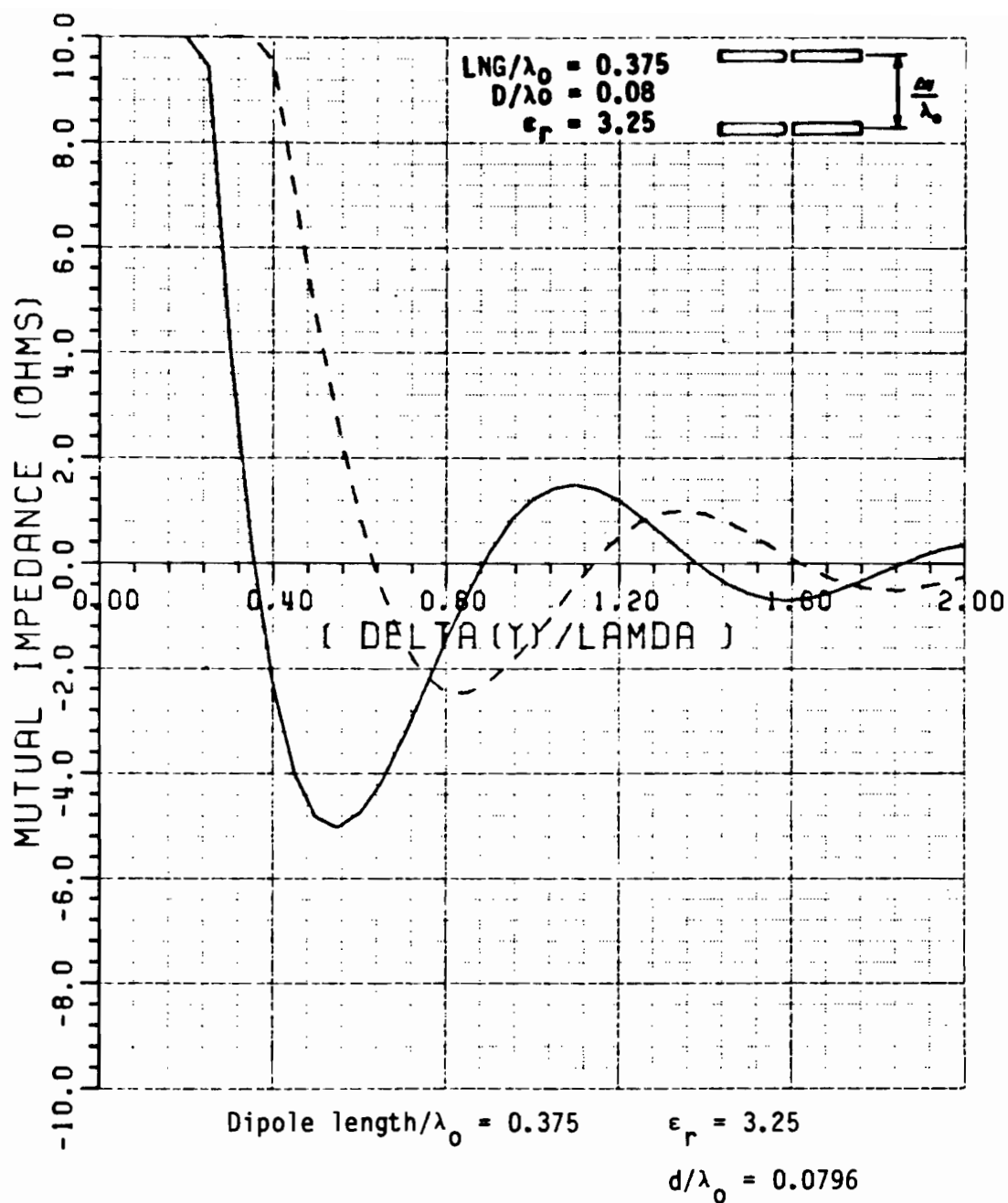
Figure 7.4. Mutual impedance of two thin strip dipoles over a grounded dielectric slab, E-plane coupling (end fire) versus the normalized separation length with respect to free space wave length.



(b) With the closed form asymptotic microstrip Green's function.

— Imaginary
 - - - Real

Figure 7.4. (continued)

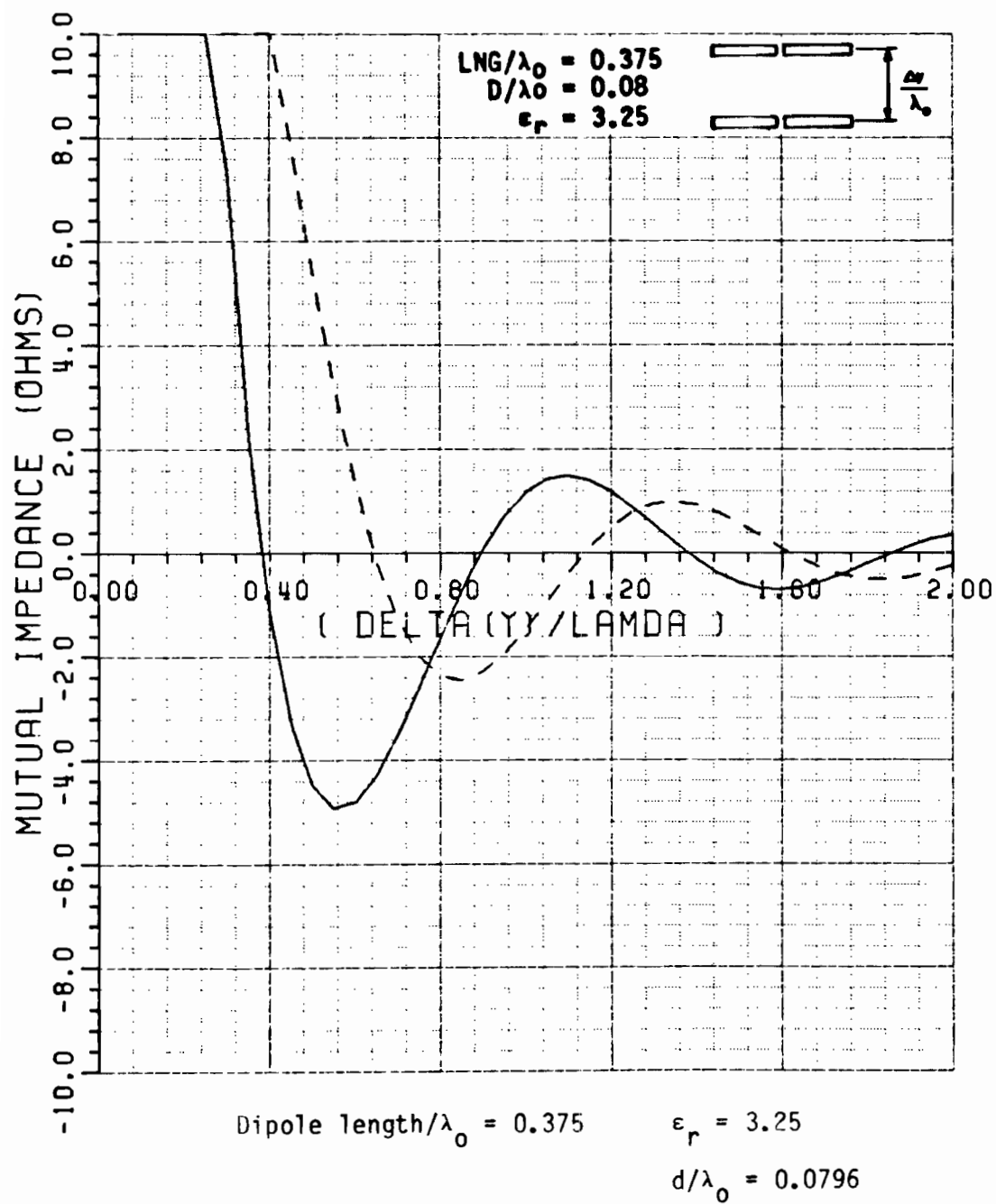


(a) With the exact numerical integration of the microstrip Green's function

—— Imaginary

----- Real

Figure 7.5. Mutual impedance of two thin strip dipoles over a grounded dielectric slab, H-plane coupling (broad side) versus the normalized separation with respect to free space wave length.



(b) With the closed form asymptotic microstrip Green's function.

— Imaginary
 ---- Real

Figure 7.5. (continued)

used for a very efficient and accurate numerical calculation of mutual coupling and the impedance matrix elements in the moment method solution of any microstrip structure. It is seen from Figure 7.4 that the (E-plane) coupling is strong and is almost a periodic function of the axial separation (Δx) without much attenuation. The dominant part of the coupling is due to the first TM surface wave which is excited most strongly in the axial direction and decays as $(\sqrt{\rho})^{-1}$. In the H-plane (broad side) case (see Figure 7.3(b)), the coupling is very strong for small lateral separations; however, it decreases very rapidly as the lateral separation increases. This is due to the fact that the space wave (higher order terms) are dominant for small lateral separation and these space waves vanish on the interface for large lateral separations. Also the first order TM surface wave has a null at broadside to the dipole.

CHAPTER VIII

CONCLUSION

A relatively simple and accurate closed form asymptotic approximation for the electric current point source microstrip dyadic surface Green's function is presented. This uniform asymptotic solution provides surprisingly good results even for very small separations of the source and field points. In addition, alternative, exact integral representations (radially propagating and steepest descent path) of microstrip dyadic Green's function are developed which are also very efficient for numerical evaluation provided the observation point is not in the immediate vicinity of the source point. For observation points in the immediate vicinity of the source point, a modification of the conventional Sommerfeld type integral representation is proposed. In contrast to the representations developed in this study, the conventional Sommerfeld integral representation converges slowly for large and even moderately large separations between the source and field points. The representations developed here do not exhibit this difficulty and are hence expected to be useful in the MM solution to a wide variety of microstrip problems.

Accuracies and efficiencies of the proposed methods have been shown through extensive numerical calculations. The input impedance of a

micro-strip dipole and the mutual impedance between two microstrip dipoles (for both the E-plane and H-plane coupling) have been found using the new representations and the utilization of the moment method. Excellent agreement between the conventional method and the new proposed representations have been demonstrated. This work is particularly useful in the moment method analysis of large microstrip antenna arrays and monolithic millimeter and microwave integrated circuit (MIMIC) where mutual coupling effects are important.

The technique which has been proposed appears to be completely general, and it appears that it can be used to treat arbitrary horizontally stratified multilayered media as well.

APPENDIX A
THE PWS SOLUTION FOR THE FREE SPACE
DYADIC GREEN'S FUNCTION $\bar{\bar{G}}^0(\bar{r}, \bar{r}')$

The free space dyadic Green's function can be constructed from the electric field \bar{E}^0 excited by an arbitrarily oriented current point source $\bar{p}_e \delta(\bar{r}-\bar{r}')$ via (2.7), namely:

$$\bar{E}^0 = -j\omega\mu_0 \bar{\bar{G}}^0(\bar{r}, \bar{r}') \cdot \bar{p}_e . \quad (A.1)$$

Since an arbitrarily oriented source may be decomposed into a transverse and longitudinal part, it is useful to treat each case separately. Note that:

$$\bar{J} = \bar{J}_t + \hat{z} J_z = \bar{p}_e \delta(\bar{r}-\bar{r}') \quad (A.2)$$

where

$$\bar{J}_t = (p_{ex} \hat{x} + p_{ey} \hat{y}) \delta(\bar{r}-\bar{r}') ; \quad J_z = p_{ez} \delta(\bar{r}-\bar{r}') . \quad (A.3)$$

Therefore,

$$\bar{E}^0 = \bar{E}^{ot} + \bar{E}^{oz} ; \quad \bar{H}^0 = \bar{H}^{ot} + \bar{H}^{oz} \quad (A.4)$$

where $(\bar{E}^{ot}, \bar{H}^{ot})$ and $(\bar{E}^{oz}, \bar{H}^{oz})$ are the fields due to transverse and vertical electric current point source, respectively; of course from the definitions given in (2.8) and (2.9)

$$\vec{E}^{ot} = \vec{E}^{<t} \quad ; \quad \vec{H}^{ot} = \vec{H}^{<t} \quad , \quad (A.5a)$$

and

$$\vec{E}^{oz} = \vec{E}^{<z} \quad ; \quad \vec{H}^{oz} = \vec{H}^{<z} \quad . \quad (A.5a)$$

Let us first consider the transverse oriented electric current point source which is located at $\vec{r}=\vec{r}'$ and has both \hat{x} and \hat{y} components of p_{ex} and p_{ey} , respectively. The fields $(\vec{E}^{<t}, \vec{H}^{<t})$ of this transverse current can be represented as in Equations (2.13) and (2.14); thus,

$$\begin{aligned} \vec{E}^{<t} = & \left[-j\omega\mu_0 \frac{\partial \Pi^{<''}}{\partial y} + \frac{\partial^2 \Pi^{<'}}{\partial x \partial z} \right] \hat{x} \\ & + \left[j\omega\mu_0 \frac{\partial \Pi^{<''}}{\partial x} + \frac{\partial^2 \Pi^{<'}}{\partial y \partial z} \right] \hat{y} + \left[\frac{\partial^2}{\partial z^2} + k_0^2 \right] \Pi^{<'}_{ot} \hat{z} \quad , \end{aligned} \quad (A.6)$$

$$\begin{aligned} \vec{H}^{<t}_0 = & \left[\frac{\partial^2 \Pi^{<'}}{\partial x \partial z} + j\omega\epsilon_0 \frac{\partial \Pi^{<'}}{\partial y} \right] \hat{x} \\ & + \left[\frac{\partial^2 \Pi^{<''}}{\partial y \partial z} - j\omega\epsilon_0 \frac{\partial \Pi^{<'}}{\partial x} \right] \hat{y} + \left[\frac{\partial^2}{\partial z^2} + k_0^2 \right] \Pi^{<''}_{ot} \hat{z} \quad , \end{aligned} \quad (A.7)$$

where

$$k_0 = \omega \sqrt{\mu_0 \epsilon_0} \quad (A.8)$$

and superscripts and subscripts "t" on $(\vec{E}^{<t}, \vec{H}^{<t})$ and $\Pi_{ot}^{>}$ denote the source is in transversal direction. The magnetic field boundary conditions (2.27) can be expressed in component form:

$$\hat{y}(H_x^{t>} - H_x^{t<}) \delta(z-z') = \hat{y}p_{ey} \delta(\vec{r}-\vec{r}') \quad , \quad (A.9)$$

$$\hat{x}(H_y^{t>} - H_y^{t<}) \delta(z-z') = \hat{x}p_{ex} \delta(\vec{r}-\vec{r}') \quad . \quad (A.10)$$

Equations (A.9) and (A.10) can be written in terms of the vector potentials $\hat{z}\Pi'$ and $\hat{z}\Pi''$. From (A.7), (A.9) and (A.10) one gets

$$\left[j\omega\epsilon_0 \left[\frac{\partial \Pi_{ot}^{>}}{\partial y} - \frac{\partial \Pi_{ot}^{<}}{\partial y} \right] + \left[\frac{\partial^2 \Pi_{ot}^{>}}{\partial x \partial z} - \frac{\partial^2 \Pi_{ot}^{<}}{\partial x \partial z} \right] \right] \delta(z-z') = p_{ey} \delta(\vec{r}-\vec{r}') \quad , \quad (A.11)$$

$$\left[-j\omega\epsilon_0 \left[\frac{\partial \Pi_{ot}^{>}}{\partial x} - \frac{\partial \Pi_{ot}^{<}}{\partial x} \right] + \left[\frac{\partial^2 \Pi_{ot}^{>}}{\partial y \partial z} - \frac{\partial^2 \Pi_{ot}^{<}}{\partial y \partial z} \right] \right] \delta(z-z') = -p_{ex} \delta(\vec{r}-\vec{r}') \quad . \quad (A.12)$$

By integrating both sides of (A.11) and (A.12) along z' and using the fact that:

$$\int \delta(\vec{r}-\vec{r}') dz' = \int \delta(\vec{\rho}-\vec{\rho}') \delta(z-z') dz' \quad (A.13)$$

$$= \delta(\vec{\rho}-\vec{\rho}') \quad (A.14)$$

one will get:

$$(H_x^{t>} - H_x^{t<}) = p_{ey} \delta(\vec{\rho}-\vec{\rho}') \quad , \quad (A.15)$$

$$(H_y^{t>} - H_y^{t<}) = p_{ex} \delta(\bar{\rho} - \bar{\rho}') \quad . \quad (A.16)$$

Now we expand the Π_{ot}' and Π_{ot}'' and $\bar{J}_t = \bar{p}_{et} \delta(\bar{r} - \bar{r}')$ in terms of plane wave spectrum (PWS) integral over the variable k_x and k_y :

$$\Pi_{ot}(r, r') = \frac{1}{4\pi^2} \iint_{-\infty}^{\infty} \tilde{\Pi}_{ot}(k_x, k_y, z, z') e^{-jk_x(x-x') - jk_y(y-y')} dk_x dk_y, \quad (A.17)$$

and

$$\bar{J}_t(r, r') = \frac{1}{4\pi^2} \iint_{-\infty}^{\infty} \tilde{\bar{J}}_t(k_x, k_y, z, z') e^{-jk_x(x-x') - jk_y(y-y')} dk_x dk_y, \quad (A.18)$$

where $\tilde{\Pi}_{ot}$ and $\tilde{\bar{J}}_t$ are the Fourier transform of Π_{ot} and \bar{J}_t . This expansion is complete [42,44], which simply means that the $\delta(\bar{\rho} - \bar{\rho}')$ can be expanded in terms of the modal plane wave $e^{-jk_x(x-x') - jk_y(y-y')}$ [42,44]. The main reason for employing this PWS expansion is that the derivative operation will transform to a multiplication operation as follows:

$$\frac{\partial}{\partial x} \Pi_{ot} \leftrightarrow -jk_x \tilde{\Pi}_{ot} \quad , \quad (A.19)$$

$$\frac{\partial}{\partial y} \Pi_{ot} \leftrightarrow -jk_y \tilde{\Pi}_{ot} \quad . \quad (A.20)$$

Therefore, the boundary conditions which contain derivative forms in the spatial domain can be transformed to algebraic equations in the spectral domain. The boundary conditions of (A.11) and (A.12) in the spectral domain will be

$$(j\omega\epsilon_0)(-jk_y)(\tilde{\Pi}_{ot}'> - \tilde{\Pi}_{ot}'<) + (-jk_x) \left(\frac{\partial}{\partial z} \tilde{\Pi}_{ot}''> - \frac{\partial}{\partial z} \tilde{\Pi}_{ot}''< \right) = p_{ey} \quad (A.21)$$

$$(-j\omega\epsilon_0)(-jk_x)(\tilde{\Pi}_{ot}^{>} - \tilde{\Pi}_{ot}^{<}) + (-jk_y) \left(\frac{\partial}{\partial z} \tilde{\Pi}_{ot}^{>} - \frac{\partial}{\partial z} \tilde{\Pi}_{ot}^{<} \right) = -p_{ex} \quad (A.22)$$

From (A.21) and (A.22) one can get:

$$\tilde{\Pi}_{ot}^{>} - \tilde{\Pi}_{ot}^{<} = \frac{1}{j\omega\epsilon_0} \frac{jk_y p_{ey} + jk_x p_{ex}}{k_x^2 + k_y^2}, \quad (A.23)$$

and

$$\frac{\partial \tilde{\Pi}_{ot}^{>}}{\partial z} - \frac{\partial \tilde{\Pi}_{ot}^{<}}{\partial z} = \frac{jk_x p_{ey} - jk_y p_{ex}}{k_x^2 + k_y^2}. \quad (A.24)$$

It is to be noted that $\tilde{\Pi}_{ot}^{>}(\bar{r}, \bar{r}')$ and $\tilde{\Pi}_{ot}^{<}(\bar{r}, \bar{r}')$ satisfy Helmholtz's equation in the source free region (see (2.15)):

$$[\nabla^2 + k_0^2] \tilde{\Pi}_{ot}^{<}(\bar{r}, \bar{r}') = 0 \quad (A.25)$$

when

$$\bar{r} \neq \bar{r}' \quad (A.26)$$

Transforming (A.25) into the spectral domain, under the validity of interchanging the differentiation and integration [42] one gets:

$$[\nabla^2 + k_0^2] \iint_{-\infty}^{\infty} \tilde{\Pi}_{ot}^{<}(k_x, k_y, z, z') e^{-jk_x(x-x') - jk_y(y-y')} dk_x dk_y = 0, \quad (A.27)$$

$$\iint_{-\infty}^{\infty} \left(\frac{\partial^2}{\partial z^2} + k_z^2 \right) \tilde{\Pi}_{ot}^{<}(k_x, k_y, z, z') e^{jk_x(x-x') - jk_y(y-y')} dk_x dk_y = 0, \quad (A.28)$$

where

$$k_z^2 = k_0^2 - (k_x^2 + k_y^2), \quad (A.29)$$

which implies

$$\left(\frac{\partial^2}{\partial z^2} + k_z^2\right) \tilde{\Pi}_{ot}^{>}(k_x, k_y, z, z') = 0 \quad . \quad (A.30)$$

Equation (A.30) is a one dimensional Helmholtz equation which can be solved along with the prescribed boundary conditions of (A.23), (A.24) and (2.16). We start with the \bar{H} mode (TE_z) case, or with the potential $\tilde{\Pi}_{ot}^{>}$ the differential equations and the boundary are as follows:

$$\left(\frac{\partial^2}{\partial z^2} + k_z^2\right) \tilde{\Pi}_{ot}^{>} = 0 \quad , \quad (A.31)$$

$$\left. \frac{\partial}{\partial z} \tilde{\Pi}_{ot}^{>} - \frac{\partial}{\partial z} \tilde{\Pi}_{ot}^{<} \right|_{z=z'} = \frac{jk_x p_{ey} - jk_y p_{ex}}{k_x^2 + k_y^2} \quad , \quad (A.32)$$

and

$$\lim_{|z| \rightarrow \infty} \left(\frac{\partial}{\partial z} \pm jk_z \right) \tilde{\Pi}_{ot}^{>} = 0 \quad . \quad (A.33)$$

It can be shown quite easily that the solution for $\tilde{\Pi}_{ot}^{>}$ is given by:

$$\tilde{\Pi}_{ot}^{>} = \frac{jk_x p_{ey} + jk_y p_{ex}}{k_x^2 + k_y^2} \frac{e^{\mp jk_z(z-z')}}{2jk_z} \quad (A.34)$$

which can be written as

$$\tilde{\Pi}_{ot}^{>} = \frac{jk_x p_{ey} + jk_y p_{ex}}{k_x^2 + k_y^2} \frac{e^{-jk_z|z-z'|}}{2jk_z} \quad . \quad (A.35)$$

For the TM case or for the $\tilde{\Pi}_0^{>}$ potential, the overall differential equation and the boundary conditions are

$$\left(\frac{\partial^2}{\partial z^2} + k_z^2\right) \tilde{\Pi}_{ot}^{\prime >} = 0 \quad (\text{A.36})$$

$$\tilde{\Pi}_{ot}^{\prime >} - \tilde{\Pi}_{ot}^{\prime <} = \frac{1}{j\omega\epsilon_0} \frac{jk_x p_{ex} + jk_y p_{ey}}{k_x^2 + k_y^2} \quad (\text{A.37})$$

$$\lim_{|z| \rightarrow \infty} \left(\frac{\partial}{\partial z} \pm jk_z\right) \tilde{\Pi}_{ot}^{\prime <} = 0 \quad (\text{A.38})$$

It can easily be shown that the solution for $\tilde{\Pi}_{ot}^{\prime <}$ is given by

$$\tilde{\Pi}_{ot}^{\prime <} = \frac{1}{j\omega\epsilon_0} \frac{jk_x p_{ex} + jk_y p_{ey}}{k_x^2 + k_y^2} \frac{\pm e^{\mp jk_z(z-z')}}{2} \quad (\text{A.39})$$

which can be written in a slightly more convenient form for later use

as:

$$\tilde{\Pi}_{ot}^{\prime <} = + \frac{1}{j\omega\epsilon_0} \frac{jk_x p_{ex} + jk_y p_{ey}}{k_x^2 + k_y^2} \frac{\partial}{\partial z'} \frac{e^{-jk_z|z-z'|}}{2jk_z} \quad (\text{A.40})$$

Note that

$$\frac{\partial \tilde{\Pi}_{ot}^{\prime <}}{\partial z} = + \frac{1}{j\omega\epsilon_0} \frac{jk_x p_{ex} + jk_y p_{ey}}{k_x^2 + k_y^2} \frac{-jk_z e^{-jk_z|z-z'|}}{2} \quad (\text{A.41})$$

From (A.17), (A.35) and (A.40) one can get

$$\Pi_{ot}^{\prime <}(\bar{r}, \bar{r}') = \frac{1}{4\pi^2} \iint_{-\infty}^{\infty} \frac{-jk_x p_{ey} + jk_y p_{ex}}{k_x^2 + k_y^2} \frac{e^{-jk_z|z-z'|}}{2jk_z} e^{-jk_x(x-x') - jk_y(y-y')} dk_x dk_y \quad (\text{A.42})$$

and

$$\Pi_{ot}^{> <}(\vec{r}, \vec{r}') = \frac{1}{4\pi^2} \iint_{-\infty}^{\infty} \frac{1}{j\omega\epsilon_0} \frac{jk_x p_{ex} + jk_y p_{ey}}{k_x^2 + k_y^2} \frac{\partial}{\partial z'} \frac{e^{-jk_z|z-z'|}}{2jk_z} e^{-jk_x(x-x') - jk_y(y-y')} dk_x dk_y \quad (A.43)$$

The fields $(\vec{E}^{> < t}, \vec{H}^{> < t})$ can be ascertained via (A.6), (A.7), (A.42) and (A.43).

Now we analyse the fields for the vertically directed point source case where

$$\vec{J}_z = \hat{z} p_{ez} \delta(\vec{r}-\vec{r}') \quad (A.44)$$

In this case one can still use the method that was employed to analyze the transversely oriented current source case. It can be shown that $\Pi_0^{> <}$ will vanish identically (no TE_z wave will be excited) and $\Pi_0^{> <}$ will be determined up to a constant; by making use of Maxwell's equation, the constant can be determined. However, we use a different but more straight forward method in this case as follows. First the fields $(\vec{E}^{0z}, \vec{H}^{0z})$ of the vertically directed current can be expressed in terms of a single vector potential, $\hat{z}\Pi_{0z}^{'}$; namely

$$\vec{H}^{0z}(\vec{r}, \vec{r}') = j\omega\epsilon_0 \nabla \times (\hat{z} \Pi_{0z}^{'}(\vec{r}, \vec{r}')) \quad (A.45)$$

where $\hat{z}\Pi_{0z}^{'}$ is a magnetic type vector potential. Also:

$$\nabla \times \vec{E}^{0z} = -j\omega\mu_0 \vec{H}^{0z} \quad , \quad (A.46)$$

$$\nabla \times \vec{H}^{0z} = j\omega\epsilon_0 \vec{E}^{0z} + \hat{z} p_{ez} \delta(\vec{r}-\vec{r}') \quad , \quad (A.47)$$

therefore

$$\nabla \times (\bar{E}^{0z} - k_0^2 \hat{z} \Pi_{0z}'(\bar{r}, \bar{r}')) = 0 \quad (\text{A.48})$$

so

$$\bar{E}^{0z} - k_0^2 \hat{z} \Pi_{0z}'(\bar{r}, \bar{r}') = -\nabla \phi_{0z} \quad (\text{A.49})$$

Then

$$\bar{E}^{0z} = k_0^2 \hat{z} \Pi_{0z}'(\bar{r}, \bar{r}') - \nabla \phi_{0z} ,$$

but from the Equations (A.47) and (A.49)

$$j\omega\epsilon_0 (\nabla \times \nabla \times \hat{z} \Pi_{0z}' - k_0^2 \hat{z} \Pi_{0z}') = -j\omega\epsilon_0 \nabla \phi_{0z} + \hat{z} p_e \delta(\bar{r} - \bar{r}') . \quad (\text{A.50})$$

It is noted that

$$\nabla \times \nabla \times = \nabla \nabla \cdot - \nabla^2 \quad (\text{A.51})$$

and if one imposes the Lorentz condition,

$$\nabla \cdot \hat{z} \Pi_{0z}' = -\phi_{0z} , \quad (\text{A.52})$$

then it follows that

$$\nabla^2 \Pi_{0z}' + k_0^2 \Pi_{0z}' = \frac{-1}{j\omega\epsilon_0} p_{ez} \delta(\bar{r} - \bar{r}') . \quad (\text{A.53})$$

Let us expand both sides of the above equation in terms of the plane wave spectrum integral introduced before, and interchange the derivative operations and integration to obtain

$$\frac{1}{4\pi^2} \iint_{-\infty}^{\infty} \left[\left[\frac{\partial^2}{\partial z^2} + (k_0^2 - (k_x^2 + k_y^2)) \right] \tilde{\Pi}'_{oz} + \frac{1}{j\omega\epsilon_0} p_{ez} \delta(z-z') \right] e^{-jk_t \cdot (\bar{\rho} - \bar{\rho}')} dk_x dk_y = 0 \quad (A.54)$$

It follows that:

$$\left[\frac{\partial^2}{\partial z^2} + (k_0^2 - k_t^2) \right] \tilde{\Pi}'_{oz} = + \frac{1}{j\omega\epsilon_0} p_{ez} \delta(z-z') , \quad (A.55)$$

Imposing the radiation condition at infinity:

$$\tilde{\Pi}'_{oz} = \frac{1}{j\omega\epsilon_0} p_{ez} \frac{e^{-jk_z |z-z'|}}{2jk_z} \quad (A.56)$$

so

$$\hat{z} \tilde{\Pi}'_{oz} = \hat{z} \frac{1}{4\pi^2} \iint_{-\infty}^{\infty} \frac{1}{j_0 \epsilon_0} p_{ez} \frac{e^{-jk_z |z-z'|}}{2jk_z} e^{-j\bar{k}_t \cdot (\bar{\rho} - \bar{\rho}')} dk_x dk_y . \quad (A.57)$$

The fields $(\bar{E}^{oz}, \bar{H}^{oz})$ can be ascertained via (A.46), (A.47) and (A.57). It is noted that

$$\tilde{\Pi}'_{oz} = \tilde{\Pi}'_{oz}^{>} ; z \geq z' \quad (A.58)$$

Finally the electromagnetic fields $(\bar{E}_0^0, \bar{H}_0^0)$ radiated by an arbitrarily oriented current point source $\bar{p}_e \delta(\bar{r} - \bar{r}')$ (transverse and longitudinal) is given by

$$\bar{E}^0 = \bar{E}^{ot} + \bar{E}^{oz} , \quad (A.59)$$

$$\bar{H}^0 = \bar{H}^{0t} + \bar{H}^{0z}, \quad (A.60)$$

or

$$\begin{aligned} \bar{E}^0 = & \left[-j\omega\mu_0 \frac{\partial \Pi_0^{<''}}{\partial y} + \frac{\partial^2 \Pi_0^{<'}}{\partial x \partial z} \right] \hat{x} + \left[j\omega\mu_0 \frac{\partial \Pi_0^{<''}}{\partial x} + \frac{\partial^2 \Pi_0^{<'}}{\partial y \partial z} \right] \hat{y} \\ & + \left[\frac{\partial^2}{\partial z^2} + k_0^2 \right] \Pi_0^{<' } \hat{z} - \frac{1}{j\omega\epsilon_0} \hat{z} \cdot \mathbf{p}_{ez} \delta(\bar{r} - \bar{r}') \end{aligned} \quad (A.61)$$

$$\begin{aligned} \bar{H}^0 = & \left[\frac{\partial^2 \Pi_0^{<'}}{\partial x \partial z} + j\omega\epsilon_0 \frac{\partial \Pi_0^{<'}}{\partial y} \right] \hat{x} \\ & + \left[\frac{\partial^2 \Pi_0^{<''}}{\partial y \partial z} - j\omega\epsilon_0 \frac{\partial \Pi_0^{<'}}{\partial x} \right] \hat{y} + \left[\frac{\partial^2}{\partial z^2} + k_0^2 \right] \Pi_0^{<''} \hat{z}, \end{aligned} \quad (A.62)$$

where

$$\Pi_0^{<''} = \Pi_{ot}^{<''}, \quad (A.63)$$

and

$$\Pi_0^{<' } = \Pi_{ot}^{<' } + \Pi_{oz}^{<' }. \quad (A.64)$$

The expressions of $\Pi_{ot}^{<''}$, $\Pi_{ot}^{<' }$ and $\Pi_{oz}^{<' }$ have been given in (A.42), (A.43) and (A.57). (A.63) and (A.64) can be written in more compact form.

$$\begin{aligned} \Pi_0^{\prime\prime} &= \frac{-1}{4\pi^2} \frac{1}{j\omega\mu_0} \iint_{-\infty}^{\infty} \frac{(\hat{z} \times \bar{p}_e)}{k_t^2} \\ &\quad \cdot \nabla_t \left[e^{-j\bar{k}_t \cdot (\bar{\rho} - \bar{\rho}')} \right] g^{\prime\prime}(kz, z, z') dk_x dk_y, \end{aligned} \quad (A.65)$$

$$\begin{aligned} \Pi_0^{\prime} &= \frac{-1}{4\pi^2} \frac{1}{j\omega\epsilon_0} \iint_{-\infty}^{\infty} \frac{(\bar{p}_e \cdot \nabla_t)}{k_t^2} \\ &\quad \left[e^{-j\bar{k}_t \cdot (\bar{\rho} - \bar{\rho}')} \right] \frac{\partial}{\partial z'} \frac{g^{\prime}(kz, z, z')}{j\omega\epsilon_0} dk_x dk_y \\ &\quad + \iint_{-\infty}^{\infty} \bar{p}_e \cdot \hat{z} e^{-j\bar{k}_t \cdot (\bar{\rho} - \bar{\rho}')} \frac{g^{\prime}(kz, z, z')}{j\omega\epsilon_0} dk_x dk_y \end{aligned} \quad (A.66)$$

where

$$k_t^2 = k_x^2 + k_y^2 \quad ; \quad \bar{k}_t = \hat{x}k_x + \hat{y}k_y ,$$

$$\bar{\rho} - \bar{\rho}' = \hat{x}(x - x') + \hat{y}(y - y') , \quad (A.67)$$

$$g^{\prime\prime}(kz, z, z') = j\omega\mu_0 \frac{e^{-jk_z|z-z'|}}{2jk_z} , \quad (A.68)$$

$$g^{\prime}(kz, z, z') = j\omega\epsilon_0 \frac{e^{-jk_z|z-z'|}}{2jk_z} , \quad (A.69)$$

$$k_z = \sqrt{k_0^2 - k_t^2} ,$$

and use has been made via the definition of transverse operator,

$$\nabla_t = \hat{x} \frac{\partial}{\partial x} + \hat{y} \frac{\partial}{\partial y} .$$

The components of the free space dyadic Green's function can be inferred via the (A.1), (A.61), (A.65) and (A.66).

APPENDIX B

RADIATION AND EDGE CONDITIONS

In Chapter II, we convert the electromagnetic vector wave equation to the two scalar Helmholtz equations:

$$[\nabla^2 + k^2] \Pi(\vec{r}, \vec{r}') = 0 \quad ; \quad \vec{r} \neq \vec{r}' \quad (\text{B.1})$$

where k is the wave number, which in general is complex, and the region of interest has a boundary at infinity. If all sources are confined in a finite region, the solution at large distance from the sources must meet a physical constraint, that is the energy must travel away from the source region. Sommerfeld constitutes this constraint as a boundary condition on a surface at infinity, known as the "radiation condition" it states [39]:

$$\lim_{r \rightarrow \infty} r [\nabla \times \vec{E} - jk\hat{r} \times \vec{E}] = 0 \quad , \quad (\text{B.2})$$

or

$$\lim_{r \rightarrow \infty} r \left(\frac{\partial \Pi}{\partial r} + jk\Pi \right) = 0 \quad , \quad (\text{B.3})$$

which implies that

$$\lim_{r \rightarrow \infty} \Pi \sim \frac{e^{-jkr}}{r} \quad (\text{B.4})$$

For the one dimensional Helmholtz equation, one has:

$$\left(\frac{d^2}{dz^2} + \kappa^2\right) \tilde{\Pi}(z, z') = 0 \quad ; \quad z \neq z' \quad . \quad (B.5)$$

The Sommerfeld radiation condition will be

$$\lim_{z \rightarrow \pm\infty} \left(\frac{\partial \tilde{\Pi}}{\partial z} \pm j\kappa \tilde{\Pi} \right) \rightarrow 0 \quad (B.6)$$

which implies

$$\lim_{z \rightarrow \pm\infty} \tilde{\Pi}(z, z') \sim e^{\mp j\kappa z} \quad (B.7)$$

This constrain also ensures uniqueness for Helmholtz's equation when the region has a boundary at infinity. Another situation which we have encountered in Chapter VI, arises when the configuration of the problem contains geometrical singularities, such as sharp edges. Since at the geometrical singularities the normal to the surface can not be defined uniquely, an additional physical condition is needed to assure the uniqueness to the solution of the field problem. This condition, first introduced by Meixner [59], is known as the edge condition. It is required that the electric and magnetic energy stored in any finite neighborhood of the edge (or wedge) be finite; it is inferred that no component of the electric or magnetic field can grow more rapidly than $\rho^{-1+\alpha}$, where ρ is the distance from the edge (see Figure B.1) and α is a positive constant.

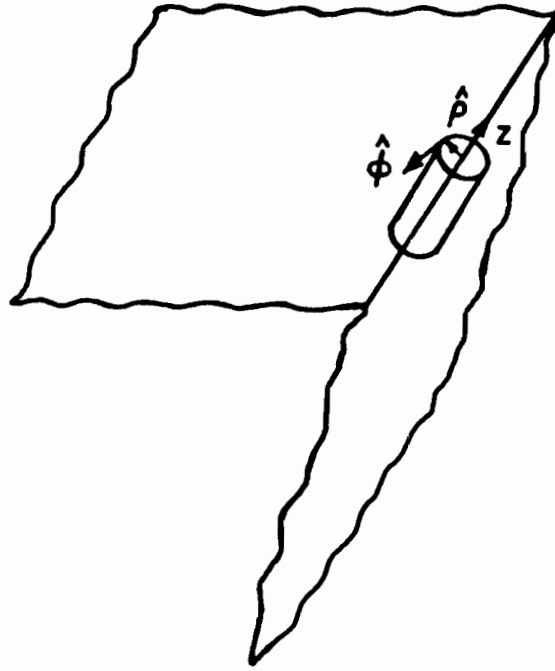


Figure B.1. Three dimensional wedge (surface singularity); the electromagnetic energy must be finite in any small finite volume (shown by small cylinder) at the neighborhood of the wedge.

These conditions constitute the surface current singularity behavior close to the edge. For the conductor microstrip patches in Chapter VI, the component of the surface current parallel to the edge at most has singularity of $\rho^{-1+\alpha}$, ($\alpha > 0$) where ρ is the distance from the edge (see Figure B.2)

$$\bar{J}(x,y) \sim \hat{x}y^{-1+\alpha} f(x) \quad . \quad (B.8)$$

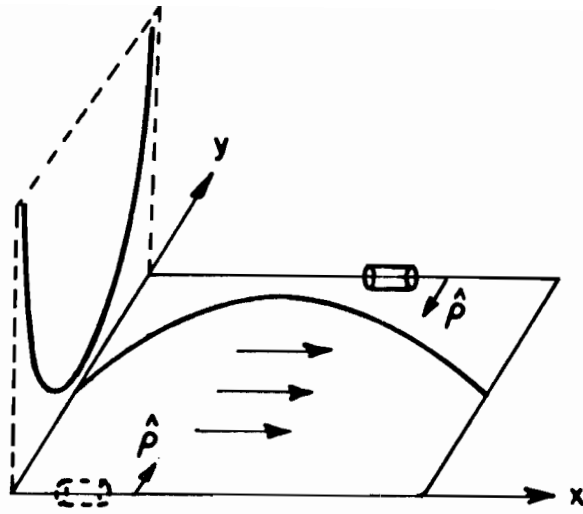


Figure B.2. Current singularity close to the edges. Current is flowing in the x direction ($\bar{J}(x,y) \sim \hat{x}y^{-1+\alpha} f(x)$).

APPENDIX C

SOMMERFELD INTEGRAL REPRESENTATION OF THE MICROSTRIP DYADIC GREEN'S FUNCTION

In this appendix the Sommerfeld integral representation of the electromagnetic fields (\vec{E}_m, \vec{H}_m) due to an arbitrarily oriented current point source $\vec{p}_e \delta(\vec{r} - \vec{r}')$ in the presence of the grounded dielectric slab will be presented. This representation will be derived from the PWS representation of (\vec{E}_m, \vec{H}_m) given in (2.46), (2.47). The Sommerfeld integral representation for the microstrip dyadic Green's function can then be inferred by inspection via (3.31).

Consider first the function I (a double Fourier integral) which essentially constitutes a typical PWS integral,

$$I = \iint_{-\infty}^{\infty} F(k_t) e^{-j(k_x(x-x') + k_y(y-y'))} dk_x dk_y, \quad (C.1)$$

where

$$k_t^2 = k_x^2 + k_y^2, \quad (C.2)$$

and we are interested in the Fourier-Bessel representation of this function [42]. Let us introduce the following transformation of variables

$$k_t = \xi \quad ; \quad k_x = \xi \cos \alpha \quad ; \quad k_y = \xi \sin \alpha \quad (C.3)$$

and

$$(x-x') = \rho \cos \phi - \rho' \cos \phi' \quad ; \quad y-y' = \rho \sin \phi - \rho' \sin \phi' \quad . \quad (C.4)$$

Note that

$$dk_x dk_y = \left| \begin{vmatrix} \frac{\partial k_x}{\partial \xi} & \frac{\partial k_y}{\partial \xi} \\ \frac{\partial k_x}{\partial \alpha} & \frac{\partial k_y}{\partial \alpha} \end{vmatrix} \right| d\xi d\alpha = \xi d\xi d\alpha \quad , \quad (C.5)$$

therefore

$$I = \iint_{-\infty}^{\infty} F(k_t) e^{-j\vec{k}_t \cdot (\vec{\rho} - \vec{\rho}')} dk_x dk_y \quad (C.6)$$

$$= \int_0^{\infty} \int_0^{2\pi} F(\xi) e^{-j(\rho \xi \cos(\alpha - \phi) - \rho' \xi \cos(\alpha - \phi'))} d\alpha \xi d\xi \quad , \quad (C.7)$$

but

$$e^{\pm j\beta \cos \gamma} = \sum_{m=-\infty}^{\infty} (\pm j)^m J_m(\beta) e^{\pm jm\gamma} \quad , \quad (C.8)$$

so the Equation (4.7) can be written as

$$I = \int_0^{\infty} F(\xi) \sum_{n=-\infty}^{\infty} \sum_{m=-\infty}^{\infty} (j)^{m-n} \int_0^{2\pi} J_n(\xi \rho) J_m(\xi \rho') e^{-j(n\phi - m\phi')} e^{-j(n-m)\alpha} d\alpha \xi d\xi \quad (C.9)$$

or,

$$I = 2\pi \sum_{n=-\infty}^{\infty} e^{-jn(\phi - \phi')} \int_0^{\infty} F(\xi) J_n(\xi \rho) J_n(\xi \rho') \xi d\xi \quad . \quad (C.10)$$

In deriving the above result use has been made from the following identity

$$\int_0^{2\pi} e^{\pm j(n-m)\alpha} d\alpha = \begin{cases} 0 & n \neq m \\ 2\pi & n = m \end{cases} \quad (C.11)$$

Equation (C.10) is the Fourier-Bessel representation of the double Fourier integral function I in (C.1). If the coordinate system is chosen so that $\rho' = 0$, then the expression (C.10) reduces (in view of $J_0(0) = 1$, $J_m(0) = 0$; $m \neq 0$) to

$$I = 2\pi \int_0^{\infty} F(\xi) J_0(\xi \rho) \xi d\xi \quad (C.12)$$

This is the Sommerfeld type integral representation of the function I which was given in terms of its PWS representation in (C.1). Now with this introduction, we rewrite the PWS representations of the electromagnetic fields (\bar{E}_m, \bar{H}_m) in (2.46) and (2.47) in the conventional form. Thus, the fields in region m ($m=0$ or 1) are:

$$\begin{aligned} \bar{E}_m = & \left[-j\omega\mu_m \frac{\partial \pi''_m}{\partial y} + \frac{\partial^2 \pi'_m}{\partial x \partial z} \right] \hat{x} + \left[j\omega\mu_m \frac{\partial \pi''_m}{\partial x} + \frac{\partial^2 \pi'_m}{\partial y \partial z} \right] \hat{y} \\ & + \left[\frac{\partial^2}{\partial z^2} + k_m^2 \right] \pi'_m \hat{z} - \frac{1}{j\omega\epsilon_0} p_{ez} \delta(\bar{r} - \bar{r}') \hat{z} \end{aligned} \quad (C.13)$$

and

$$\begin{aligned} \bar{H}_m = & \left[\frac{\partial^2 \pi''_m}{\partial x \partial z} + j\omega\epsilon_m \frac{\partial \pi'_m}{\partial y} \right] \hat{x} + \left[\frac{\partial^2 \pi''_m}{\partial y \partial z} - j\omega\epsilon_m \frac{\partial \pi'_m}{\partial x} \right] \hat{y} \\ & + \left[\frac{\partial^2}{\partial z^2} + k_m^2 \right] \pi''_m \hat{z}, \end{aligned} \quad (C.14)$$

in which

$$\pi_m'' = \frac{1}{4\pi^2} \frac{1}{j\omega\mu_m} \iint_{-\infty}^{\infty} \frac{-(\hat{z}_x \hat{\rho}_e)}{k_t^2} \cdot \nabla_t g_m''(\kappa, z, z') e^{-j\bar{k}_t \cdot (\bar{\rho} - \bar{\rho}')} dk_x dk_y, \quad (C.15)$$

and

$$\pi_m'' = \frac{1}{4\pi^2} \frac{1}{(j\omega\epsilon_m)} \frac{1}{(j\omega\epsilon_0)} \iint_{-\infty}^{\infty} \left(\frac{-\bar{\rho}_{et}}{k_t^2} \cdot \frac{\partial}{\partial z'} \nabla_t + \rho_{ez} \right) \cdot g_m'(\kappa, z, z') e^{-j\bar{k}_t \cdot (\bar{\rho} - \bar{\rho}')} dk_x dk_y, \quad (C.16)$$

with

$$\bar{\rho}_e = \bar{\rho}_{et} + \hat{z} \rho_{ez}, \quad (C.17)$$

and g_m'' and g_m' are given in (2.77), (2.78) and, (2.83) and (2.84). As usual, ∇_t denotes the transverse (to z). Laplacian operator,

$$\nabla_t = \hat{x} \frac{\partial}{\partial x} + \hat{y} \frac{\partial}{\partial y}, \quad (C.18)$$

which can also be expressed as

$$= \hat{\rho} \frac{\partial}{\partial \rho} + \frac{1}{\rho} \hat{\phi} \frac{\partial}{\partial \phi}. \quad (C.19)$$

In the following, the conventional Sommerfeld integral representation of π_m'' and π_m' will be derived from their PWS integral representations. Using the procedure in Equations (C.1) through (C.11), and perform the Del operation in (C.15) and (C.16), knowing the fact that $J_0'(x) = -J_1(x)$, and let $\rho' \rightarrow 0$; then one will get

$$\pi_m'' = \frac{1}{2\pi} \frac{1}{j\omega\mu_m} \int_0^\infty (\hat{z} \times \bar{p}_e) \cdot \hat{\rho} g_m''(\kappa, z, z') J_1(\xi\rho) d\xi, \quad (C.20)$$

and

$$\begin{aligned} \pi_m' = \frac{1}{2\pi} \frac{1}{j\omega\epsilon_m} \frac{1}{j\omega\epsilon_0} \{ & \int_0^\infty \bar{p}_e \cdot \hat{\rho} \frac{\partial}{\partial z'} g_m'(\kappa, z, z') J_1(\xi\rho) d\xi \\ & + \int_0^\infty \bar{p}_e \cdot \hat{z} g_m'(\kappa, z, z') J_0(\xi\rho) d\xi \} \end{aligned}, \quad (C.21)$$

where

$$\kappa = \sqrt{k^2 - \xi^2}, \quad (C.22)$$

there, k will take the value of the wave number of air or dielectric, k_0 and k_1 and

$$\hat{\rho} = \hat{x} \cos\phi + \hat{y} \sin\phi. \quad (C.23)$$

Equations (C.20) and (C.21) are the Sommerfeld integral representations of the Hertzian potentials for a grounded dielectric slab excited by an electric point current source. The explicit expressions of g_m'' and g_m' are given in (2.77), (2.78), (2.83) and (2.84) with k_t replaced by ξ in (2.82) via (3.15). The Sommerfeld representations for the electric and magnetic fields can be found readily via Equations (C.13) and (C.14) after noting that

$$\frac{\partial}{\partial x} \leftrightarrow \cos\phi \frac{\partial}{\partial \rho} - \frac{1}{\rho} \sin\phi \frac{\partial}{\partial \phi}; \quad \frac{\partial}{\partial y} \leftrightarrow \sin\phi \frac{\partial}{\partial \rho} + \frac{1}{\rho} \cos\phi \frac{\partial}{\partial \phi}. \quad (C.24)$$

The explicit values of the electric field \bar{E}_m in component form are

$$\bar{E}_m = \hat{x} \bar{E}_{mx} + \hat{y} \bar{E}_{my} + \hat{z} \bar{E}_{mz}, \quad (C.25)$$

where

$$\begin{aligned}
 E_{mx} = & \frac{1}{2\pi} \left\{ p_{ex} \left[\int_0^\infty (\sin^2\phi \xi J_1'(\xi\rho) + \frac{\cos^2\phi}{\rho} J_1(\xi\rho)) g_m''(\kappa, z, z') d\xi \right. \right. \\
 & + \frac{1}{j\omega\epsilon_m} \frac{1}{j\omega\epsilon_0} \int_0^\infty (\cos^2\phi \xi J_1'(\xi\rho) + \frac{\sin^2\phi}{\rho} J_1(\xi\rho)) \frac{\partial^2}{\partial z \partial z'} g_m'(\kappa, z, z') d\xi \\
 & + p_{ey} \cos\phi \sin\phi \left[\int_0^\infty (-J_1'(\xi\rho)\xi + \frac{1}{\rho} J_1(\xi\rho)) (g_m''(\kappa, z, z') \right. \\
 & \quad \left. \left. - \frac{1}{j\omega\epsilon_m} \frac{1}{j\omega\epsilon_0} \frac{\partial^2}{\partial z \partial z'} g_m'(\kappa, z, z') d\xi \right] \right. \\
 & \left. + p_{ez} \frac{1}{j\omega\epsilon_m} \frac{1}{j\omega\epsilon_0} \cos\phi \int_0^\infty J_0'(\xi\rho)\xi^2 \frac{\partial}{\partial z} g_m'(\kappa, z, z') d\xi \right\}, \quad (C.26)
 \end{aligned}$$

$$\begin{aligned}
 E_{my} = & \frac{1}{2\pi} \left\{ -p_{ex} \sin\phi \cos\phi \left[\int_0^\infty (\xi J_1'(\xi\rho) + \frac{1}{\rho} J_1(\xi\rho)) (g_m''(\kappa, z, z') \right. \right. \\
 & \left. \left. + \frac{1}{j\omega\epsilon_m} \frac{1}{j\omega\epsilon_0} \frac{\partial^2}{\partial z \partial z'} g_m'(\kappa, z, z') d\xi \right] \right. \\
 & + p_{ey} \left[\int_0^\infty -(\cos^2\phi \xi J_1'(\xi\rho) + \frac{\sin^2\phi}{\rho} J_1(\xi\rho)) g_m''(\kappa, z, z') d\xi \right. \\
 & + \frac{1}{j\omega\epsilon_m} \frac{1}{j\omega\epsilon_0} \int_0^\infty (\sin^2\phi \xi J_1'(\xi\rho) \\
 & \quad \left. + \frac{\cos^2\phi}{\rho} J_1(\xi\rho)) \frac{\partial^2}{\partial z \partial z'} g_m'(\kappa, z, z') d\xi \right] \\
 & \left. + p_{ey} \frac{1}{j\omega\epsilon_m} \frac{1}{j\omega\epsilon_0} \sin\phi \left[\int_0^\infty J_0'(\xi\rho)\xi^2 \frac{\partial}{\partial z} g_m'(\kappa, z, z') d\xi \right] \right\} \quad (C.27)
 \end{aligned}$$

and

$$\begin{aligned}
 E_{mz} = & \frac{1}{2\pi} \frac{1}{j\omega\epsilon_m} \frac{1}{j\omega\epsilon_0} \left\{ p_{ex} \cos\phi \int_0^\infty \left(\frac{\partial^2}{\partial z^2} + k_m^2 \right) \frac{\partial}{\partial z'} g'_m(\kappa, z, z') J_1(\xi\rho) d\xi \right. \\
 & + p_{ex} \sin\phi \int_0^\infty \left(\frac{\partial^2}{\partial z^2} + k_m^2 \right) \frac{\partial}{\partial z'} g'_m(\kappa, z, z') J_1(\xi\rho) d\xi \\
 & \left. + p_{ez} \int_0^\infty \left(\frac{\partial^2}{\partial z^2} + k_m^2 \right) \frac{\partial}{\partial z'} g'_m(\kappa, z, z') J_0(\xi\rho) \xi d\xi \right\} - \frac{1}{j\omega\epsilon_0} p_{ez} \delta(\vec{r}-\vec{r}')
 \end{aligned} \tag{C.28}$$

Equations (C.26) through (C.28) directly provide the Sommerfeld representation for the single layer microstrip dyadic Green's function via (3.31) which provides an explicit relationship between the fields and the corresponding Green's function.

APPENDIX D

ANALYTIC PROPERTY OF $\kappa(\xi) = \sqrt{k^2 - \xi^2}$ IN THE COMPLEX ξ PLANE

As mentioned in Chapter IV, the Green's Function integrands contain branch-point singularities at

$$\xi = \pm k_0^2 \quad . \quad (D.1)$$

To assure a unique specification of integrands in the complex ξ plane, it is necessary to discuss the analytic properties of the double valued function $\kappa(\xi)$.

For analytic convenience let's assume that the medium is slightly lossy;

$$k_0 = k' - jk'' \quad , \quad (D.2)$$

where k' and k'' are both positive and real and

$$k' \gg k'' \quad . \quad (D.3)$$

The lossless case can be treated as a limiting case when $k'' \rightarrow 0$. Because of the radiation condition given in Appendix B, which specifies either an outgoing or evanescent wave for large distance from the source, the double valued function $\kappa(\xi)$ has to satisfy the following conditions along any path in the ξ plane, namely

$$\text{Im } \kappa(\xi) < 0 \quad , \quad (\text{D.4})$$

and

$$\text{Re } \kappa(\xi) > 0 \quad . \quad (\text{D.5})$$

To specify $\kappa(\xi)$ uniquely, it is convenient to view the complex $\xi = \xi' + j\xi''$ as a two sheeted surface with the sheets connected along the branch cuts. In each sheet $\kappa(\xi)$ is a single-valued and analytic function of ξ . If ξ changes continuously, the value of $\kappa(\xi)$ becomes discontinuous only if a branch cut is crossed, in which the sign of $\kappa(\xi)$ is changed. The choice of the branch cuts is arbitrary, but for our particular problem, a set of branch cuts will be defined based on the restrictions given by Equations (D.4) and (D.5).

The branch cut of $\kappa(\xi)$ in the ξ -plane is defined such that $\text{Im}\kappa(\xi) < 0$ on one sheet, say, the top or proper sheet, and $\text{Im}\kappa(\xi) > 0$ on the bottom or improper sheet. This definition implies that the two sheets are joined together by the curve defined by $\text{Im}(\kappa(\xi)) = 0$, which therefore locates the desired branch cut [42,60].

As a first step to specify this branch cut, let's write $\kappa^2(\xi)$ as

$$\kappa^2(\xi) = k^2 - \xi^2 = (k' - jk'')^2 - (\xi' + j\xi'')^2 \quad , \quad (\text{D.6})$$

which can be written as:

$$\kappa^2(\xi) = (k'^2 - k''^2 - \xi'^2 + \xi''^2) + j(-2)(k'k'' + \xi'\xi'') \quad (\text{D.7})$$

The complex ξ -plane can be subdivided by the curves $\text{Re}(\kappa^2(\xi)) = 0$ and $\text{Im}(\kappa^2(\xi)) = 0$, as shown in Figure D.1, where the horizontally shaded region corresponds to $\text{Re}(\kappa^2(\xi)) < 0$ and vertically shaded regions

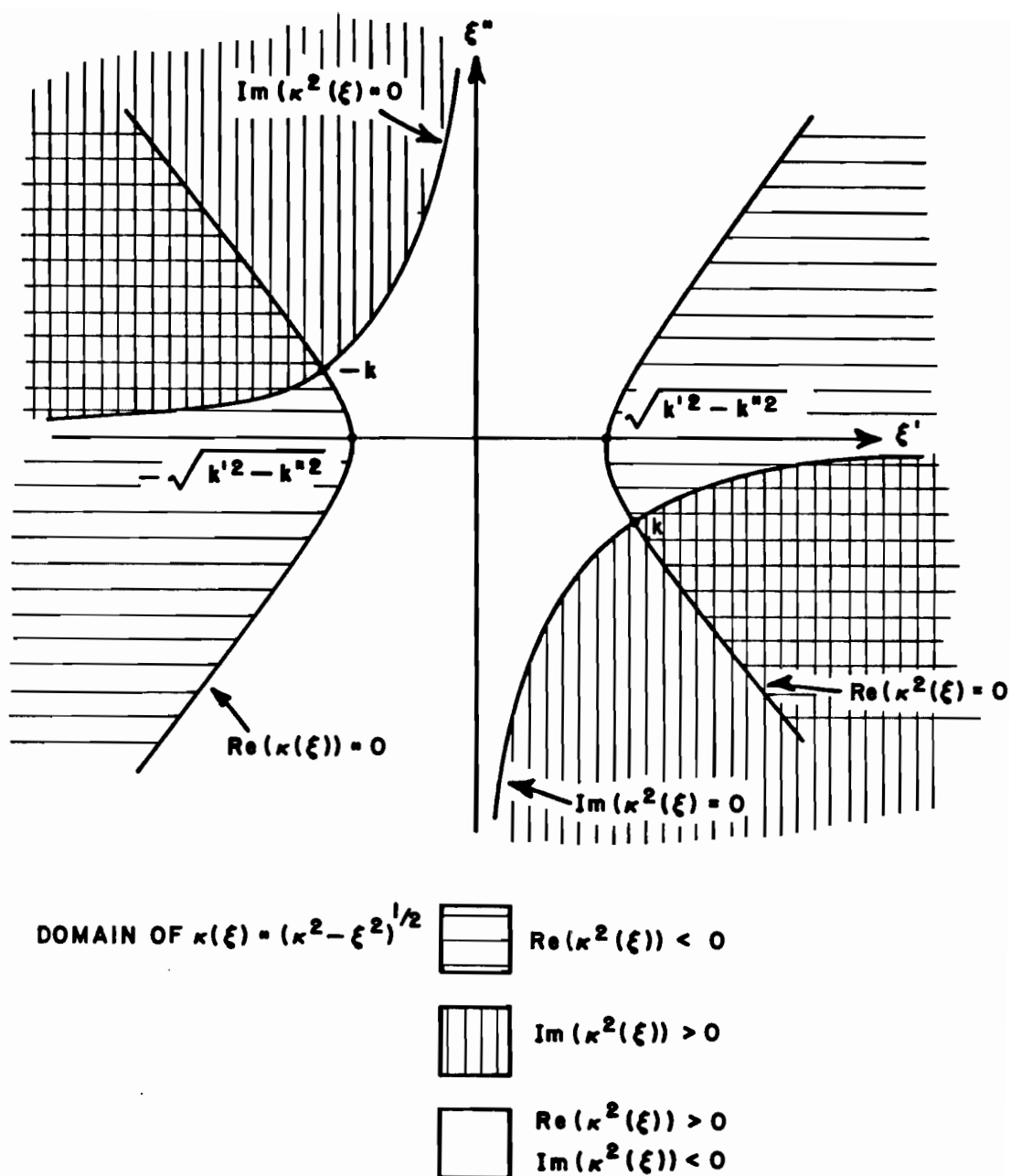


Figure D.1. Regions in the complex ξ separated by curves $\text{Re}(\kappa^2(\xi))=0$ and $\text{Im}(\kappa^2(\xi))=0$.

correspond to $\text{Im}(\kappa^2(\xi)) > 0$. The unshaded regions correspond to both $\text{Re}(\kappa^2(\xi)) > 0$ and $\text{Im}(\kappa^2(\xi)) < 0$.

Recall that the locus of $\text{Re}(\kappa^2(\xi)) = 0$ in the ξ plane is given by the equation:

$$k'^2 - k''^2 - \xi'^2 + \xi''^2 = 0 \quad , \quad (\text{D.8})$$

which is the equation of a hyperbola and the locus of $\text{Im}(\kappa^2(\xi)) = 0$ in the ξ plane is given by the equation:

$$k'k'' + \xi'\xi'' = 0 \quad , \quad (\text{D.9})$$

or

$$\xi'' = - \frac{k'k''}{\xi'} \quad . \quad (\text{D.10})$$

To insure that $\text{Im}(\kappa(\xi)) < 0$ on the entire top sheet, it is required that the argument of $\kappa^2(\xi)$ be restricted to the following domain:

$$2\pi < \text{Arg}(\kappa^2(\xi)) < 4\pi \quad , \quad (\text{D.11})$$

which implies

$$\pi < \text{Arg}(\kappa(\xi)) < 2\pi \quad . \quad (\text{D.12})$$

This, in turn, prescribes the choice of the branch cut; that is

$$\text{Im}(\kappa^2(\xi)) = 0 \quad , \quad (\text{D.13})$$

and

$$\text{Re}(\kappa^2(\xi)) > 0 \quad . \quad (\text{D.14})$$

The branch cuts of the function $\kappa(\xi)$ have been uniquely specified and shown by wiggly lines in Figure D.2. On the bottom sheet, it follows from Equation (D.11) that

$$0 < \text{Arg}(\kappa^2(\xi)) < 2\pi \quad , \quad (\text{D.15})$$

which implies:

$$0 < \text{Arg}(\kappa(\xi)) < \pi \quad . \quad (\text{D.16})$$

The top and bottom sheet are shown in Figures D.3. The signs of $\text{Re}(\kappa^2(\xi))$ and $\text{Im}(\kappa^2(\xi))$ on the entire two-sheeted ξ plane are summarized in Table (D.1). As the limiting case shown $\kappa \rightarrow 0$, the two sheeted ξ plane has been shown in Figure D.4 and the top and bottom sheets have been shown in Figure D.5.

TABLE D.1
SIGNS OF $\text{Re}(\kappa(\xi))$ AND $\text{Im}(\kappa(\xi))$

$\text{Re}(\kappa(\xi))$	$\text{Im}(\kappa(\xi))$
Top Sheet + -	-
Bottom Sheet + -	+

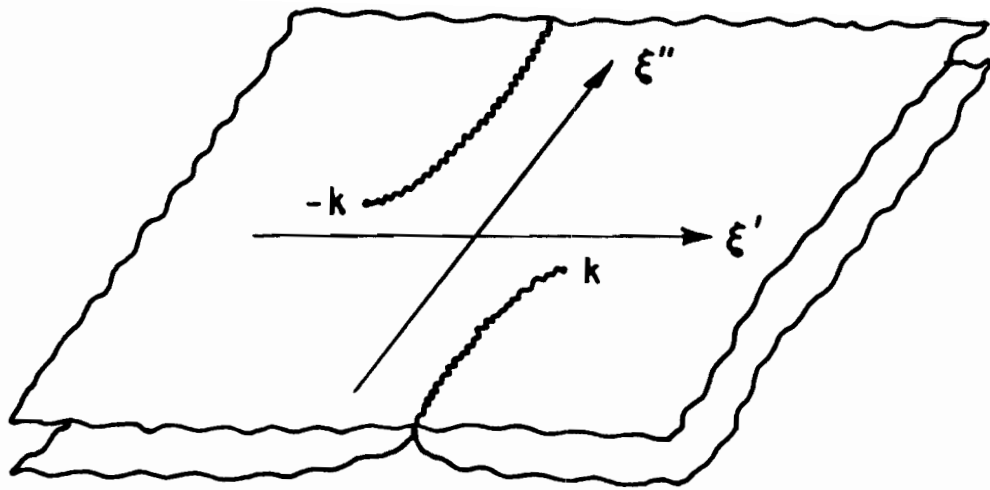


Figure D.2. Two sheeted ξ plane connected with the branch cut defined by $\text{Im}(\kappa^2(\xi))=0$.

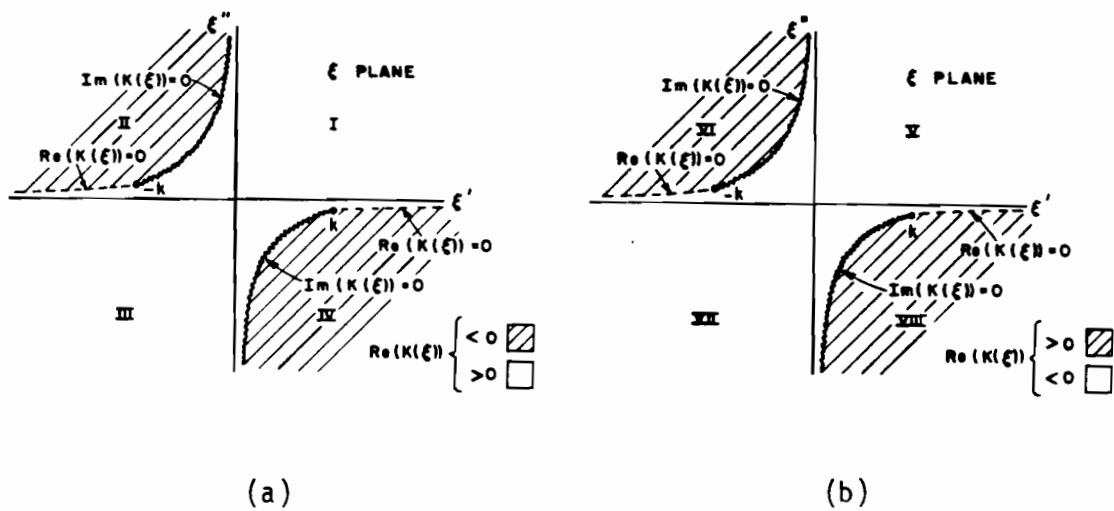


Figure D.3. Entire two-sheeted ξ -plane.
 (a) Top sheet $\text{Im}(\kappa(\xi)) < 0$, (b) Bottom sheet: $\text{Im}(\kappa(\xi)) > 0$

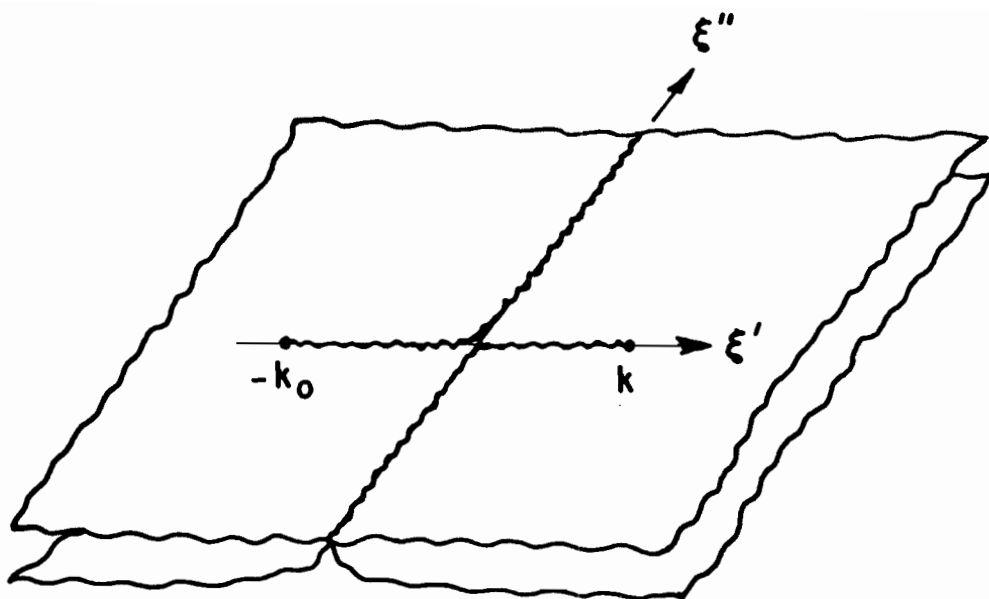


Figure D.5. Two sheeted ξ plane connected with branch cut defined by $\text{Im}(\kappa^2(\xi))=0$; ($\kappa'' \rightarrow 0$).

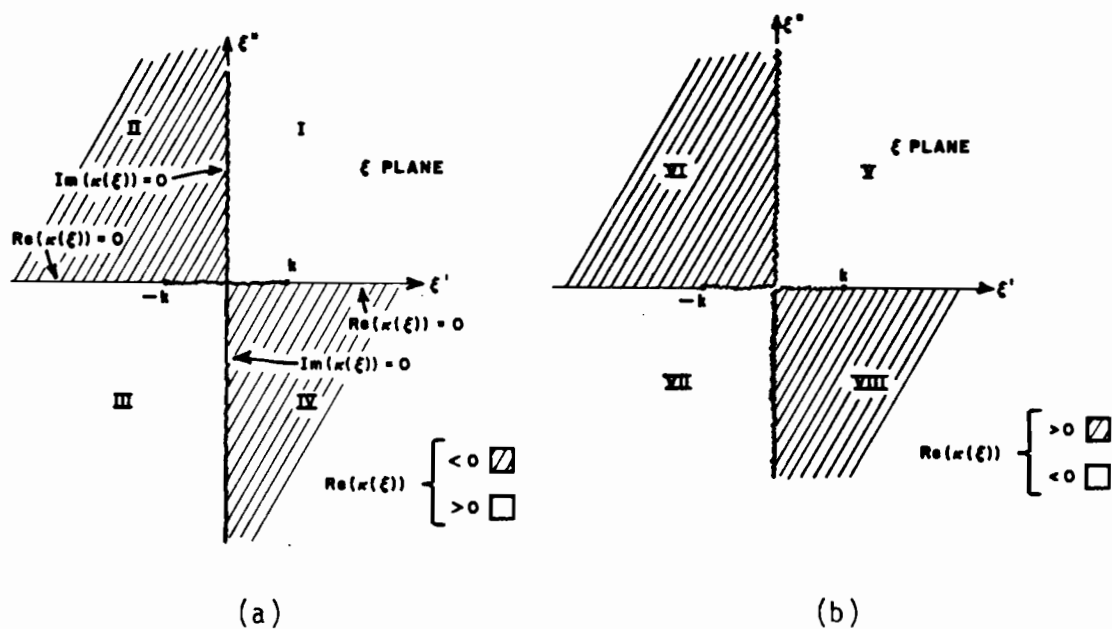


Figure D.6. Entire two-sheeted ξ -plane, lossless medium $\kappa'' \rightarrow 0$.
 (a) Top sheet $\text{Im}(\kappa(\xi)) < 0$, (b) Bottom sheet $\text{Im}(\kappa(\xi)) > 0$

APPENDIX E

$\xi = k \sin w$ TRANSFORMATION

In order to formulate the asymptotic expansion of integral representation of the field quantities, it is desirable to introduce a complex variable w via the transformation [42,60]

$$\xi = k \sin w \quad (E.1)$$

$$w = \sin^{-1} (\xi/k) \quad (E.2)$$

which identifies w as a complex angle variable and makes the branch point $\kappa(\xi)=(k^2-\xi^2)^{1/2}=0$ a regular point in w plane.

It is evident that a multiplicity of w values corresponds to the same value of ξ . Thus, the entire ξ plane can be mapped into various adjacent sections of "strip" 2π in the w plane. The inverse function $\sin^{-1} (\xi/\kappa)$ in the ξ plane is multiple valued, implying the existence of branch points in that plane. The branch points occur at those points in the ξ plane that mapping derivatives $(\frac{d\xi}{dw}=k\cos w)$ vanish. Note that:

$$\xi' + j\xi'' = k \sin w' \cosh w'' + j k \cos w' \sinh w'' \quad , \quad (E.3)$$

$$\xi = \xi' + j \xi'' \quad , \quad (E.4)$$

and

$$W = w' + jw'' \quad , \quad (E.5)$$

where ξ' , ξ'' , w' , w'' and k are all real quantities.

$$\kappa(\xi) = \kappa' + j\kappa'' = k \cos w \quad (\text{E.6})$$

$$= k(\cos w' \cosh w'' - j \sin w' \sinh w'') \quad (\text{E.7})$$

Thus to ensure that the mapping of ξ plane to w plane is one to one, we explicitly express the inverse transformation, that is [60]:

$$\sin w = \frac{\xi}{k} \quad , \quad (\text{E.8})$$

$$\cos w = \sqrt{\frac{k^2 - \xi^2}{k}} \quad , \quad (\text{E.9})$$

$$\cos w + j \sin w = e^{jw} \quad , \quad (\text{E.10})$$

so

$$w = -j \ln \left(\frac{\sqrt{k^2 - \xi^2} + j\xi}{k} \right) \quad , \quad (\text{E.11})$$

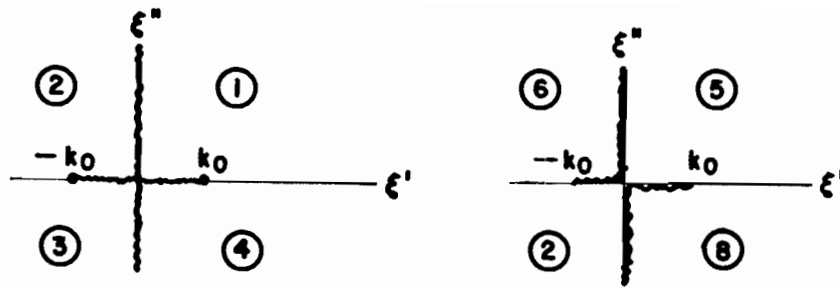
where

$$\ln(z) = \ln|z| + j \arg(z) \quad , \quad (\text{E.12})$$

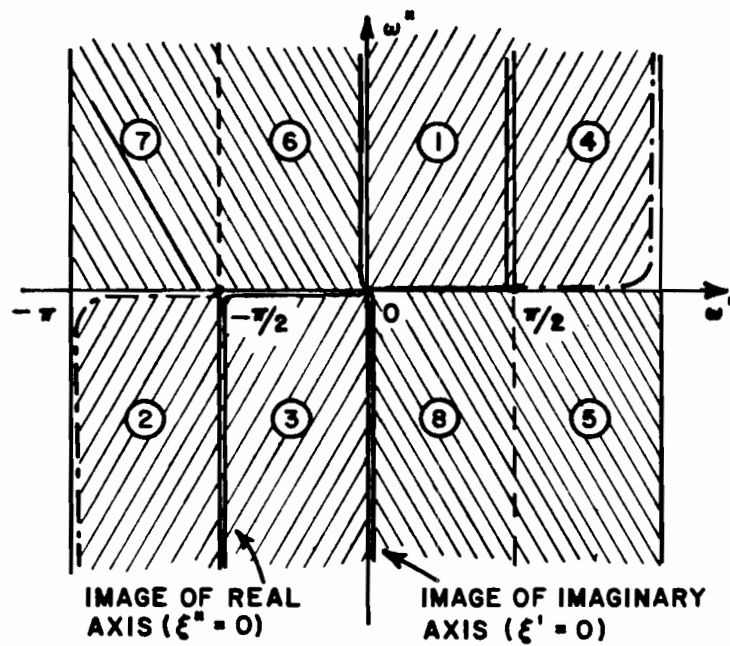
and the $\arg(z)$ must be confined to the strip of 2π . The principle branch argument will be confined to:

$$-\pi < \arg(z) < \pi \quad . \quad (\text{E.13})$$

So the Equations (E.11) and (E.12) will map the two-sheeted ξ plane into the strip $-\pi < w' < \pi$ in the w plane. The top sheet of the ξ plane as shown in Figure E.1(b) maps into the strip $-\frac{\pi}{2} < w' < \frac{\pi}{2}$, shaded with a slanted line of 45° , and branch cuts of $\kappa(\xi)$ in the ξ plane ($\kappa''(\xi)=0$) will be a dashed-dotted line in Figure E.1(b).



(a) Two sheeted ξ plane (lossless medium)



 TOP SHEET OF $\kappa(\xi) - \text{Im}(\kappa(\xi)) < 0$

 BOTTOM SHEET OF $\kappa(\xi) - \text{Im}(\kappa(\xi)) > 0$

----- IMAGE OF BRANCH CUTS $\text{Im}(\kappa(\xi)) = 0$

Figure E.1. Mapping from two sheet complex ξ plane to complex w plane, k is real; lossless case.

Note that the regions (2) and (4) are not adjacent in the w plane, even though they have a common point at $\xi=0$ in the ξ -plane. This is a consequence of the branch point singularity in $L_{\eta}z$ in mapping function at Equation (E.11).

If k becomes complex (lossy medium), then

$$k = k' + jk'' \quad , \quad (E.14)$$

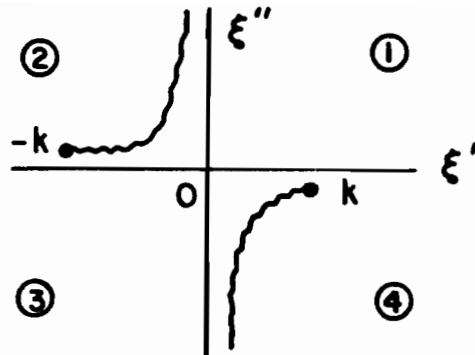
and

$$\kappa'(\xi) = k' \cos w' \cosh w'' + k'' \sin w' \sinh w'' \quad , \quad (E.15)$$

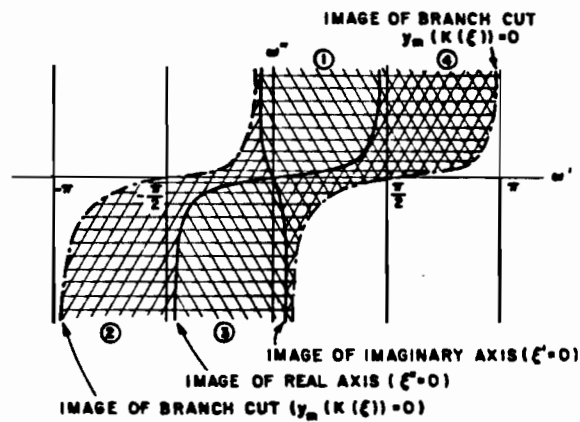
$$\kappa''(\xi) = k'' \cos w' \cosh w'' - k' \sin w' \sinh w'' \quad . \quad (E.16)$$

The curves $\kappa'(\xi)=0$ and $\kappa''(\xi)=0$ in the complex w plane depicted are in Figure E.2 as $|w''| \rightarrow \infty$. These curves are asymptotic to the lines $w' = \frac{\pi}{2} \pm \Delta$, [42], where:

$$\Delta = \tan^{-1} \left(\frac{|k''|}{|k'|} \right) \quad . \quad (E.17)$$



(a) Two Sheeted ξ Plane (Lossy Medium)



(b) Periodic w Complex Plane

$$\kappa = \kappa' + j\kappa''$$

$$\kappa'' < 0$$

— Image of $\text{Im}(\kappa(\xi)) = 0$

--- Image of $\text{Re}(\kappa(\xi)) = 0$

 Top Sheet

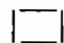
 Bottom Sheet

Figure E.2. Mapping from the sheeted ξ complex plane to the complex w plane; k is the complex (lossy case).

APPENDIX F

MUTUAL IMPEDANCE BETWEEN A PAIR OF ANTENNAS

Consider an antenna system consists of two elements, as shown in Figure F.1.

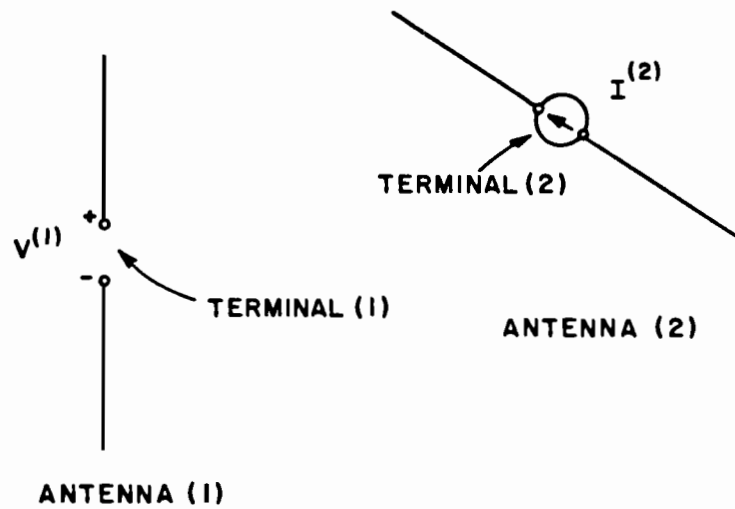


Figure F.1. Two element antenna system $I(2)$, an impressed current on antenna terminal (2); $v(1)$ is the induced open circuited voltage in antenna terminal (1).

The mutual impedance between the terminal (1) and (2) is defined as:

$$Z_{12} = \frac{V(1)}{I(2)} \quad (F.1)$$

where $V(1)$ is the open circuited induced voltage at the terminal (1) due to the current source at the terminal (2).

The mutual admittance at the terminal (1) is defined as:

$$Y_{12} = \frac{I(1)}{V(2)} \quad (F.2)$$

Where $I(1)$ is the short circuited current induced at the terminal (1) due to the voltage source $V(2)$ at the terminal (2), (see Figure F.2).

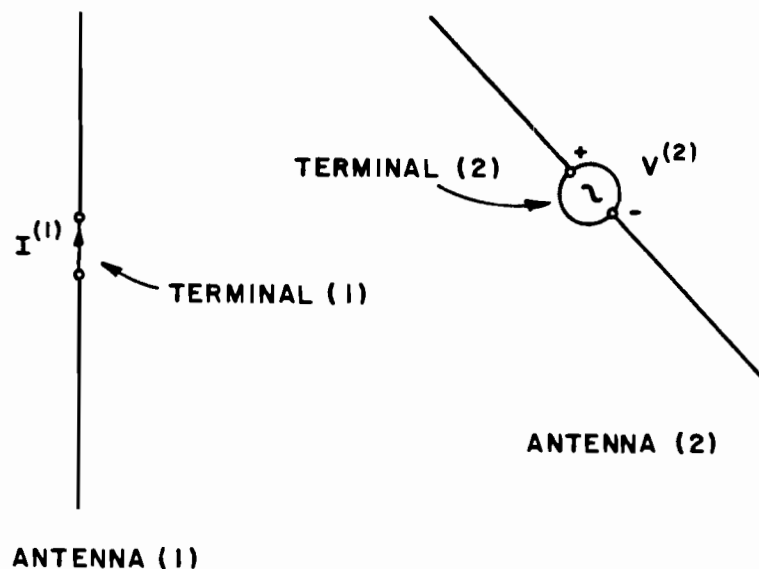


Figure F.2. Two element antenna system. $V(2)$ is an impressed voltage on antenna terminal (2); $I(1)$ is the induced short circuited current in antenna terminal (1).

By the reciprocity (in the isotropic media)

$$Z_{12} = Z_{21} \quad , \quad (F.3)$$

and

$$Y_{12} = Y_{21} \quad . \quad (F.4)$$

Now let's suppose that the voltage source $V^{(2)}$ is uniformly distributed in the interval $z_2; z_3$, then the mutual admittance can be written as [61]:

$$Y(z_2) = \frac{1}{(z_3 - z_2)} \int_{z_2}^{z_3} Y_{z_1, z} (z_1, z') dz \quad . \quad (F.5)$$

The left hand side can be interpreted as the induced current at $z=z_1$ due to a unit voltage source distributed in the interval z_2 and z_3 .

But from the reciprocity theorem, one can infer

$$Y_{z_1, (z_2; z_3)} = Y_{(z_2; z_3), z_1} \quad . \quad (F.6)$$

The right hand side can be interpreted as the average current $I^{(2)}$ at the interval $z_2; z_3$, due to the unit voltage at z_1 . From the above discussion one can deduce that:

$$Y_{(z_0; z_1), (z_2; z_3)} = \frac{1}{(z_1 - z_0)} \frac{1}{(z_3 - z_2)} \int_{z_0}^{z_1} \int_{z_2}^{z_3} Y(z', z'') dz' dz'' \quad (F.7)$$

and also from the reciprocity:

$$Y(z_0; z_1), (z_2, z_3) = Y(z_2; z_3), (z_0; z_1) \quad , \quad (F.8)$$

which states that the average current in the interval z_0 and z_1 due to the unit voltage distributed in the interval z_2 and z_3 is equal to the average current distributed in later intervals due to the unit voltage distributed in the former interval. This is called the reciprocity of the current distribution [62]. The reciprocity of the voltage distribution can be formulated via the mutual impedance, likewise. Now consider a short circuited antenna in the presence of an incident electric field \bar{E} , as shown in Figure F.3. The infinitesimal induced voltage along the antenna directed at \hat{p} is:

$$dv = \bar{E} \cdot \hat{p} \, d\ell \quad . \quad (F.9)$$

The current induced at the point z_1 via (F.5) is given by

$$I(z_1) = - \int \bar{E} \cdot \hat{p} \, Y_{z_1, z'}(z, z') \, dz' \quad , \quad (F.10)$$

or from the reciprocity:

$$I(z_1) = - \int \bar{E} \cdot \hat{p} \, Y_{z', z_1}(z', z) \, dz' \quad . \quad (F.11)$$

$Y_{z', z}(z', z)$ is the induced current distribution along the z' due to a unit voltage source at z_1 . In other words, $Y_{z, z'}(z', z)$ is the current distribution in the transmitting mode when a unit voltage is impressed at z_1 . Therefore, one can write:

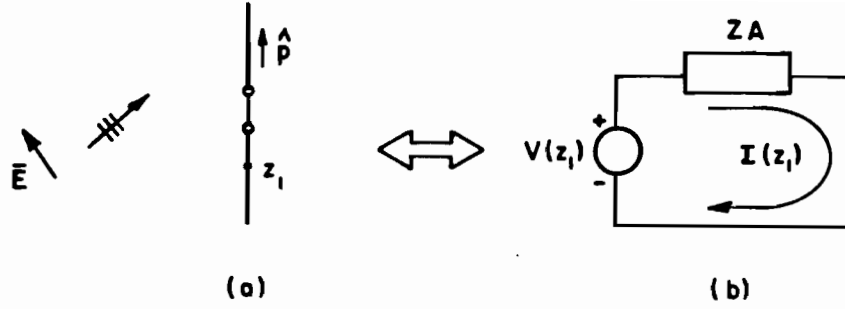


Figure F.3. Short circuited antenna exposed to the incident electric field \bar{E} , and its equivalent circuit.

$$I(z_1) = -\int \bar{E} \cdot \hat{p} I^t(z') dz' \quad , \quad (F.12)$$

and the voltage at z_1 will be

$$\begin{aligned} V(z_1) &= Z_A I(z_1) \quad , \\ &= -Z_A \int \bar{E} \cdot \hat{p} I^t(z') dz' \quad , \end{aligned} \quad (F.13)$$

where Z_A is the input impedance seen at $z=z_1$, which numerically is equal to $(I^t(z_1))^{-1}$. Therefore, (F.13) can be written as

$$V(z_1) = \frac{-1}{I^t(z_1)} \int \bar{E} \cdot \hat{p} I^t(z') dz' \quad , \quad (F.14)$$

where $V(z_1)$ is the open circuit voltage induced at $z=z_1$ as the antenna is exposed to the incident field \bar{E} .

Note that at the presence of the load, Z_L , as shown in Figure F.4, the total voltage across the load will be,

$$V_L = \frac{V(z_1)}{Z_A + Z_L} Z_L \quad . \quad (F.15)$$

Consider the two arbitrary shape antennas (q) and (r) as shown in Figure F.5. According to the Equation (F.14) the voltage induced at the terminal q due to the impressed current I_r at the terminal r will be:

$$V_{qr} = -\frac{1}{I_q} \iiint_{V_q} \bar{E}^r \cdot \bar{J}^{tq} dv \quad . \quad (F.16)$$

Where \bar{J}^{tq} is the transmitted current along the antenna q due to unit voltage at terminal (q) which symbolically is represented as a general volumetric current, \bar{J}^{tq} contained in the volume V_q ; I_q is the terminal current and \bar{E}^r is the electric field due to the impressed current source I_r at the terminal r.

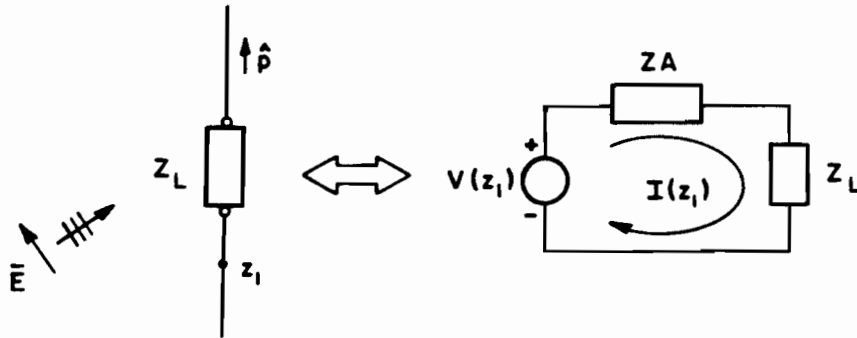


Figure F.4. Loaded antenna exposed to the incident field \bar{E} .

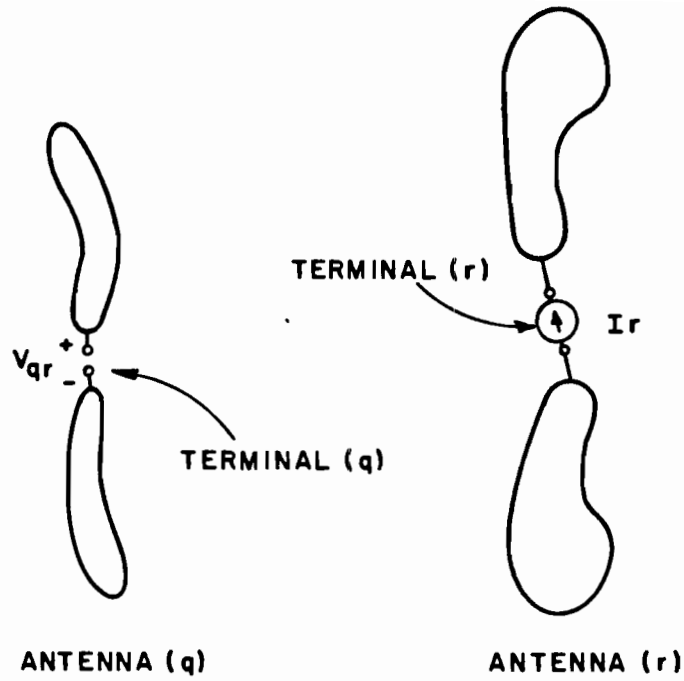


Figure F.5. Two general coupled antennas (q) and (r).

Hence the mutual impedance Z_{qr} between the two antennas (r) and (q) will be

$$Z_{qr} = \frac{V_{qr}}{I_r} \quad , \quad (F.19)$$

which can be written as

$$Z_{qr} = - \frac{1}{I_q I_r} \iiint_{V_q} \bar{E}^r \cdot \bar{J}^{tq} dv \quad , \quad (F.20)$$

and the input impedance can be found via:

$$Z_{qq} = - \frac{1}{I_q^2} \iiint_{V_q} \bar{E}^q \cdot \bar{J}^{tq} dv \quad . \quad (F.21)$$

APPENDIX G

GENERAL TE AND TM POLES AND RESIDUES OF THE GROUNDED DIELECTRIC/FERRITE SLAB; (SURFACE WAVE AND LEAKY WAVES)

In this appendix, the general TE and TM poles and their associated residues of g_0'' , g_0' , given (2.77) and (2.83), U , V and W given in (4.7)-(4.9) and (5.17)-(5.19) will explicitly be derived.

Techniques for finding the TE and TM poles in the complex ξ plane (see Chapter IV) will be presented.

Consider the Equation (4.3), the finite sum refers to the discrete spectrum of the modal waves. These are due to the poles of the reflection coefficient of g_0'' and g_0' given in Chapter II, that is

$$g_0'' = \frac{\omega\mu_0}{2\kappa_0} \left[e^{-j\kappa_0|z-z'|} + r'' e^{-j\kappa(z+z')} \right], \quad (G.1)$$

$$g_0' = \frac{\omega\epsilon_0}{2\kappa_0} \left[e^{-j\kappa_0|z-z'|} - r' e^{-j\kappa(z+z')} \right], \quad (G.2)$$

where

$$r'' = \frac{\kappa_0 + j\kappa_1 \cotan \kappa_1 d / \mu_r}{\kappa_0 - j\kappa_1 \cotan \kappa_1 d / \mu_r}; \quad r' = - \frac{\kappa_0 - j\kappa_1 \tan \kappa_1 d / \epsilon_r}{\kappa_0 + j\kappa_1 \tan \kappa_1 d / \epsilon_r} \quad (G.3)$$

and

$$\kappa = \sqrt{\mu_r \epsilon_r k_0^2 - \xi^2} \quad (G.4)$$

The residue of g_0'' and g_0' is defined as,

$$\text{Res}(g_0'') \Big|_{\xi=\xi_{p''}} = \frac{\omega \mu_0}{2 \sqrt{k_0^2 - \xi_{p''}^2}} e^{-j \sqrt{k_0^2 - \xi_{p''}^2} (z+z')} \frac{N''(\xi_{p''})}{\frac{d}{d\xi} (D''(\xi))} \Big|_{\xi=\xi_{p''}}, \quad (G.5)$$

$$\text{Res}(g_0') \Big|_{\xi=\xi_{p'}} = \frac{\omega \epsilon_0}{2 \sqrt{k_0^2 - \xi_{p'}^2}} e^{-j \sqrt{k_0^2 - \xi_{p'}^2} (z+z')} \frac{N'(\xi_{p'})}{\frac{d}{d\xi} (D'(\xi))} \Big|_{\xi=\xi_{p'}}, \quad (G.6)$$

where $N''(\xi)$, $D''(\xi)$, $N'(\xi)$ and $D'(\xi)$ are recognized via (G.3) and the following expressions,

$$\Gamma''(\xi) = \frac{N''(\xi)}{D''(\xi)} \quad ; \quad \Gamma'(\xi) = \frac{N'(\xi)}{D'(\xi)} \quad . \quad (G.7)$$

But,

$$\begin{aligned} \frac{d}{d\xi} (D''(\xi)) \Big|_{\xi_{p''}} &= \frac{d}{d\xi} \left(\sqrt{k_0^2 - \xi^2} - \frac{j}{\mu_r} \sqrt{\mu_r \epsilon_r k_0^2 - \xi^2} \cotan(d \sqrt{\mu_r \epsilon_r k_0^2 - \xi^2}) \right) \Big|_{\xi=\xi_{p''}} \\ &= \frac{-\xi_{p''}}{\sqrt{k_0^2 - \xi_{p''}^2}} \left[1 - \frac{j}{\mu_r} \frac{\sqrt{k_0^2 - \xi_{p''}^2}}{\sqrt{\mu_r \epsilon_r k_0^2 - \xi_{p''}^2}} (\cotan(d \sqrt{\mu_r \epsilon_r k_0^2 - \xi_{p''}^2}) \right. \\ &\quad \left. - d \sqrt{\mu_r \epsilon_r k_0^2 - \xi_{p''}^2} (1 + \cotan^2(d \sqrt{\mu_r \epsilon_r k_0^2 - \xi_{p''}^2})) \right] \end{aligned} \quad (G.8)$$

$$\begin{aligned}
\left. \frac{d}{d\xi} (D'(\xi)) \right|_{\xi_p} &= \frac{d}{d\xi} \left(\sqrt{k_0^2 - \xi^2} + j \frac{\sqrt{\mu_r \epsilon_r k_0^2 - \xi^2}}{\epsilon_r} \tan(d \sqrt{\mu_r \epsilon_r k_0^2 - \xi^2}) \right) \\
&= \frac{-\xi_{p'}}{\sqrt{k_0^2 - \xi_{p'}^2}} \left[1 + \frac{j}{\epsilon_r} \frac{\sqrt{k_0^2 - \xi_{p'}^2}}{\sqrt{\mu_r \epsilon_r k_0^2 - \xi_{p'}^2}} \left(\tan(d \sqrt{\mu_r \epsilon_r k_0^2 - \xi_{p'}^2}) \right. \right. \\
&\quad \left. \left. + d \sqrt{\mu_r \epsilon_r k_0^2 - \xi_{p'}^2} (1 + \tan^2(d \sqrt{\mu_r \epsilon_r k_0^2 - \xi_{p'}^2})) \right) \right]
\end{aligned}
\tag{G.9}$$

Therefore the explicit expressions of the residues of g_0'' and g_0' (TE and TM mode) will be

$$\begin{aligned}
\text{Res}(g_0'') \Big|_{\xi=\xi_{p''}} &= \frac{\omega \mu_0}{-\xi_{p''}} \cdot \\
&\frac{e^{-j\sqrt{k_0^2 - \xi_{p''}^2}(z+z')} \sqrt{k_0^2 - \xi_{p''}^2}}{1 - \frac{j}{\mu_r} \frac{\sqrt{k_0^2 - \xi_{p''}^2}}{\sqrt{\mu_r \epsilon_r k_0^2 - \xi_{p''}^2}} (\cotan(d \sqrt{\mu_r \epsilon_r k_0^2 - \xi_{p''}^2}) - d \sqrt{\mu_r \epsilon_r k_0^2 - \xi_{p''}^2} (1 + \cotan^2(d \sqrt{\mu_r \epsilon_r k_0^2 - \xi_{p''}^2})))}
\end{aligned}
\tag{G.10}$$

$$\text{Res}(g'_0) \Big|_{\xi=\xi_{p'}} = \frac{\omega \epsilon_0}{-\xi_{p'}} \cdot$$

$$\frac{e^{-j\sqrt{k_0^2 - \xi_{p'}^2}(z+z')} \sqrt{k_0^2 - \xi_{p'}^2}}{\left[1 + \frac{j \sqrt{k_0^2 - \xi_{p'}^2}}{\epsilon_r \sqrt{\mu_r \epsilon_r k_0^2 - \xi_{p'}^2}} \left(\tan(d\sqrt{\mu_r \epsilon_r k_0^2 - \xi_{p'}^2}) + d\sqrt{\mu_r \epsilon_r k_0^2 - \xi_{p'}^2} (1 + \tan^2(d\sqrt{\mu_r \epsilon_r k_0^2 - \xi_{p'}^2})) \right) \right]}$$

(G.11)

also note that

$$\frac{\partial^2}{\partial z \partial z'} \text{Res}(g'_0) = -(k_0^2 - \xi_{p'}^2) \text{Res}(g'_0) \quad . \quad (G.12)$$

From the above analysis, explicit expressions of residues $\text{Res}_U(\zeta_{n''})$, $\text{Res}_V(\zeta_{n'})$, $\text{Res}_W(\zeta_{n''})$ and $\text{Res}_W(\zeta_{n'})$ introduced in (4.7) through (4.9) and $R_U(\zeta_{n''})$, $R_V(\zeta_{n'})$, $R_W(\zeta_{n''})$ and $R_W(\zeta_{n'})$ given in (5.17) through (5.19) can readily be found. Note that

$$\zeta^2 = k_0^2 - \xi^2 \quad , \quad (G.13)$$

and

$$\text{Res}_U(\zeta_{p''}) = R_U(\zeta_{p''}) H_0^2(p\xi_{p''}) e^{-j\sqrt{k_0^2 - \xi_{p''}^2} z} \quad , \quad (G.14)$$

where

$$R_U(\zeta_{p''}) = \frac{1}{2}$$

$$\sqrt{k_0^2 - \xi_{p''}^2}$$

$$\left[1 - \frac{j}{\mu_r} \frac{\sqrt{k_0^2 - \xi_{p''}^2}}{\sqrt{\mu_r \epsilon_r k_0^2 - \xi_{p''}^2}} \left(\cotan(d\sqrt{\mu_r \epsilon_r k_0^2 - \xi_{p''}^2}) - d\sqrt{\mu_r \epsilon_r k_0^2 - \xi_{p''}^2} (1 + \cotan^2(d\sqrt{\mu_r \epsilon_r k_0^2 - \xi_{p''}^2})) \right) \right] \quad (G.15)$$

also,

$$\text{Res}_V(\zeta_{p'}) = R_V(\zeta_{p'}) H_0^2(\rho \xi_{p'}) e^{-j\sqrt{k_0^2 - \xi_{p'}^2} z} \quad (G.16)$$

where

$$R_V(\zeta_{p'}) = \frac{1}{2} (k_0^2 - \xi_{p'}^2)$$

$$\left[1 + \frac{j}{\epsilon_r} \frac{\sqrt{k_0^2 - \xi_{p'}^2}}{\sqrt{\mu_r \epsilon_r k_0^2 - \xi_{p'}^2}} \left(\tan(d\sqrt{\mu_r \epsilon_r k_0^2 - \xi_{p'}^2}) + d\sqrt{\mu_r \epsilon_r k_0^2 - \xi_{p'}^2} (1 + \tan^2(d\sqrt{\mu_r \epsilon_r k_0^2 - \xi_{p'}^2})) \right) \right] \quad (G.17)$$

and

$$\text{Res}_W(\zeta_{p''}) = R_W(\zeta_{p''}) H_0^2(\rho \xi_{p''}) e^{-j\sqrt{k_0^2 - \xi_{p''}^2} z} \quad (G.18)$$

where

$$R_W(\xi_{p''}) = \frac{1}{2} \frac{1}{(k_0^2 - \xi_{p''}^2)} \cdot \left[1 - \frac{j}{\mu_r} \frac{\sqrt{k_0^2 - \xi_{p''}^2}}{\sqrt{\mu_r \epsilon_r k_0^2 - \xi_{p''}^2}} (\cotan(d\sqrt{\mu_r \epsilon_r k_0^2 - \xi_{p''}^2}) - d\sqrt{\mu_r \epsilon_r k_0^2 - \xi_{p''}^2} (1 + \cotan^2(d\sqrt{\mu_r \epsilon_r k_0^2 - \xi_{p''}^2}))) \right] \cdot \frac{1}{\sqrt{k_0^2 - \xi_{p''}^2} + j \frac{\sqrt{\mu_r \epsilon_r k_0^2 - \xi_{p''}^2}}{\epsilon_r} \tan(d\sqrt{\mu_r \epsilon_r k_0^2 - \xi_{p''}^2})} \quad (G.19)$$

finally

$$\text{Res}_W(\xi_{p'}) = R_W(\xi_{p'}) H_0^2(\rho \xi_{p'}) e^{-j\sqrt{k_0^2 - \xi_{p'}^2} z} \quad , \quad (G.20)$$

where

$$R_W(\xi_{p'}) = \frac{1}{2} \frac{1}{(k_0^2 - \xi_{p'}^2)} \cdot \left[1 + \frac{j}{\epsilon_r} \frac{\sqrt{k_0^2 - \xi_{p'}^2}}{\sqrt{\mu_r \epsilon_r k_0^2 - \xi_{p'}^2}} (\tan(d\sqrt{\mu_r \epsilon_r k_0^2 - \xi_{p'}^2}) + d\sqrt{\mu_r \epsilon_r k_0^2 - \xi_{p'}^2} (1 + \tan^2(d\sqrt{\mu_r \epsilon_r k_0^2 - \xi_{p'}^2}))) \right] \cdot \frac{1}{\sqrt{k_0^2 - \xi_{p'}^2} - j \frac{\sqrt{\mu_r \epsilon_r k_0^2 - \xi_{p'}^2}}{\mu_r} \cotan(d\sqrt{\mu_r \epsilon_r k_0^2 - \xi_{p'}^2})} \quad , \quad (G.21)$$

The poles $\xi_{p''}$ and $\xi_{p'}$ are the roots of the denominators r'' and r' ,

$$D''(\xi) = \frac{\sqrt{k_0^2 - \xi^2} - j \frac{\sqrt{\mu_r \epsilon_r k_0^2 - \xi^2}}{\mu_r}}{\mu_r} \cotan(d \sqrt{\mu_r \epsilon_r k_0^2 - \xi^2}) = 0 \Big|_{\xi=\xi_{p''}} \quad (G.22)$$

$$D'(\xi) = \frac{\sqrt{k_0^2 - \xi^2} + j \frac{\sqrt{\mu_r \epsilon_r k_0^2 - \xi^2}}{\epsilon_r}}{\epsilon_r} \tan(d \sqrt{\mu_r \epsilon_r k_0^2 - \xi^2}) = 0 \Big|_{\xi=\xi_{p'}} \quad (G.23)$$

In the following the existence of the roots of D'' and D' will be discussed.

First let us consider $D''(\xi)$ (TE Case); for the lossless medium, D'' does not have any real roots for the values $|\xi| < k_0$. Let us define,

$$q = jd\sqrt{k_0^2 - \xi^2} \quad ; \quad p = d\sqrt{\mu_r \epsilon_r k_0^2 - \xi^2} \quad , \quad (G.24)$$

therefore

$$D'' = q + \frac{(p)\cotan(p)}{\mu_r} = 0 \quad (G.25)$$

and also from (G.24),

$$q^2 + p^2 = (\mu_r \epsilon_r - 1)(k_0 d)^2 \quad . \quad (G.26)$$

The solutions of the above equations (for the real p and q) are readily obtained graphically. The roots corresponding to positive values of q lie on the proper sheet (surface waves), and the roots corresponding to the negative values of q lie in the improper sheet of the Riemann surfaces (leaky waves). One observes that for the range of

$$(n+1/2) \pi < (\mu_r \epsilon_r - 1)^{1/2} (k_0 d) < (n+3/2) \pi , \quad (G.27)$$

there exists (n) solutions which correspond to the positive value of q (surface waves). No solution exists in the proper Reimann sheet for $(\mu_r \epsilon_r - 1)^{1/2} k_0 d < \pi/2$. Therefore the surface waves are subjected to a low frequency cut off. For the $\mu_r \epsilon_r k_0 < |\xi|$, p will be imaginary, and one will get,

$$\mu_r q - |p| \coth |p| = 0 , \quad (G.28)$$

and

$$q^2 - |p|^2 = (\mu_r \epsilon_r - 1)(k_0 d)^2 . \quad (G.29)$$

there will be no roots for the above equation for $\mu_r > 1$. Nevertheless, for $\mu_r = 1$, the solution exists on the improper sheet if $(\mu_r \epsilon_r - 1)^{1/2} k_0 d$ would be less than unity. When this condition holds there will not be any solution for a surface wave (no roots on the proper sheet).

To determine the complex roots, let us define,

$$q = u + jv ; \quad p = x + jy , \quad (G.30)$$

then, (G.25) will be

$$\mu_r (u + jv) = -(x + jy) \cotan (x + jy) , \quad (G.31)$$

or

$$u = -\frac{1}{\mu_r} \frac{\frac{x \tan x}{\cosh^2 y} + \frac{y \tanh y}{\cos^2 x}}{\tan^2 x + \tanh^2 y} , \quad (G.32)$$

$$v = \frac{1}{\mu_r} \frac{\frac{-y \tan x}{\cosh^2 y} + \frac{x \tanh y}{\cos^2 x}}{\tan^2 x + \tanh^2 y} \quad . \quad (G.33)$$

From the above equations, it is found that u is negative for all values of x and y ; therefore, the real value of q is always negative (see (G.30)). Hence, the complex roots are located on the improper sheet of the Riemann surface.

By eliminating the variable q , of (G.25) and (G.26), with $\mu_r=1$ one will have

$$\frac{p}{\sin p} = \pm \ell \quad (G.34)$$

which implies

$$\frac{x}{\sin x} = \pm \ell \cosh y ; \quad \cos x = \pm \frac{1}{\ell} \frac{y}{\sinh y} \quad (G.35)$$

where

$$\ell = k_0 d \sqrt{\mu_r \epsilon_r - 1} \quad ; \quad \mu_r = 1 \quad . \quad (G.36)$$

The infinite number of complex root p can be found via the solution of (G.35). It is to be noted that if $x+jy$ is a solution, $(\pm x \pm jy)$ are also the solutions of the above equations. Let $x, y > 0$; the solution exists for $\ell > \pi/2$. The roots are located in the vicinity of $x = n\pi - \pi/2$, where n is any integer [63]. For large values of x , the corresponding value of y is given by

$$y = \text{Ln}\left((2n-1) \frac{\pi}{\ell}\right) \quad . \quad (G.37)$$

It is to be noted that the roots for $n\pi < x < (2n+1)\pi/2$ for $n=1,2,\dots$ are the only valid solutions and satisfy the condition of $xy = -uv$ in (G.26). For $\mu_r \neq 1$, the same procedure should be followed; however, more complicated equations will be sought.

In the following, the roots of $D'(\xi)$ (TM Case) will be studied. For the lossless medium $D'(\xi)$ does not have any real roots for values $|\xi| < k_0$. Consider again,

$$q = jd \sqrt{k_0^2 - \xi^2} \quad ; \quad p = d \sqrt{\mu_r \epsilon_r k_0^2 - \xi^2} \quad , \quad (G.38)$$

$$D' = q - \frac{(p)\tan(p)}{\epsilon_r} = 0 \quad (G.39)$$

and

$$q^2 + p^2 = (\mu_r \epsilon_r - 1)(k_0 d)^2 \quad . \quad (G.40)$$

The solutions of these two equations (for real p and q) is readily obtained graphically. Corresponding roots of the positive q give rise to (proper) surface waves, and the negative q contributes to the (improper) leaky waves. One also observes that for the range of

$$n\pi < (\mu_r \epsilon_r - 1)^{1/2} k_0 d < (n+1)\pi \quad , \quad n=0,2,1\dots \quad , \quad (G.41)$$

there exists (n) solutions which correspond to the positive value of q (surface waves). At least one solution exists for arbitrary small values of $(\mu_r \epsilon_r - 1)^{1/2} k_0 d$, therefore for the (TM) case, no low frequency cut off exists for the surface wave excitation. The solutions of (G.39) and (G.40) are readily obtained graphically. The Newton-Raphson or

perturbation technique [64] can also be used to find the roots of these equations more accurately which will be discussed later in this section. For the $\mu_r \epsilon_r k_0 < |\xi|$, p will be imaginary, and one will have,

$$\epsilon_r q - |p| \tanh |p| = 0 \quad , \quad (G.42)$$

$$q^2 - |p|^2 = (\mu_r \epsilon_r - 1) (k_0 d)^2 \quad . \quad (G.43)$$

There will be no roots for the above equations, for $\epsilon_r > 1$. However, for $\epsilon_r = 1$, the solution exists on the improper sheet if $(\mu_r \epsilon_r - 1)^{1/2} k_0 d$ would be less than unity. If this condition holds, unlike the TE case there still exists a surface wave solution on the proper sheet.

To determine the complex roots, let us define again,

$$q = u + jv \quad ; \quad p = x + jy \quad , \quad (G.44)$$

then one will have

$$\epsilon_r (u + jv) = (x + jy) \tan (x + jy) \quad (G.45)$$

or

$$u = - \frac{1}{\epsilon_r} \frac{\frac{x \cotan x}{\sinh^2 y} + \frac{y \coth y}{\sin^2 x}}{1 + \cotan^2 x \coth^2 y} \quad , \quad (G.46)$$

$$v = \frac{1}{\epsilon_r} \frac{\frac{x \coth y}{\sin^2 x} - \frac{y \cotan x}{\sinh^2 y}}{1 + \cotan^2 x \coth^2 y} \quad . \quad (G.47)$$

Like the roots of $D''(\xi)$, it is found that u of the above equation is always negative, therefore the complex roots of $D'(\xi)$ are also located

on the improper sheet of the Riemann surface. Let us eliminate the variable $q=u+jv$ from the Equations (G.39) and (G.40), where $p=x+jy$.

$$\epsilon_r(u+jv) = (x+jy)\tan^2(x+jy) \quad , \quad (G.48)$$

$$\epsilon_r(u+jv)^2 + (x+jy)^2 = \ell^2 \quad , \quad (G.49)$$

or

$$\frac{1}{\epsilon_r^2} (x+jy)^2 (\tan^2(x+jy) + \epsilon_r^2) = \ell^2 \quad , \quad (G.50)$$

so

$$(x^2-y^2) \left[\left((1+\epsilon_r^2) + (\epsilon_r^2-1)A \right) (1+A) + (\epsilon_r^2-1)B^2 \right] - 4Bxy - \epsilon_r^2 \ell^2 \left((1+A)^2 + B^2 \right) = 0 \quad , \quad (G.51)$$

and

$$(x^2-y^2)B + xy \left[\left((1+\epsilon_r^2) + (\epsilon_r^2-1)A \right) (1+A) + (\epsilon_r^2-1)B^2 \right] = 0 \quad , \quad (G.52)$$

where

$$A = \cos(2x) \cosh(2y) \quad ; \quad B = \sin(2x) \sinh(2y) \quad . \quad (G.53)$$

The infinite number of the complex root $(x+jy)$ can be found via the solution of (G.51) and (G.52). It is to be noted that if $(x+jy)$ is a solution, $(\pm x \pm jy)$ are also the solutions of the above equations. Also note that the valid solutions must satisfy the condition of $xy = -\epsilon_r uv$ in order that (G.40) be satisfied.

In the following, the Newton-Raphson and perturbation method will be discussed. Both of these methods are successfully employed to find the surface wave and leaky wave roots.

In the Newton-Raphson approach, one can use the following argument,

$$F(\xi_1) \cong F(\xi_0) + (\xi_1 - \xi_0)F'(\xi_0) \cong 0 \quad (G.54)$$

where the right hand side is the two-term Taylor expansion of $F(\xi_1)$ around ξ_0 . Hence,

$$\xi_1 \cong \xi_0 - \frac{F(\xi_0)}{F'(\xi_0)}, \quad (G.55)$$

thus, after n iterations, one can have

$$\xi_{n+1} = \xi_n - \frac{F(\xi_n)}{F'(\xi_n)} \quad (G.56)$$

which is a convergent process. Of course, the number of iterations is related to the initial guess of the root ξ_0 .

If $k_0 d \ll 1$ (which is usually the case) the perturbation method can also be invoked to find the roots more efficiently. Let

$$\xi = k_0 \alpha, \quad (G.57)$$

then the Equation (G.39) will be

$$\frac{\sqrt{\alpha^2 - 1} - \sqrt{\mu_r \epsilon_r - \alpha^2}}{\epsilon_r} \tan k_0 d \sqrt{\mu_r \epsilon_r - \alpha^2} = 0 \quad (G.58)$$

Lets assume that the substrate thickness is very small compared to the space wavelength,

$$\delta = k_0 d \ll 1, \quad (G.59)$$

the unperturbed solution, $\delta=0$,

$$\alpha_0 = 1. \quad (G.60)$$

Therefore, we assume

$$\alpha \cong \alpha_0 + \beta \quad , \quad (G.61)$$

where β can be expressed in the power series of δ , that is

$$\beta = \sum_{n=1}^{\infty} a_n \delta^n \quad . \quad (G.62)$$

After substitution of (G.61) into (G.58) one will have

$$\frac{\sqrt{(1+\beta)^2 - 1} - \sqrt{\mu_r \epsilon_r - (1+\beta)^2}}{\epsilon_r} \tan\left(\delta \sqrt{\mu_r \epsilon_r (1+\beta)^2}\right) = 0 \quad (G.63)$$

or

$$\sqrt{\beta(\beta+2)} - \frac{\delta}{\epsilon_r} (\mu_r \epsilon_r - 1 - \beta(\beta+2)) \cong 0 \quad , \quad (G.64)$$

so

$$\beta \cong 0.5 \left[(\mu_r \epsilon_r - 1) \frac{\delta}{\epsilon_r} \right]^2 \quad , \quad (G.65)$$

where use has been made from the Taylor expansions of $\tan(x)$ and $\sqrt{1+x}$ around $x=0$.

Therefore the perturbation solution of (G.39) will be;

$$\xi_p \cong k_0 \left(1 + 0.5 \left[\frac{k_0 d}{\epsilon_r} (\mu_r \epsilon_r - 1) \right]^2 \right) \quad . \quad (G.66)$$

It is worth mentioning that if the perturbation solution of (G.66) is used as an initial value for (G.56), the roots of the D' can be found within a few iterations, usually less than five.

APPENDIX H

UNIFORM ASYMPTOTIC EXPANSION OF THE CANONICAL INTEGRAL

In this appendix, a complete asymptotic expansion of the canonical integral

$$I(\Omega) = \int_{\Gamma} F(z) e^{\Omega q(z)} dz, \quad (H.1)$$

will be presented; where Ω is a large positive parameter and $q(z)$ has a first order saddle point.

First we discuss this problem when $F(z)$ has no singularity near the saddle point. Next we treat this integral as $F(z)$ exhibits many first order poles near the saddle point. We generalize the method presented by Van der Waerden and extensively studied by Felsen [42]. The property of the transition function encounter in the nearby singularity cases, will also be discussed.

A. COMPLETE ASYMPTOTIC EXPANSION

Let's assume for the time being that, $F(z)$ and $q(z)$ to be analytic functions along the integration path Γ of which its end points are at infinity and Ω is some large positive parameter.

An asymptotic evaluation of $I(\Omega)$ can be performed, if $\text{Re}(q(z))$ has a maximum value at z_s , so that $\text{Re}(q(z)) < \text{Re}(q(z_s))$ on the remainder of the integration path. Since Ω is very large, it follows that $\exp(\Omega q(z_s))$ has a maximum at z_s and decreases very rapidly away from z_s , which the function $F(z)$ is regular and slowly varying at the vicinity of z_s . In general, the exponent will not have the above described behavior along the given contour Γ , but along some other path Γ' , steepest descent path. One then attempts to deform the path from Γ into Γ' , with proper account being taken of any interfering singularities of $F(z)$, (such as poles or branch points) in the complex z -plane [42], [65], (see Figure H.1).

It has been shown [42], [44] that the point(s), where the maximum contribution to the integral occurs, are "saddle" or "stationary points" of the function $q(z)$, defined by the vanishing derivative of $q(z)$. The desired path Γ' is one on which $\text{Im}(q(z))$ remains constant. Let us use a pertinent transformation from z to the s plane,

$$q(z) = \tau(s) \quad (\text{H.2})$$

such that the point z_s in the complex z -plane is chosen to correspond to $s=0$ in the complex s plane.

$$I(\Omega) = \int_{\Gamma''} F(z) \frac{dz}{ds} e^{\Omega \tau(s)} ds, \quad (\text{H.3})$$

where

$$\frac{dz}{ds} = \frac{\tau'(s)}{q'(z)} \quad (\text{H.4})$$

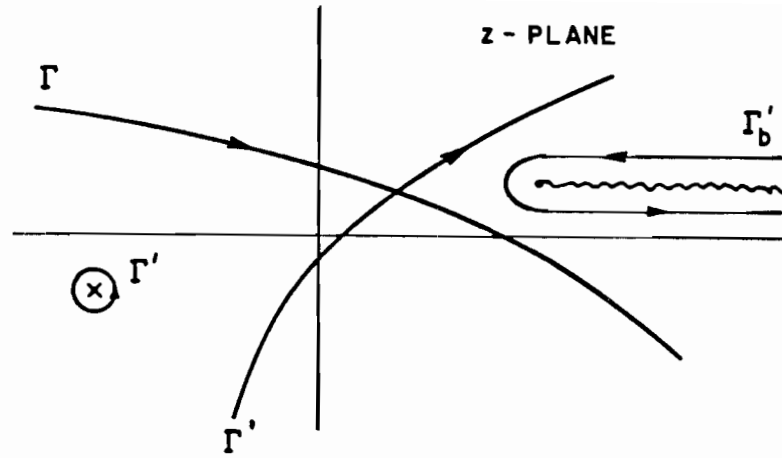


Figure H.1. Deformation contour of Γ into steepest descent path Γ' .

where Γ'' represents the mapping of the path Γ' in the z -plane into the s -plane.

In order to assure the regularity of $F(z) \frac{dz}{ds}$ [42], the derivative (dz/ds) must not vanish along the path Γ'' and especially around $s=0$. Also, $\tau'(s)$ must have a zero at $s=0$ of the same order as that of $q'(z)$ at z_s . In the case of an isolated first-order saddle point, $q'(z)$ has a first-order zero at z_s so one possible expansion of $\tau(s)$ satisfying the above requirement is

$$\tau(s) = q(z_s) - s^2 . \quad (\text{H.5})$$

The steepest-descent path Γ'' in the s plane, along which $\text{Im}\tau(s)$ is constant, clearly is the real s axis. Thus, the integral of (H.1) becomes

$$I(\Omega) = e^{\Omega q(z_s)} \int_{-\infty}^{\infty} G(s) e^{-\Omega s^2} ds \quad (\text{H.6})$$

where

$$G(s) = F(z) \frac{dz}{ds}, \quad (\text{H.7})$$

and

$$\frac{dz}{ds} = \frac{-2s}{q'(z)} \quad . \quad (\text{H.8})$$

Since $G(s)$ assumed to be regular near $s=0$ it can be expanded into a power series of s

$$G(s) = G(0) + G'(0)s + G''(0) \frac{s^2}{2!} + \dots + G^{(n)}(0) \frac{s^n}{n!} \quad , \quad (\text{H.9})$$

which converges uniformly inside a circle with finite radius r centered at $s=0$, and r being the distance to the nearest singularity of $G(s)$, so:

$$I(\Omega) \sim e^{\Omega q(z_s)} \sum_{n=0}^{\infty} \frac{G^{(n)}(0)}{n!} \int_{-\infty}^{\infty} s^n e^{-\Omega s^2} ds \quad , \quad (\text{H.10})$$

but

$$\int_{-\infty}^{\infty} s^n e^{-\Omega s^2} ds = \begin{cases} \frac{\Gamma(1+n)/2}{\Omega^{(1+n)/2}} & n \text{ even} \\ 0 & n \text{ odd} \end{cases} \quad (\text{H.11})$$

where $\Gamma(x)$ is the gamma function

$$\Gamma(1/2) = \sqrt{\pi} \quad (\text{H.12})$$

and

$$\Gamma(z+1) = z\Gamma(z) . \quad (\text{H.13})$$

Alternately,

$$\int_{-\infty}^{\infty} s^{2m} e^{-\Omega s^2} ds = (-1)^m \frac{d^m}{d\Omega^m} \int_{-\infty}^{\infty} e^{-\Omega s^2} ds , \quad (\text{H.14})$$

which is

$$= (-1)^m \frac{d^m}{d\Omega^m} \sqrt{\frac{\pi}{\Omega}} . \quad (\text{H.15})$$

Therefore

$$I(\Omega) \sim e^{\Omega q(z_S)} \sum_{n=0}^{\infty} \frac{G^{(2n)}(0)}{(2n)!} \frac{(-1)^n d^n}{d\Omega^n} \sqrt{\frac{\pi}{\Omega}} \quad (\text{H.16})$$

as $\Omega \rightarrow \infty$.

Equation (H.16) constitutes the complete asymptotic expansion of integral (H.1) as $\Omega \rightarrow \infty$. It follows from the recognition that the ratio between successive terms of the series approaches zero as $\Omega \rightarrow \infty$, for any N , [42].

The asymptotic expansion of (H.16) requires knowledge of the derivatives of

$$G(s) = F(z)\phi(s) , \quad (\text{H.17})$$

where

$$\phi(s) = \frac{dz}{ds} , \quad (\text{H.18})$$

evaluated at $s=0$, ($z=z_S$). By direct differentiation of (H.17) one finds that

$$G(0) = F(z_S)\phi(0) , \quad (H.19)$$

$$G(0) = F'(z_S) [\phi(0)]^2 + F(z_S)\phi'(0) , \quad (H.20)$$

$$G''(0) = F''(z_S) [\phi(0)]^3 + 3F'(z_S)\phi(0)\phi'(0) + F(z_S)\phi''(0) , \quad (H.21)$$

•
•
• .

To obtain the value of the derivatives of $\phi(s)$ at $s=0$, one can expand the function $q(z)$ around the saddle point z_S for which $q'(z_S)=0$ and invert the resulting series [42].

Note that:

$$\begin{aligned} q(z) &= \tau(s) , \\ &= q(z_S) - s^2 , \end{aligned} \quad (H.22)$$

so

$$q(z) = q(z_S) + q'(z_S)(z-z_S) + \frac{q''(z_S)}{2!} (z-z_S)^2 + \frac{q^{(3)}(z_S)}{3!} (z-z_S)^3 \dots , \quad (H.23)$$

which implies

$$-s^2 = (z-z_S)^2 \frac{q''(z_S)}{2!} + (z-z_S)^3 \frac{q^{(3)}(z_S)}{3!} + \dots . \quad (H.24)$$

The inverse of this series is regular and vanishes at $s=0$. So, in view of the definition of $\phi(s) = \frac{dz}{ds}$, we may expand $(z-z_S)$ in terms of s around the saddle point $s=0$, one will get:

$$\begin{aligned} (z-z_S) &= 0 + (s-0)\phi(0) + \frac{(s-0)^2}{2!} \phi'(0) + \frac{(s-0)^3}{3!} \phi''(0) + \\ &\quad \frac{(s-0)^4}{4!} \phi^{(3)}(0) \dots . \end{aligned} \quad (H.25)$$

It follows that:

$$(z-z_s)^2 = \phi^2(0)s^2 + \phi(0)\phi'(0)s^3 + \left(\frac{\phi^2(0)}{4} + \frac{\phi(0)\phi''(0)}{3}\right)s^4 + \dots, \quad (\text{H.26})$$

$$(z-z_s)^3 = \phi^3(0)s^3 + \frac{3}{2}\phi^2(0)\phi'(0)s^4 + \dots, \quad (\text{H.27})$$

$$(z-z_s)^4 = s^4\phi^4(0) + \dots, \quad (\text{H.28})$$

We substitute (H.25), (H.26), (H.27) and (H.28) into (H.24) and equate the coefficient of like powers of s on both sides:

$$\begin{aligned} -s^2 &= [\phi^2(0)s^2 + \phi(0)\phi'(0)s^3 + \left(\frac{\phi^2(0)}{4} + \frac{\phi(0)\phi''(0)}{3}\right)s^4 + \dots] \cdot \\ &\quad \frac{q''(z_s)}{2} + [\phi^3(0)s^3 + \frac{3}{2}\phi^2(0)\phi'(0)s^4 + \dots] \frac{q^{(3)}(z_s)}{3!} + \\ &\quad [\phi^4(0)s^4 + \dots] \frac{q^{(4)}(z_s)}{4!} + \dots, \end{aligned} \quad (\text{H.29})$$

which gives:

$$\begin{aligned} &[1 + \phi^2(0) \frac{q''(z_s)}{2}]s^2 + [\phi(0)\phi'(0) \frac{q''(z_s)}{2} + \phi^3(0) \frac{q^{(3)}(z_s)}{3!}]s^3 + \\ &\quad \left\{ \left[\frac{\phi^2(0)}{4} + \frac{\phi(0)\phi''(0)}{3} \right] \frac{q''(z_s)}{2} + \frac{3}{2}\phi^2(0)\phi'(0) \frac{q^{(3)}(z_s)}{3!} + \right. \\ &\quad \left. \phi^4(0) \frac{q^{(4)}(z_s)}{4!} \right\} s^4 + \dots = 0. \end{aligned} \quad (\text{H.30})$$

One will get:

$$\phi(0) = \pm \sqrt{\frac{-2}{q''(z_s)}} \quad , \quad (\text{H.31})$$

$$\phi'(0) = \frac{2}{3} \frac{q^{(3)}(z_s)}{[q''(z_s)]^2} \quad , \quad (\text{H.32})$$

and

$$\begin{aligned} \phi''(0) &= \frac{1}{2} \left[\frac{1}{q''(z_s)} \right]^2 \sqrt{\frac{-2}{q''(z_s)}} \left\{ q^{(4)}(z_s) - \frac{5}{3} \frac{[q^{(3)}(z_s)]^2}{q''(z_s)} \right\} \\ &\vdots \\ &\vdots \end{aligned} \quad (\text{H.33})$$

Recall that

$$G(0) = F(z_s)\phi(0) \quad , \quad (\text{H.34})$$

$$G'(0) = F'(z_s)[\phi(0)]^2 + F(z_s)\phi'(0) \quad , \quad (\text{H.35})$$

and

$$\begin{aligned} G''(0) &= F''(z_s)[\phi(0)]^3 + 3F'(z_s)\phi(0)\phi'(0) + F(z_s)\phi''(0) \quad , \\ &\vdots \\ &\vdots \end{aligned} \quad (\text{H.36})$$

so the integral (H.16) becomes

$$\begin{aligned} I(\Omega) &\sim e^{\Omega q(z_s)} \sqrt{\frac{-2\pi}{\Omega q''(z_s)}} \\ &\left\{ F(z_s) + \frac{1}{4\Omega} \left[F(z_s) \frac{3q^{(4)}(z_s)q''(z_s) - 5[q^{(3)}(z_s)]^2}{6[F''(z_s)]^3} + \right. \right. \\ &\quad \left. \left. + 2F'(z_s) \frac{q^{(3)}(z_s)}{[q''(z_s)]^2} - 2 \frac{F''(z_s)}{q''(z_s)} \right] + O\left(\frac{1}{\Omega^2}\right) + \dots \right\} \end{aligned} \quad (\text{H.37})$$

The higher order terms can be found accordingly. Furthermore, the branch of the square root in (H.37) is ascertained by noting that

$$\phi(s) = \left. \frac{dz}{ds} \right|_{z=z_s} = \left| \sqrt{\frac{-2}{q''(z_s)}} \right| e^{j\phi_s} \quad (\text{H.38})$$

where ϕ_s is the angle between the tangent to the SDP at $z=z_s$ and the positive real axis [66], (see Figure H.2).

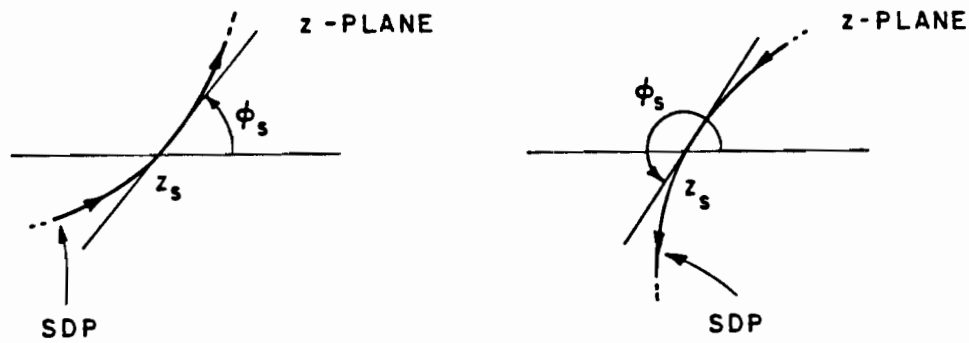


Figure H.2. Definition of the angle ϕ_s . The direction of integration along the path SDP is indicated by the arrowhead [66].

Pole Singularities Close to the Saddle Point

The above evaluation can no longer be performed, when the $F(z)$ has pole singularities at $z=z_i$'s near the first order saddle point z_s since $G(s)$ in (H.6) will possess corresponding pole singularities at $s=b_i$'s, in the vicinity of $s=0$; b_i 's in general are complex poles. Recall that

$$I(\Omega) = e^{\Omega q(z_s)} \int_{-\infty}^{\infty} G(s) e^{-\Omega s^2} ds \quad (\text{H.39})$$

where

$$G(s) = T(s) + \sum_{i=1}^N \frac{a_i}{s-b_i}, \quad (\text{H.40})$$

a_i 's are the residue of $G(s)$ at $s=b_i$, and $T(s)$ is regular at $s=b_i$. Note that the radius of convergence of $T(s)$ is uninfluenced by the presence of the poles, so the original integral becomes:

$$I(\Omega) = e^{\Omega q(z_s)} \left\{ \int_{-\infty}^{\infty} T(s) e^{-\Omega s^2} ds + \sum_{i=1}^N a_i \int_{-\infty}^{\infty} \frac{e^{-\Omega s^2}}{s-b_i} ds \right\}. \quad (\text{H.41})$$

$T(s)$ can be expanded in power series around $s=0$, and then the integration can be performed term by term. This will result in an expression similar to (H.10). So:

$$T(s) = \sum_{n=0}^{\infty} \frac{T^{(n)}(0)}{n!} s^n, \quad (\text{H.42})$$

which is:

$$= \sum_{n=0}^{\infty} (G^{(n)}(0) + (n!) \sum_{i=1}^N \frac{a_i}{b_i^{n+1}}) \frac{s^n}{n!} . \quad (\text{H.43})$$

The second integral in (H.42) can be written as:

$$\int_{-\infty}^{\infty} \frac{e^{-\Omega s^2}}{s-b} ds = -\frac{1}{b} \sqrt{\frac{\pi}{\Omega}} F(\pm \sqrt{j\Omega b^2}) , \quad (\text{H.44})$$

where

$$F(\pm \sqrt{x}) = \pm 2j\sqrt{x} e^{jx} \int_{\pm \sqrt{x}}^{\infty} e^{-j\tau^2} d\tau ; \quad \text{Im}(b) \gtrless 0 \quad (\text{H.45})$$

called the transition function [68]. The analytic property of this function will be discussed later. Therefore, (H.41) will be:

$$I(\Omega) \sim e^{\Omega q(z_s)} \left\{ \sum_{n=0}^{\infty} \left[\frac{G^{(2n)}(0)}{(2n)!} + \sum_{i=1}^N \frac{a_i}{b_i^{2n+1}} \right] [(-1)^n \frac{d^n}{d\Omega^n} \sqrt{\frac{\pi}{\Omega}} - \frac{a_i}{b_i} \sqrt{\frac{\pi}{\Omega}} F(\pm \sqrt{j\Omega b_i^2})] \right\} \quad (\text{H.46})$$

which can be written as:

$$I(\Omega) \sim e^{\Omega q(z_s)} \sqrt{\frac{\pi}{\Omega}} \left[G(0) + \sum_{i=1}^N \frac{a_i}{b_i} (1 - F(\pm \sqrt{j\Omega b_i^2})) + \sum_{n=1}^{\infty} \frac{2^{-2n}}{n! \Omega^n} \left[G^{(2n)}(0) + (2n)! \sum_{i=1}^N \frac{a_i}{b_i^{2n+1}} \right] \right] \quad (\text{H.47})$$

Where use has been made via

$$\left[(-1)^n \frac{d^n}{d\Omega^n} \sqrt{\frac{\pi}{\Omega}} \right] = \frac{\Gamma\left(\frac{(2n+1)}{2}\right)}{\Omega^{\frac{(2n+1)}{2}}} ; \quad n=0,1,2,\dots , \quad (\text{H.48})$$

and

$$\Gamma(\alpha+1) = \alpha\Gamma(\alpha) \quad ; \quad \Gamma\left(\frac{1}{2}\right) = \sqrt{\pi} \quad (\text{H.49})$$

$$2^{2\alpha-1} \Gamma(\alpha)\Gamma\left(\alpha+\frac{1}{2}\right) = \sqrt{\pi} \Gamma(2\alpha) \quad . \quad (\text{H.50})$$

Equation (H.47) is a complete asymptotic expansion of integral (H.1) in which the presence of the simple poles have been taken into account by the mean of transition function $F(\pm\sqrt{x})$. It is worth noting that as $|\sqrt{x}| \rightarrow \infty$, the $F(|\sqrt{x}|) \rightarrow 1$, (see (H.73)). This implies that if the poles are sufficiently far from the saddle point, expression of (H.47) will simplify to (H.37).

On The Uniformity of the Uniform Asymptotic Expansion

Consider again (H.47), we are going to show that as one of the poles, say b_k , goes to SDP, $\text{Im}(b_k) \rightarrow 0$, or goes to the saddle point, $b_k \rightarrow 0$, the solution remains regular.

Recall that:

$$b_k = \pm \sqrt{q(z_s) - q(z_0)} \quad , \quad (\text{H.51})$$

where the proper branch can be inferred as follows:

$$b_k^2 = q(z_s) - q(z_0) \quad , \quad (\text{H.52})$$

If one expands b_k^2 around the saddle point z_s ;

$$b_k^2 = 0 - (z_0 - z_s)q'(z_s) - \frac{(z_0 - z_s)^2}{2!} q''(z_s) - \frac{(z_0 - z_s)^3}{3!} q^{(3)}(z_s) \dots, \quad (\text{H.53})$$

$$b_k^2 \approx -\frac{(z_0 - z_s)^2}{2!} q''(z_s) \left\{ 1 + \frac{(z_0 - z_s)^3}{3} - \frac{q^{(3)}(z_s)}{q''(z_s)} + \dots \right\}, \quad (H.54)$$

so

$$b_k \approx \frac{(z_0 - z_s)}{h} \left\{ 1 + \frac{(z_0 - z_s)}{3} - \frac{q^{(3)}(z_s)}{q''(z_s)} + \dots \right\}^{1/2}, \quad (H.55)$$

where

$$h = \sqrt{\frac{-2}{q''(z_s)}} = \left(\frac{dz}{ds} \right) \Big|_{z=z_s}, \quad (H.56)$$

which its proper branch has been defined in (H.38).

As $b_k \rightarrow 0$, one will have

$$b_k \approx \frac{z_0 - z_s}{h} \rightarrow 0, \quad (H.57)$$

so the proper branch of (H.51) can be ascertained from the above equation.

As $\text{Im}(b_k) \rightarrow 0$, (H.47) (in view of (H.45), (H.64) and (H.75)) can be written as

$$I(\Omega) \sim e^{\Omega f(z_s)} \left[\pm j\pi a_k e^{-\Omega b_k^2} + \sqrt{\frac{\pi}{\Omega}} \left[G(0) + \frac{a_k}{b_k} (1 - F(\pm \sqrt{j\Omega} b_k^2)) \right. \right. \\ \left. \left. + \sum_{\substack{i=1 \\ i \neq k}}^N \frac{a_i}{b_i} (1 - F(\pm \sqrt{j\Omega} b_i^2)) + \sum_{n=1}^{\infty} \frac{2-2n}{n! \Omega^n} [G^{(2n)}(0) + (2n)! \sum_{i=1}^N \frac{a_i}{b_i^{2n+1}}] \right] \right] \quad (H.58)$$

which either (+) or (-) sign can be properly used. This implies that as the pole b_k approaches to SDP, $\text{Im}(b_k) \rightarrow 0$, the principle value of $I(\Omega)$

remains the same, either the pole b_k approaches to SDP from above or from below.

As the pole b_k goes to the saddle point, $b_k \rightarrow 0$, (H.47) remains regular and given by

$$(H.59) \quad I(\Omega) \sim e^{\Omega f(z_s)} \sqrt{\frac{\pi}{\Omega}} \left[\left(G(0) + \frac{a_k}{b_k} \right) + \sum_{\substack{i=1 \\ i \neq k}}^N \frac{a_i}{b_i} (1 - F(\pm \sqrt{j\Omega b_i^2})) \right. \\ \left. + \sum_{n=1}^{\infty} \frac{2-2n}{n! \Omega^n} \left[G^{(2n)}(0) + (2n)! \sum_{i=1}^N \frac{a_i}{b_i^{2n+1}} \right] \right]$$

where in the derivation of (H.59) use has been made from the small argument approximation of the transition function given by (H.74), that is

$$F(\pm \sqrt{j\Omega b_k^2}) \approx \pm j b_k \sqrt{\pi \Omega} e^{-j\Omega b_k^2} \quad (H.60)$$

The discontinuous nature of the above equations are consistent with the amount of the contribution of the poles as they cross the steepest descent path. Therefore, the overall asymptotic expansion of $I(\Omega)$ remains smooth and continuous regardless of the position of the poles.

Analytic Property of the Transition Function $F(\pm \sqrt{j\Omega b^2})$

Let's consider (H.44):

$$I_0(\Omega, b) = \int_{-\infty}^{\infty} \frac{e^{-\Omega s^2}}{s-b} ds \quad , \quad (H.61)$$

strictly speaking $I_0(\Omega, b)$ is defined only for $\text{Im}(b) \neq 0$ and does not exist when b is real or zero. The analytic property of $I_0(\Omega, b)$ reveals that the integral is discontinuous across the real s axis. To show the discontinuity of $I_0(\Omega, b)$ as b crosses the real axis, one may construct the difference $D(\Omega, b)$:

$$D(\Omega, b_r) = \lim_{\delta \rightarrow 0} (I_0^+(\Omega, b_r + j\delta) - I_0^-(\Omega, b_r - j\delta)) \quad (\text{H.62})$$

where

$$b = b_r \pm j\delta \quad (\text{H.63})$$

where $I_0^+(\Omega, b_r + j\delta)$ is the value of $I(\Omega, b)$ as b approaches the real axis from the above, and $I_0^-(\Omega, b_r - j\delta)$ is the value of $I(\Omega, b)$ as b approaches the real b axis from below. The path integrations indented at $s = b_r \pm j\delta$ as shown in Figure H.3, [42]. Note that in $D(\Omega, b_r)$, the contribution of the integrals from the straight portions of the path cancel, then it remains a small circular contour enclosing the pole at $s = b$, therefore:

$$D(\Omega, b_r) = 2\pi j e^{-\Omega b^2} \quad (\text{H.64})$$

which gives the amount of discontinuity of $I_0(\Omega, b)$ as b crosses the real axis. Equation (H.61) can be written as [67]

$$I_0(\Omega, b) = be^{-\Omega b^2} \int_{-\infty}^{\infty} \frac{e^{-\Omega(s^2 - b^2)}}{s^2 - b^2} ds \quad (\text{H.65})$$

$$= be^{-\Omega b^2} \int_{\Omega}^{\infty} e^{\xi b^2} \int_{-\infty}^{\infty} e^{-\xi s^2} ds d\xi, \quad (\text{H.66})$$

therefore,

$$I_0(\Omega) = b\sqrt{\pi} e^{-\Omega b^2} \int_{\Omega}^{\infty} \frac{e^{\xi b^2}}{\sqrt{\xi}} d\xi . \quad (\text{H.67})$$

where the path of integration goes to infinity so that $\text{Re}(\xi b^2) < 0$ at infinity, and use has been made from the formula

$$\frac{1}{s-b} = \frac{s}{s^2-b^2} + \frac{b}{s^2-b^2} , \quad (\text{H.68a})$$

and

$$\frac{e^{-\Omega(s^2-b^2)}}{s^2-b^2} = \int_{\Omega}^{\infty} e^{-\xi(s^2-b^2)} d\xi . \quad (\text{H.68b})$$

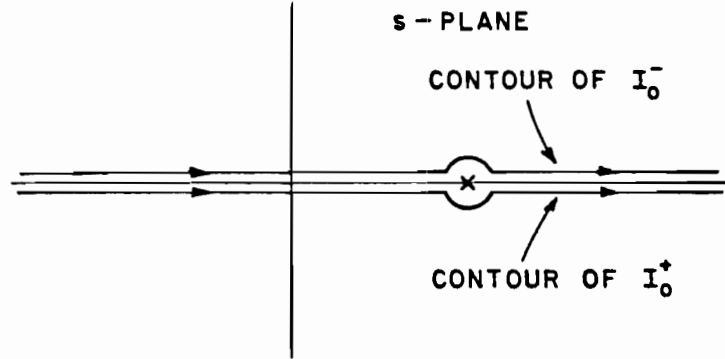


Figure H.3. Contour of integrations of $I_0^{\pm}(\Omega, b_r \pm j\delta)$.

In order to write the $I_0(\Omega, b)$ in terms of complex Fresnel's integral, the new variable is introduced. Let

$$u = \pm \sqrt{j\xi b^2} \quad ; \quad d\xi = -2j \frac{u}{b^2} du \quad , \quad (H.69)$$

$$I_0(\Omega, b) = -\frac{1}{b} \sqrt{\frac{\pi}{\Omega}} \left[\pm 2j \sqrt{j\Omega b^2} e^{j(j\Omega b^2)} \left(\int_{\pm \sqrt{j\Omega b^2}}^{\infty} e^{-ju^2} du \right) \right] ; \text{Im}(b) \gtrless 0 \quad (H.70)$$

The expression inside the brackets is called the transition function [68], generalized to complex arguments,

$$F(\pm \sqrt{j\Omega b^2}) = 2j(\pm \sqrt{j\Omega b^2}) e^{j(j\Omega b^2)} \int_{\pm \sqrt{j\Omega b^2}}^{\infty} e^{-ju^2} du ; \text{Im}(b) \gtrless 0 \quad (H.71)$$

The transition function is a double valued function in terms of the argument $(j\Omega b^2)$. The sign ambiguity is resolved by imposing the following condition:

$$-3 \frac{\pi}{4} < \arg(\pm \sqrt{j\Omega b^2}) < \frac{\pi}{4} \quad . \quad (H.72)$$

Equation (H.72) can be explained more clearly, if one constructs a two-sheeted Riemann surface in a (ξb^2) plane with a cut along the positive real axis. One sheet of Riemann surface will be mapped onto the left hand side of $y=x$ line (shaded area) and the other sheet will be mapped on the right hand side of $y=x$ (unshaded area), as shown in Figure H.4. The choice of the sign of the square root $(\pm \sqrt{j\xi b^2})$ in the change of variable (H.70) will indicate which Riemann sheet will map onto the shaded region, and which onto the unshaded region. One will choose this

sign in such a way that the sheet containing the path of integration will be mapped onto the shaded region. Note that if $\text{Im}(b) > 0$, (the pole located in the upper half of the s plane), the integration path is on the top sheet, so $\bar{u} = -e^{j\pi/4} b/\sqrt{\Omega}$; whereas if $\text{Im}(b) < 0$, (the pole located in the lower half of the s plane), the integration path is on the bottom sheet, so $\bar{u} = +e^{j\pi/4} b/\sqrt{\Omega}$. In the $u = \sqrt{j\Omega} b^2$ plane, the path of integration is any path that starts from $\bar{u} = \pm e^{j\pi/4} b/\sqrt{\Omega}$ and goes to infinity in the fourth quadrant (see Figure H.5). It is noteworthy that as the pole $s=b$ crosses the real axis in the s plane, ($\text{Im}(b)$ flips the sign), the value of the transition function, $F(\sqrt{j\Omega} b^2)$ changes discontinuously. However, this is expected, because the path of integration of the original integral (H.61) goes along the real axis, and as the pole crosses the real axis, one must add (or subtract) the residue contribution of the pole to (or from) the integral (see (H.64)).

The asymptotic expansion of $F(\sqrt{\alpha})$, $|\sqrt{\alpha}| \gg 1$, in descending powers of α can be obtained via the repeated integration by parts [69], that is

$$F(\sqrt{\alpha}) \sim 1 + \frac{1}{-2j\alpha} + \frac{3}{-4\alpha^2} + \frac{15}{8j\alpha^3} + \frac{105}{16\alpha^4} + \dots ; \quad |\alpha| \gg 1 . \quad (\text{H.73})$$

The transition function has also an ascending power series, when $|\sqrt{\alpha}| \ll 1$. This expansion can be obtained by expanding the $\exp(-ju^2)$ term in a power series, and integrating term by term,

$$F(\sqrt{\alpha}) \sim e^{j(\alpha+\pi/4)} [\sqrt{\pi\alpha} - 2\alpha e^{j\pi/4} - \frac{2}{3} \alpha^2 e^{-j\pi/4} + \dots] ; \quad |\alpha| \ll 1 . \quad (\text{H.74})$$

If $\text{Im}(b) \rightarrow 0$; $I_0(\Omega, b)$ in (H.61) via (H.64) can be considered as a generalized function [42], that is

$$\lim_{\delta \rightarrow 0} I_0(\Omega, b_r \mp j\delta) = -\frac{1}{b_r} \sqrt{\frac{\pi}{\Omega}} (F(\pm \sqrt{j\Omega} b_r^2) \mp j\sqrt{\pi\Omega} b_r e^{-\Omega b_r^2}), \quad (\text{H.75})$$

also the following relationship between $F(+\sqrt{j\Omega} b)$ and $F(-\sqrt{j\Omega} b)$ exists,

$$F(-\sqrt{j\Omega} b) = F(+\sqrt{j\Omega} b) - 2j \sqrt{\pi\Omega} b e^{-\Omega b^2} \quad (\text{H.76})$$

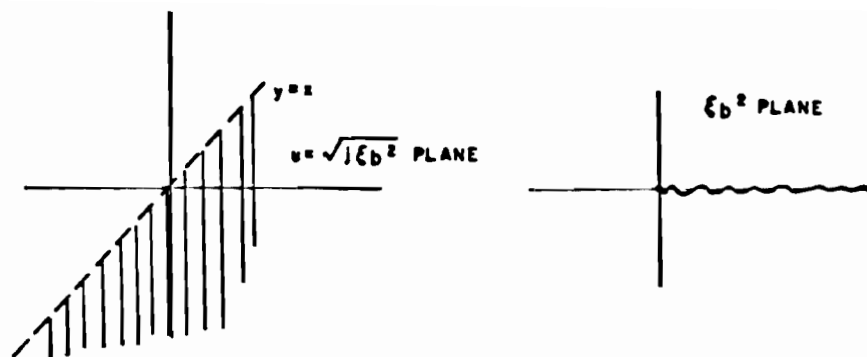


Figure H.4. Mapping of the two sheeted (ξb^2) plane onto $u = \sqrt{j\xi b^2}$ plane.

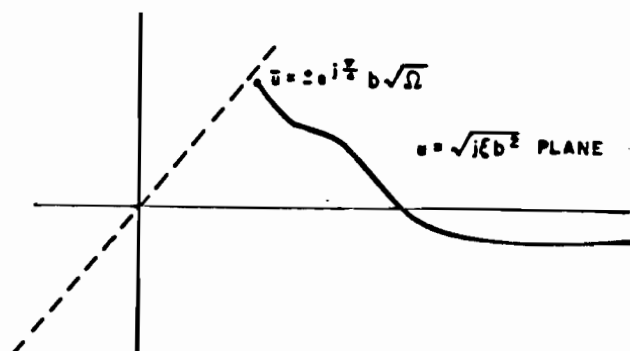


Figure H.5. Integration path of the complex Fresnel's integral in the $u = \sqrt{j\xi b^2}$ plane.

APPENDIX I

$$\text{A UNIFORM ASYMPTOTIC EXPANSION OF } \int_{-\infty}^{\infty} \frac{H_0^2(k_0 \rho \sqrt{1-\eta^2}) e^{-jk_0 \eta z}}{\eta - (\frac{\zeta_p}{k_0})} d\eta$$

In this appendix, a uniform asymptotic expansion of the above integral associated with the uniform asymptotic approximation of I given in (5.4) and (5.16) will be derived.

Let us consider the integral A,

$$A = \int_{-\infty}^{\infty} \frac{H_0^2(k_0 \rho \sqrt{1-\eta^2}) e^{-jk_0 \eta z}}{\eta - (\frac{\zeta_p}{k_0})} d\eta, \quad (I.1)$$

where ζ_p is in general a complex pole (surface wave or leaky wave of the integrand $F(\zeta)$ in (5.1)). The integral A can be asymptotically approximated as

$$A \sim \sqrt{\frac{2}{\pi k_0 \rho}} e^{j\pi/4} \int_{-\infty}^{\infty} \frac{1}{\sqrt{1-\eta^2}} \frac{e^{-jk_0(\rho\sqrt{1-\eta^2} + \eta z)}}{\eta - (\frac{\zeta_p}{k_0})} d\eta, \quad (I.2)$$

where the large argument approximation of the Hankel function has been utilized,

$$H_0^2(x) \sim \sqrt{\frac{2}{\pi x}} e^{j\pi/4} e^{-jx} \left(1 + \frac{j}{8x}\right); \quad x \gg 1. \quad (I.3)$$

Although the steepest descent path evaluation can be directly performed, it is more convenient to do the angular spectrum mapping; for more detail see Appendix E. Let

$$\eta = \cos \gamma \quad ; \quad \frac{d\eta}{d\gamma} = -\sin \gamma \quad , \quad (I.4)$$

$$\sqrt{1-\eta^2} = \pm \sin \gamma \quad , \quad (I.5)$$

$$\eta = \cos(\gamma' + j\gamma'') = \cos \gamma' \cos \gamma'' - j \sin \gamma' \sinh \gamma'' \quad . \quad (I.6)$$

Thus, the two sheeted complex η plane can be mapped into various adjacent sections of "strip" 2π in the complex γ plane $(-\frac{\pi}{2} < \text{Real}(\gamma) < \frac{3}{2}\pi)$.

$$A \sim \sqrt{\frac{2}{\pi k_0 r \sin \theta}} e^{j\pi/4} \int_{\Gamma} \left(1 + \frac{j}{8k_0 r \sin \theta \sin \gamma}\right) \frac{1}{\sqrt{\sin \gamma}} \frac{e^{-jk_0 r \cos(\theta-\gamma)}}{\cos \gamma - (\epsilon_p/k_0)} \sin \gamma \, d\gamma \quad , \quad (I.7)$$

Γ is the original path of integration in the complex γ plane, and the minus sign (-) in Jacobian of $\frac{d\eta}{d\gamma}$ in (I.4) has been taken into account via the direction of integration over the Γ path; also use has been made of the following definition,

$$\rho = r \sin \theta; \quad z = r \cos \theta; \quad \tan \theta = \frac{\rho}{z} \quad . \quad (I.8)$$

It is noted that the above integral has a saddle point at $\gamma_s = \theta$. Let

$$q(\gamma) = -j \cos(\theta - \gamma) \quad , \quad (I.9)$$

$$q'(\gamma) = j \sin(\theta - \gamma) \quad ; \quad \gamma_s = \theta \quad (\text{saddle point}), \quad (I.10)$$

and

$$q(\gamma_s) = -j \quad . \quad (I.11)$$

Figure I.1 depicts the original path (Γ) and steepest descent path Γ_{SDP} in the complex γ plane. Some pole singularities (surface wave and leaky wave) of the original integrand $F(\zeta)$ in (5.1) have been shown in Figure I.1 also. The original integral A can be written in terms of the SDP integral plus the residue contributions of the poles which may be captured during the path deformation; so

$$\begin{aligned} A \sim & 2\pi j N(\zeta_p) H_0^2 (\rho \sqrt{k_0^2 - \zeta_p^2}) e^{-j\zeta_p z} \\ & + \sqrt{\frac{2}{\pi k_0 r \sin \theta}} e^{j\pi/4} \int_{\Gamma_{SDP}} \left(1 + \frac{j}{8k_0 r \sin \theta \sin \gamma}\right) \\ & \frac{\sqrt{\sin \gamma}}{\cos \gamma - \cos \gamma_p} e^{-jk_0 r \cos(\theta - \gamma)} d\gamma ; \quad \eta_p = \left(\frac{\zeta_p}{k_0}\right) , \end{aligned} \quad (I.12)$$

where

$$\cos(\gamma_p) = \frac{\zeta_p}{k_0} ; \quad (I.13)$$

$$\gamma_p = \cos^{-1} \left(\frac{\zeta_p}{k_0} \right) , \quad (I.14)$$

$$N(\zeta_p) = \begin{cases} 1 & \text{if } \gamma_p \text{ lies in regions B or C,} \\ -1 & \text{if } \gamma_p \text{ lies in region A ,} \\ 0 & \text{if } \gamma_p \text{ lies outside regions A, B or C} \end{cases} \quad (I.15)$$

of the Figure (I.1), and Γ_{SDP} is the path on which the following condition holds:

$$\text{Im } q(\gamma) = \text{Im}(q(\gamma_s)) , \quad (I.16)$$

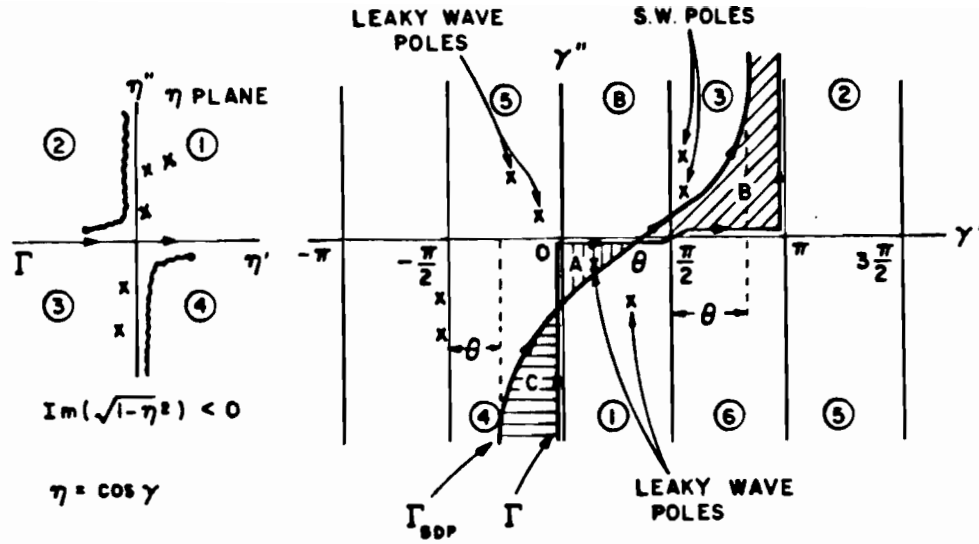


Figure I.1. Angular spectrum mapping where $n=\cos\gamma$; the leaky and surface wave poles and the contour integration of Γ and Γ_{SDP} in (I.1) and (I.12) respectively are shown.

or

$$\operatorname{Re}(\cos(\theta-\gamma)) = 1 \quad . \quad (I.17)$$

The Γ_{SDP} can be transformed into the real axis via the following transformation:

$$q(\gamma) - q(\gamma_S) = -s^2 \quad , \quad (I.18)$$

or

$$\cos(\theta-\gamma) = 1 - js^2 \quad ; \quad \sin(\theta-\gamma) = \pm s\sqrt{s^2+2j} \quad , \quad (I.19)$$

also

$$\frac{d\gamma}{ds} = \frac{2j}{\sqrt{s^2+2j}} ; \quad \left. \frac{d\gamma}{ds} \right|_{s=0} = \sqrt{\frac{-2}{q''(\gamma_s)}} = \sqrt{2} e^{j\pi/4} . \quad (I.20)$$

Equation (I.12) can now be written in canonical form,

$$A \sim 2\pi j N(\zeta_p) H_0^2 (\rho \sqrt{k_0^2 - \zeta_p^2}) e^{-j\zeta_p z} \\ + \sqrt{\frac{2}{\pi k_0 r \sin\theta}} e^{j\pi/4} e^{-jk_0 r} \int_{-\infty}^{\infty} G(s) e^{-k_0 r s^2} ds , \quad (I.21)$$

where

$$G(s) = \left(1 + \frac{j}{8k_0 r \sin\theta \sin\gamma}\right) \frac{\sqrt{\sin\gamma}}{\cos\gamma - \cos\gamma_p} \frac{d\gamma}{ds} . \quad (I.22)$$

The complete asymptotic expansion of the above canonical integral has been discussed in Appendix H. It is noted that $G(s)$ has a simple pole at $s=b$, from (H.40), $G(s)$ can be written as

$$G(s) = T(s) + \frac{\text{Res}(b)}{s-b} , \quad (I.23)$$

where $T(s)$ is regular at $s=b$. The value of b can be found from (H.51),

$$b = \sqrt{q(\gamma_s) - q(\gamma_p)} = \sqrt{-j(1 - \cos(\gamma_p - \theta))} \\ = \pm \sqrt{2} e^{-j\pi/4} \sin\left(\frac{\gamma_p - \theta}{2}\right) , \quad (I.24)$$

where the proper branch can be inferred from (H.51) - (H.52), and (I.18), that is;

$$\lim_{\gamma_p \rightarrow \gamma_s} b \equiv \frac{\gamma_p - \gamma_s}{\sqrt{\frac{2}{-q''(\gamma_s)}}} = \frac{\gamma_p - \theta}{\sqrt{2}} e^{-j\pi/4} , \quad (I.25)$$

which implies that (+) must always be chosen in (I.24). The residue of pole at $\gamma=b$ can be found from (I.2),

$$\begin{aligned} \text{Res}(b) &= \lim_{n \rightarrow n_p} (n - n_p) \frac{1}{\sqrt{1-n^2} (n - n_p)} , \\ &= \frac{1}{\sqrt{1-n_p^2}} ; \quad n_p = \frac{\zeta_p}{k_0} . \end{aligned} \quad (I.26)$$

The leading term of the uniform asymptotic expansion of (I.21) for $k_0 r \gg 1$ can be readily written via (H.39)-(H.47),

$$\begin{aligned} A \sim M(k_0 r, \zeta_p) &= 2\pi j N(\zeta_p) H_0^2(\rho \sqrt{k_0^2 - \zeta_p^2}) e^{-j\zeta_p z} \\ &+ 2j \frac{e^{-jk_0 r}}{k_0 r} \left(1 + \frac{j}{8k_0 r \sin^2 \theta}\right) \left(\frac{1}{\cos \theta - n_p}\right. \\ &\left. + \frac{1}{2\sqrt{\sin \theta} \sqrt{1-n_p^2} \sin(\frac{\gamma_p - \theta}{2})} \left(1 - F(\mp \sqrt{2k_0 r} \sin^2(\frac{\gamma_p - \theta}{2}))\right)\right) \end{aligned} \quad (I.27)$$

where $F(\mp \sqrt{x})$ is called the transition function given in (H.71). The (+) or (-) signs in (I.27) will be resolved by using the minus sign (-) if the pole $\gamma_p = \cos^{-1}(\frac{\zeta_p}{k_0})$ are above the SDP ($\text{Im}(b) > 0$) and the plus sign (+) otherwise ($\text{Im}(b) < 0$), (See also Figure I.1).

For the microstrip geometries where the source and observation points both lie on the substrate, one will have

$$z=0 \quad \text{or} \quad \theta = \pi/2 , \quad (I.28)$$

and the uniform asymptotic form of A for $k_0 \rho \gg 1$ will be given by,

$$\begin{aligned}
A \sim M(k_p, \zeta_p) &= 2\pi j N(\zeta_p) H_0^2 (\rho \sqrt{k_0^2 - \zeta_p^2}) e^{-j\zeta_p z} \\
&\quad - 2j \frac{e^{-jk_0 \rho}}{k_0 \rho \eta_p} \cdot \left(1 + \frac{j}{8k_0 \rho}\right) \cdot \\
&\quad \left(1 - \frac{\eta_p}{\sqrt{2} \sqrt{1-\eta_p^2} (\sqrt{1-\eta_p^2})} \left(1 - F(\mp \sqrt{k_0 \rho (1-\eta_p^2)})\right)\right), \quad (I.29a)
\end{aligned}$$

where the proper branch of $\sqrt{1-\eta_p^2}$ is chosen in such a way that

$$\text{Imag}(\sqrt{1-\eta_p^2}) > 0 \quad \text{if} \quad \text{Imag}(\eta_p) < 0. \quad (I.29b)$$

It is worth noting that if

$$\eta_p = \frac{\zeta_p}{k_0} \ll 1 \quad \text{or} \quad |\gamma_p| \approx \frac{\pi}{2}, \quad (I.30)$$

then the first two terms inside the bracket of (I.29) will be canceled,

$$\begin{aligned}
1 - \frac{\eta_p}{\sqrt{2} (\sqrt{1-\eta_p^2}) (\sqrt{1-\eta_p^2})} &\approx 1 - \frac{\eta_p}{\sqrt{2} (1 - \frac{1}{4} \eta_p^2) (\frac{\eta_p}{\sqrt{2}})} \\
&= 1 - \frac{1}{1 - \frac{1}{4} \eta_p^2} \approx 0, \quad (I.31)
\end{aligned}$$

where use has been made from the following formula,

$$(1-x)^\alpha \approx 1 - \alpha x \quad x \ll 1, \quad (I.32)$$

and the leading term of uniform asymptotic expansion of A in I.1 simplifies to,

$$\begin{aligned}
A \sim M(k_0 \rho, \zeta_p) &= 2\pi j N(\zeta_p) H_0^2 (\rho \sqrt{k_0^2 - \zeta_p^2}) e^{-j\zeta_p z} \\
&\quad 2j \frac{e^{-jk_0 \rho}}{k_0 \rho \eta_p} \cdot \left(1 + \frac{j}{8k_0 \rho}\right) F(\mp \eta_p \sqrt{\frac{k_0 \rho}{2}}) \quad \eta_p = \frac{\zeta_p}{k_0} \ll 1. \quad (I.33)
\end{aligned}$$

REFERENCES

- [1] S. Barkeshli, P.H. Pathak "An Efficient Approach for Evaluating the Planar Microstrip Green's Function", International IEEE AP-S Symposium and National Radio Science Meeting at Philadelphia, PA, June 9-13, 1986.
- [2] D.A. Jackson, and N.G. Alexopoulos, "An Asymptotic Extraction Technique for Evaluating Sommerfeld-type Integrals", IEEE Trans. on Antennas and Propagation, Vol. AP-34, pp. 1467-1470.
- [3] D.A. Jackson and N.G. Alexopoulos, "An Asymptotic Extraction Technique for the Real-Space Evaluation of Sommerfeld-Type Integrals", International IEEE AP-S Symposium and National Radio Science Meeting at Philadelphia, PA, June 9-13, 1986.
- [4] G.A. Deschamps, "Microstrip Microwave Antennas " presented at 3rd USAF Symposium on Antennas 1953
- [5] H. Gutton and G. Baissinot, "Flat Aerial for Ultra High Frequencies," French Patent No. 703113, 1955.
- [6] K.R. Carver and J.W. Mink, "Microstrip Antenna Technology," IEEE Trans. on Antennas and Propagation, Vol. AP-29, No. 1, pp. 2-24, January 1981.
- [7] E.V. Byron "A New Flush-Mounted Antenna Element for Phased Array Application," in Proc. Phased-Array Antennas Symposium, pp. 187-192, 1970.
- [8] R.E. Munson, "Conformal Microstrip Antennas and Microstrip Phased Arrays," IEEE Trans. on Antennas and Propagation, Vol. AP-22, No. 1, pp. 74-77, Jan. 1974.
- [9] D.M. Pozar, "Consideration for Millimeter Wave Printed Antennas," IEEE Trans. on Antennas and Propagation, Vol. AP-31, No. 5, pp. 740-747, Sept. 1983.
- [10] Y.T. Lo, D.P. Harrison, D. Solomon, G.A. Deschamps and F.R. Ore, "Study of Microstrip Antennas, Microstrip Phased Arrays, and Microstrip Feed Networks," Rome Air Development Center, Tech. Rpt. TR-77-406, Oct. 1977.
- [11] A.G. Derneryd, "A Theoretical Investigation of the Rectangular Microstrip Antenna Element," Rome Air Development Center, Tech. Rpt. TR-77-206, June, 1977.

- [12] K.R. Carver, "A Model Expansion Theory for the Microstrip Antenna," Dig. Int. Symp. Antennas Propagation Soc., Seattle, WA, pp. 101-104 June 1979.
- [13] K.R. Carver, "Practical Analytical Techniques for the Microstrip Antenna," Proc. Workshop Printed Circuit Antenna Tech., New Mexico State University, Las Cruces, pp. 711-720, Oct. 1979.
- [14] Y.T. Lo, D. Solomon and W.F. Richards, "Theory and Experiment on Microstrip Antennas," IEEE Trans. on Antennas and Propagation, Vol. AP-27, No. 2, pp. 137-145, March 1979.
- [15] W.F. Richards and Y.T. Lo, "An Improved Theory for Microstrip Antennas and Applications," IEEE Trans. on Antennas and Propagation, Vol. AP-29, No. 1, pp. 38-46, January 1981.
- [16] E.H. Newman and P.Tulyathan, "Analysis of Microstrip Antennas Using Moment Methods," IEEE Trans. on Antennas and Propagation, Vol. AP-29, No. 1, pp. 47-53, Jan 1981.
- [17] J.H. Richmond and E.H. Newman, "Dielectric Coated Wire Antennas," Radio Science, Vol. 11, pp. 13-20, January 1976.
- [18] E.H. Newman, "Strip Antennas in a Dielectric Slab " IEEE Trans. on Antennas and Propagation, Vol. AP-26, pp. 647-653, Spet. 28, 1978.
- [19] N.K. Uzunoglu, N.G. Alexopoulos and J.G. Fikioris, "Radiation Properties of Microstrip Dipoles," IEEE Trans. AP, Vol. AP-27, No. 6, pp. 853-858, November 1979.
- [20] J.R. Mosig and F.E. Gardiol, "The Near Field of An Open Microstrip Structure," IEEE AP-S International Symposium, pp. 379-382, 1979.
- [21] D.M. Pozar, "Input Impedance and Mutual Coupling of Rectangular Microstrip Antennas," IEEE Trans. AP, Vol. AP-30, No. 6, pp. 1191-1196, November 1982.
- [22] I.E. Rana and N.G. Alexopoulos, "Current Distribution and Input Impedance of Printed Dipoles," IEEE Trans. AP, Vol. AP-29, No. 1, pp. 99-105, January 1981.
- [23] N.G. Alexopoulos and I.E. Rana, "Mutual Impedance Computation between Printed Dipoles," IEEE Trans. AP, Vol. AP-29, No. 1, pp. 106-111, January 1981.
- [24] M. Siegel, and R.W.P. King, "Electromagnetic Fields in a Dissipative Half-Space-A Numerical Approach", Journal of Applied Physics, Vol. 41, No. 6, p. 2415-2423, May 1970.

- [25] G.J. Burke, and E.K. Miller, "Modeling Antennas Near to and Penetrating a Lossy Interface", IEEE Trans. on Antennas and Propagation, Vol. AP-32, pp. 1040-1049, October 1984.
- [26] W.A. Johnson, and D.G. Dudley, "Real Axis Integration of Sommerfeld Integrals, Source and Observation Points in Air", Radio Science, Vol. 18, pp. 175-186, 1983.
- [27] L. Tsang, R., R. Brown, J.A. Kong, G. Simmons, "Numerical Evaluation of Electromagnetic Fields Due to Dipole Antennas in the Presence of Stratified Media", Journal of Geophysical Research, Vol. 29, No. 14, pp. 2077-2080, May 1974.
- [28] A. Mohsen, "On the Evaluation of Sommerfeld Integrals", IEE Proc. H., Microwaves, Opt. and Antennas, Vol. 129, pp. 177-182, 1982.
- [29] J.A. Kong, Shen Liang-Chi and Leung Tsong, "Field of an Antenna Submerged in a Dissipative Dielectric Medium", IEEE Trans on Antennas and Propagation, Vol. AP-25, pp. 887-889, November 1977.
- [30] P. Parhami, Y. Rahmat-Sami, and R. Mittra, "An Efficient Approach for Evaluating Sommerfeld Integrals Encountered in the Problem of a Current Element Radiating Over Lossy Ground", IEEE Trans., Vol. AP-18, pp. 100-104, 1980.
- [31] K.A. Michalski, "On the Efficient Evaluation of Integrals Arising in the Sommerfeld Half-Space Problem, IEE Proc., H, Microwaves, Opt., and Antennas, Vol. 32, pp. 312-318, 1985.
- [32] P.B. Katehi, and N.G. Alexopoulos, "Real Axis Integration of Sommerfeld Integrals with Application to Printed Circuit Antennas", J. Math. Phys., Vol. 24(3), pp. 527-532, March 1983.
- [33] P.W. Hawkes, Ed., Advances in Electronics and Electron Physics, A Dynamical Radiation Model for Microstrip Structures (by J.R. Mosig and F.E. Gardiol), Academic Press, 1982.
- [34] I. Choi, "An Efficient Representation for the Planar Microstrip Green's Function," Ph.D. Dissertation, The Ohio State University, Dec. 1986.
- [35] D.M. Pozar, "Improved Computational Efficiency for the Moment Method Solution of Printed Dipoles and Patches", Electromagnetics, Vol. 3, No. 3-4, pp. 299-309, July-Dec. 1983.
- [36] J.R. Mosig, and T.K Sarkar, "Comparison of Quasi-Static and Exact Electromagnetic Fields from a Horizontal Electric Dipole Above a Lossy Dielectric Backed by an Imperfect Ground Plane", IEEE Trans. Microwave Theory and Technique, Vol. MTT-34, No. 4, pp. 379-387, April 1986.

- [37] S. Barkeshli, P.H. Pathak, "Radially Propagating and Steepest Descent Path Representation of the Planar Microstrip Dyadic Green's Function," paper submitted to Journal of Radio Science.
- [38] S. Barkeshli, P.H. Pathak, and M. Marin, "An Asymptotic Closed Form Microstrip Surface Green's Function for the Efficient Moment Method Analysis of Mutual Coupling In Microstrip Antenna Arrays," paper submitted for publication to IEEE Trans. on Antennas and Propagation.
- [39] A. Sommerfeld, Partial Differential Equations in Physics, New York, Academic Press, 1949.
- [40] J.R. Wait, Antenna Theory, Part 2, (Editors, Collin and Zucker), New York, McGraw-Hill, 1969.
- [41] A. Banos, Dipole Radiation in the Presence of a Conducting Half Space, New York, Pergamon Press, 1966.
- [42] L.B. Felsen and N. Marcuvitz, Radiation and Scattering of Waves, Englewood Cliffs, NJ: Prentice-Hall, 1973.
- [43] J.A. Kong, Theory of Electromagnetic Waves, John Wiley and Sons, Second Edition, 1986.
- [44] R.G. Kouyoumjian, "Advanced Electromagnetic Theory," unpublished notes of ELEC 816,817,819, The Ohio State University, Department of Electrical Engineering, 1983.
- [45] C.T. Tai, "Dyadic Green's Function", unpublished notes, The Ohio State University, Winter 1985.
- [46] P.H. Pathak, "On the Eigenfunction Expansion of Electromagnetic Dyadic Green's Functions, IEEE Trans. on Antennas and Propagation, Vol. AP-31, pp. 837, 1983.
- [47] P.E. Mayes, The Equivalence of Electric and Magnetic Sources, GRE Trans. Antenn. Prop. Vol. 6:295-296, 1958.
- [48] Van Bladel, Electromagnetic Fields, Hemisphere Publishing Corporation, New York, 1985.
- [49] S. Barkeshli, P.H. Pathak, "On the Dyadic Green's Function of the Multilayered Dielectric/Ferrite Media", presented at the 1987 International IEEE AP-S and National Radio Science Meeting at Blacksburg, VA, June 15-19, 1987.

- [50] S. Barkeshli and P.H. Pathak, "On the Dyadic Green's Function for an Infinite Periodic Array of Arbitrary Oriented Dipole in a Multi-layered Media", presented at international IEEE AP-S Symposium and National Radio Science Meeting at Blacksburg, VA, June 15-19, 1987.
- [51] S.A. Schelkunoff, Field Equivalence Theorems, Comm. on Pure and Appl. Math., Vol. 4, pp. 43-59, June, 1951.
- [52] R.F. Harrington, Field Computation by Moment Method, Robert E. Krieger Publ. Company, Malabar, Florida, 1982.
- [53] L.V. Kantorovich and V.I. Krylor, Approximate Method of Higher Analysis, 4th Ed., translated by C.P. Benster, John Wiley and Sons, Inc., New York, Chapter IV, 1969.
- [54] V.H. Rumsey, "Reaction Concept in Electromagnetic Theory," Phy. Rev., Vol. 94, pp. 1483-1491, June 1959.
- [55] S. Silver (Ed.), Microwave Antenna Theory and Design, MIT Radiation Laboratory Series, Vol. 12, McGraw-Hill Book Co., New York, 1949.
- [56] R.E. Collin, Foundations for Microwave Engineering, McGraw Hill, 1966.
- [57] W.A. Imbriale, Numerical and Asymptotic Techniques in Electromagnetics, (R. Mittra, Editor), Springer-Verlay, New York, Heidelberg, Berlin, 1975.
- [58] E.H. Newman, "The Equivalent Separation(s) for the Self-Impedance of Thin Stripes", IEEE Transactions on Antenna and Propagation, Vol. AP-35, No. 1, Jan. 1987.
- [59] J. Meixner, "The Behavior of Electromagnetic Fields at Edges Ins. Math. Sci. Research, Report EM-72, New York University, New York, Dec. 1954.
- [60] R. Mittra and S.W. Lee, Analytical Techniques in the Theory of Guided Waves, MacMillan Co., New York, Collier-MacMillan Ltd., London, 1971.
- [61] B.A. Munk, "Advanced Antenna Theory", unpublished notes of ELEC 910, The Ohio State University, Winter, 1984.
- [62] S.A. Schelkunoff and H.T. Friis, Antennas Theory and Practice, Wiley and Sons, 1952.

- [63] Robert E. Collin, Field Theory of Guided Waves, McGraw Hill Book Company, New York, 1960.
- [64] J. Kevorkian and J.D. Cole, "Perturbation Methods in Applied Mathematics", Springer-Verlag, N.Y. Heidelberg, Berlin (1981).
- [65] D.L. Hutchins and R.G. Kouyoumjian, "Asymptotic Series Describing the Diffraction of a Plane Wave by a Wedge", Report No. 2183, The Ohio State Univ., ElectroScience Lab, Cos., OH, Dec. 15, 1969.
- [66] R.H. Schafer and R.G. Kouyoumjian, "Higher Order Terms in the Saddle Point Approximation", Proceedings of the IEEE, Vol. 55, pp. 1496-1497, August 1967.
- [67] L.M. Brekhovskikh, Waves in Layered Media, pp. 264-266, New York: Academic Press, 1960.
- [68] R.G. Kouyoumjian and P.H. Pathak, "A Uniform Geometrical Theory of Diffraction for an Edge in a Perfectly Conducting Surface", Proc. IEEE, Vol. 62, pp. 1448-1461, 1974.
- [69] P.C. Clemmow, The Plane Wave Spectrum Representation of Electromagnetic Fields, New York: Permamon Press, Ltd., 1966.
- [70] M. Marin, S. Barkeshli and P.H. Pathak, "On the Location of Surface and Leaky Wave Poles for the Grounded Dielectric Slab," paper submitted to IEEE Trans. on Antennas and Propagation.